EPA-650/4-74-034

August 1974

Environmental Monitoring Series

4

AEROSOL FORMATION FROM GAS-PHASE REACTIONS OF OZONE AND OLEFIN IN THE PRESENCE OF SULFUR DIOXIDE

Office of Research and Development
National Environmental Research Center
U.S. Environmental Protection Agency
Research Triangle Park, N.C. 27711

Research reports of the Office of Research and Development, Environmental Protection Agency, have been grouped into five series. These five broad categories were established to facilitate further development and application of environmental technology. Elimination of traditional grouping was consciously planned to foster technology transfer and a maximum interface in related fields. The five series are:

1. Environmental Health Effects Research
2. Environmental Protection Technology
3. Ecological Research
4. Environmental Monitoring
5. Socioeconomic Environmental Studies

This report has been assigned to the ENVIRONMENTAL MONITORING series. This series describes research conducted to develop new or improved methods and instrumentation for the identification and quantification of environmental pollutants at the lowest conceivable significant concentrations. It also includes studies to determine the ambient concentrations of pollutants in the environment and/or the variance of pollutants as a function of time or meteorological factors.

This report has been reviewed by the Office of Research and Development, EPA, and approved for publication. Approval does not signify that the contents necessarily reflect the views and policies of the Environmental Protection Agency, nor does mention of trade names or commercial products constitute endorsement or recommendation for use.

EPA-650/4-74-034

AEROSOL FORMATION FROM GAS-PHASE REACTIONS OF OZONE AND OLEFIN IN THE PRESENCE OF SULFUR DIOXIDE

by

David N. McNelis

National Environmental Research Center
Las Vegas, Nevada 89114

Program Element No. 21 AKB
ROAP No. 38

EPA Project Officer: William E. Wilson

Chemistry and Physics Laboratory
National Environmental Research Center
Research Triangle Park, North Carolina 27711

NATIONAL ENVIRONMENTAL RESEARCH CENTER
OFFICE OF RESEARCH AND DEVELOPMENT
U.S. ENVIRONMENTAL PROTECTION AGENCY
RESEARCH TRIANGLE PARK, NORTH CAROLINA 27711

August 1974

DISTRIBUTION STATEMENT

This report is available to the public, for a nominal cost, through the National Technical Information Service, 5285 Port Royal Road, Springfield, Virginia 22151.

This report is a dissertation submitted to the faculty of the University of North Carolina in partial fulfillment of the requirements for the degree of Doctor of Philosophy in the Department of Environmental Sciences and Engineering.

ABSTRACT

The loss of visibility in atmospheres laden with photochemical smog is largely attributed to the presence of sulfate aerosols. This facet was thought to be the most objectionable effect of the sulfate species and is reflected in the establishment of the National Ambient Air Quality Standard for sulfur dioxide. Recent reviews, however, have indicated that the adverse health effects appear more strongly associated with suspended particulate sulfate than with the sulfur dioxide.

The dark-phase reaction of olefin-ozone-sulfur dioxide was studied in an attempt to elucidate the mechanism involved in the oxidative consumption of the sulfur dioxide. The effect of several variables on the reaction stoichiometry and on the aerosol production was also investigated. These variables included the reactant concentrations, the relative humidity, molecular oxygen concentration and the olefin species although propylene was the primary olefin studied.

The stoichiometry of the propylene-ozone reaction was found to be a smooth function of the initial concentration ratio of these species. The olefin/ozone consumption was 1 for a system in which the olefin was initially in excess and 1 for a system having an initial ozone excess. The consumption ratio was unaffected by the addition of sulfur dioxide or by varying the relative humidity over the range of 20 to 38 percent.

Molecular oxygen had a significant effect on the reaction stoichiometry and product formation in the propylene-ozone thermal reaction. The propylene/ozone consumption ratio was lower in a system in which the molecular oxygen concentration was reduced. Oxygen apparently also contributed to the regeneration of ozone and the production of the hydroxyl radical species, both of which interacted with the propylene and with products of the reaction.

A tentative mechanism has been proposed for the oxidative consumption of sulfur dioxide in the propylene-ozone-sulfur dioxide system based on the observations made during these studies. Secondary reactions are a distinctive feature of this model which incorporated relatively few reactions to explain the major characteristics of the systems studied.

Aerosol formation occurred in the dark reaction of propylene and ozone although the particulate formed did not grow to a size which efficiently scattered light. The addition of sulfur dioxide markedly enhanced both the formation and subsequent growth of the aerosol. The same general patterns of aerosol formation, growth and decay were observed throughout the series of experiments over a broad range of initial conditions. These patterns are consistent with a model which includes homogeneous nucleation, condensation and coagulation processes.

An apparent equilibrium surface area was established for the aerosol when the addition to the total surface area by condensation was equal to the loss by coagulation. A strong correlation was found to exist between this equilibrium surface area and the volumetric conversion rate. It was also found that the correlation could be extended considerably in range to include data from other experiments in which the aerosol was photochemically generated. The establishment of the equilibrium surface area is due, therefore, to the physical processes rather than the chemical mechanism leading to its formation.

Table of Contents

		Page
List of Tables		vii
List of Figures		viii
I.	Introduction	1
II.	Review of Previous Work	7
	A. Studies of the Olefin-Ozone System	7
	B. Mechanism of the Olefin-Ozone Reaction	8
	C. Reactions with Sulfur Dioxide	14
	D. Aerosol Production in Hydrocarbon Systems	15
III.	Theory of Aerosol Formation, Growth and Decay.	20
	A. Nucleation	21
	B. Condensation	26
	C. Coagulation	29
IV.	Experimental Arrangement and Procedures	34
	A. Experimental Design and Arrangement	34
	B. Experimental Apparatus	41
	1. Reactor	41
	2. Ozone Analysis	44
	3. Ambient and Dew Point Temperatures Measurements	46
	4. Sulfur Dioxide Analysis	47
	5. Hydrocarbon Analysis	49
	6. Infrared Spectroscopic Product Analysis	50
	7. Sulfur Balance Determination	52
	8. Light Scattering Measurements	53
	9. Condensation Nuclei Count Determination	55
	10. Sub-microscopic Aerosol Analysis	56
	11. Optical Particle Analysis	61
	C. Experimental Procedures	63

V. Experimental Results and Discussion 71

A. Reactant Consumption Data and Reaction Stoichiometry 71

B. Product Analysis 94

C. Tentative Reaction Mechanism 111

D. Sulfate Analysis and Sulfur Mass Balance 114

E. Light Scattering Measurements 119

F. Aerosol Development 123

G. Aerosol Measurements by Single Particle Light Scattering 158

VI. Conclusions and Recommendations 162

References 168

Appendices 175

1. Product Analysis by Fourier Transform Infrared Spectroscopy. 175

2. Observed and Predicted Reactant Concentrations for Gas Phase Experiments. 176

3. Aerosol Droplet Number, Surface Area, and Volume Concentrations Distributions for Aerosol Experiments. 196

LIST OF TABLES

TABLE		PAGE
2-1	Summary of Rate Constant Data	10
2-2	Relative Rate Constants	17
3-1	Coagulation Constants for Unequal Sized Particles	31
4-1	Permeability of Tedlar and Scotchpak to Gases and Vapors	42
4-2	Data Table for Number, Surface Area and Volume Distribution	62
5-1	Summary of Experimental Conditions and Initial Reactant Concentrations	72
5-2	Summary of Stoichiometric Data and Acetyaldehyde Production	75
5-3	Product Analysis by Fourier Transform Infrared Spectroscopy	105
5-4	Summary of Sulfuric Acid Analysis by X-ray Fluorescence Spectroscopy and Liquid Chromatography	116
5-5	Volumetric Conversion Rate, Total Volume at 80 Minutes, Mean Volume Diameter Growth Rate, Coagulation Constant and Sulfur Dioxide Consumption at 80 Minutes for Aerosol Experiments	138
5-6	Initial Sulfur Dioxide Reaction Rate and Oxidative Rate	141
5-7	Calculated Sulfur Dioxide Consumption based on the Observed Volume Concentration	141

LIST OF FIGURES

FIGURE		PAGE
4-1	Schematic of Experimental Arrangement	36
4-2	Laboratory Arrangement for Olefin-Ozone-Sulfur Dioxide Studies	38
4-3	Aerosol Measurement Instrumentation	39
4-4	Fourier Transform Infrared Spectrometer	40
4-5	Variation of Relative Humidity with Time due to the Permeation of Water Vapor	43
4-6	Schematic of Reactor Port Arrangement	45
4-7	Schematic of the Electrical Aerosol Size Analyzer	58
4-8	Relationship Between Electrical Mobility and Particle Size for Diffusion Charging where $N_o = 1 \times 10^7$ (ions/cm^3)(sec)	60
4-9	Calibration Data for Optical Aerosol Analyzer	64
4-10	Variation of Reactant Concentration with Time Due to Wall Losses	69
5-1	Variation of Concentration with Time for Propylene-Ozone-Sulfur Dioxide Reaction	78
5-2	Variation of Concentration with Time for Ethylene-Ozone-Sulfur Dioxide Reaction	79
5-3	Stoichiometry of Olefin-Ozone Reaction versus Initial Reactant Concentration Ratio	80
5-4	Concentration of Acetyaldehyde Produced versus Propylene Reacted for Nine Propylene-Ozone Experiments	86
5-5	Sulfur Dioxide Consumption versus Propylene Reacted for Different Initital Sulfur Dioxide Concentrations	88
5-6	Sulfur Dioxide Consumption versus Ozone Reacted for Different Initial Sulfur Dioxide Concentrations	89
5-7	Variation of the Apparent Rate Constant with Time Due to Secondary Reactions	92

LIST OF FIGURES (Continued)

FIGURE		PAGE
5-8	Infrared Absorption Spectra of Reactor Contents - Runs 31 and 21	96
5-9	Infrared Spectra in Region of Carbon Monoxide Absorption - Runs 31 and 21	97
5-10	Infrared Spectra in Region of Carbon Monoxide Absorption - Runs 78 and 79	99
5-11	Infrared Spectra in Region of Carbon Monoxide Absorption - Runs 81 and 82	100
5-12	Infrared Spectra in Region of Carbon Monoxide Absorption - Runs 60 and 65	101
5-13	Infrared Absorption Spectra of Reactor Contents - Runs 28 and 29	104
5-14	Comparison of Results for Sulfuric Acid Analysis	118
5-15	Variation of the Scattering Coefficient, Visual Range, Surface Area Concentration and Sulfur Dioxide Concentration with Time for a Propylene-Ozone-Sulfur Dioxide Experiment	121
5-16	Variation of the Scattering Coefficient, Visual Range, Surface Area Concentration and Sulfur Dioxide Concentration with Time for an Ethylene-Ozone-Sulfur Dioxide Experiment	122
5-17	Aerosol Particle Number, Surface Area and Volume Development for a Propylene-Ozone Experiment	124
5-18	Total Volume, Number, Reciprocal of Number and Surface Area Concentration versus Time for the Developing Sulfuric Acid Aerosol - Run 101A	126
5-19	Total Volume, Number, Reciprocal of Number and Surface Area Concentration versus Time for the Developing Sulfuric Acid Aerosol - Run 101B	127
5-20	Total Volume, Number, Reciprocal of Number and Surface Area Concentration versus Time for the Developing Sulfuric Acid Aerosol - Run 102	128
5-21	Total Volume, Number, Reciprocal of Number and Surface Area Concentration versus Time for the Developing Sulfuric Acid Aerosol - Run 103	129

LIST OF FIGURES (Continued)

FIGURES		PAGE
5-22	Total Volume, Number, Reciprocal of Number and Surface Area Concentration versus Time for the Developing Sulfuric Acid Aerosol - Run 104	130
5-23	Total Volume, Number, Reciprocal of Number and Surface Area Concentration versus Time for the Developing Sulfuric Acid Aerosol - Run 105	131
5-24	Total Volume versus Sulfur Dioxide Consumption at T + 80 Minutes	143
5-25	Variation of the Equilibrium Surface Area with Volumetric Conversion Rate	145
5-26	Initial Volumetric Conversion Rate versus Product of Initial Propylene and Ozone Concentrations for Different Initial Sulfur Dioxide Concentrations	147
5-27	Development of the Volume Distribution with Time - Run 101A	148
5-28	Development of the Volume Distribution with Time - Run 101B	149
5-29	Development of the Volume Distribution with Time - Run 102	150
5-30	Development of the Volume Distribution with Time - Run 103	151
5-31	Development of the Volume Distribution with Time - Run 104	151
5-32	Development of the Volume Distribution with Time - Run 105	152
5-33	Variation of Volume Mean Diameter with Time for Six Aerosol Experiments	154
5-34	Rate of Change in Mean Volume Diameter versus Volumetric Conversion Rate	157
5-35	Variation of Aerosol Size Distribution with Time as Measured with Optical Particle Size Analyzer - Run 31	159
5-36	Variation of Aerosol Size Distribution with Time as Measured with Optical Particle Size Analyzer - Run 29	160

AEROSOL FORMATION FROM GAS PHASE REACTIONS OF OZONE AND OLEFIN IN THE PRESENCE OF SULFUR DIOXIDE

CHAPTER I

INTRODUCTION

A major source of the sulfur burden of our atmosphere results from the combustion of solid and liquid fossil fuels. These fuels contain significant quantities of sulfur as inorganic sulfides, sulfur containing organic compounds and some small fraction as sulfates. It is estimated that sulfur dioxide accounts for upwards of 95% of the sulfur released from the fuel combustion (Smith and Gruber, 1966).

There are several undesirable effects attributed to this contaminant which include the degradation of materials, retardation of plant growth and production, and of most importance, the direct impact on man's health. In addition, literature reviews by Bufalini (1971) and Altshuller and Bufalini (1971) provide many references citing the conversion of sulfur dioxide to aqueous sulfuric acid droplets as one of the most basic photochemical reactions. The exact physical and chemical mechanisms which enter into this conversion are not adequately understood but the resulting aerosol is known to contribute significantly to visibility reduction. The scatter and absorption of visible radiation by gas molecules and particulates are the causes of atmospheric visibility reduction. Small particles (0.1 to 1 μm diameter) suspended in the atmosphere are particularly effective in scattering visible light.

Until recently, this loss of visibility was thought to be the most objectionable effect of the sulfate aerosol. The sulfur dioxide

ambient air quality standards were based on judgemental decisions using the best available data. A review of the standard using the Community Health Environmental Surveillance System (CHESS) data indicated that this standard has a defensible base. This same review, however, has added a new facet to the problem, i.e., the fact that the adverse health effects for certain health indicators, particularly asthma, appear more strongly associated with suspended particulate sulfate than with sulfur dioxide (Environmental Protection Agency, 1974). If new toxicological data supports this finding then data collection and analysis should be directed toward developing sulfate criteria. Of paramount concern at the present is the complete lack of knowledge concerning the relationship of sulfur dioxide to suspended sulfate levels. Additional information is also needed relative to the rate of conversion of sulfur dioxide to sulfate. The standard will require another review when these data are available particularly if they indicate that the simple control of sulfur dioxide is not the most efficient way of protecting man's health from exposure to sulfur compounds.

In the atmosphere sulfur dioxide is oxidized by either gas phase, catalytic or photochemical processes. In irradiated olefin-oxides of nitrogen systems decay of sulfur dioxide and formation of sulfuric acid do not occur to any appreciable extent until most of the nitric oxide is converted to nitrogen dioxide. Nitrogen trioxide is formed in the reaction of ozone with nitrogen dioxide and the organic peroxides which earlier reacted with the nitric oxide begin to accumulate. Reaction with one of these oxidizing species rather than the direct photooxidation of the sulfur dioxide probably accounts for most of the sulfate aerosol generation. The oxidative interaction with the surfaces of aerosol droplets or particles could also account in part for the decay of the

sulfur dioxide. The significance of this mode would depend on the reactant concentrations, the physical/chemical nature of the aerosol and its surface area. The rate of this type of reaction may be limited by the diffusion of sulfur dioxide to the active surfaces or by its diffusion into and reactions throughout the aerosol material. The third process, i.e., the photochemical reaction of sulfur dioxide when irradiated by sunlight, has perhaps been the most thoroughly invesitgated. In particle-laden air, the oxidation can proceed by a number of paths with the aerosol surface serving as a catalyst for chemical reactions involving the photochemical products. In particle-free air, the oxidation proceeds along fixed paths with components of the vapor phase. The primary photochemical reaction involves the absorption of solar radiation by the sulfur dioxide followed by reactions of the excited sulfur dioxide molecules with molecular oxygen to form an intermediate sulfate species. It is suggested that this intermediate then reacts with molecular oxygen to the sulfur trioxide and ozone (Blacet, 1952).

These processes are, for the most part, poorly understood and become considerably more complex when in the presence of other air pollutants. In recent years, however, major advances in the knowledge of homogeneous gas phase reactions have been accomplished although the factors governing the gas to particle conversions remain largely unresolved and are only briefly discussed in published reviews of the chemistry of air pollution.

Generally, aerosol production in gas phase reactions has been monitored by condensation nuclei counters and integrating light scattering instruments. Both of these instruments provide evidence of the presence of the aerosol but lack the ability to yield a quantitative analysis of the mass or volumetric conversion rate or a size distribution of the aerosol produced. The condensation nuclei counter provides

a count of the number of nuclei present per unit volume. The nuclei are grown to a common size and their number concentration is sensed by the attenuation of a light beam. The light scattering devices measure the integrated scattering which changes as the size distribution, refractive index and the concentration of the aerosol change over the span of the measurement period.

Because of the inability of investigators to control or isolate the various gaseous components or environmental factors leading to aerosol production under field conditions, many of the studies designed to investigate aerosol formation are conducted in chambers under controlled environmental conditions. The photochemical systems studied usually involve a hydrocarbon, nitric oxide, and sulfur dioxide. In dark phase systems ozone is also introduced as a reactant.

A review of the literature indicates that the thermal reaction of olefins and ozone in the presence of sulfur dioxide yields a sulfate aerosol (Groblicki and Nebel, 1971 and Cox and Penkett, 1972). Recent technological advances in both gas phase and aerosol measurement instrumentation now permits selected aspects of the olefin-ozone-sulfur dioxide reaction with its attending aerosol production to be more thoroughly investigated. The principal advances relative to the studies undertaken are the flame photometric detection of total sulfur, the application of the chemiluminesence reaction of ethylene and ozone to ozone analysis, the development of the Fourier transform infrared spectrometer for gas phase product analysis and the electrical mobility analyzer for the in situ measurement of submicroscopic aerosols. Two new techniques have also been applied to the sulfate analysis of filter samples. X-ray fluoresence is being used to measure the total sulfur as well as other

elements and compounds, and liquid chromatography is being used to analyze for water soluble sulfates.

Data developed in these studies serve to develop a qualitative understanding of the overall photochemical smog formation process as well as to provide detailed quantitative input into newly developed photochemical smog predictive models. Finally, these data, particularly those dealing with mass or volumetric conversion rates, mechanism and gas phase product yields, serve to provide the information necessary to establish criteria which ultimately are used as the basis for standards for control.

Propylene was selected as the primary olefin to be studied because it is a common atmospheric hydrocarbon, has moderate reactivity with ozone and is a relatively simple molecule. Ethylene was also studied but, like other first members in homologous series, is atypical. Neither of these olefins produces organic aerosols in reaction with ozone.

The general aims of the research reported herein were to elucidate selected aspects of the oxidative mechanism of sulfur dioxide and to measure its mass conversion rate from the gaseous to the condensed state.

More specifically, the objectives of this research were:

1. to design a reaction vessel and sampling system which would permit the study of selected dark phase reactions under controlled conditions and reactant concentrations and which would yield reproducible results.

2. to study the kinetics of the olefin-ozone-sulfur dioxide system and to determine factors which influence the stoichiometry of the olefin-ozone reaction and the formation of selected gas phase products.

3. to assess and characterize the aerosol formed including measurements of the size distribution, mass concentration, number concentration and total light scattering both as a function of time and of system component concentrations.

4. to infer from the aforementioned measurements the physical/chemical mechanism leading to the formation and growth of the aerosol.

5. to advance a tentative mechanism for the oxidative consumption of sulfur dioxide in the olefin-ozone-sulfur dioxide system based on information contained in the literature and on the measurements reported herein.

CHAPTER II

REVIEW OF PREVIOUS WORK

A. Studies of the Olefin-Ozone System

The stoichiometry of the ethylene-ozone and the propylene-ozone reactions were studied by Hanst et al. (1958). Within experimental error they found a 1:1 ratio of olefin to ozone consumption. The initial concentration ratios of the reactants in these studies were 1:1 for ethylene and ozone and 3.36:1 for the propylene and ozone. Stedman et al. (1973) reported similar results for various initial reactant concentrations where they show 1:1 stoichiometry by observation of equal decrements of the reactants. Vbraski and Cvetanović (1960) and Wei and Cvetanović (1963) studied this reactions at much higher concentrations (20,000 ppm olefin and 4,000 ppm ozone) and found a quite different result, i.e., the ratio of olefin to ozone consumed varied from 1.4 to 2.0 for the different olefins studied. This difference was attributed (Hanst et al., 1958) to the possible further reaction of the zwitterions formed in the initial olefin-ozone reaction with olefins at the high concentrations. At lower concentrations, however, the zwitterion was postulated to undergo unimolecular decomposition. One other study, i.e., that of Bufalini and Altshuller (1965), reports data for olefin-ozone consumption ratios although propylene is not included. This ratio was found to increase with increasing olefin concentration and level off when the olefin concentration was in excess.

One other paramenter which has received cursory examination is the

initial molecular oxygen concentration in the reactor. Oxygen can participate in the reaction either as a scavenger of radicals or by contributing to the formation of species which alter the consumption ratio of the initial reactants. Cox and Penkett (1972) and Stedman et al. (1973) report the independence of the olefin-ozone reaction from the molecular oxygen concentration. In both cases, nitrogen was employed as the diluent gas and in the Cox and Penkett study, the oxygen mole fraction was estimated at 0.2%. Wei and Cvetanović (1963), however, found that in the absence of molecular oxygen the consumption ratio was close to unity while in the presence of oxygen as previously reported, this ratio increased to 1.4 - 2.0 depending on the olefin studied. The departure from 1:1 stoichiometry was believed to be due to a secondary attack on the olefin. An oxygen effect was also reported by Ripperton et al. (1972) in their studies of the dark phase reaction of cyclohexene and ozone. A decrease in aerosol formation was noted concurrent with a decrease in the molecular oxygen content.

Cadle and Schadt (1952, 1953) studied the effect of varying the reactor temperature and found no statistically significant change in the bimolecular rate constant. The temperature was varied from 8 to 27°C in the ozone and 1-hexene reaction and from 20 to 50°C in the ozone-ethylene reaction.

B. Mechanism of the Olefin-Ozone Reaction

The rate constants for the reaction of ethylene and propylene, both terminally bonded olefins, with ozone are fairly well known. The primary step of the ozonalysis reaction most commonly cited is the Criegee mechanism (1954, 1955) which leads to the formation of a stable carbonyl

and a zwitterion as

$$O_3 + OL \xrightarrow{k_1} RC^{+}HOO^{-} + RCHO \qquad (1)$$

where R can be a hydrogen atom, an alkyl group or an alkyl group containing an alcohol functional group. This mechanism has been confirmed for reactions in solution (Bailey, 1958 and Criegee, Blust and Zinke, 1954) and as has been assumed by recent investigators to be operative in gas phase reactions by analogy. The zwitterion species has never been reported as being observed in the vapor phase. It was found to be a relatively stable and long-lived species in the studies in solution. However, in the gas phase, if this species has an appreciable lifetime, then there should exist an observable difference in the rate of reactant consumption and product formation. The observation of such a difference has only been reported in one study, i.e., that of Cox and Penkett (1972) and was interpreted as suggesting that an intermediate having an appreciable lifetime is involved in at least one path to product formation.

Representative rate constants for this ozonalysis reaction and many of those to follow are listed in Table 2-1 along with the appropriate references.

For propylene, two modes of the mechanism are reported, one yielding formaldehyde and an acetyl zwitterion and the other yielding acetylaldehyde and the formyl zwitterion. The zwitterions are unstable intermediates which can, according to Leighton (1961), react with an aldehyde or ketone to form the ozonide (using the acetyl zwitterion as the example)

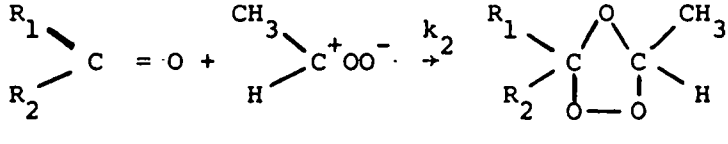

(2)

Table 2-1

Summary of Rate Constant Data

Rate Constant	Value	Units	Reference
k_1	1.82×10^{-2}	$ppm^{-1}min^{-1}$	Garvin and Hampson, 1974
k_{11}	1.47×10^{-3}	"	Stedman et al., 1970
k_{14}	2.13×10^{4}	"	Stuhl, 1973
k_{15}	2.93	"	Niki et al., 1972
k_{16}	2.35×10^{4}	"	Niki et al., 1972
k_{17}	2.35×10^{4}	"	Niki et al., 1972
k_{18}	2.05×10^{2}	"	Garvin and Hampson, 1974
k_{19}	2.58×10^{-17}	$ppm^{-2}min^{-1}$	Garvin and Hampson, 1974
k_{20}	4.40×10^{-3}	$ppm^{-1}min^{-1}$	Heicklen, 1973
k_{21}	1.47×10^{-4}	"	Garvin and Hampson, 1974
k_{22}	8.36×10^{3}	"	Washida et al., 1973
k_{23}	2.27	"	Garvin and Hampson, 1974
k_{24}	8.37×10^{1}	"	Hampson et al., 1973
k_{25}	$(2.93 - 29.3)\times 10^{4}$	"	Garvin and Hampson, 1974
k_{26}	1.57×10^{-4}	"	Hendry, 1974

It can decompose,

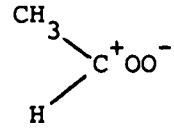

$$\xrightarrow{k_3} CH_4 + CO_2 \quad (3)$$

$$\xrightarrow{k_4} CH_3OH + CO \quad (4)$$

$$\xrightarrow{k_5} CH_2{=}C{=}O + H_2O \quad (5)$$

$$\xrightarrow{k_6} CH_3COOH \quad (6)$$

$$\xrightarrow{k_7} \text{HCOOH (from formyl zwitterion)} \quad (7)$$

it can rearrange

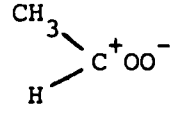

$$\xrightarrow{k_8} \quad (8)$$

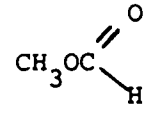

$$\xrightarrow{k_9} \quad (9)$$

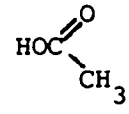

or it can dimerize

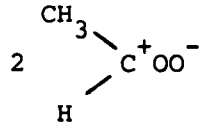

$$\xrightarrow{k_{10}} \quad (10)$$

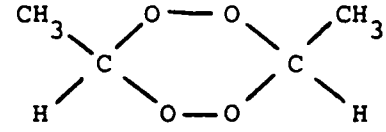

Three reactions with oxygen have also been proposed, the first two of which are chain initiating steps

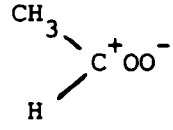

$$+ O_2 \xrightarrow{k_{11}} \cdot OH + CH_3\overset{O}{C}OO\cdot \quad (11)$$

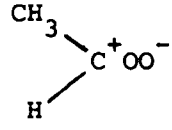

$$+ O_2 \xrightarrow{k_{12}} CH_3\cdot + CO_2 + \cdot HO_2 \quad (12)$$

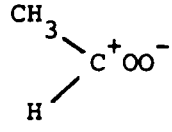

$$+ O_2 \xrightarrow{k_{13}} O_3 + CH_3CHO \quad (13)$$

These latter reactions can potentially account for the apparent excess in olefin consumption observed in some of the studies previously discussed. The ozone generated would simply react with additional olefin while the formation of hydroxyl or hydroperoxy radicals is chain initiating and can drive the system. This role of the hydroxyl radical was discussed by Leighton (1961) and Weinstock (1971). Niki et al. (1972) proposed a hydroxyl radical chain mechanism for the propylene system which included the reactions

$$\cdot OH + CH_3CH{=}CH_2 \xrightarrow{k_{14}} CH_3\dot{C}H - CH_2OH \qquad (14)$$

$$CH_3\dot{C}H - CH_2OH + O_2 \xrightarrow{k_{15}} CH_3\overset{OO\cdot}{\overset{|}{C}}H - CH_2OH \qquad (15)$$

$$\cdot OH + CH_3CHO \xrightarrow{k_{16}} H_2O + CH_3\overset{O}{\overset{\|}{C}}\cdot \qquad (16)$$

$$\cdot OH + HCHO \xrightarrow{k_{17}} H_2O + H\overset{O}{\overset{\|}{C}}\cdot \qquad (17)$$

Hydroxyl radicals react with hydrocarbons either by hydrogen atom abstraction or by addition. The propylene reaction also proceeds via and addition to the double bond or by hydrogen abstraction resulting in the radical formation. The aldehyde-hydroxyl radical reaction also yields a free radical. As the acetyl, formyl and hydroxyl radicals are chain carriers, the aldehyde products of the olefin-ozone reaction can sustain chain reactions. The rate of the reaction of the aldehydes with ozone, however, is negligible compared to propylene (Bufalini, 1974).

Carbon monoxide, another product of the ozone-olefin reaction will also react with the hydroxyl radical (Baulch et al., 1968)

$$\cdot OH + CO \xrightarrow{k_{18}} CO_2 + H\cdot \qquad (18)$$

$$H\cdot + O_2 + M \xrightarrow{k_{19}} M + \cdot HO_2 \qquad (19)$$

The rate constant for the reaction of the hydroxyl radical with carbon monoxide is about two orders of magnitude lower than for its reaction with propylene or the two aldehydes. The reaction of carbon monoxide with ozone is considerably slower (Pressman et al., 1970) with a reported rate constant of $\leq 5.9 \times 10^{-10}$ ppm^{-1} min^{-1}.

Other reactions have been reported as follows which involve the reactants or principal products of the olefin-ozone reaction:

$$CH_3O\cdot + CO \xrightarrow{k_{20}} \dot{C}H_3 + CO_2 \tag{20}$$

$$\cdot HO_2 + CO \xrightarrow{k_{21}} \cdot OH + CO_2 \tag{21}$$

$$HC\overset{O}{\overset{\|}{\cdot}} + O_2 \xrightarrow{k_{22}} \cdot HO_2 + CO \tag{22}$$

$$\cdot HO_2 + O_3 \xrightarrow{k_{23}} \cdot OH + 2O_2 \tag{23}$$

$$\cdot OH + O_3 \xrightarrow{k_{24}} \cdot HO_2 + O_2 \tag{24}$$

$$\cdot OH + \cdot HO_2 \xrightarrow{k_{25}} H_2O + O_2 \tag{25}$$

$$\cdot HO_2 + HCHO \xrightarrow{k_{26}} H_2O_2 + HC\overset{O}{\overset{\|}{\cdot}} \tag{26}$$

$$\cdot HO_2 + CH_3CHO \xrightarrow{k_{27}} H_2O_2 + CH_3C\overset{O}{\overset{\|}{\cdot}} \tag{27}$$

O'Neal and Blumstein (1973) proposed a new mechanism for the gas phase olefin-ozone reaction involving biradical intermediates which react by various modes. One mode of their mechanism includes the Criegee split already discussed. The other major mode involves the ring opening of the initial adduct into a species having two active sites, i.e., a biradical which can react in a variety of ways. These involve three different intramolecular hydrogen abstractions and rearrangements of the biradical intermediates.

C. Reactions with Sulfur Dioxide

A biradical species was also proposed by an unnamed referee for the mechanism used by Cox and Penkett (1972) in their ozone-olefin studies conducted in the presence of sulfur dioxide. It was this biradical or zwitterion species or an addition complex which was proposed by those investigators as being the reactive intermediate responsible for the oxidation of the sulfur dioxide. Likewise, Groblicki and Nebel (1971) suggested the oxidizing species as being a reactive intermediate but included an ozonide, an epoxide or a free radical as the potential identity of that species.

Species which have been identified as capable of oxidizing the sulfur dioxide are the hydroxyl radical, hydroperoxy radical and ozone. The rate constants for the ozone and the hydroperoxy radical reactions are quite slow relative to the rate constant with the hydroxyl radical and for the three reactions are $\leq 2.93 \times 10^{-7}$ (Davis et al., 1974), 1.32 (Payne et al., 1973) and 5.58×10^{2} (Wood et al., 1974) $ppm^{-1}min^{-1}$ respectively. Other radical species which may also be considered for their potential as the oxidizing agent are the alkoxyl, peroxyakyl and the acetyl radicals.

A three step mechanism has been proposed by Cox and Penkett (1972) to describe this olefin-ozone-sulfur dioxide system. The scheme presented was independent of the nature of the intermediate species and of other removal processes for this species in the system. Their mechanism postulates the following steps:

$$\text{Olefin} + \text{Ozone} \xrightarrow{k_1} \text{Intermediate (I)} + \text{Aldehyde}$$

$$\text{I} \xrightarrow{k_2} \text{Wall, Decomposition, Reaction, etc.}$$

$$\text{I} + SO_2 \xrightarrow{k_3} SO_3 + \text{aldehyde}$$

The time rate of change in concentration of the intermediate species $[R_I]$ can be expressed as

$$[R_I]_{total} = \alpha k_1[Ol][O_3] - k_2\ [I] - k_3[I][SO_2] \qquad \text{II-1}$$

where α is the fraction of the ozone molecules reacting which lead to the formation of the short-lived intermediate. They incorporated the assumptions that the rate of formation of the intermediate species is proportional to the initial rate of the olefin-ozone reaction and that a pseudo steady state concentration of the intermediate species is established, i.e., $(dI/dt)_{total} = 0$. If follows then

$$[I] = \frac{\alpha k_1\ [Ol][O_3]}{k_2 + k_3\ [SO_2]} \qquad \text{II-2}$$

and

$$-R_{SO_2} = R_{SO_3} = k_3[SO_2][I] = \frac{\alpha k_3 k_1[Ol][O_3][SO_2]}{k_2 + k_3\ [SO_2]}$$

$$\frac{R_{O3}}{R_{SO_3}} = -\frac{1}{\alpha}\quad\{1 + \frac{k_2}{k_3\ [SO_2]}\}. \qquad \text{II-4}$$

If the two assumptions are valid, then a plot of this latter relationship, i.e., R_{O3}/R_{SO2} vs $[SO_2]^{-1}$ would yield, via the intercept, the fraction of ozone which reacts to form the oxidizing intermediate and via the slope, the ratio of the second to third step rate constants. Cox and Penkett presented such a graph for the olefins studied (hexene, 2-methyl pentene, trans-2-butene, cis-2-butene and cis-2-pentene) although only the initial rates and reactant concentrations were used.

D. Aerosol Production in Hydrocarbon Reactions

Prager et al. (1960), Wei and Cvetanović (1963), Rasmussen (1964), and Ripperton et al. (1972) all observed aerosol formation in the reaction of certain hydrocarbons and ozone alone. Actually, only the

olefins out of the group of hydrocarbon categories consisting of olefins, paraffins, aromatics and aldehydes, react readily with ozone in the gas phase. Table 2-2, developed by Niki et al. (1972), presents relative rate constants for atomic oxygen and the hydroxyl radical as well as for ozone in their reactions with the different hydrocarbon classes.

Groblicki and Nebel (1971) likewise observed aerosol formation in the dark phase reaction of various olefinic hydrocarbons and ozone. The hydrocarbon concentration used in their studies was 4 ppm and the ozone concentration was 0.6 ppm. A condensation nuclei count during these studies showed that a-pinene, 1-heptene, 3-heptene and styrene produced approximately 10^7 particles/cm^3 when added to a chamber containing ozone. Cyclopentene, propylene and 2,4,4-trimethyl-1-pentene with ozone resulted in the formation of about 4×10^5 particles/cm^3 while the other hydrocarbons studied either produced less aerosol than the propylene or none at all.

Very few studies of the olefin-ozone-sulfur dioxide thermal reaction have been conducted which included an investigation of aerosol formation factors. And, as previously indicated, aerosol measurement instrumentation was used to yield some integrated parameter on the aerosol such as the light scattering coefficient, visibility reduction or total nuclei count and not to provide a quantitative analysis of the aerosol produced. Groblicki and Nebel (1971) used a Sinclair-Phoenix Smoke Photometer to monitor the formation of a light scattering aerosol in their studies which included sulfur dioxide as a reactant. They concluded that no light scattering aerosol was formed unless propylene, ozone and sulfur dioxide were all present and the amount of aerosol increases with the

Table 2-2

Relative Rate Constants[a]

Compound	Relative Rate Constants*		
	O	O_3	OH
Olefins			
Propylene	1.0	1.0	1.0
Ethylene	0.2	0.3	0.1
Isobutene	4.4	1.7 ∿ 2	2.5
Trans-2-Butene	4.9	2.8 ∿ 36	4.2
2-Methyl-2-Butene	14	2.4	7.1
Tetramethylethylene	18	3.9 ∿ 62	8.6
Aromatics			
Benzene	.007	---	≤0.05
Xylene	---	<0.2	1.1
Aldehydes			
Formaldehyde	0.05	---	0.9
Acetaldehyde	.15	---	0.9
Proprionaldehyde	∿ .2	---	1.8
Alkanes			
n-Butane	.008	---	0.24

*Absolute Rate Constants ($ppm^{-1}min^{-1}$) for Propylene

O	O_3	OH
1.76×10^{3}	1.75×10^{-2}	2.49×10^{4}

[a]Source of Table: Niki et al. (1972).

amount of ozone added to the system. They also concluded that the sulfate aerosol formed was ammonium sulfate.

Cox and Penkett (1972) used a condensation nuclei counter to test for the presence of aerosol during some of their experiments. The major effort, however, relative to the aerosol analysis, consisted of determining the mass of sulfur collected in bubblers containing hydrogen peroxide and on membrane filters. Radiochemical techniques were used to determine the mass of the ^{35}S collected based on the amount of radioactivity present after correcting for counter efficiency and radioactive decay. A deionized water extraction of one filter yielded a strongly acidic solution containing sulfate ions and it was concluded, therefore, that the aerosol was sulfuric acid droplets.

The aerosol formation during the Cox and Penkett studies was observed to follow second order kinetics. They also concluded that the aerosol formation was not significantly affected by surface reactions. This conclusion was based on the results of an experiment during which an iron oxide aerosol was added to the reaction vessel increasing the effective surface area by a factor of 2 to 3. The rate of ozone consumption and the rate of the sulfate aerosol formation were not significantly affected by the additional surface.

The role of water vapor concentration on aerosol formation in the sulfur dioxide- ozone -cis-2-butene system was studied over a range of relative humidities from about 10-78% and over a range of initial sulfur dioxide concentrations (0.2 - 3.61 ppm). The aerosol formation rate was observed to decrease with increasing relative humidity for all of the sulfur dioxide concentrations studied. Wall losses for all of the system components also increased but the decrease in the aerosol formation rate was too large to be accounted for by this type of loss.

Water vapor, it was concluded, inhibits the aerosol formation in the olefin-ozone-sulfur dioxide reaction.

Clark (1972) conducted a comprehensive study of the formation and growth of aerosols produced by the photooxidation of sulfur dioxide. The advent of the recently developed Whitby Aerosol Analyzer permitted for the first time, a study of the nucleation and growth of a forming submicroscopic aerosol. This instrument was an earlier version of the electrical mobility analyzer used in the study reported on in this paper and has been described by Whitby and Clark (1966). A 625 ft^3 FEP Teflon bag was used as the containment vessel and the ultraviolet irradiation was provided by a cylindrical bank of fluorescent lamps. The lamps used had about the same spectral energy distribution as sunlight over the wavelength range of interest, i.e., 2900 to 3400 Å for SO_2 photooxidation. Two important factors relative to the use of these lights are that they essentially provide full ultraviolet energy output instantaneously and that they do not introduce excessive heat into the system.

The sulfur dioxide concentration ranged from 0.049 to 2.88 ppm during these studies which yielded volumetric conversion rates of from 0.389 to 22.9 $\mu m^3/cm^3$-hr. The volume concentration was observed to increase non-linearly with time during the initial stages of the runs which was attributed to a nucleation process. The increase in the volume concentration was later characterized by a constant rate of condensation of material from the vapor to the condensed state. The calculated total surface area of the aerosol formed during these studies was found to achieve an apparent equilibrium value which appeared to be a function of the volumetric conversion rate.

CHAPTER III

THEORY OF AEROSOL FORMATION, GROWTH AND DECAY

Aerosols can be divided into two major classifications according to the mechanisms involved in their formation. Aerosols of large individual particle size are primarily formed either by the communition or nebulization of bulk materials into discrete particles small enough to remain suspended in the gaseous medium. The much smaller aerosols are formed by chemical reactions leading to polymerized species or by the physical agglomeration of molecules leading from the vapor to the condensed phase. This formation mode is commonly referred to as 'gas to aerosol conversion'.

This report is concerned with only the second classification, i.e., the transformation to particulate material resulting from the phase transition from the gas to the liquid state. The photooxidation of sulfur dioxide and the oxidative consumption of sulfur dioxide in the thermal reactions involving certain hydrocarbons and ozone are examples of reactions that result in gas to aerosol conversions. The initial step in the agglomeration process is the nucleation of molecules from a supersaturated vapor. These nuclei may consist of clusters of the condensable molecular species or foreign material (ions or particles) of submicroscopic size. The growth of the newly formed embryos continues by the diffusion of condensable material from the saturated vapor phase directly onto the existing particulate surface. These processes individually and in concert affect the time-dependent size distribution

spectra of the aerosol. One other physical mechanism which influences this distribution is coagulation. This process is an agglomerative interaction which occurs if the concentration of the aerosol droplets is sufficiently high.

A. Nucleation

Nucleation is the first step in one type of gas to liquid or solid phase transition process. Homogeneous nucleation refers to the spontaneous formation of molecular aggregates or embryos resulting from the random collisions of molecules in a supersaturated vapor. The nucleation is termed heterogeneous if the condensation process occurs on a pre-existing solid or liquid phase, i.e., foreign particles or charged ions. Prerequisite to any self-nucleation is the establishment of a supersaturated vapor in the gas volume. The supersaturated vapor develops in chemical reactions between gaseous components only when the saturated vapor pressure of the reaction products is less than the saturated vapor pressure of the reactants.

The classical treatment of nucleation is included in works by a number of authors including Amelin (1967) and Mason (1971). The experimental effort described in this paper involved a system which was initially free of particles or ions. The treatment to follow, therefore, is devoted to spontaneous homogeneous nucleation.

The embryos which rapidly form as a result of the statistical fluctuations in the gaseous medium are also dissipated by evaporation or breakup because of these same local thermal and density variations. Only if the nuclei exceed some critical size (g^*) will they survive and continue to grow by condensation on the embryonic surfaces. The free energy of the system is at its maximum value when the size of the nuclei is g^*.

This variation of free energy in a supersaturated system with droplet size can be plotted as

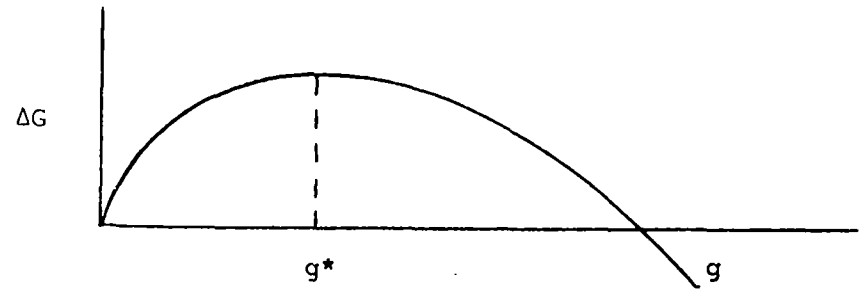

where ΔG is the incremental change in free energy and g is the number of molecules in the aggregate. The supersaturated vapor is in a metastable state with the chemical potential of the vapor being greater than that of the condensed phase, i.e., $\mu_a > \mu_b$. The embryos will develop only if they grow to a state where they are more stable than the vapor phase or grow with a decrease in free energy to $g > g^*$. In the case of heteromolecular homogeneous nucleation, a three dimensional plot is required to accurately represent the change in free energy.

The total change in the free energy of a system upon the formation of an embryo of g molecules is described by the Gibbs free energy function for an isothermal, isobaric change as

$$\Delta G = (\mu_b - \mu_a)g + \pi d^2 \sigma \qquad \text{(III-1)}$$

where μ_a = chemical potential/molecule in the vapor system

μ_b = chemical potential/molecule in the condensed phase

d = diameter of the molecular aggregate

σ = surface tension

The second term on the right is the surface free energy which goes from zero to this value upon nucleation and is significant because of the large surface to volume ratio for these small clusters.

In order to form nuclei of size g*, $d\Delta G/dg$ must be at a maximum, i.e., $d\Delta G/dg = 0$. By differentiation of equation III-1 this condition is satisfied when

$$\mu_b - \mu_a = \frac{2\pi\sigma d^2}{3g} . \qquad \text{III-2}$$

The critical free energy change is, therefore,

$$\Delta G^* = \frac{\pi d^{*2} \sigma}{3} \qquad \text{III-3}$$

where d* = the diameter of the critical nucleus containing g* molecules.

An alternative expression relating the critical diameter for continued growth by condensation to the degree of saturation can be developed from equation III-2 by expressing g in terms of the density and diameter of the condensed molecular cluster and the difference in the chemical potential of the vapor and the condensed phases in terms of the saturation ratio (S). This relationship was first developed by Kelvin (1870) and can be expressed as

$$\ln S = \frac{4 M \sigma}{\rho R T d^*} \qquad \text{III-4}$$

where M = molecular weight of the droplet

ρ = density of the droplet

R = universal gas constant

T = temperature.

S, the saturation ratio or degree of supersaturation is expressed by the equality

$$S = \frac{p}{p_\infty (T)} \qquad \text{III-5}$$

where p = vapor pressure in the gas phase and

p_∞ (T) = saturated vapor pressure over a plane surface of the liquid at the temperature T.

The rate at which vapor molecules are impinging per unit area on the embryonic surface is given by

$$\beta = \eta\, p\, (2\pi\, M\, R\, T)^{-\frac{1}{2}} \qquad \text{III-6}$$

where η = Avogadro's number

and the rate of incorporation assuming an accommodation coefficient of unity is simply the product of the impingement rate β and the surface area. And finally, the rate of nucleation in embryos/cm^3-sec can be expressed as

$$\frac{dN}{dt} = \pi\, d^{*2}\, \beta \exp\, (-\Delta G^*/kT) \qquad \text{III-7}$$

where N = number concentration of embryos cm^{-3} and

k = Boltzman's constant.

The preexponential term is a kinetic factor the expression of which differs among various investigators (Becker and Doring, 1935; Reiss, 1950; Mason, 1971; and Mirabel and Katz, 1974).

From the foregoing discussion, it follows that homogeneous nucleation occurs in a gas volume only if $S \geq S^*$, i.e., at some critical supersaturation condition. The critical supersaturation condition is arbitrarily defined as that which will produce embryos capable of further growth at the rate of one per unit volume per unit time. The vapor supersaturation ratio is included in the exponential term in equation III-7 and the rate of nucleation, therefore, increases sharply with the degree of supersaturation.

The critical supersaturation required for spontaneous homogeneous nucleation can be calculated from that equation by setting dN/dt = 1. As vapor supersaturation increases it can also be seen from equation III-4 that the embryo diameter decreases and from equation III-7 that the number of embryos increases.

One of the earlier works dealing with the kinetics of the sulfur trioxide and water reaction was conducted by Goodeve et al. (1934). The resultant product of this reaction, molecular hydrogen sulphate, was observed to be in a state of supersaturation and condensed to produce sulfuric acid molecular aggregates. They concluded from their reaction velocity measurements that about one collision in one hundred results in an association, and further, that the lack of a reaction in the balance of the collisions was possibly due to an energy of activation, a steric factor or the necessity of a third body collision to remove the energy of association.

The self-nucleation rate for the sulfuric acid-water system was theoretically treated by Doyle (1961). The rate of the transition was characterized by a vector model developed by Reiss (1950) and adapted for their study. The existence of a saddle point was assumed on the free energy surface, and the rate of flow of embryos through this pass in the energy barrier was used to approximate the rate of nucleation. The nucleation rate was calculated and tabulated as a function of the partial pressure of the sulfuric acid in the vapor phase for a system at 25°C and 50% relative humidity. These data indicate that self-nucleation becomes appreciable at sulfuric acid partial pressures of about 10^{-9} mm although, according to Doyle, the rate is uncertain by three to four orders of magnitude at this pressure. He attributed the source of the error to the failure of the liquid droplet model at this supersaturation, uncertainties in the acid partial pressure and uncertainties concerning the nature of the dominant acid-bearing species at elevated humidities.

Limited theoretical studies of the rate of formation of critical sized molecular clusters at relative humidities have recently been conducted by Kiang et al. (1973) for the sulfuric acid-water system.

Relative humidity is demonstrated to be a dominant factor in gas to particle conversions. Their data indicates that only about 3×10^9 sulfuric acid molecules/cm^3 are required to achieve a unit nucleation rate (cm^{-3} sec^{-1}) in a system at 10% relative humidity. The errors associated with this theoretical treatment relate to uncertainties in the nucleation theory for small molecular aggregates.

B. Condensation

Growth of the molecular aggregates formed as a result of spontaneous nucleation continues by two processes, condensation and thermal coagulation. The initial growth of the newly formed droplet due to the direct condensation of material from the vapor phase is rapid according to classical theories relative to the early growth due to coagulation. Homogeneous nucleation followed by surface condensation occurs, according to equation III-4 when the supersaturation in the gas volume exceeds some critical value. Once an embryo exists, e.g., from the heteromolecular nucleation of sulfur trioxide and water, it becomes a soluble nucleus upon which condensation can occur. The equilibrium vapor pressure over this newly formed surface is lowered according to its composition and concentration. Condensation will occur on this surface, therefore, at a lower supersaturation level than required for the primary nucleation or for condensation on an insoluble particle of the same size. When the solution droplet is in equilibrium with its surrounding air, its vapor pressure must equal the partial pressure of the water vapor, and the saturation ratio equals the relative humidity of the air.

An expression for the equilibrium water vapor pressure at the surface of a droplet of solution is given by Mason (1971) as

$$\ln \frac{p'}{p_\infty} = \frac{\sigma' M}{\rho' RdT} - \frac{P M}{\rho' RT} \qquad \text{III-8}$$

where p' = equilibrium vapor pressure over the solution droplet

σ' = surface tension of the solution

M = molecular weight of water

ρ' = density of the solution

P = osmotic pressure of the solution.

Mason also gives an expression for the osmotic pressure for solutions whose densities vary linearly with concentration as

$$P = \left(\frac{R\,T\,\rho}{M}\right) \ln\left(1 + \frac{i\,n_1}{n_2}\right) \qquad \text{III-9}$$

where ρ = density of water

n_1 = moles of solute

n_2 = moles of water

i = factor which depends on the composition and the concentration of the solute.

The density of sulfuric acid solutions does not vary linearly with concentration (Chemical Engineers Handbook, 1963) although over the range of about 15 - 50% acid the relationship is nearly linear. The combination of equations III-8 and III-9 yields two predictions relative to the percent acid for the equilibrium system of sulfuric acid and water. First, the percent acid decreases with increasing relative humidity for a fixed particle size and secondly, the percent acid increases with particle size for a constant relative humidity.

The rate of condensation on a droplet suspended in a gaseous medium is expressed by the Maxwell equation (1890) corrected by Fuchs (1959) for the influence of the droplet diameter as

$$\frac{dq}{dt} = \frac{2\pi\,D\,d\,M}{R\,T\,\zeta}\,(p - p_T) \qquad \text{III-10}$$

where q = quantity of vapor in the gas

D = vapor diffusion coefficient

ζ = a coefficient the value of which depends on the Knudsen number

p_T = equilibrium vapor pressure at the droplet temperature.

The influence of the Knudsen number on the rate of condensation can perhaps be better understood by defining the characteristics of the transfer process regimes. The Knudsen number (K_n) itself is defined as the ratio of the gas mean free path (l) to the particle radius, i.e., $K_n = 2l/d$.

In the free molecule regime where $d \leq .01$ μm and $K_n \to \infty$ the particles behave as giant molecules and do not disrupt the random collisions of the molecules of the medium. Transport properties for this regime may be evaluated from the kinetic theory of gases.

The continuum regime includes large particles, i.e., $d \geq 1$ μm and $K_n \to 0$. In this region, the transfer processes are adequately described by the equations of continuum mechanics. The molecular structure of the medium is not included in the description.

The region between these two extremes is referred to as the transition regime, i.e., where $0.01 \lesssim d \lesssim 1$ μm and $13.2 \gtrsim K_n \gtrsim 0.132$. Particles in this size range disrupt the random motion of molecules in the medium, and the molecular structure of the medium is still needed to describe the system.

A comprehensive treatment of the transport processes and the transfer equations for an isolated sphere in these three regimes is presented by Hidy and Brock (1970). The condensation rate can, therefore, be approximated through the use of the equations for the mass flux on the surfaces of a spherical droplet.

As a droplet increases in size, the coefficient ζ decreases

approaching unity for d >> 1 and the Maxwell equation applies. Expressed in terms of particle growth this equation becomes

$$\frac{dd}{dt} = \frac{4\ D\ M}{R\ T\ d}\ (p - p_T). \qquad \text{III-11}$$

For smaller droplets the coefficient increases and varies according to the accommodation coefficient which is sensitive to the molecular structure of the liquid.

If the nuclei exceeds the critical diameter (equation III-4) in a supersaturated system, then it will continue to grow with a decrease in the free energy. The transition would, according to theory, be rapid and the droplet formed would grow without limit. In practical systems which can be conceived, however, the supersaturation does not remain constant as the embryos compete for the condensable vapor which is being consumed at an increasing rate. The supersaturation, therefore, diminishes and the upper limit for the growth of the droplets is restricted.

C. Coagulation

Following the rapid growth of the newly formed nuclei by condensation, the continued growth of the particles or droplets will be dominated by coagulation assuming that the number concentration remains above about $10^4/cm^3$. Coagulation is a coalescence of the nuclei due to the occurrence of random collisions caused by the aerosol undergoing Brownian motion. The theory predicting a second-order decay for the aerosol originated with Smoluchowski (1917) who applied the diffusion equations to the Brownian motion of hard non-interacting spheres thermally agitated in a continuum. This aspect of aerosol stability has been extensively treated by Fuchs (1964) and more recently by Hidy and Brock (1970) and Husar (1971). The basic coagulation equation follows from a consideration

of the number of collisions which occur per unit volume and time in an aerosol due to diffusion and the number of particles is reduced by one with each collision. The equation describing the decay of the number concentration of equally sized aerosol particles is given as

$$\frac{dN}{dt} = - K N^2 \qquad \text{III-12}$$

where N = the number concentration per unit volume cm^{-3} and

K = the coagulation constant (cm^3 sec^{-1}) which is given by

$K = 4\pi\ d\ D$ (D here being the particle diffusion coefficient).

The value of K increases sharply as the system becomes more polydisperse and decreases as the particle size increases. The coagulation constant for unequal size particles is given by Fuchs (1964) as

$$K(d_1,d_2) = 4\pi \left(\frac{d_1 + d_2}{2}\right)\left(\frac{D_1 + D_2}{2}\right) \beta \qquad \text{III-13}$$

where $d_1 + d_2$ = the diameter of the absorbing sphere in Fuchs' model

$D_1 + D_2$ = the coefficient of relative diffusion for the two particles

β = a correction factor necessary to account for the concentration discontinuity which exists at the surface of the absorbing sphere and is a function of the aerosol transfer process regime. Values of $K(d_1,d_2)$ are given in Table 3-1 from which it is evident that the size distribution of the aerosol will rapidly become devoid of small particles and the size of the larger particle is not significantly affected by the interaction. Several more elaborate approaches than the limiting sphere calculations of Fuchs have been performed including those of Sahni (1966), Smirnov (1969) and Walter (1973). The results have not significantly altered the values obtained from the original work.

Table 3-1

Coagulation Constants for unequal sized particles

$K(d_1 d_2) \times 10^{-10}$ $(cm^3 sec^{-1})$[a]

d_1 (μm) \ d_2 (μm)	.002	.004	.01	.02	.04	.1	.2	.4	1	2	4	10	20
.002	4.5												
.004	7.5	6											
.01	30	13	9										
.02	90	40	15	12									
.04	300	110	35	17	11								
.1	1600	550	120	40	15	7.2							
.2	5000	1400	270	80	25	8	5.2						
.4	13000	4100	600	170	47	11	5.3	4.0					
1	37000	9500	1600	420	115	24	9	4.7	3.4				
2	77000	20000	3200	940	230	45	16	7.1	3.7	3.2			
4	160000	40000	6600	1700	450	90	30	12	5.2	3.4	3.0		
10	400000	100000	16000	4300	1100	220	72	28	10.3	5.6	3.7	3.0	
20	800000	200000	30000	8500	2200	430	140	54	19	9.6	5.5	3.3	3.0

[a]Adapted from Fuchs, 1964

One other phenomena affects the size distribution of the aging aerosol, i.e., the sedimentation of the largest particles. The net tendency of the interactions which occur in the aerosol including the nucleation, condensation, coagulation and sedimentation is for the size distribution to become self-preserving in time. A similarity theory to describe the shape uniformity was originally presented by Friedlander (1960). Subsequently Clark and Whitby (1967) presented data from a number of investigations properly normalized to demonstrate this self-preservation. The data reported encompassed a wide range of experimental conditions and suggest that a similarity spectrum forms in a matter of hours for atmospheric aerosols originating from a number of different sources and conditions. The similarity spectrum fit, however, was not that predicted by the theory and at present there exists no direct verification of the theory (Hidy and Brock, 1970).

Upon integration, equation III-12 becomes

$$\frac{1}{N} - \frac{1}{N_o} = Kt \qquad \text{III-14}$$

where N_o = the initial particle concentration. The straight line relationship between time and the reciprocal of the particle concentration dictated by this equation implies that K is invariant in time. The value of K derived from this relationship has been the main experimental fact reported by previous investigators in treating gas to particle conversions. This limitation in quantitative aerosol analysis was primarily due to the lack of the sophisticated instrumentation necessary to characterize the small particles generated by the binary homogeneous nucleation process.

A term to account for the deposition of aerosol particles on the walls or floor of an experimental chamber was added to equation III-12

by Langstroth and Gillespie (1947). The decrease in the number concentration due to this 'wall loss' is proportional to N, the concentration at any time t and the change in concentration can be expressed as

$$-\frac{dN}{dt} = \beta N + KN^2 \qquad \text{III-15}$$

where β = the coefficient for wall loss. In a chamber which is not mechanically stirred, deposition on the walls must be diffusive. The small particles are transported near the wall by convective diffusion and deposited on it by molecular diffusion through a stagnant air layer at the containment surface. The thickness of this layer was reported by Langstroth and Gillespie to 20 μm although the value varies considerably among investigators. One of the more recent theoretical treatments was performed by Van DeVate (1972) in which a thickness of 0.85 mm was calculated for the stagnant air layer. The coefficient β, accounting for the wall layer is given by Fuchs (1964) as

$$\beta = \frac{SD}{V\S} \qquad \text{III-16}$$

where S = the surface area of the chamber

V = the chamber volume

§ = the thickness of the wall layer. Implicit in this expression for the wall loss constant is the bias of the wall for small particles and the dependence of this term on the surface to volume ratio of the chamber.

CHAPTER IV

EXPERIMENTAL ARRANGEMENT AND PROCEDURES

A. Experimental Design and Arrangement

The experimental series discussed in this paper was designed to provide insight into the oxidative consumption of the reactant-sulfur dioxide and into the subsequent growth of the resultant aerosol. Initial experiments were conducted on the propylene-ozone system for comparative purposes and to establish a baseline for later studies conducted in the presence of sulfur dioxide. Nitrogen was used as the diluent gas in certain of these studies to test the role of molecular oxygen on the reaction kinetics and on the reaction stoichiometry. Two levels of relative humidity were also established in the reactor in an attempt to determine the influence of that parameter on the gas-phase reaction.

These same parameters as well as the initial reactant concentrations were varied in the studies which included sulfur dioxide. The propylene and ozone were varied from conditions of olefin excess to ozone excess and two levels of sulfur dioxide were used. Target concentrations of the primary reactants, propylene, ozone and sulfur dioxide, were generally as close to representative atmospheric levels as possible consistent with the limitations imposed by the instrumentation used. This limitation is most restrictive in the measurement of the time history for low total reactant consumption. A few runs were made at elevated concentrations to obtain a higher product yield thereby increasing the sensitivity for the measurement of minor reaction products.

A high concentration of carbon monoxide was added to two of olefin-ozone-sulfur dioxide runs to make use of its capacity as a hydroxyl radical scavenger in determining the participation of that species in the reaction. Acetyaldehyde, which is reportedly formed as a result of the propylene-ozone reaction, was investigated to determine its reactivity in the presence of ozone or conversely its stability as a product of the primary reaction.

A series of low reactant consumption runs were made wherein the volumetric conversion rate was limited in order to follow more closely the aerosol formation and growth.

Finally, a limited number of ethylene and ozone and ethylene-ozone-sulfur dioxide experiments were conducted to determine similarities with the propylene reactions and to observe the aerosol formation characteristics.

A schematic outlining the complete laboratory arrangement is shown in Figure 4-1. The reaction containment vessel is shown at the top of the figure while the reactant introduction system is shown on the right side. This system includes the gas cylinders, the pressure and flow regulation, ozonization and humidification. The diluent gas stream was initially split twice with a metered fraction of the total flow passing through the humidifier. Upon recombination there were two air streams of similar properties, i.e., composition, flow, humidity and temperature. Ozone was added to one of these inlet lines and the olefin and the sulfur dioxide to the other thereby limiting the reactions to the confines of the reactor.

The aerosol measuring instrumentation is shown directly below the reactor where it was physically located. The positioning of these devices was dictated by the requirement to minimize aerosol line losses.

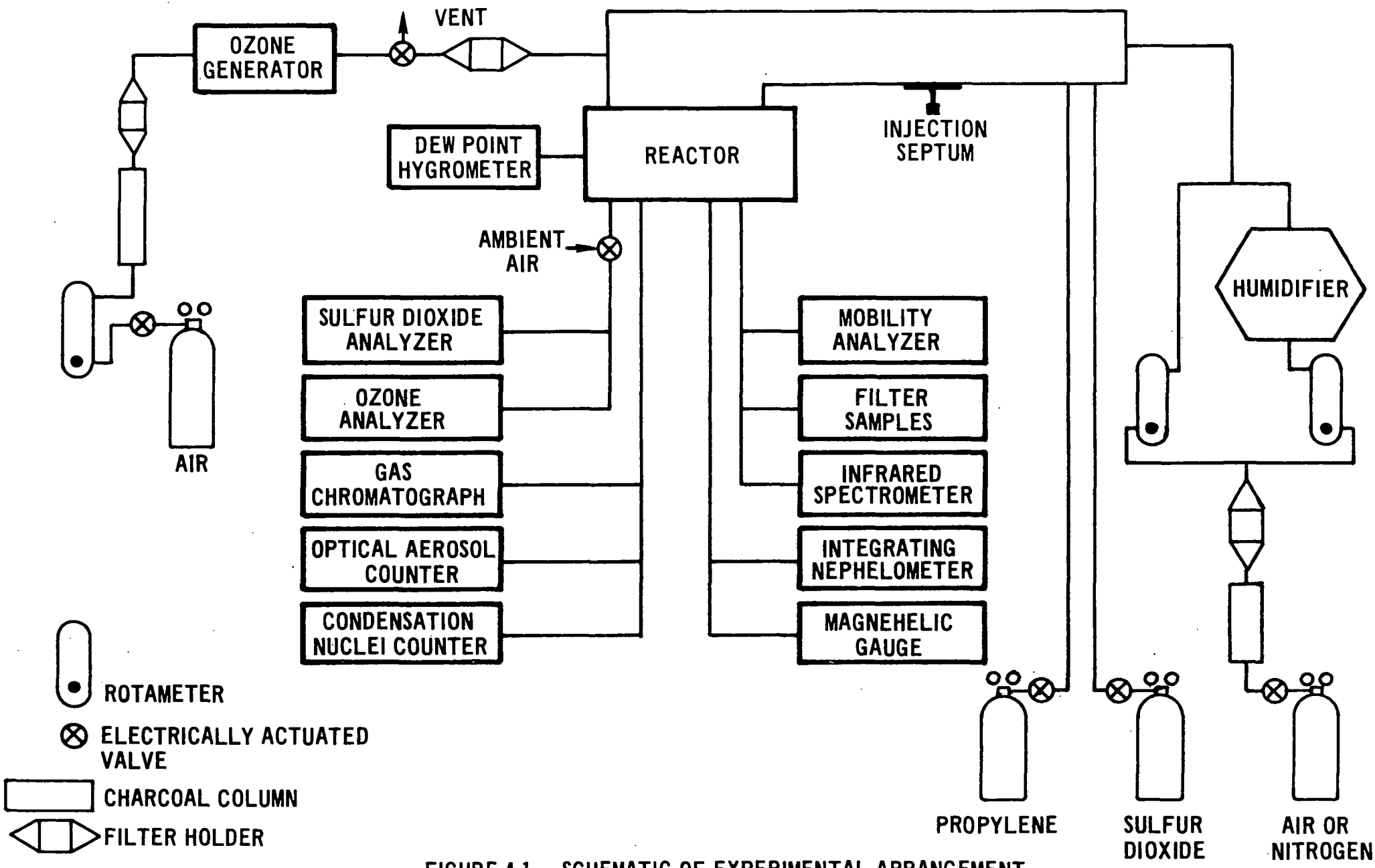

FIGURE 4-1 . SCHEMATIC OF EXPERIMENTAL ARRANGEMENT.

The gas-phase instrumentation is shown on the left along with the dew point hygrometer. The volume of the reactor would not permit continuous sampling by all of the instrumentation shown although to eliminate dynamic instabilities and to minimize the response time of the instrumentation it was necessary to have all measurement devices in continuous operation. The ambient air inlet shown at the upper left allows the sulfur dioxide analyzer and the ozone analyzer to be switched to sample the room air and the reactor intermittently. Similar arrangements were made for the remainder of the instruments.

A photograph of the major portion of the instrumentation used routinely during this study is shown as Figure 4-2. The reactor is shown at the top center and the aerosol instrumentation directly below except for the integrating nephelometer. This latter device, the sampling section of which is oriented vertically, is located immediately to the left of the reaction vessel. The reactant introduction system can be seen in the background near the center of the picture. The gas chromatograph is shown on the right and the sulfur dioxide and ozone analyzers are to the left of the aerosol instrumentation table. At the extreme left is a computer and display scope used for the processing of data from the optical particle analyzer.

Figure 4-3 is a picture of the front panels of the condensation nuclei counters, the optical particle analyzer and the electrical mobility analyzer with its control module. Figure 4-4 is a picture of the Fourier transform infrared spectrometer. The "folded path" cell is in the background with the detectors, interferometer and recorder in the foreground.

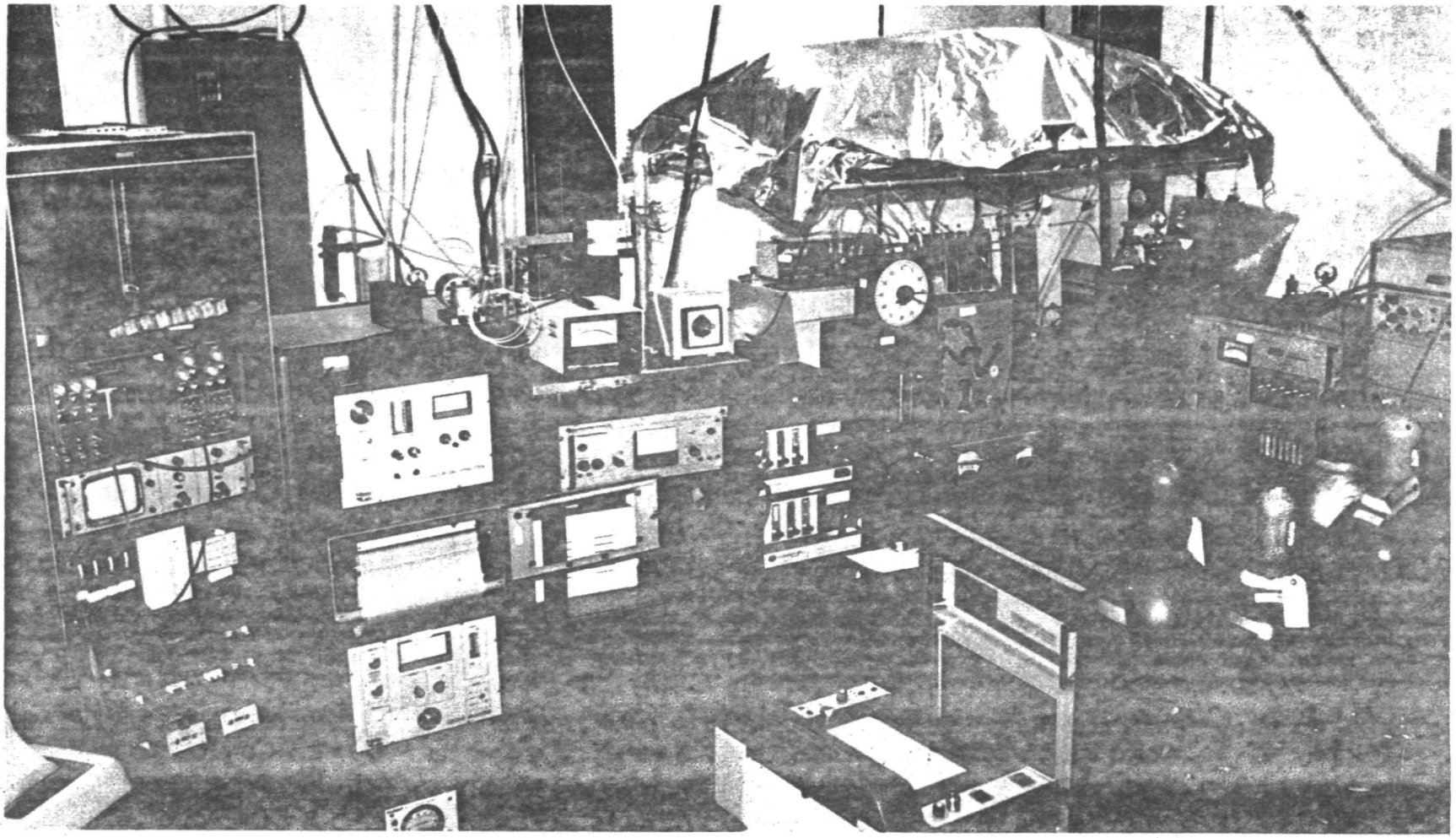

FIGURE 4-2. LABORATORY ARRANGEMENT FOR OLEFIN-OZONE-SULFUR DIOXIDE STUDIES.

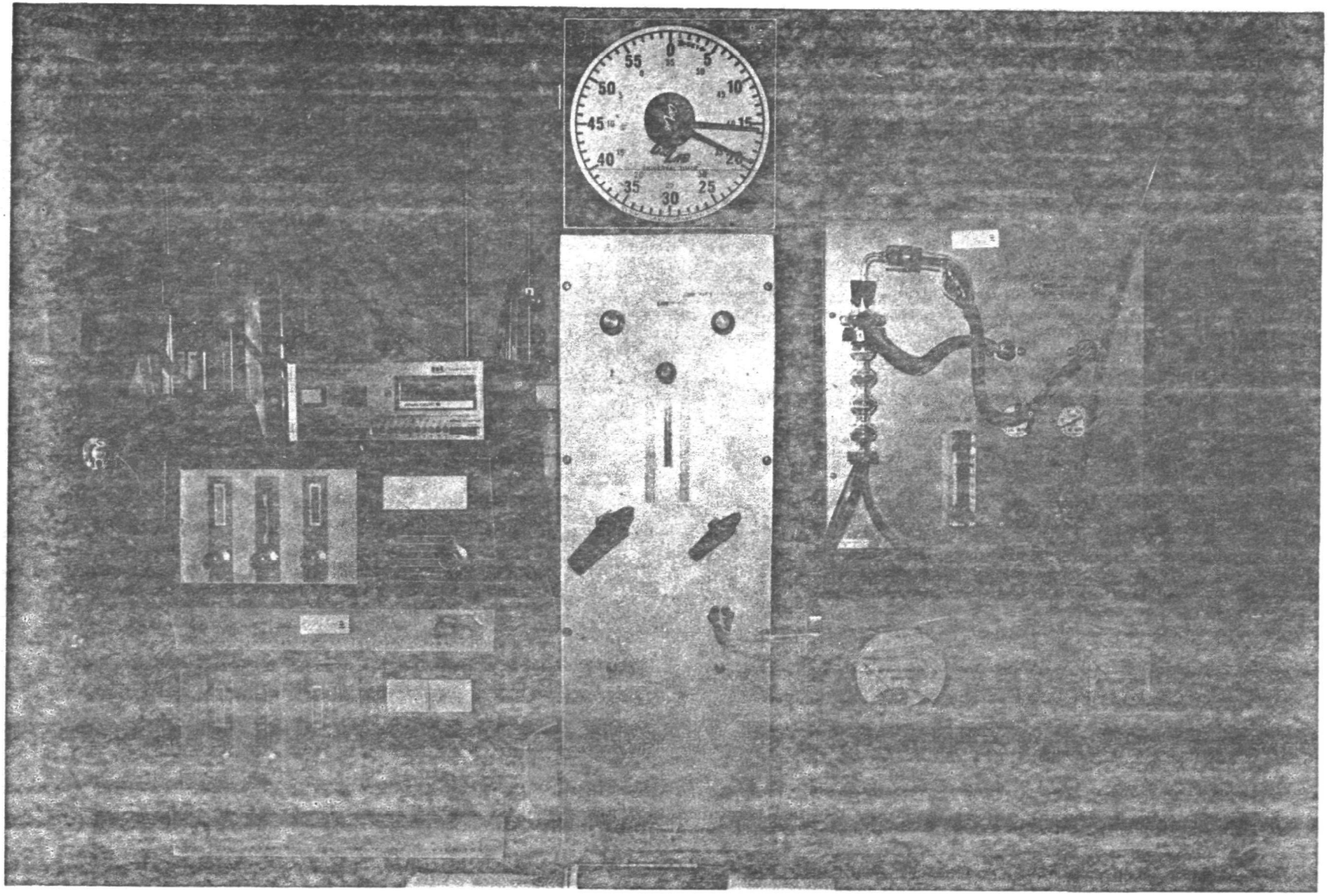

FIGURE 4-3. AEROSOL MEASUREMENT INSTRUMENTATION.

FIGURE 4-4. FOURIER TRANSFORM INFRARED SPECTROMETER

B. Experimental Apparatus

1. Reactor

The reaction bag was constructed of Dupont "Tedlar" PVF film which was folded and then heat sealed along three sides. When inflated the bag took on a pillowcase configuration. It was approximately 1.83m in length and 0.94m in width and when fully inflated contained approximately 437 liters. The surface to volume ratio for the fully inflated bag was $7.87m^{-1}$.

"Tedlar" was selected for the reactor because of its low reactivity with the type of compounds encountered in these studies. The bag configuration was employed because, in addition to its economy and simplicity, the pressure in the system remains constant at ambient atmospheric pressure as the volume is depleted by sampling. A dilution correction is required when rigid walled containers are used and makeup air is added to replace the sampled volume.

An aluminized polyester bag (3M Company 'Scotchpak') was constructed and placed over the "Tedlar" bag to eliminate the transmission of ultraviolet radiation and also to reduce the rate of permeation of gases and vapors into or out of the reactor. A polyethylene tape was used to seal the sections of this bag together. Permeation rates for several gases and vapors are shown in Table 4-1 for the two materials in cm^3 or $g/(100\ cm^2)(24\ hrs)$ per mil thickness. The permeation of water vapor through the "Tedlar" was measured at a time when the relative humidity in the laboratory was 54% and the ambient temperature was 27°C. Figure 4-5 shows the increase in the relative humidity with time which is estimated at 57.4 mg $H_2O/(100\ cm^2)(24\ hrs)$ per mil. The permeation of water vapor was again measured but this time through both the "Tedlar" and the 'Scotchpak'. Over the anticipated lifetime of the experiments

Table 4-1

Permeability of Tedlar[a] and Scotchpak[b] to Gases and Vapors

Tedlar	
Gases	$cm^3/(100\ cm^2)(24\ hrs)(mil)$ at 23.5°C
Oxygen	.50
Nitrogen	.04
Carbon Dioxide	1.7
Hydrogen	9.0
Vapors	$g/(100\ cm^2)(24\ hrs)(mil)$ at 23.5°C
Water	.50 (37.8°C, 90%RH)
Ethyl Alcohol	.08
Benzene	.22
Acetic Acid	.11
Scotchpak	
Gases	$cm^3/(100\ cm^2)(24\ hrs)$ at 1 atmosphere
Oxygen	.05
Carbon Dioxide	.05
Air	<.02
Vapors	$g/(100\ cm^2)(24\ hrs)$
Water	.003 (37.8°C, 95%RH)

[a]Adapted from DuPont Company

[b]Adapted from 3M Company

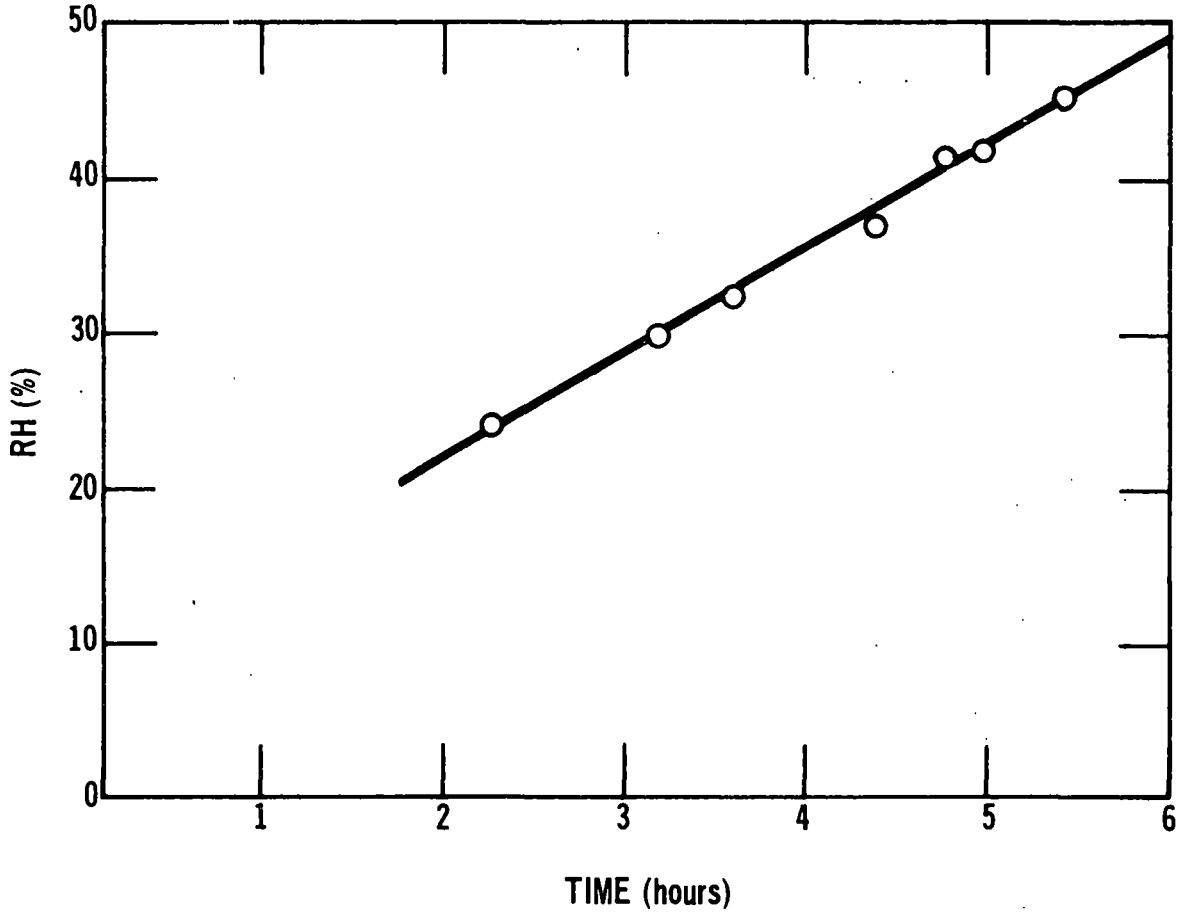

FIGURE 4-5. VARIATION OF RELATIVE HUMIDITY WITH TIME DUE TO THE PERMEATION OF WATER VAPOR.

to be conducted, one to two hours, no change in the relative humidity could be detected within the resolution of the instrumentation used.

The reactor was supported horizontally on a lattice frame suspended from the laboratory ceiling and about two meters above the floor. Air was permitted to circulate freely about the outer bag. Seven Swagelok O-Seal, ¼" O.D. stainless steel (316) adapters were fitted to the bag with threaded teflon blocks in the pattern shown in Figure 4-6. Additional thickness was provided at these points by the addition of a layer of the polyethylene tape. Two of the ports were used to introduce the reactants into the system and the other five were reserved for sampling.

2. Ozone Analysis

A Meloy Laboratories, Incorporated, Model OA350 Ozone Analyzer was used to monitor the ozone concentration in the reactor. The gas sample and ethylene are delivered simultaneously to a mixing zone where they react and produce chemiluminescence in the 430 μm region. This light is photometrically detected and is directly proportional to the ozone concentration. The photocurrent thus produced from this flameless reaction is converted to a voltage, amplified and then is available as an analog signal and/or is displayed on a panel meter.

Oxidizing species other than ozone and reducing species which might be expected to be encountered during this series of experiments do not interfere with the analysis.

The instrument has six operating ranges to cover the span of from 0 to 10 ppm and its minimum detectable sensitivity is 0.001 ppm.

Primary calibration of the analyzer was achieved by generating an ozone atmosphere in the reactor, the concentration of which was determined

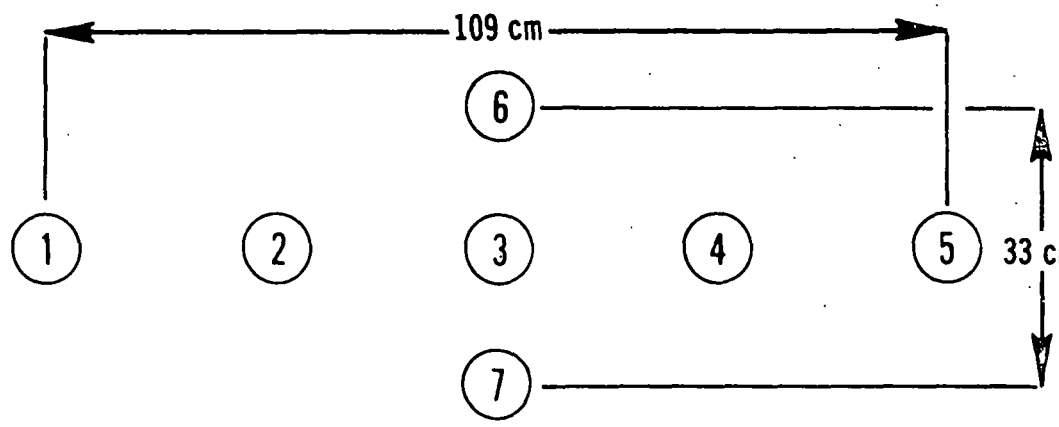

1 OZONE AND DILUENT GAS INLET
2 MAGNEHLIC GAUGE, INTEGRATING NEPHELOMETER
3 VACUUM, ELECTRICAL MOBILITY ANALYZER, IR SPECTROMETER, FILTER SAMPLES
4 OZONE AND SULFUR DIOXIDE ANALYZERS
5 DEW POINT HYGROMETER
6 OPTICAL PARTICLE ANALYZER, CONDENSATION NUCLEI COUNTER, GAS CHROMATOGRAPH

FIGURE 4-6. SCHEMATIC OF REACTOR PORT ARRANGEMENT.

using the Reference Method for the Measurement of Photochemical Oxidants (Environmental Protection Agency, 1971). The instrument was spanned on the concentration value thus obtained. A three-way solenoid value was installed, which when energized, closed the sample inlet port and allowed ambient air to pass through a charcoal filter. This provided ozone free air to the reaction chamber for a zero calibration.

The instrument also has an integral ozone generator (Pen-Ray ultra-violet lamp) which provides a constant ozone source on demand to the detector. This secondary calibration was used to monitor the stability of the analyzer and to determine primary calibration requirements.

3. Ambient and Dew Point Temperature Measurements

A Cambridge Systems, Incorporated, Model 880 Dew Point Hygrometer was used to sense the dew point temperature dynamically in the reactor and was also used to monitor a remote Yellow Springs Instrument Company Thermistor, Model 410X. The thermistor had a 3.4 second time constant, an active element 5.1 cm in length and was used to sense the temperature in the bag.

The hygrometer measures the dew point of a gas sample by presenting a metal surface to the gas which will be at the temperature of the metal. The surface is cooled to the dew point temperature of the gas being sampled and condensation occurs. At the dew point temperature, an equilibrium condition exists and the rate at which molecules leave the surface water is equal to the rate at which water molecules enter the surface water.

An optical system senses the presence of condensate on the metal surface which is mirrored and an optical-thermal feedback system adjusts and maintains the surface at the dew point temperature.

The range of the hygrometer is -40°C to 50°C, its accuracy is ±1.1°C and with this method being a primary measurement, no calibration is required.

The relative humidity of the gas sample defined as the ratio of the actual vapor pressure in the gas to the saturation vapor pressure with respect to water at the prevailing dry bulb temperature can be calculated as follows:

$$\text{Relative humidity} = \frac{\text{Saturation Vapor Pressure over water at Dew Point Temp.}}{\text{Saturation Vapor Pressure over water at Ambient Temp.}}$$

The Smithsonian Meteorological Tables (list, 1958) were used to obtain the appropriate saturation vapor pressure data.

4. Sulfur Dioxide Analysis

A Meloy Laboratories, Incorporated, Model SA 185-2 Flame Photometric Detector Sulfur Analyzer was used to monitor the sulfur dioxide concentration in the reactor. This instrument provides real time analysis by monitoring the intensity of light emitted by sulfur as it passes through a hydrogen rich flame. High detection sensitivity is achieved by the geometrical arrangement of the burner block and the photomultiplier tube and specificity by a narrow band pass (394 μm) filter. Sulfur containing molecules are converted to an S_2 species in the hydrogen rich flame. The hydrogen and hydroxyl radicals which are also produced in the flame react with the S_2 to form activated S_2* as follows:

$$\cdot H + \cdot H + S_2 \rightarrow S_2^* + H_2$$

$$\cdot OH + \cdot H + S_2 \rightarrow S_2^* + H_2O$$

Radiation with a maximum intensity at 394 μm is emitted when this excited S_2* species reverts to a lower energy state. The intensity of the light

produced is directly proportional to a power slightly less than the square of the sulfur concentration.

The range of the instrument is 0-1 ppm and its minimum detection sensitivity is 0.005 ppm.

Calibration of the sulfur analyzer was achieved through the use of a 2 cm long, Metronics Associates, Incorporated, Dynacal Permeation tube (#2140) and a constant temperature (30°C) Meloy SO_2 Gas Calibrator Model CS-10. The use of permeation tubes to generate low concentrations of gases has been described by O'Keeffe and Ortman (1966). The permeation rate of the tube was calibrated gravimetrically over a period of 18 hours using a Cahn Vacuum Electro Balance System Model R100 at 25°C as 558 μg/min.

The concentration of SO_2 in ppm can be expressed as

$$c(\text{ppm}) = \frac{R}{F}\,\frac{22.4}{M}\,\frac{T}{273}\,\frac{760}{P} \qquad \text{IV-1}$$

where R = permeation rate (μg/min)

F = Gas flow rate (ml/min)

M = molar gas volume at operating conditions

T = Temperature of the gas (°K) and

P = Pressure of the gas (mm Hg).

The change in permeation rate with temperature is given by (Meloy, 1972):

$$\log R_2 = \log R_1 + 2950\,\frac{T_2 - T_1}{T_2 T_1} \qquad \text{IV-2}$$

The permeation rate, therefore, for this series of experiments was 812.4 μg/min at the 30°C operating temperature and the output concentration used for spanning the sulfur analyzer was 0.365 ppm.

The instrument zero was achieved by passing air through an internal charcoal column prior to its passage into the burner block.

As this instrument is a total sulfur analyzer, a Millipore Mitex (teflon) LSWP filter was added to the sample inlet to eliminate any contribution from the sulfate aerosol.

A Lear Siegler, Incorporated, Model III Second Derivative Air Analyzer was used to measure the sulfur dioxide concentration in the reactor when nitrogen was used as the diluent gas. This instrument measures the curvature or rate of change of the slope of intensity with respect to wavelength for the absorption of ultraviolet radiation at a prescribed wavelength. Its minimum detectable concentration for sulfur dioxide is 10 ppb using the 6.3ℓ, 1 m long, multipass cell. Its relatively large volume and high sampling rate made extensive use of this instrument impractical. The output signal from the ultraviolet photomultiplier tube was recorded on an integral component Honeywell Electronik 193.

5. Hydrocarbon Analysis

A Tracor, Incorporated, Model MT150 Gas Chromatograph was used to monitor the concentration of the unreacted olefin and the product acetyaldehyde in the reactor. A flame ionization detector measured the difference in the ion current due to the combustion of the sample. Sample was continuously drawn at 100 cm^3/min through a 5cm^3 loop the contents of which could be injected via an eight position pneumatic valve into the chromatographic column. Poropak Q was used to pack the 2.75 m column for the adsorption and desorption of the sample gases. This material provides good separation based on the vapor pressure of gases and allows for complete resolution of the peaks of interest. The column was operated in an isothermal mode (85°C) and regenerated for 30 minutes at 230°C (Intersociety Committee, 1972).

An analysis, using a 200 cm^3 sample injection and a silica gel adsorption column, of the cylinder air used during the series of experiments indicated the presence of methane, small amounts of ethane and propane and trace levels of acetylene, n-butane, isobutane and isopentane. None of these gases interfere with the analysis or react with ozone or sulfur dioxide under the conditions of the experiment.

Calibration of the gas chromatograph was achieved by injecting specified microliter quantities of pure olefin in the gas phase into a 51 ℓ "Tedlar" bag along with carrier air. Calibration samples from this bag were periodically injected into the chromatographic column correcting for wall loss in the bag.

Operation of the column in the isothermal mode along with the semi-continuous calibration allowed for the quantification of the gaseous components by the measurement of peak heights which were recorded on a Honeywell Incorporated Electronik - 193 chart recorder.

6. Infrared Spectroscopic Product Analysis

A Fourier Transform Infrared Spectrometer was used to measure the product inventory in the reactor at a terminal point in some of the experimental runs. This system consisted of two detectors operated at liquid nitrogen temperature, a cell, a helium-neon laser for path alignment, a Nerst glower as a source of the infrared radiation, a Digilab Incorporated, Model 496 scanning Michelson interferometer, a Data General Nova 1200 dedicated computer for processing interferograms and spectra, a teletype for user control and a Digilab Digital Plotter for plotting the spectra. One of the detectors, indium antimonide, was used to scan the frequency region 2000 cm^{-1} to 3000 cm^{-1} and the other, mercury-cadmium-telluride, to scan the region 700 cm^{-1} to 1200 cm^{-1}. The glass

cell was 2.5 m long and with the mirrored surfaces on the ends, path lengths of 140 and 160 m were used for the measurements. The operation of a system of this type has been described in a recent article by Hanst, et al., (1973).

In operation the cell was evacuated and then allowed to fill to ambient atmospheric pressure by opening a valve connecting the cell with the reactor. The infrared radiation from the Nernst glower entered the interferometer where a scanning mirror projected a sine wave modulation on each optical frequency passing through the cell to the detectors. The superposition of the modulated frequencies reaching the detector constitute the interferogram which is related to the spectrum through the Fourier transform. A reference spectrum was taken before each experimental run which consisted of the diluent gas humidified to match the water content of the run to follow. The digitized reference spectrum was stored in the computer memory and was accessed after the sample was collected in the cell. The ratio of the sample spectrum to the reference was computed and plotted. The Lambert-Beer law was used to compute the concentrations from the equation

$$C = \frac{\ell n\left(\frac{I_o}{I}\right)}{k\ell} \qquad \text{IV-3}$$

where I_o = the intensity of the radiation at the particular wave number for zero absorption

I = the absorption diminished intensity

k = the absorption coefficient

ℓ = the path length used and

C = the concentration to be determined.

The absorption coefficients used in this study were obtained from reference spectra of an extensive series of molecular species previously studied at the National Environmental Research Center, Research Triangle Park, North Carolina.

7. Sulfur Balance Determination

Two techniques were used to determine the total sulfur content of the sulfate aerosol formed in the olefin-ozone-sulfur dioxide reaction. The first of these involved the use of Dupont Instruments Model 820 Liquid Chromatograph and a Technicon Corporation Auto Analyzer to determine the concentration of water soluble sulfates. This method is the subject of a technical report in preparation by Tejada (1974).

The aerosol was collected on Millipore Corporation, Fluoropore FGLP (0.2 μm pore size) 37 mm diameter filters. The filter was extracted with a 60/40 isopropyl alcohol (IPA)/water solution and the extract pumped through a cation exchange resin (Dowex 50W - X2) to remove interferences. The extract is then pumped through a column of solid barium chloranilate where barium sulfate precipitates out. An equivalent amount of reddish colored acid chloranilate ion is released and measured colorimetrically. This method has a sensitivity better than 0.5 μg $SO_4^{=}$/ml in 60% IPA.

Calibration of this method was accomplished by preparing solutions of sulfuric acid in IPA/water to span the concentration range of the samples being analyzed.

The second method made use of X-ray fluoresence techniques to measure the total sulfur collected on the filters. A Lawrence Berkeley Laboratory X-ray Fluoresence Spectrometer which incorporated a dedicated Texas Instruments computer Model T1960A and used three secondary targets, i.e., Ti, Mo, and Tb to optimize the sensitivity over the periodic

table was used for this analysis. A Northern Scientific Corporation 1024 Channel ADC together with the computer served as a pulse height analyzer conducting an energy sort of the X-ray pulses. The spectrometer has been described in reports by Landis et al. (1970) and by Goulding et al. (1972). The composition of the samples was determined by irradiating them for 400 seconds with monochromatic X-rays and observing the characteristic K and L X-rays. The secondary fluorescer, in this case, Ti, was used to produce the near monochromatic X-ray source. The fluoropore filter was selected for this analysis because of its low mass and very low level of impurities (Dzubay and Stevens, 1973) in addition to its high efficiency for collecting small particles. A standard Millipore Corporation Field Monitor was used as the filter holder with the addition of one extra retainer incorporated as a spacer in an attempt to insure a uniform deposition distribution on the filter surface.

The analyzer was calibrated using evaporated foils of a number of elements and compounds. The smooth calibration curve drawn through these points was used to determine elements for which foils were not available. Individual spectra of up to forty elements are stored in the computer along with a spectrum from a blank filter. These spectra are compared with the sample spectra using a stripping procedure in order to determine the concentration of each element.

8. Light Scattering Measurements

A Meteorology Research, Incorporated, Model 1500 Integrating Nephelometer was used to measure the light scattering coefficient (b_{scat}) as a function of time during the experimental runs. The design, operation and calibration of this instrument have been described by Charlson et al. (1969).

The sampled gas is drawn into a cylindrical optical assembly with a flash lamp mounted behind an opal glass screen on one side. A photomultipler tube is mounted in one end of the assembly to detect the scattered light from the flash illuminated volume. A light trap and a calibration mechanism are mounted on the opposite end. A reference phototube is located in the illuminated volume. This volume is defined by means of the physical arrangement which is such that the photomultiplier tube is not visible from the flash lamp position. Light received at the photomultiplier tube is due, therefore, to scatter from particulate material in the illuminated volume. The reference phototube senses the light directly from the flash lamp and automatically eliminated the effect of fluctuations in flash lamp output. Ultraviolet cutoff filters, (~4100 Å) are used with both phototubes to relate the instruments response more nearly to the visible spectrum and to eliminate spurious radiation in the ultraviolet region.

The effective wavelength of the nephelometer is 500 nm for either aerosols or particle-free gases. The human eye is most sensitive, however, to radiation at 550 nm. Horvath and Noll (1968) have shown theoretically and Alquist and Charlson (1969) have shown experimentally that the measured scattering can be related to light scattered at the other wavelength as $b_{550} \simeq 0.84\ b_{500}$.

The normal sampling rate of this instrument is approximately 140 lpm but because of the limited reactor volume the sampling rate was reduced to approximately 300 cm^3/min. The nephelometer output is independent of flow rate and a range of time constants and flash lamp rates are selectable. For these studies a flash lamp rate of one per second and a ten second time constant were used.

Primary calibration of this instrument was achieved by sampling Freon-12 and spanning the instrument on the tabulated light scattering coefficient ($3.6 \times 10^{-4} m^{-1}$) which was derived from the Rayleigh theory based on its measured refractive index (Charlson et al., 1969). A secondary calibration method is built into the instrument and consists of a shutter arrangement on the end of the optical assembly opposite the phototube. A white surface behind the shutter is illuminated via a fiber optic light pipe and the light reflected has been optically calibrated against gases of known scattering coefficients.

There are two secondary meter scales with this instrument which do not indicate the results of any measurement but rather relationships that have extensive empirical support and some theoretical justification. The visual range scale is based on the limiting contrast for daytime visual determination of 0.02. The resulting relationship is

$$L_v(m) \simeq \frac{3.9}{b_{550}} \simeq \frac{4.7}{b_{500}} . \qquad \text{IV-4}$$

The other scale, i.e., mass concentration, relates the mass of material in a box one meter in cross section and of length L_v as

$$L_v \times \text{Mass} = 1.8 \ g/m^2 \qquad \text{IV-5}$$

(Charlson et al., 1969). The instrument panel meter displays the mass concentration using the relationship between that parameter and the light scattering coefficient which is indicated on the primary scale as

$$\text{mass} \ (\mu g/m^3) = 3.8 \times 10^5 \ b_{scat}(m^{-1}) . \qquad \text{IV-6}$$

Values for both of these secondary scales were calculated from the b_{scat} measurements made during the experimental runs and are reported herein.

9. Condensation Nuclei Count Determination

An Environmental One Corporation, Model Rich 100 Condensation

Nuclei Counter was used to monitor the number concentration of particles $\geq$ 0.0025 μm diameter. The instrument operates on the principle of a cloud chamber in which submicroscopic droplets grow to micrometer size as a result of condensation of water from a supersaturated environment. The sample air is diverted, at an approximate frequency of once per second, to a humidifier and then to a cloud chamber where the volume is rapidly expanded. The supersaturation achieved as a result of the adiabatic expansion reaches in excess of 300%. A light beam is focused on a solid state light sensitive element across the expansion chamber. The beam is attenuated by the growing aerosol the extent of which is proportional to the number concentration of the aerosol particles. At the end of each cycle the chamber in pressurized and flushed out.

The concentration range of the counter is from 300 to 10^7 particles/cm^3 and has a linear response, as reported by the manufacturer, through the 0-$3x10^5$ particles/cm^3 range scale and a non-linear response on the 0-10^7 particles/cm^3 scale. The response time of the instrument is five seconds at 50 cm^3/sec.

Calibration by the manufacturer is based on the Pollack counter the developmental history of which is given by Nolan (1972).

10. Sub-microscopic Aerosol Analysis

A Thermo-Systems, Incorporated, Model 3030 Electrical Aerosol Size Analyzer was used to measure with time the size distribution of the growing sulfate aerosol in the 0.003 to 1 μm size range. The design, operation and performance of a prototype of this instrument is described in a paper by Liu et al. (1973) and is based on the principle of "diffusion charging-mobility analysis" described by Whitby and Clark (1966).

A flow schematic of the commercial model of the electrical mobility analyzer is shown in Figure 4-7. The sample aerosol is introduced into a charging region where it is exposed to unipolar positive ions produced in a corona discharge. The charged aerosol then passes through the mobility analyzer which consits of a precipitator, a high-efficiency current collecting filter and an electrometer sensor. The collection rod, to which a variable negative voltage is applied, is immersed in a sheath of clean air surrounded by an annular cylinder of the aerosol. Small particles with high electrical mobility are drawn to the collection rod under an applied voltage and larger particles are collected on the current collecting filter. The voltage on the rod is periodically increased and particles of discrete size increments will be collected on the rod with a concurrent decrease in the electrometer current. Particles with a sufficiently high electrical mobility are collected on the rod for a discrete voltage while those of lower mobility are sensed by the electrometers. The cutoff mobility at which precipitation on the rod occurs is given by:

$$Z_p = \frac{Q_T[\ln(r_2/r_1)]}{2\pi\ VL} \qquad \text{IV-7}$$

where Q_T = the total air flow

r_1 = the inner electrode radius of the precipitator

r_2 = the outer electrode radius of the precipitator

L = the length of the collecting rod and

V = the applied voltage.

The mobility distribution of the aerosol is thus measured from which the size distribution is inferred. This inference is based on the electrical mobility of the aerosol being a monotonically decreasing function of the particle size. Whitby and Clark (1966) report that for analyzers in

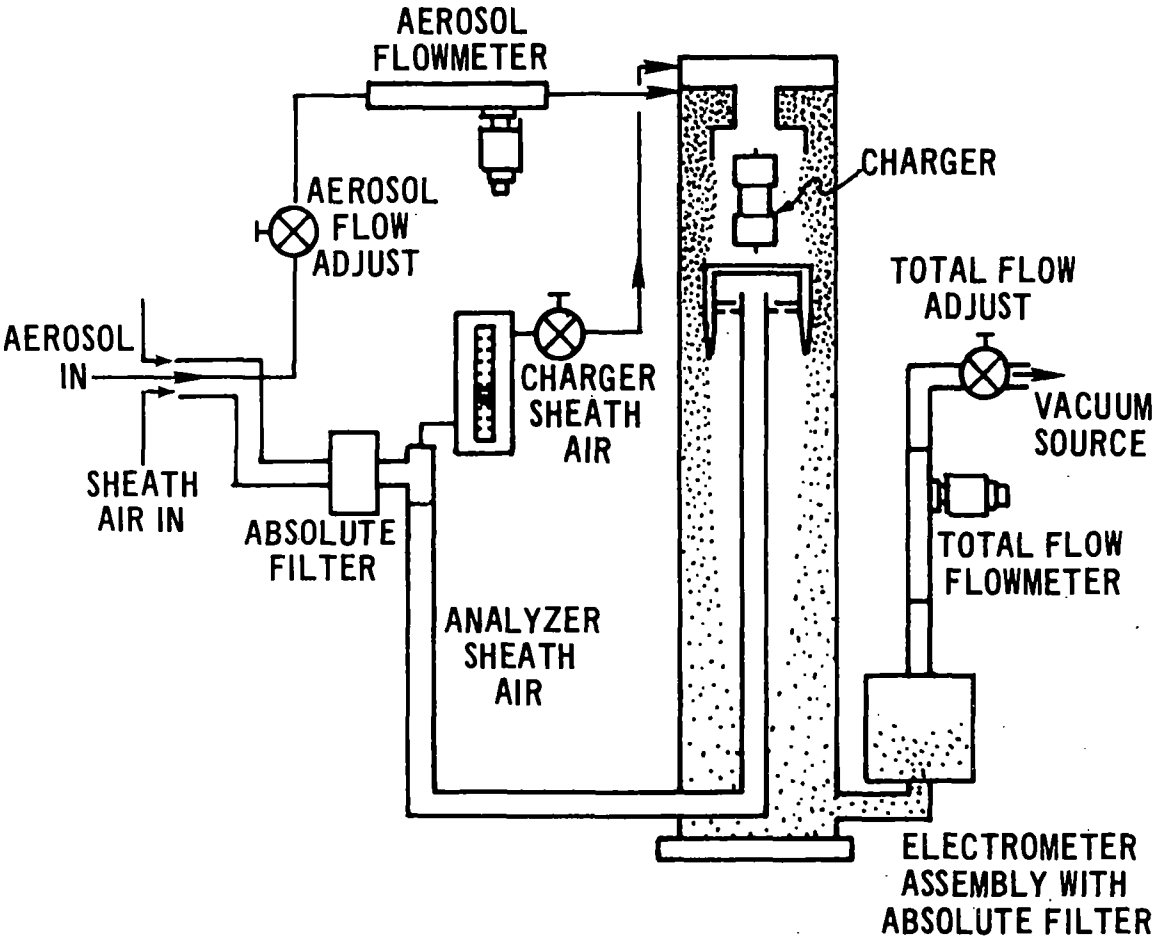

FIGURE 4-7. SCHEMATIC OF THE ELECTRICAL AEROSOL SIZE ANALYZER. [TAKEN FROM THERMO-SYSTEMS INCORPORATED, 1974].

which the conditions approximate diffusion charging this relationship holds for particles up to approximately 1 μm in diameter.

Figure 4-8, adapted from the work of Bademosi (1971), shows the relationship between the electrical mobility and the particle size for diffusion charging for the conditions used in the design of this instrument, i.e., $N_o t = 1 \times 10^7$ (ions/cc)(sec). N_o is the positive ion concentration in the charging region and t is the residence time in that region. Up to approximately 0.02 μm, the mean charge on the particles is one unit and, therefore, for this size and smaller particles, the method provides an accurate sizing technique as the mobility Z_p is related to the particle radius by the equation,

$$Z_p = 300 \frac{eC}{6\pi r\eta} \qquad (cm^2/volt\text{-}sec) \qquad \text{IV-8}$$

where e = the elementary charge unit is esu

C = the Cunningham Correction factor

η = the viscosity of the air and

r = the particle radius.

The mobility dependence decreases significantly with particle size beginning at about 0.2 μm and is essentially zero for particles greater than 1 μm in diameter. The definition of the upper end of the distribution curve has, therefore, a higher degree of uncertainty than, for example, the region between 0.02 and 0.2 μm. Below 0.02 μm the distribution of charges on the particles is either zero or one. The determination of the fraction of particles charged and the diffusion loss becomes increasingly more tenuous as the particle size decreases.

On this instrument the particle size interval from 0.0032 to 1.0 μm has been divided into ten equal geometrical size intervals. The reported

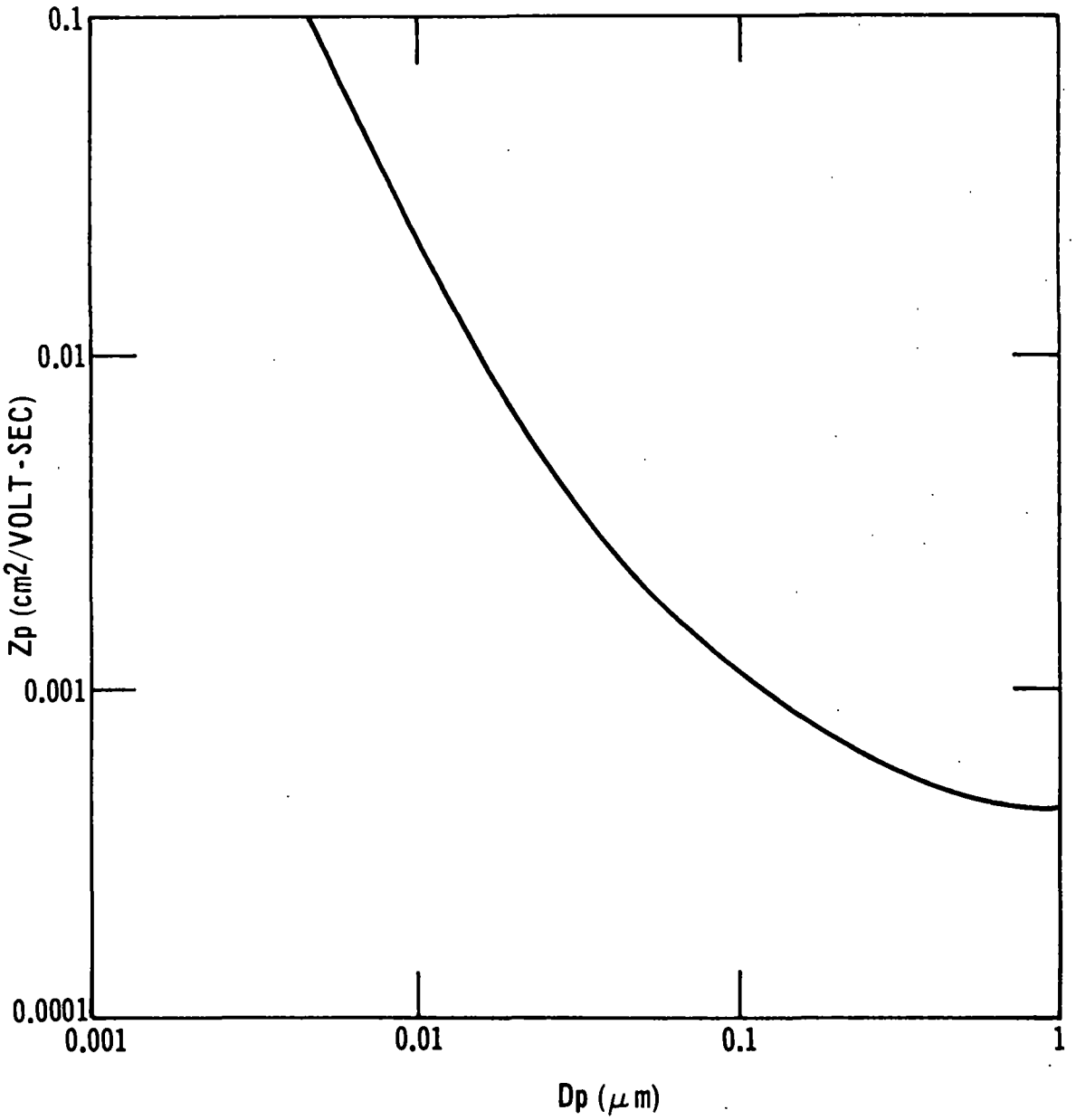

FIGURE 4-8. RELATIONSHIP BETWEEN ELECTRICAL MOBILITY AND PARTICLE SIZE FOR DIFFUSION CHARGING WHERE $N_o t = 1 \times 10^7$ (ions/cc)(sec). [ADAPTED FROM THE WORK OF BADEMOSI, 1971].

diameter for each interval is the geometric mean size. Table 4-2 shows the computational sheet used to calculate the standard and the normalized size distributions of count, surface area and volume. The calibration constant $\Delta N/\Delta I$ is calculated from the expression

$$\frac{\Delta N}{\Delta I} = Q_s \, \bar{n}_p \, e \, f_c f_p \qquad \text{IV-9}$$

where Q_s = the sample air flow

$\bar{n}_p$ = the mean particle charge

e = the elementary unit charge in coulombs and

f_c = the fraction of charged particles and

f_p = the number collected on the current collecting filter.

An absolute calibration of this instrument has not been accomplished to date although an effort to determine the finite resolution of the analyzer accounting for the charge distribution on the particles is under study at the Particle Technology Laboratory, University of Minnesota.

11. Optical Particle Analysis

A Royco Instruments, Incorporated, Model 220 optical aerosol counter was used to measure the size distribution of aerosol particles from approximately 0.3 to 10 μm in diameter. The basic principle of this instrument is that the light from a tungsten lamp is projected into a viewing volume through which a dilute aerosol is passed, ideally with only a single particle in the viewing volume at a time. The light scattered at 90° from the focused beam is sensed by a photomultiplier tube and converted to a voltage signal. The amount of light scattered is related not only to the size of the particle but also to its shape, absorbtivity, refractive index and orientation. For this study the shape of the aerosol droplets are spherical and the absorbtivity and refractive

Table 4-2. Data Table for Number, Surface Area and Volume Distribution[a]

D_p	Dpi	$\Delta N/\Delta I$	Collector Voltage	$I \times 10^{-12}$ Amp.	$\Delta I \times 10^{-12}$ Amp.	ΔN Part./CC	$\frac{\Delta N}{\Delta \log D_p}$ $\Delta N \times 4$	$\frac{\Delta S}{\Delta N}$ πd^2	$\frac{\Delta S}{\Delta \log D_p}$ $\Delta S \times 4$	$\frac{\Delta V}{\Delta N}$ $1/6\pi d^3$	$\frac{\Delta V}{\Delta \log D_p}$ $\Delta V \times 4$
.0032			20	_____							
	.0042	1.102×10^7			_____	_____	_____	5.54(-5)	_____	3.88(-8)	_____
.0056			62	_____							
	.0075	3.596×10^6			_____	_____	_____	1.77(-4)	_____	2.21(-7)	_____
.0100			196	_____							
	.0133	1.069×10^6			_____	_____	_____	5.56(-4)	_____	1.23(-6)	_____
.0178			593	_____							
	.0237	3.062×10^5			_____	_____	_____	1.76(-3)	_____	6.97(-6)	_____
.0316			1220	_____							
	.0422	9.866×10^4			_____	_____	_____	5.59(-3)	_____	3.93(-5)	_____
.0562			2183	_____							
	.0750	4.775×10^4			_____	_____	_____	1.77(-2)	_____	2.21(-4)	_____
.100			3515	_____							
	.133	2.356×10^4			_____	_____	_____	5.56(-2)	_____	1.23(-3)	_____
.178			5387	_____							
	.237	1.356×10^4			_____	_____	_____	1.76(-1)	_____	6.97(-3)	_____
.316			7152	_____							
	.422	7.781×10^3			_____	_____	_____	5.59(-1)	_____	3.93(-2)	_____
.562			8642	_____							
	.750	4.461×10^3			_____	_____	_____	1.77	_____	2.2(-1)	_____
1.000			9647	_____							
							N= ÷4		S= ÷4		V= ÷4

[a]Taken from Thermo Systems Incorporated, 1974

index are fairly constant so that this counter can classify by size as well as count the droplets.

The signal from the Royco was processed by a Nuclear Data, Incorporated, system consisting of a Particle Sizing Amplifier, a Model ND 560 Analog to Digital Converter and a ND 812 Computer. An ND 4410 Control Function Module, an ND Tape Cassette, a teletypewriter and a Hewlett Packard 1208 B Display Scope were used to manipulate, display and record the distribution data.

Calibration of this instrument was accomplished by a number of techniques. To compensate for degradation of the lamp, the counter is equipped with a light pulse generator (mechanical chopper) to simulate the passage of particles. The amplification is adjusted until the signal reaches the calibration value. A zero check is made by placing a membrane filter over the sample inlet. The prime calibration procedure consisted of generating an aerosol of monodisperse latex spheres (refractive index 1.6) and sampling the suspended material with the optical aerosol analyzer. The size of the spheres used were 0.3, 0.357, 0.481, 0.794 and 1.011 μm and their corresponding peak channels were recorded with the multi-channel analyzer. The calibration data for this system is shown in Figure 4-9.

C. Experimental Procedures

The reactor was flushed with diluent gas three times before each run to sweep out unreacted and product species from previous experiments. The bag was evacuated via a vacuum line to yield a maximum deflection on the Dwyer magnehelic gauge, $\leq$ - 0.5 inches of water. The reactor was then filled with the diluent gas humidified to the same degree as for the experiment which was to follow. The diluent gas was passed through a

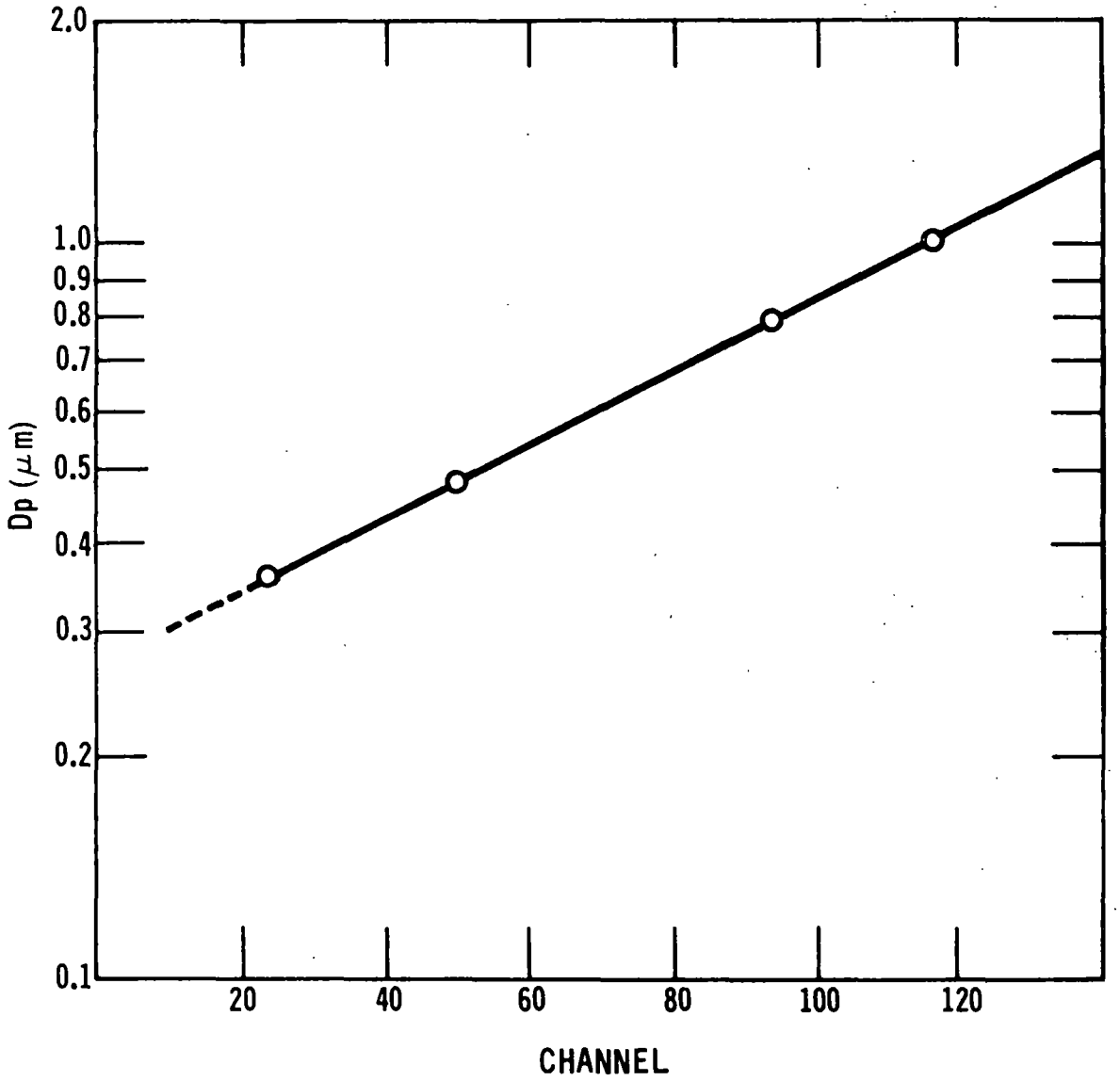

FIGURE 4-9. CALIBRATION DATA FOR OPTICAL AEROSOL ANALYZER.

charcoal column followed by a 142mm Millipore type AAWP filter (0.8 μm mean pore size) prior to its introduction into the reactor to remove contaminant aerosols and undesirable reactive gaseous species. The diluent gases used in this experimental series were compressed air made from a mixture of liquid oxygen and liquid nitrogen and compressed nitrogen (High Purity Grade).

A complete set of background measurements was made with the total instrument complement to confirm the essentially zero concentrations of the reactive species and particulate material. The condensation nuclei counter typically indicated a background nuclei count of about 400 condensation nuclei per cubic centimeter and its reported range is $300\text{-}10^7$ cn/cm^3. If during these background measurements, positive concentration values (other than the cn/cm^3 level cited) were recorded, then the flushing procedure was continued until a zero value was observed.

The propylene used for the reactor was a calibration mixture (Linde) of 945 ppm in nitrogen while that used for the calibration of the gas chromatograph was CP grade ($\geq$99.5%) and was introduced into the reactor by being injected into the diluent gas stream from a gas tight syringe. The sulfur dioxide was also in a calibration mixture, in this case from Scott Research Laboratories, Incorporated and contained 89 ppm in nitrogen. An Orec Model 03V1 OZONATOR was used to provide the desired ozone concentration. Zero grade air was passed through a charcoal column and a Millipore type AAWP filter before being exposed to the mercury vapor lamp in the ozonizer. A Millipore type FALP (teflon) filter (1μm mean pore size) was used on the output of the ozone generator to remove any condensation nuclei which might be photochemically generated by the ultraviolet lamp. The carbon monoxide which was used for two of the runs was CP grade and was injected into the diluent stream in the same manner as was the ethylene.

The propylene, sulfur dioxide and the diluent gas were delivered to the reactor at a constant rate and mixture ratio over a five minute period. The humidification was provided as previously mentioned, by passing a metered portion of the diluent gas through bubblers containing distilled water and immersed in a Forma Scientific Model 2800 Constant Temperature Bath and Circulator. The ozone was fed into one of the two diluent gas streams for a portion of the five minute period depending on the concentration desired. Ozone was not, however, added during the last thirty seconds of the filling time thereby permitting the other reactants and diluent gas introduced during that terminal period to mix thoroughly with the ozone. Electrically actuated solenoid values were used to initiate and terminate the introduction of the gas phase components into the reactor and this flow was controlled through Brooks Instrument Division flowmeters and Parker-Hannefin needle valves. The reactor was filled for each experiment to a positive pressure indication on the magnehelic gauge of 0.1" of water above ambient.

The total gas flow into the bag was about 90 lpm which was considered adequate to insure uniform mixing of the reactants. The reactor was not mechanically stirred during the experiments as the thermal gradients which existed in and about the reactor were found to be adequate in maintaining homogeneity among the gaseous species. Wilson et al. (1971) studied the effect of stirring in a series of chamber experiments and noted a decrease in the amount of aerosol with increased stirring rate. If the stirring was sufficiently fast, the observation of light scattering aerosol could be completely eliminated. The composition of the reactants also influenced the effect noted with increased stirring. Cox and Penkett (1972) observed a similar result in that when forced circulation was used during their experiments, the effective rate of gaseous diffusion to

their reactor walls was increased by a factor of about five. The effect of stirring was not found to be a critical parameter on aerosol growth in systems with initial low nuclei counts during studies conducted by Kocmond et al. (1973). Aerosol decay by coagulation in the dark, however, was noted to be significantly increased by stirring.

Sampling was initiated immediately after the reaction vessel was full and was generally intermittent. The electronics portion of the instrumentation was kept operating while the pneumatic system was off in some cases and cycled to sample room air in others. These measures were necessitated because of the limited total volume in the reactor and the large sampling volume demands of the instruments. The experiments were designed to last until one of the principal reactants, i.e., the olefin or ozone had been consumed by $\geq$ 90%.

A Westronics, Incorporated, Model M11E Multipoint Recorder was used to record the ambient temperature and the output of the ozone and sulfur dioxide analyzers, the condensation nuclei counter, the integrating nephelometer, and the dew point hygrometer. The output of the flame ionization detector in the gas chromatograph was recorded on the Honeywell Electronik 193 Strip Chart Recorder. The Royco optical particle data was stored in the memory of the Nuclear Data ND 812 computer system and printed out on a teletypewriter. The data output from the electrical mobility analyzer was manually recorded. The analog output from the various instruments was digitized and recorded along with the other digital data on computer cards for subsequent data manipulation.

A series of measurements was performed to determine the loss of the reactants in the containment vessel. Propylene, ozone and sulfur dioxide, were introduced into the reactor individually along with the diluent gas and their concentration monitored over an extended period of time. The

loss of the reactant species could be a function of molecular diffusion to and reactions with the reactor walls and/or reactions with species not purged from the bag after previous runs or introduced with the species under study.

The observed loss for these three species was apparently the result of a first order reaction, with the species irreversibly lost to the walls of the reactor. Figure 4-10 shows the linear relationship resulting from a plot of the logarithm of concentration versus time for the three species for typical decay measurement runs. The slopes of the lines are the rate constants for the wall loss reaction as predicted from the following equations:

$$\frac{d[A]}{dt} = -k[A] \qquad \text{IV-10}$$

where A = some hypothetical species and

k = the velocity constant.

The equation simply states that the rate of the wall loss reaction is directly proportional to the concentration of the reactant present. By integration the equation becomes:

$$\ln[A] = -kt + \text{constant} \qquad \text{IV-11}$$

from which the value of k can be obtained. Reaction rates are also often reported in terms of the half life of the species in the system. For the first order reaction the half life is related to the rate constant by

$$t_{\frac{1}{2}} = \frac{.693}{k}. \qquad \text{IV-12}$$

The rate constants and half lifes measured for the three species in the reaction containment vessel were as follows:

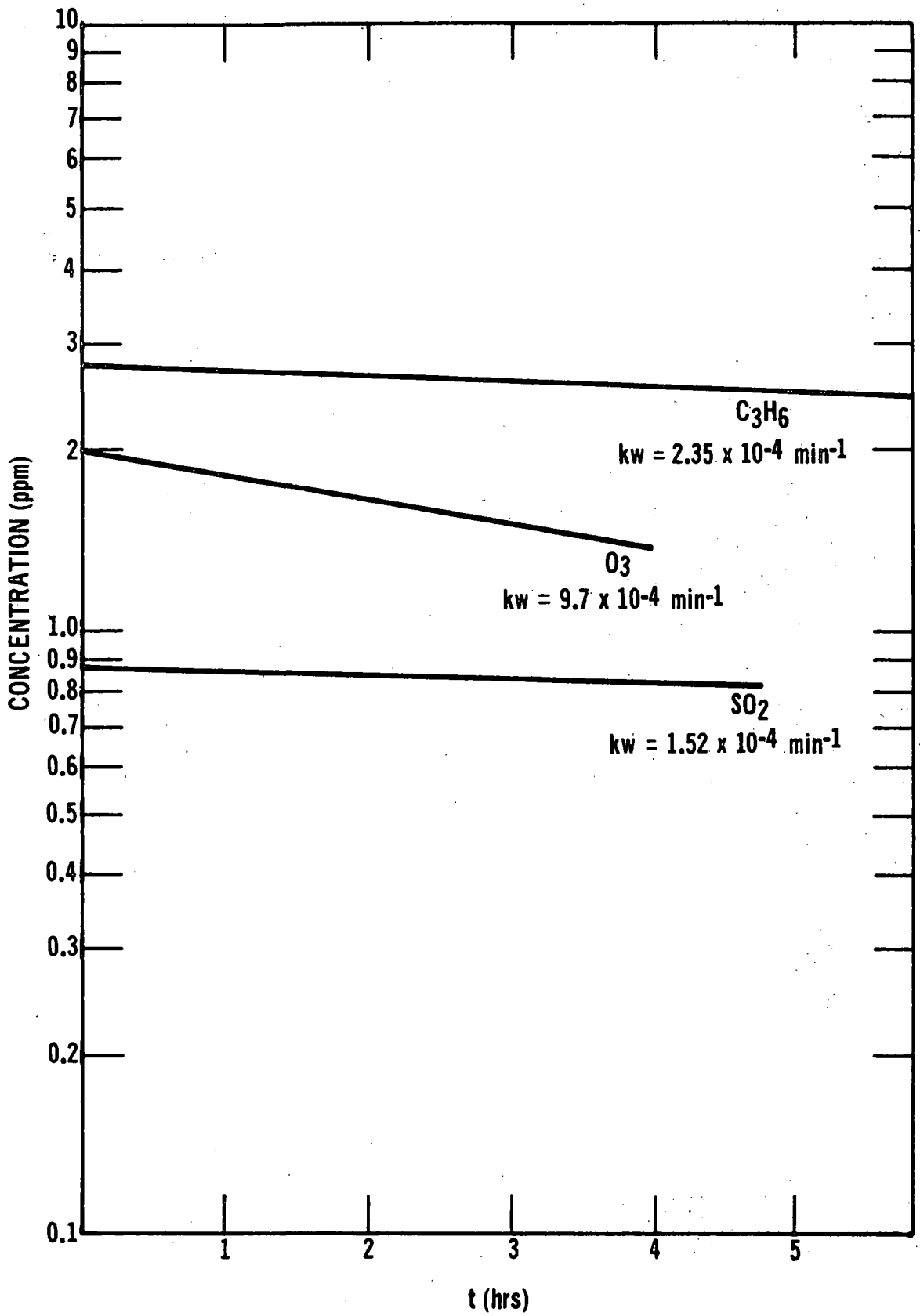

FIGURE 4-10. VARIATION OF REACTANT CONCENTRATION WITH TIME DUE TO WALL LOSSES.

	Propylene	Ozone	Sulfur Dioxide
Rate Constant (k)	$2.35 \times 10^{-4} min^{-1}$	$9.7 \times 10^{-4} min^{-1}$	$1.52 \times 10^{-4} min^{-1}$
Half Life ($t_{\frac{1}{2}}$)	49.1 hrs.	11.9 hrs.	76.0 hrs.

The data from several experiments were corrected for these different rates of loss due to wall deposition although the net result was insignificant and is not included in this report.

CHAPTER V

Experimental Results and Discussion

The experimental results obtained during this study generally relate to two separate yet interrelated scientific fields. The first few sections of this chapter deal with the analysis of gas phase reactants and products while the later sections are concerned with the gas to particle conversion process and the growth of the newly-formed aerosol. The interrelationships are made clear throughout the treatment to follow. Extensive use has been made of tables and figures in supplementing the discussion of the experimental results.

A tabulation of the gas phase products observed by the Fourier Transform Infrared Spectrometer for eleven runs is included in the Appendix as is the listing of the observed and predicted values of the reactant concentrations as a function of time for the basic series of nineteen gas phase experiments. The droplet number, surface area and volume concentration distributions at several different times are also tabulated in the Appendix for a series of six aerosol experiments.

A. Reactant Consumption Data and Reaction Stoichiometry

Several series of olefin-ozone-sulfur dioxide experiments were conducted to obtain information relative to the stoichiometry of the olefin-ozone reaction, the influence of sulfur dioxide on the reaction, the role of molecular oxygen and the effect of varying the relative humidity on the system. A summary of the initial conditions for one series of nineteen experiments is shown in Table 5-1. Sixteen of these runs

Table 5-1. Summary of Experimental Conditions and Initial Reactant Concentrations

Propylene

Run	T(°C)	RH (%)	Olefin (ppm)	Ozone (ppm)	Sulfur Dioxide (ppm)	Olefin/Ozone
91	24	26	2.580	1.660	0	1.554
92	24	39	3.012	1.651	0	1.824
93	24	23	2.753	2.573	0	1.070
94	25	37	2.930	2.683	0	1.092
21	27	19	8.125	2.882	0	2.819
31	28	19	8.555	2.714	.5250	3.153
25	24	22	1.878	2.377	.5827	.790
26	25	22	3.547	1.080	.6206	3.284
27	25	22	3.461	.983	.1939	3.522
86	24	23	.922	1.969	.2010	.468
87	26	20	1.112	2.056	.6507	.541
88	23	25	3.281	.274	.2075	12.00
89	26	21	3.318	.295	.6373	11.26
90	25	21	2.739	1.970	.5803	1.390

Table 5-1. Continued

Run	T(°C)	RH (%)	Olefin (ppm)	Ozone (ppm)	Sulfur Dioxide (ppm)	Olefin/Ozone
			Propylene			
98	25	23	2.825	2.025	.2039	1.395
95	25	20	3.025	1.813	.5582	1.669
			Ethylene			
97	26	22	3.112	2.102	.5884	1.480
28	27	22	11.85	3.807	0	3.113
29	28	20	12.50	3.617	.5294	3.456

included propylene as the olefin species while the other three involved ethylene. The observed temperature with one standard deviation for the propylene runs was 25.1 ± 1.9°C while the measured relative humidity was 21.8 ± 2.0% for low water vapor concentration runs and 38.0 ± 1.9% for the higher level runs. The initial concentration of propylene ranged from about 0.9 to 8.6 ppm for this series and for ozone the range was from about 0.3 to 2.8 ppm. The initial sulfur dioxide concentration was in general, at one of three levels, 0.0, 0.2, or 0.6 ppm. The ratio of the initial concentrations of the two principal reactants typically ranged from about 0.5 to 3.5 with this initial olefin-ozone concentration ratio being about 12 for two of the runs.

The amount of the reactants consumed in this series of experiments is summarized in Table 5-2. Also shown is the percentage of one of the principal reactants which was consumed at the point at which the time averaged stoichiometric change was measured. This percentage generally referred to the quantity of ozone reacted as the olefin was usually in excess. Ozone was in excess, however, for runs 86 and 87 and the percentage refers to the amount of the propylene consumed. The amount of sulfur dioxide reacted ranged from about 0.02 to 0.2 ppm in this series. Only acetyaldehyde, of the stable aldehyde products formed in the olefin-ozone reaction, could be measured with the gas chromatographic arrangement used. This species, which is formed in the reaction of ozone with propylene, was followed in time for several of the experiments and the concentration value attained near the end of the run is included in Table 5-2. Due to the longer time required for the acetyaldehyde to elute from the gas chromatographic column and because of the lower sensitivity for its measurement, it was not followed on every experiment.

Table 5-2. Summary of Stoichiometric Data and Acetyaldehyde Production

Propylene

Run	ΔOL (ppm)	ΔO_3 (ppm)	ΔSO_2 (ppm)	$\Delta OL/\Delta O_3$	% O_3 Reacted	CH_3CHO (ppm)
91	1.811	1.463	0	1.238	.88	n.m.
92	1.957	1.499	0	1.306	.91	n.m.
93	1.852	2.315	0	.800	.90	n.m.
94	1.975	2.415	0	.818	.90	n.m.
21	3.917	2.610	0	1.501	.90	1.65
31	3.934	2.468	.174	1.594	.91	1.80
25	1.630	1.702	.180	.958	.72	.73
26	1.498	.978	.141	1.532	.92	.45
27	1.468	.889	.058	1.651	.90	.58
86	.817	1.050	.078	.778	.88*	n.m.
87	.954	1.109	.151	.860	.86*	.48
88	.501	.249	.022	2.011	.91	n.m.
89	.539	.270	.052	1.996	.92	n.m.
90	1.999	1.757	.205	1.138	.89	.82

Table 5-2. Continued

Run	ΔOL (ppm)	ΔO_3 (ppm)	ΔSO_2 (ppm)	$\Delta OL/\Delta O_3$	% O_3 Reacted	CH_3CHO (ppm)
Propylene						
98	2.084	1.805	.102	1.155	.89	.84
95	1.721	1.633	.165	1.054	.90	.79
Ethylene						
97	1.265	.980	.183	1.291	.47	
28	4.557	3.039	0	1.500	.80	
29	4.964	2.876	.299	1.726	.80	

n.m. not measured

* % OL Reacted

Acetyaldehyde is not a product of the reaction of ozone with ethylene and would not, therefore, be expected to be present in those runs.

The variation of concentration with time for a typical propylene-ozone-sulfur dioxide run is shown in Figure 5-1. The near 1:1 stoichiometric consumption for the two principal reactants is readily apparent in the near constant difference in their concentrations with time for this experiment. The consumption of the sulfur dioxide is markedly slower than it is for the other two reactants. The acetyaldehyde production is also shown and as it does not appear to follow linearly the loss of the propylene, the process leading to its appearance is more complex than if it were formed in a single bimolecular reaction.

The reaction involving propylene can be contrasted with a run in which ethylene was the olefin reacted with the ozone. The variation of the concentration for the reactants in the ethylene experiment is shown in Figure 5-2. The initial concentrations for this run were about the same as they were for the propylene experiment and although the same trends in consumption are observed, the reaction proceeds much more slowly.

The data listed in Tables 5-1 and 5-2 were used to plot the variation in the apparent stoichiometry of the olefin-ozone reaction with the initial reactant concentration ratio (Figure 5-3). There are a total of thirteen data points plotted which represent ozone-propylene reactions conducted in air. The line drawn through the points appears to satisfy these data and was fixed by eye. Ten of these thirteen experiments were conducted in the presence of sulfur dioxide. The presence of the sulfur dioxide had no apparent effect on the stoichiometry of the primary reaction as all of the data closely follow a smooth curve. This result indicates that the oxidative consumption of the sulfur dioxide is due to a reactive product of the propylene-ozone reaction rather than to a primary reactant

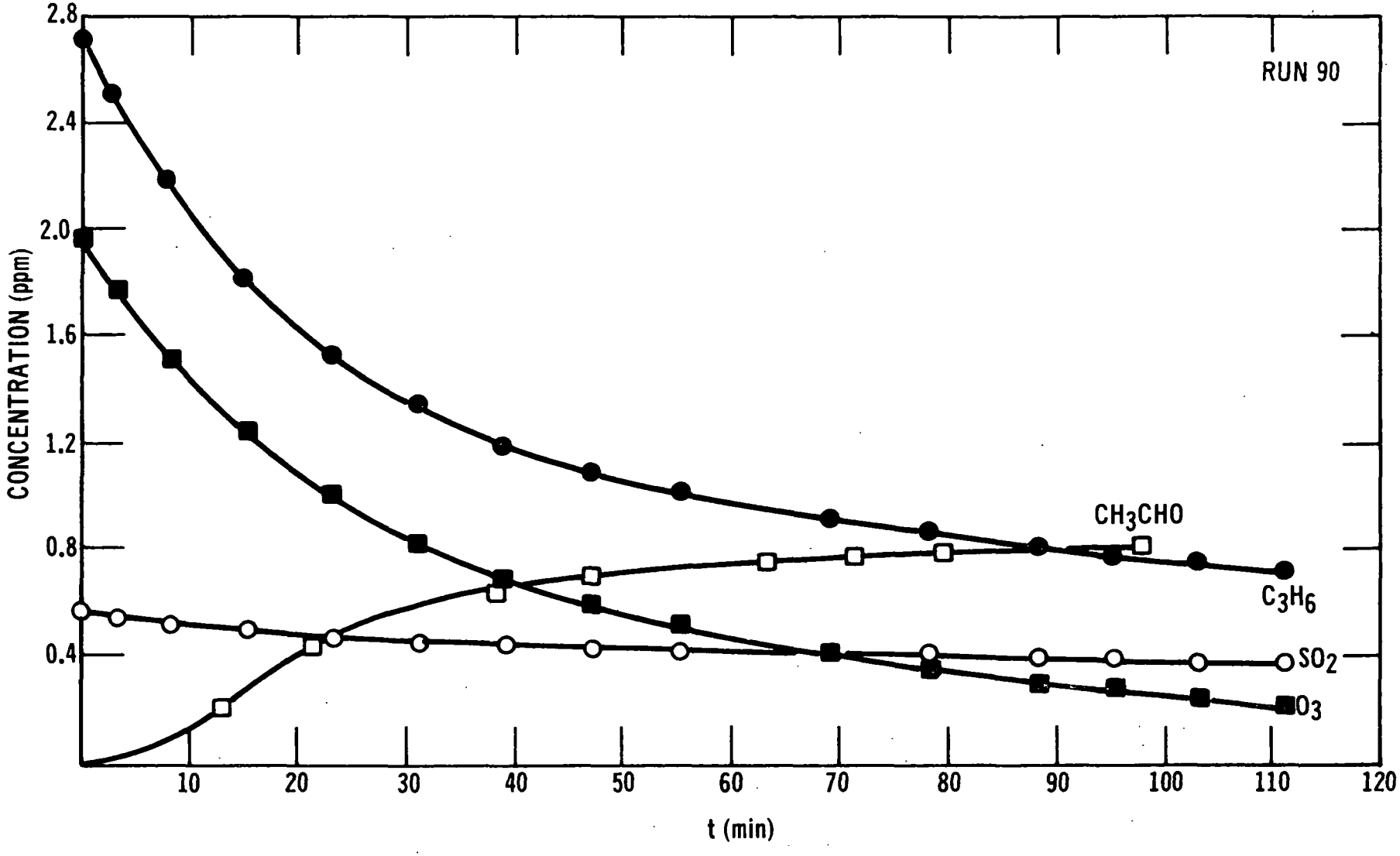

FIGURE 5-1. VARIATION OF CONCENTRATION WITH TIME FOR PROPYLENE-OZONE-SULFUR DIOXIDE REACTION.

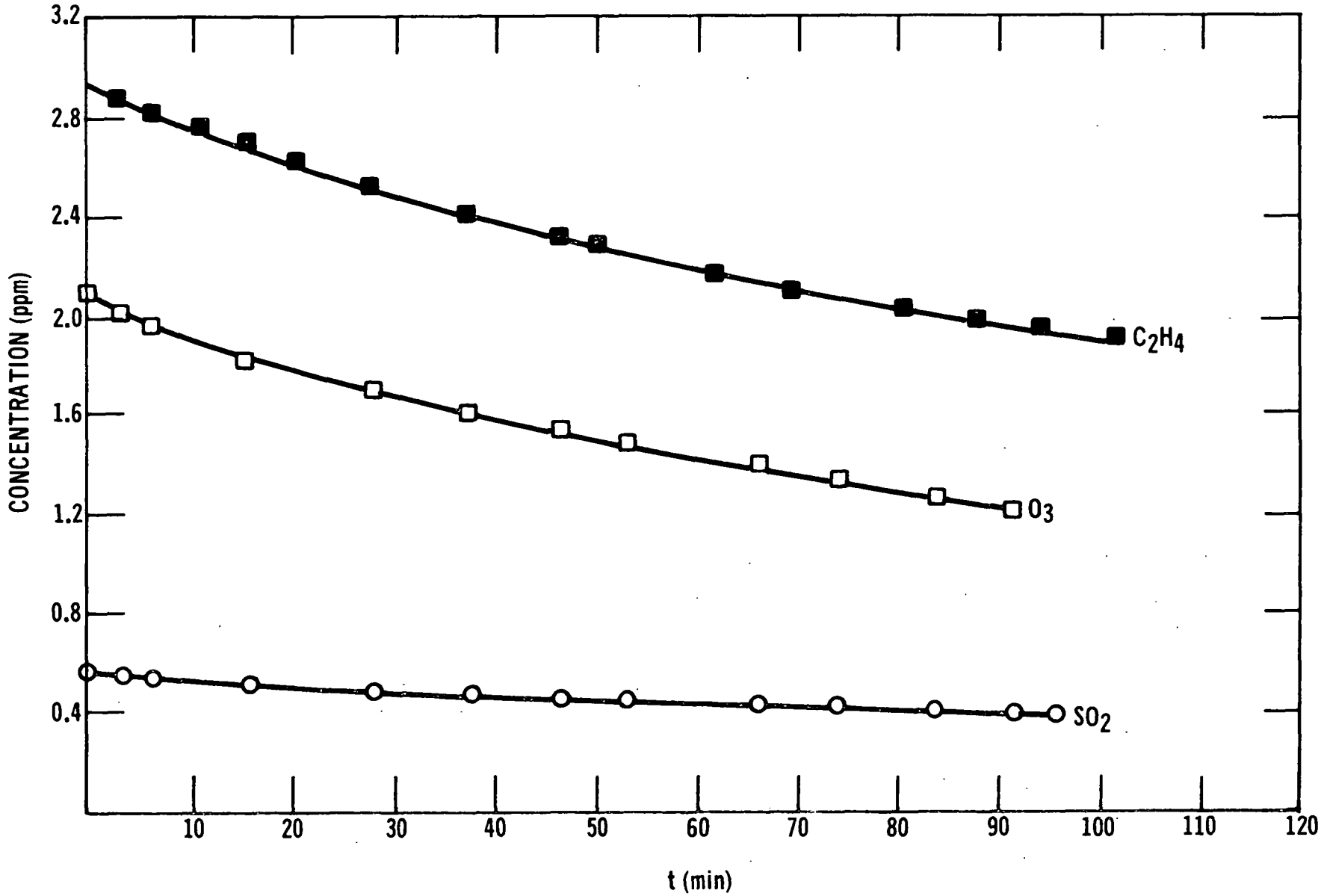

FIGURE 5-2. VARIATION OF CONCENTRATION WITH TIME FOR ETHYLENE-OZONE-SULFUR DIOXIDE REACTION.

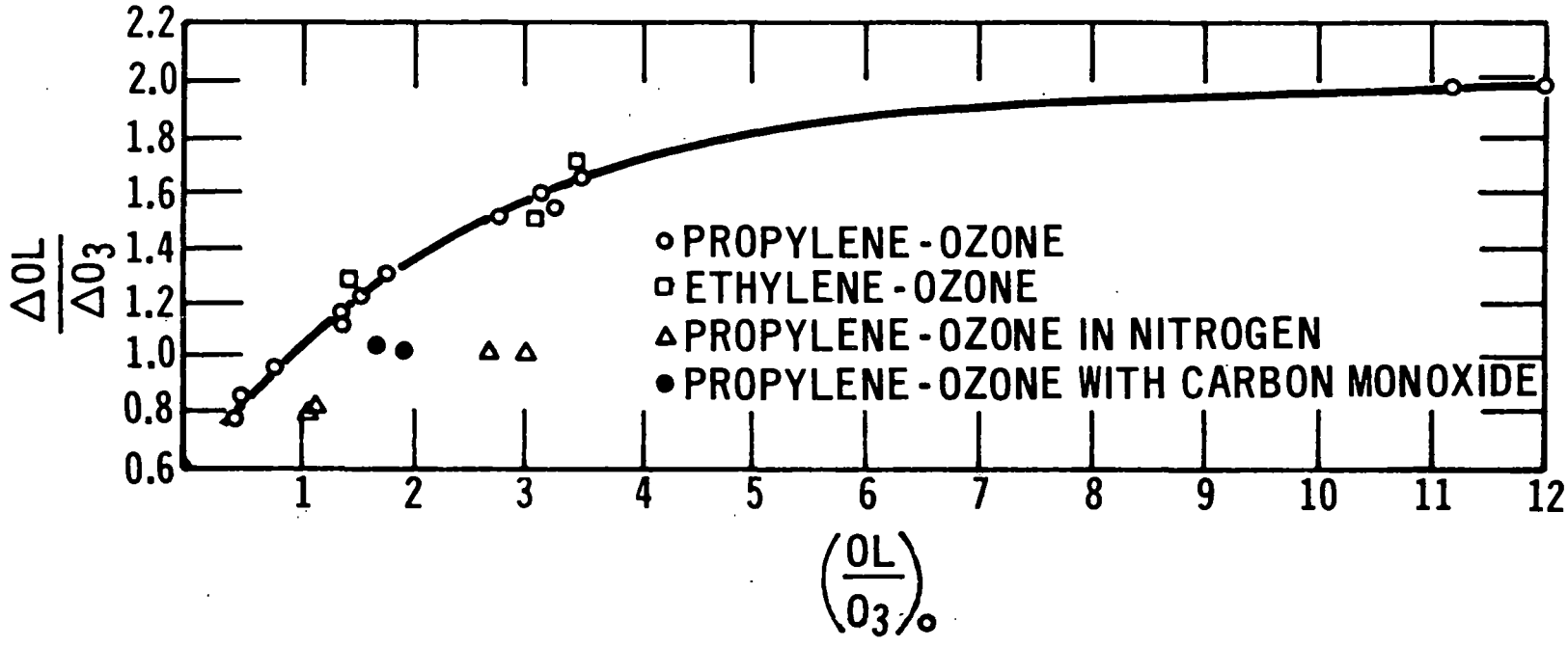

FIGURE 5-3. STOICHIOMETRY OF OLEFIN-OZONE REACTION VERSUS INITIAL REACTANT CONCENTRATION RATIO.

such as ozone. This conclusion was fully substantiated through an experiment in which ozone and sulfur dioxide were the only reactants. The consumption of those species in this experiment was slow enough so as not to be distinguished from losses attributable to wall effects.

The nature of the reactive product of the olefin-ozone reaction which results in the consumption of the sulfur dioxide has been studied by Cox and Penkett (1972). Evidence that this product is a short-lived intermediate of the primary reaction was derived from experiments in which the sulfur dioxide was introduced at different times after the initiation of the olefin-ozone reaction. When the sulfur dioxide was added after the ozone had sufficient time to react with the olefin, the aerosol formation was barely perceptible, whereas when the sulfur dioxide was initially present or added shortly after the run began, the aerosol formation was significant.

The data shown in Figure 5-3 indicate that the reaction is complicated by secondary reactions. The apparent stoichiometry of the reaction is decidedly affected by the initial concentration ratio. In general, a system which initially has propylene in excess results in a consumption ratio of the propylene to ozone greater than one while in a system which initially has an ozone excess condition the value of this ratio is less than one. These results are in general agreement with those reported by Wei and Cvetanović (1963) for experiments conducted at much higher reactant concentrations. Several olefins including propylene were studied by those investigators and the consumption ratio was found to vary from 1.4-2.0 for the different olefins in the high olefin excess system. Bufalini and Altshuller (1965) also studied a series of olefins but in concentrations much closer to values used in this study and observed a similar trend. Preliminary results from two current studies

in progress elsewhere are also in good qualitative agreement with those reported herein. One of these, directed by Williamson (1974), makes use of high initial reactant concentrations and is projected to include propylene. Initial results for the ethylene system indicate a consumption ratio of less than one for the ozone rich system and equal to or greater than one for the ethylene rich system. The other investigation is being conducted by Niki (1974) and makes use of propylene concentrations ranging from 2.0 to 5.8 ppm and ozone concentrations from about 1.4 to 8.3 ppm. The stoichiometry which they have observed for these propylene studies ranges from 0.9:1 to 1.4:1. For the study reported herein, the consumption ratio varies over the range of experimental conditions used from about 0.8 to 2.0 and it appears to approach this latter value as a limit. When a condition of initial ozone excess exists, these data would support a postulate that either ozone is interacting with products of the primary olefin-ozone reaction or that propylene is being produced. Similarly for a system which is initially rich in propylene these data could support a postulate that propylene interacts with a reactive product of the initial reaction and/or that ozone is being produced as a result of a secondary reaction. A reaction that could result in the production of ozone is shown as reaction 13, Chapter II, as postulated by Bufalini and Altshuller (1965) and involves an interaction of the reactive intermediate with molecular oxygen.

The three ethylene-ozone-sulfur dioxide experiments are also included in Figure 5-3. These data follow the same general trend as do the data from the propylene system and the slightly increased scatter is believed due to the method of olefin introduction into the reactor. The propylene was metered into the system at a constant rate for the entire reactor filling period while the ethylene was injected via a septum into the

diluent gas stream. It appears that the sulfur dioxide is oxidized by a reactive product of the primary reaction in the ethylene system in analogy to the oxidative process in the propylene system.

The molecular oxygen concentration was sharply reduced for several runs in an attempt to determine whether oxygen has a role in the reaction. The results of four of these experiments in which nitrogen was used as the diluent gas are recorded on Figure 5-3. An obvious reduction in the propylene to ozone consumption ratio occurred indicating that molecular oxygen plays a significant role in modifying the consumption of one or both of the primary reactants. This result runs contrary to that reported recently by Cox and Penkett (1972) and Stedman et al. (1973). Those investigators concluded as a result of their studies that molecular oxygen does not affect the stoichiometry of the primary olefin-ozone reaction.

Wei and Cvetanović (1963) studied the reaction of high concentrations of several olefins including propylene with ozone in the gas phase both in the presence and in the absence of molecular oxygen and found a lower consumption ratio in the absence of the oxygen. Data collected in the current study by Niki (1974) led him to the conclusion that oxygen has a pronounced effect on the olefin-ozone system.

The observation of this molecular oxygen effect has led to the postulate that a secondary attack on the propylene is occurring in this reaction. As the consumption ratio changes in the presence or absence of molecular oxygen, a secondary attack on the olefin by the reactive intermediate can be eliminated as being responsible for the stoichiometric change. Other reactions which could account for the oxygen effect and the deviation from 1:1 stoichiometry are those which involve an interaction of the intermediate species and molecular oxygen, e.g., reactions 11-13

in Chapter II-B. The products are the hydroxyl and the peroxyacetyl radicals, the methyl radical, carbon dioxide and the hydroperoxy radical, and ozone and acetylaldehyde for the three reactions respectively. Each of these reactions, therefore, results in the production of a species capable of further interacting with the olefin in a chain propagating reaction. The three species formed also react with carbon monoxide although the rate constant for the reaction of the hydroxyl radical with carbon monoxide is approximately 10^6 times greater than the reaction with the hydroperoxy radical and about 10^{12} greater than the reaction of carbon monoxide with ozone. The addition of an appropriate concentration of carbon monoxide to serve as a scavenger in the system should, therefore, provide a convenient method of testing for the formation and presence of the hydroxyl radical. As the hydroxyl radical would also react with the olefin and sulfur dioxide in the system in addition to any aldehydes formed and other minor products of the olefin reaction, a sufficient carbon monoxide concentration was needed to affect the overall reaction stoichiometry significantly. In other words, it was desired to cause the loss of the hydroxyl radical, if present, to be greater in its reaction with carbon monoxide than its total loss in all of its other possible reactions. This can be expressed in functional form as

$$k_{18}\,[\cdot OH][CO] \geq [\cdot OH]\,\{k_{14}[C_3H_6] + k_{16}[CH_3CHO] + k[SO_2] + \ldots\} \qquad \text{V-1}$$

The right hand side of this expression is dominated by the olefin reaction because of the magnitude of k_{14} and a typical olefin concentration used in these studies. For an initial propylene concentration of 3 ppm, for example, a carbon monoxide concentration of about 300 ppm would cause the loss of the hydroxyl radical to be equal to the loss from the total of the other reactions.

Two experiments in which 458 ppm of carbon monoxide was added to the propylene-ozone-sulfur dioxide system were conducted and the stoichiometric results are included in Figure 5-3. These results substantiate the postulate relative to the formation of the hydroxyl radical in this reaction and its subsequent secondary attack on the olefin species.

One final result included graphically in Figure 5-3 is the lack of an effect of a change in the relative humidity on the olefin-ozone reaction over the range studied. The propylene runs included one experiment conducted in air and two in nitrogen for which the relative humidity was elevated to about 38 percent. Cox and Penkett (1972) observed a water vapor concentration effect on the sulfur dioxide consumption with a decrease in the sulfur dioxide oxidation rate occurring with increasing relative humidity. The data from two runs in the study reported herein showed a slight but similar trend. The consumption of sulfur dioxide in run 60, which was conducted in an atmosphere at 20 percent relative humidity, was 0.071 ppm/ppm of ozone consumed while for run 65 conducted at a relative humidity of 36 percent, this ratio was 0.066 ppm/ppm of ozone consumed. The products of these two experiments as measured with the infrared spectrometer do not reflect an effect due to the variation in the relative humidity.

The acetyaldehyde concentration produced in several of the experiments was plotted against the amount of propylene reacted (Figure 5-4). Each of the data points represents a separate run. The measurements of both the olefin and the aldehyde were made at the same time, late in the experiments. The line drawn was determined by fitting the data to a linear function by the method of least squares. The slope of the regression line forced through the origin is 0.44 which also indicates the mean yield of acetyaldehyde in these reactions. The data included are

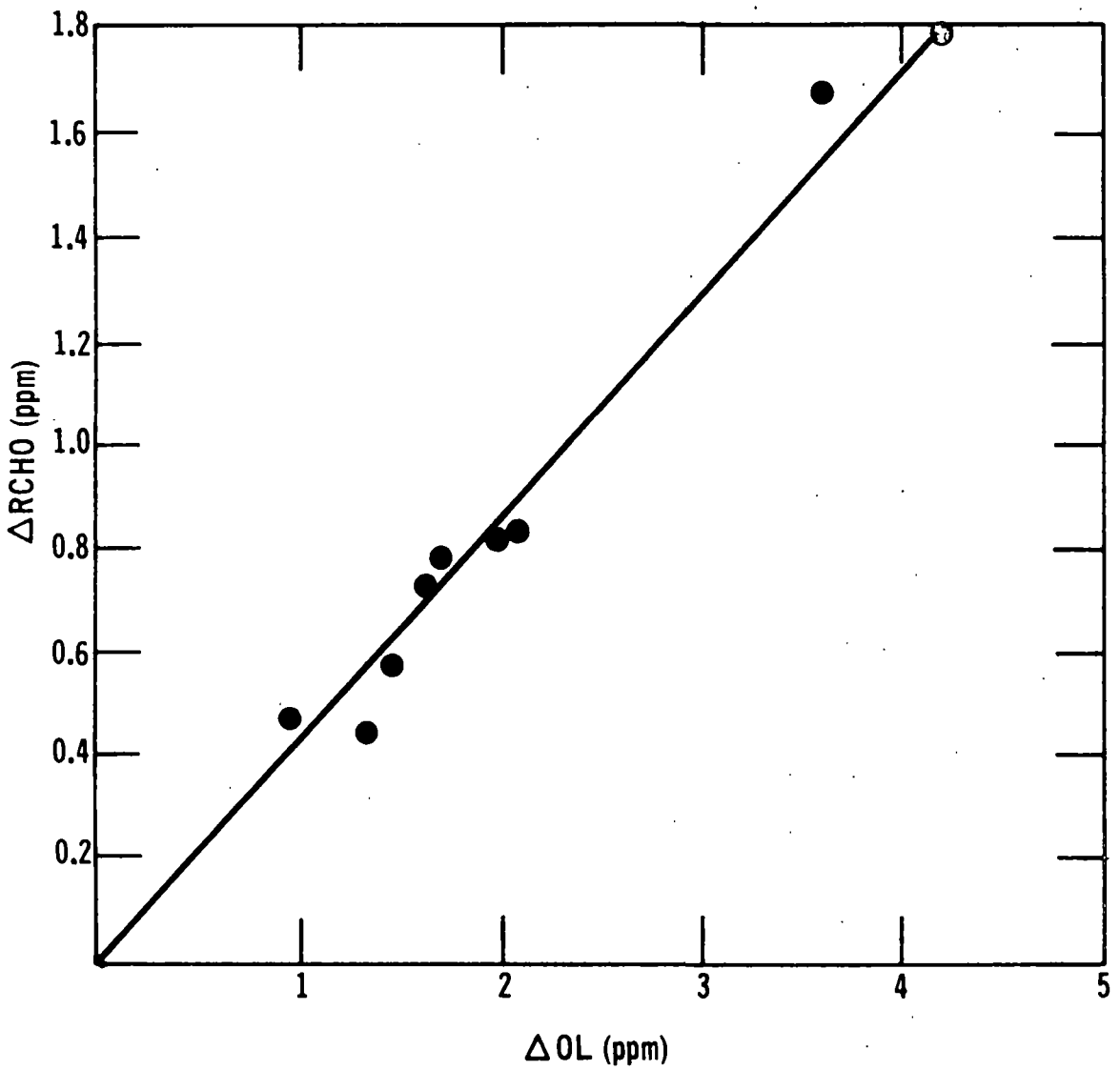

FIGURE 5-4. CONCENTRATION OF ACETYALDEHYDE PRODUCED VERSUS PROPYLENE REACTED FOR NINE PROPYLENE-OZONE EXPERIMENTS.

from experiments conducted in the presence of sulfur dioxide, the oxidative step of which purportedly produces acetyaldehyde. The contribution from that step amounted to approximately thirteen percent according to data from runs 30 and 21 reported in the product analysis table in the Appendix. Making an adjustment for the contribution from the sulfur dioxide oxidation reaction the modified production of 0.38 ppm of acetyaldehyde per ppm of propylene reacted is in close agreement with the results reported by Scott et al. (1957) and Wei and Cvetanović (1963).

A relationship between the consumption of the sulfur dioxide and one or both of the primary reactants was also sought. Using the data from runs in which the initial olefin to ozone concentration ratio was equal to or greater than one, the plots shown in Figures 5-5 and 5-6 were developed. By including the initial sulfur dioxide concentration in the plot, it can be seen from Figure 5-5 that an apparent linear relationship can be established between the formation of the sulfur species and the olefin reacted. These lines were constructed by fitting the data by the method of least squares and forcing the regression line through the origin. The sulfur dioxide concentrations employed in this analysis with one standard deviation were 0.605 ± 0.028 and 0.202 ± 0.007 ppm. The data plotted in Figure 5-6 demonstrate the non-linearity of the relationship between the amounts of ozone consumed and the sulfur dioxide produced. These data further enforce the postulate concerning the identity of the oxidizing species for the sulfur dioxide as being a reactive product of the propylene reaction.

The data plotted in Figure 5-3 and previously discussed show that the stoichiometry of the propylene-ozone reaction for these experiments was generally other than 1:1. As the reactant consumption ratio dropped when the partial pressure of the molecular oxygen was reduced, it was

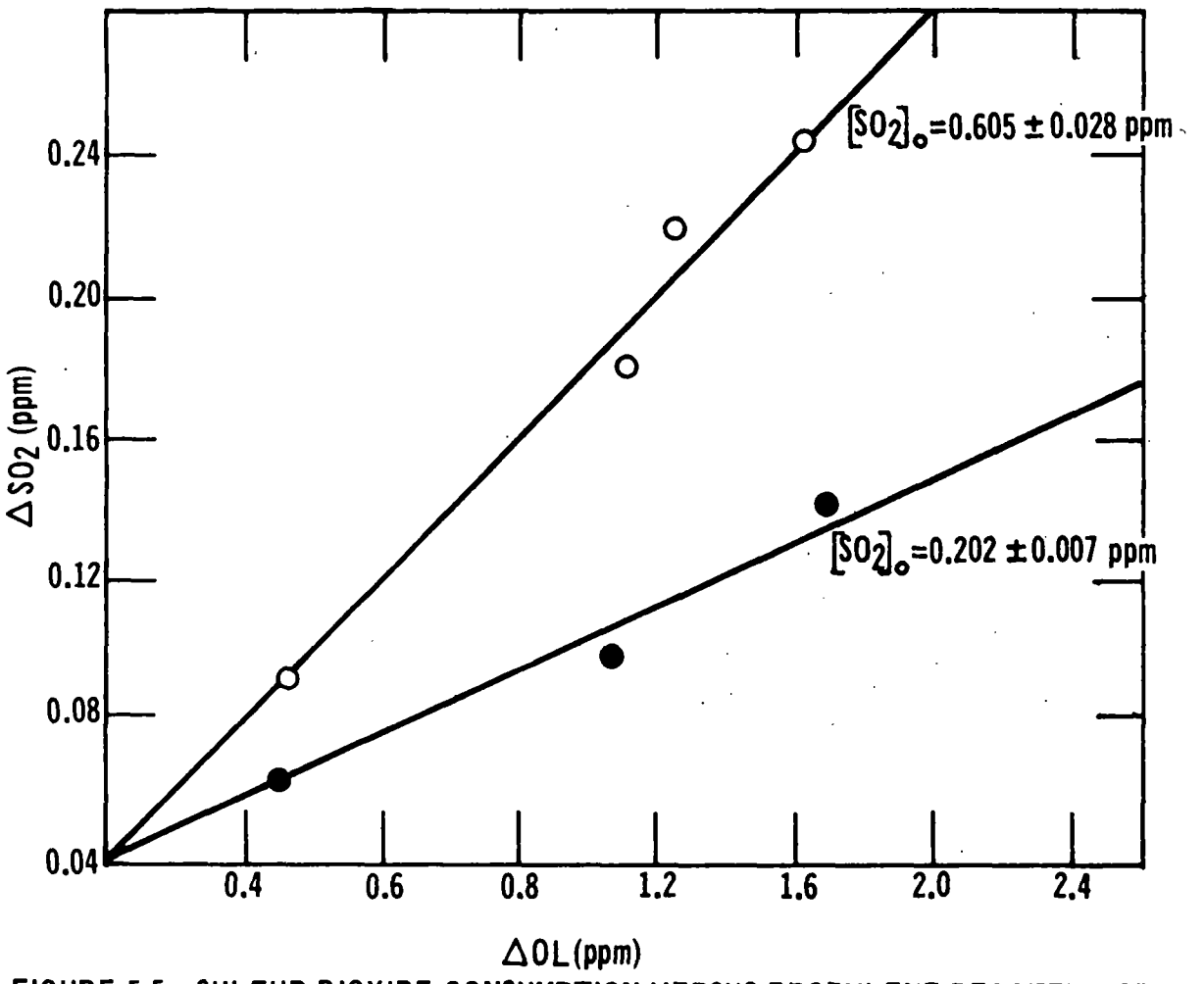

FIGURE 5-5. SULFUR DIOXIDE CONSUMPTION VERSUS PROPYLENE REACTED FOR DIFFERENT INITIAL SULFUR DIOXIDE CONCENTRATIONS.

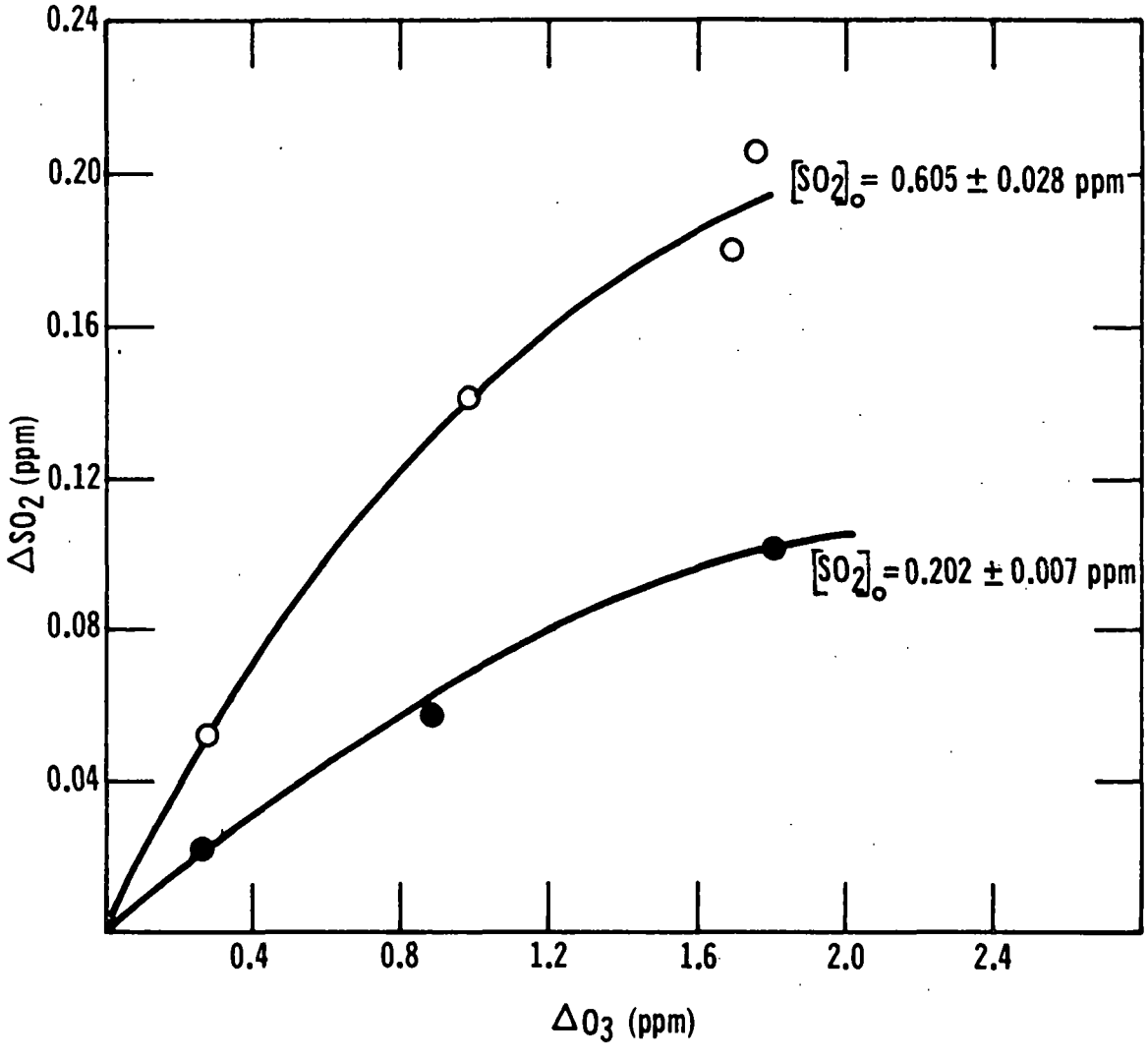

FIGURE 5-6. SULFUR DIOXIDE CONSUMPTION VERSUS OZONE REACTED FOR DIFFERENT INITIAL SULFUR DIOXIDE CONCENTRATIONS.

speculated that ozone and/or the hydroxyl radical were being produced in the reaction of a product of the ozone-propylene reaction with oxygen. The reduction of the reactant consumption ratio when the carbon monoxide was added enforced the speculation relative to the formation of the hydroxyl radical which was subsequently scavenged by the carbon monoxide. These measurements do not, however, demonostrate whether the change in stoichiometry with the changing propylene/ozone initial condition is due to the production of propylene, enhanced consumption of ozone or to an interaction of these species with reaction products. To investigate further the reaction mechanism with regard to the stoichiometry, the variation of the functions $\frac{R_{OL}}{[OL][O_3]}$ and $\frac{R_{O3}}{[OL][O_3]}$ with time was noted. If the only reactions involving these species were with each other then $R_{OL} = R_{O3}$ and the plots of the rate over reactant product versus time would yield a straight line of zero slope, and the value of the function would be equal to the second order rate constant. If, however, a plot of one of the functions initially displays a negative slope, then that species is being produced in the reaction according to

$$\frac{-R_{O3}}{[OL][O_3]} = k_1 - k_2 \frac{[A][B]}{[OL][O_3]} \qquad \text{V-2}$$

where $[A][B]$ = product of the concentration of reactants A and B leading to the ozone production and

k_2 = rate constant of the hypothetical bimolecular reaction.

Conversely, if a plot of one of the functions were to display a positive slope initially then that species is being consumed by another process as

$$\frac{-R_{OL}}{[OL][O_3]} = k_1 + k_2 \frac{[A]}{[O_3]} \qquad \text{V-3}$$

The variation of these two functions with time for run 98 is shown

in Figure 5-7. The resultant curves are typical for the series of experiments conducted in that the R_{OL} function, i.e., the function which includes R_{OL}, increases with time to some maximum and then decreases to a value that is approximately equal to that of the R_{O3} function. The function which includes R_{O3} also increases with time but at a much slower rate and without the peak typical of the other curve. The values of the functions at the reported zero time are approximately equal and represent the rate constant for the propylene ozone-reaction.

Some mention is warranted, at this point, on how the derivatives of the reactant concentrations with respect to time were estimated. The first five data points were fitted to a second order polynomial from which the value of the third point and its derivative were estimated. The first observed data point was then dropped and the sixth added to establish a new set of five data points to be fitted. This operation was continued through the total set of data collected and was performed using a computer program of the Statistical Analysis System (SAS) (Service, 1972). Values required which were beyond the range of the observed data were estimated by extrapolation. This latter feature was implemented repeatedly during this study to obtain the concentration and rate at the zero time.

One additional factor affecting the absolute accuracy of the initial R_{OL} and R_{O3} values is the fact that the primary reaction actually commenced at a time prior to the zero time reported on these plots. The reported zero time, as previously indicated, was taken as the time at which the reaction vessel became full.

Data of the type reported in Figure 5-7 provide a measure of the second order rate constant for the propylene-ozone reaction and yield semi-quantitative information on the reaction stoichiometry. The reaction

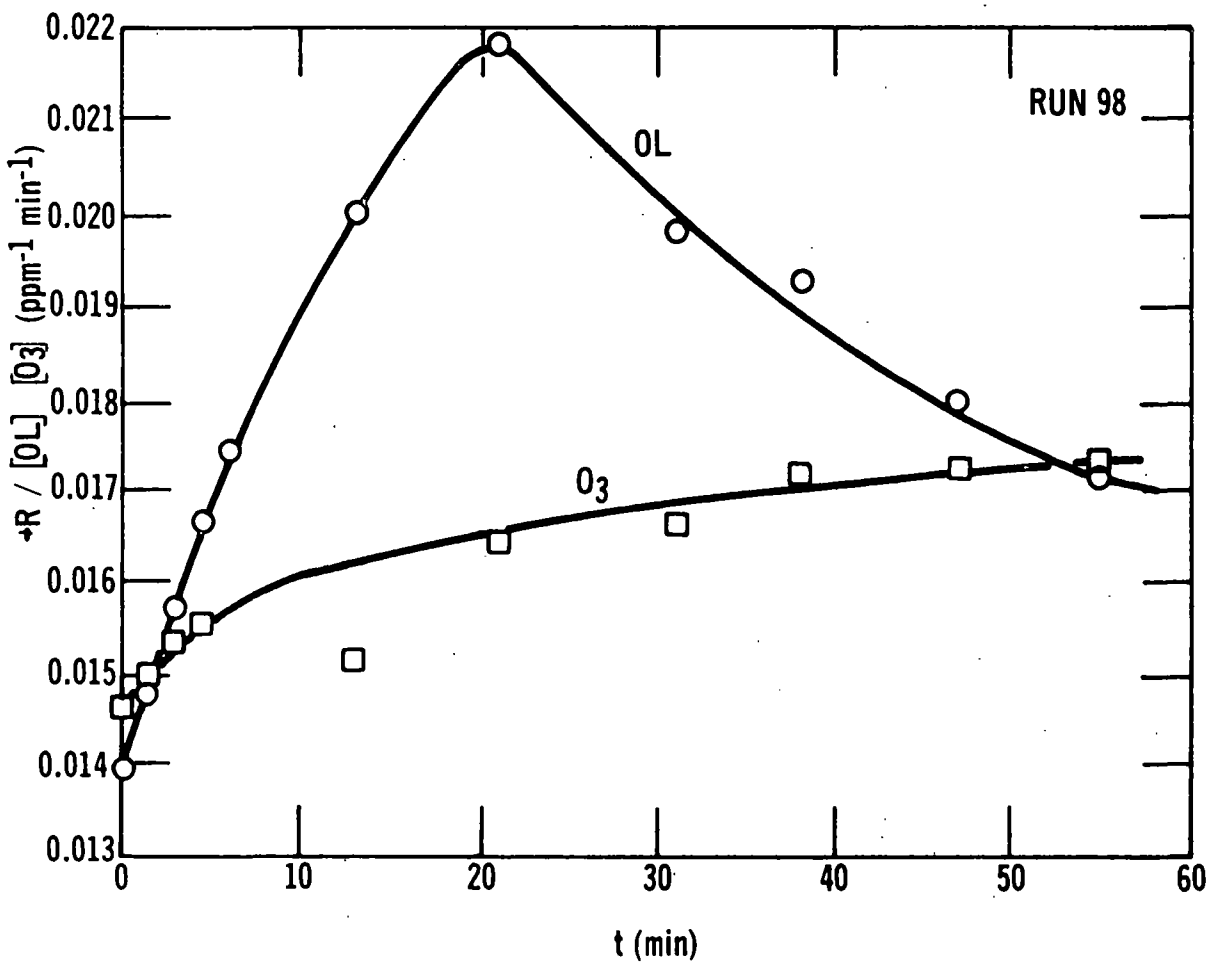

FIGURE 5-7. VARIATION OF THE APPARENT RATE CONSTANT WITH TIME DUE TO SECONDARY REACTIONS.

which involves R_{O3} is observed in the figure to increase with time suggesting that ozone is being consumed by a product of the principal reaction. The postulated generation of ozone by a secondary reaction, e.g., the reaction of the unstable intermediate with molecular oxygen, is either nonexistent or is completely masked by the enhanced ozone consumption. The product or products responsible for the additional loss of ozone are unidentified at this time but are known not to include the products measured and reported later in this paper. The rate of reaction of ozone with the aldehydes and carbon monoxide is too slow to be of significance while the yield of the other products is too low to influence the disappearance of the ozone. The slowness of the acetyaldehyde-ozone reaction relative to that of propylene with ozone was confirmed by conducting one experiment with acetyaldehyde and ozone as the sole reactants. The rate of loss of the ozone in the system with the aldehyde was such that over the lifetime of a typical experiment in this series it could not be distinguished from the first order loss of the ozone to the walls of the reactor. An equation of the form of V-3 may itself be symbolic with the second term representing several reactions.

The other curve in Figure 5-7 indicates that propylene is also being subjected to a secondary reaction. The postulate concerning the formation of the hydroxyl radical in a reaction involving the intermediate species and molecular oxygen can be used to explain that curve. As the hydroxyl radical is formed and reacts with propylene the function plotted rises to its maximum value. Formaldehyde and acetyaldehyde are produced in the propylene-ozone reaction and eventually compete for the hydroxyl radical causing the function $\frac{-R_{OL}}{[OL][O_3]}$ to diminish to some equilibrium value.

The value of k_1 based on the propylene rate data for run 98 was 1.46×10^{-2} ppm^{-1} min^{-1} and based on the ozone rate data was 1.39×10^{-2} ppm^{-1} min^{-1}. The mean and one standard deviation for k_1 computed from the thirteen runs conducted in air and based on the rate of change in the ozone concentration was $1.40 \pm .38$ ($\times 10^{-2}$ ppm^{-1} min^{-1}). For these runs, the function $\frac{-R_{OL}}{[OL][O_3]}$ was generally equal to or greater than $\frac{-R_{O3}}{[OL][O_3]}$ while for the runs conducted in the reduced oxygen atmosphere this relationship was reversed. This trend indicates that the relative rate of olefin involvement in secondary reactions had diminished with the oxygen depletion.

The initial olefin/ozone concentration ratio was 12 for run 88 and, therefore, the ozone would be expected to behave in a pseudo first order rate. The initial concentration of the ozone was 0.27 ppm and the R_{O3} function was essentially constant displaying only a slight increase over the period of the experiment. The first order rate constant for run 88 based on ozone was 1.34×10^{-2} ppm^{-1} min^{-1}.

B. Product Analysis

An inventory of the products formed in the gas phase reactions of propylene with ozone, propylene-ozone-sulfur dioxide, ethylene with ozone and ethylene-ozone-sulfur dioxide was conducted by studying the infrared absorption spectrum of the gaseous components in the reactor at a time when approximately 90% of the ozone had been reacted (80% for the ethylene runs). The volume of the glass sample cell was about 60 liters and long infrared absorption path lengths were achieved by 'folding' the beam with mirrors placed near the ends of the cell. The operation of the Fourier Transform Infrared Spectrometer is described in Chapter IV-B,6. Before each experimental run, a reference or background

spectrum of the properly humidified diluent gas was obtained and the sample spectrum from the run was subsequently ratioed against this background measurement. The ratio recording technique eliminates many of the interferences which may otherwise obscure the regions of interest and increases the detectability limits for the system.

Ratio recordings for three spectral regions, 700-1200 cm^{-1}, 2000-2300 cm^{-1} and 2600-3000 cm^{-1}, are shown in Figure 5-8 for runs 21 and 31. The infrared absorption path length for both of these measurements was 160 m through air at one atmosphere which contained the products of the propylene-ozone and the propylene-ozone-sulfur dioxide runs respectively. Spectral regions which include strong water and carbon dioxide absorption bands were excluded from these measurements because of the significant interference which they cause on quantitative product analysis. The concentrations of the identified product compounds calculated from the spectrum which appears at the top of Figure 5-8 are 0.94 ppm carbon-monoxide, 3.44 ppm formaldehyde, 1.59 ppm acetyaldehyde and a trace amount of formic acid. The regions of primary propylene, formaldehyde and acetyaldehyde absorption are marked with a range bar and the prominent absorption peak(s) used in the calculation are identified. The lower spectrum in Figure 5-8 is for the experiment (run 21) conducted without any sulfur dioxide. The product concentrations calculated from this spectrum are 0.93 ppm for carbon monoxide, 3.21 ppm for formaldehyde, 1.49 ppm for acetyaldehyde, 0.2 ppm for ketene and again a trace of formic acid was observed.

A ratio plot with scale expansion of the region from 2000-2300 cm^{-1} for the two experimental runs is shown in Figure 5-9. The scale expansion technique tends to make the absorption lines more obvious without increasing the background noise. The upper spectrum shows the carbon monoxide

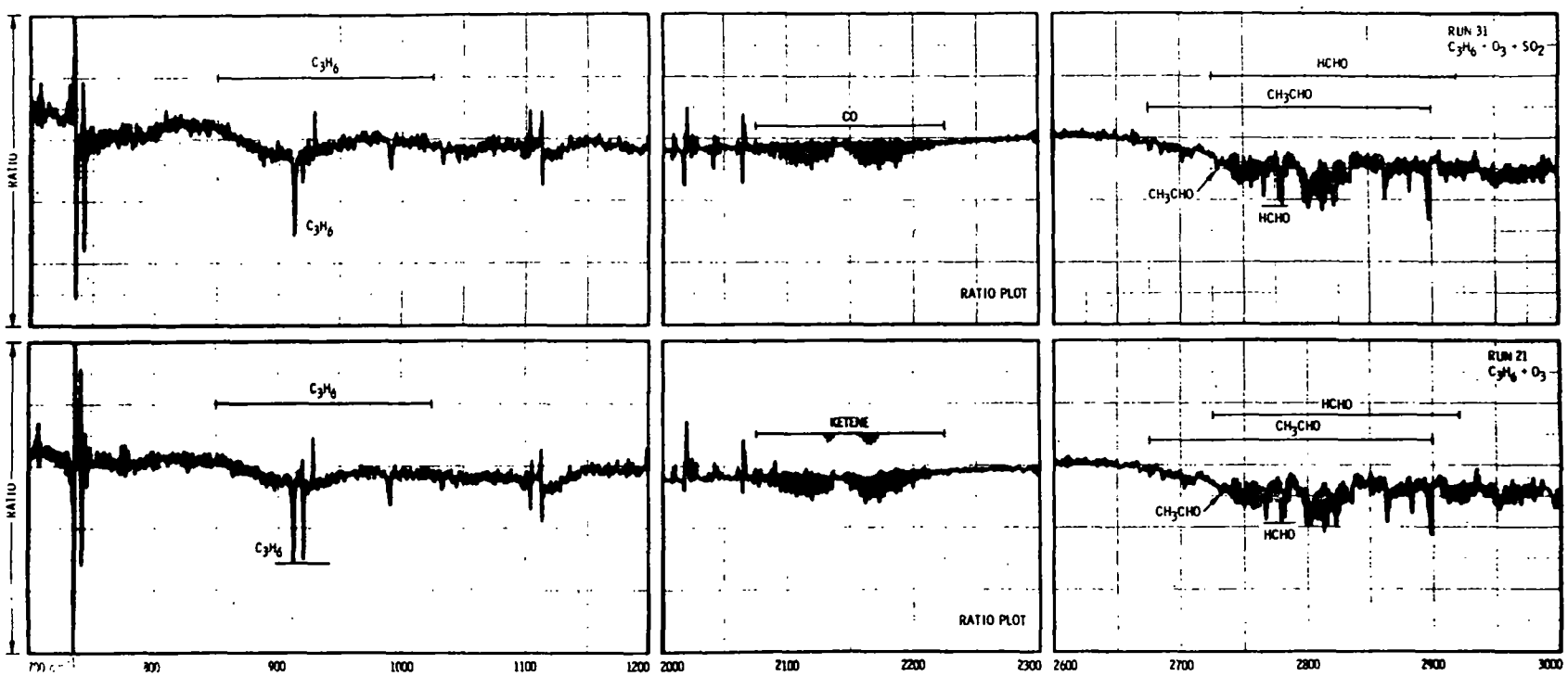

FIGURE 5-8. INFRARED ABSORPTION SPECTRA OF REACTOR CONTENTS.

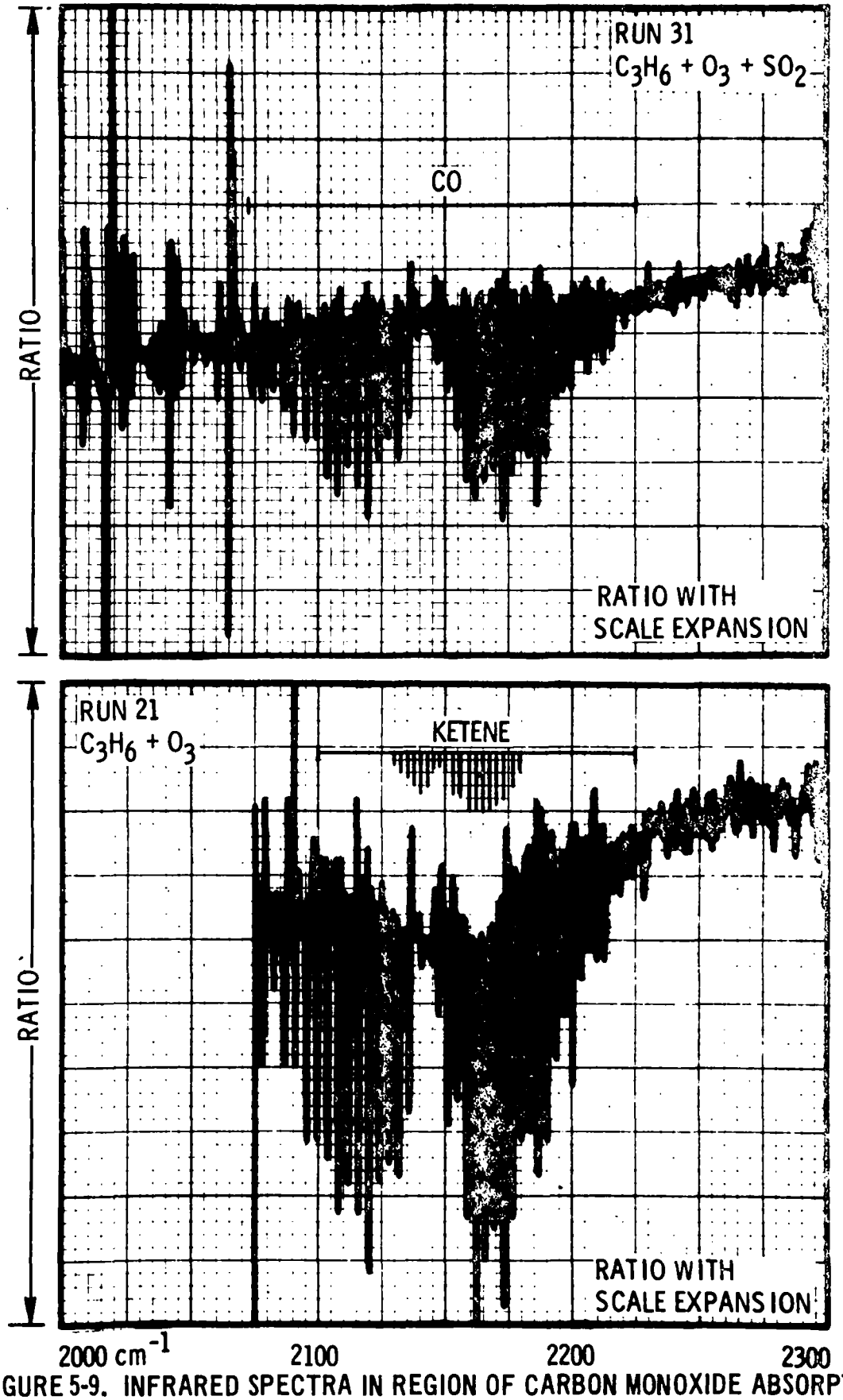

FIGURE 5-9. INFRARED SPECTRA IN REGION OF CARBON MONOXIDE ABSORPTION.

continuum for the run conducted in the presence of sulfur dioxide while the lower plot shows a ketene spectrum superimposed on the carbon monoxide continuum for the run which did not include sulfur dioxide. The ketene is identified by the double indentation on the carbon monoxide continuum with the right lobe characteristically being slightly deeper and broader. The appearance of ketene as a product of the propylene-ozone reaction has been previously reported (Scott et al., 1957) and has been postulated to result from the disassociation of the acetyl form of the zwitterion species (Leighton 1961) as shown by reaction 5 in Chapter II-B. The dramatic disappearance of the ketene spectrum in the presence of sulfur dioxide indicates that the reaction rate of the oxidizing species with the sulfur dioxide is much faster than is the rate of the decomposition reaction.

Ratio plots, with scale expansion of the spectral region which includes ketene, for two additional propylene-ozone experiments conducted in air at one atmosphere are shown in Figure 5-10. The relative humidity in the reactor was approximately 19% for run 78 and 33% for run 79. The presence of ketene in both of these runs and at approximately the same concentration is readily apparent. Nitrogen was used as the diluent gas for the product spectra shown in Figure 5-11. Run 81 was conducted in an atmosphere at 36% relative humidity while the relative humidity for run 82 was about 20%. The formation of ketene in those runs in an atmosphere with a sharply depleted molecular oxygen content is also apparent. Ratio plots of two more runs conducted in the presence of sulfur dioxide are shown in Figure 5-12 for which the relative humidity was 20 and 36% respectively. There is no ketene observable in these product absorption spectra nor in that of run 31 previously discussed.

Ratio recordings of the three spectral regions, 700-1200 cm^{-1},

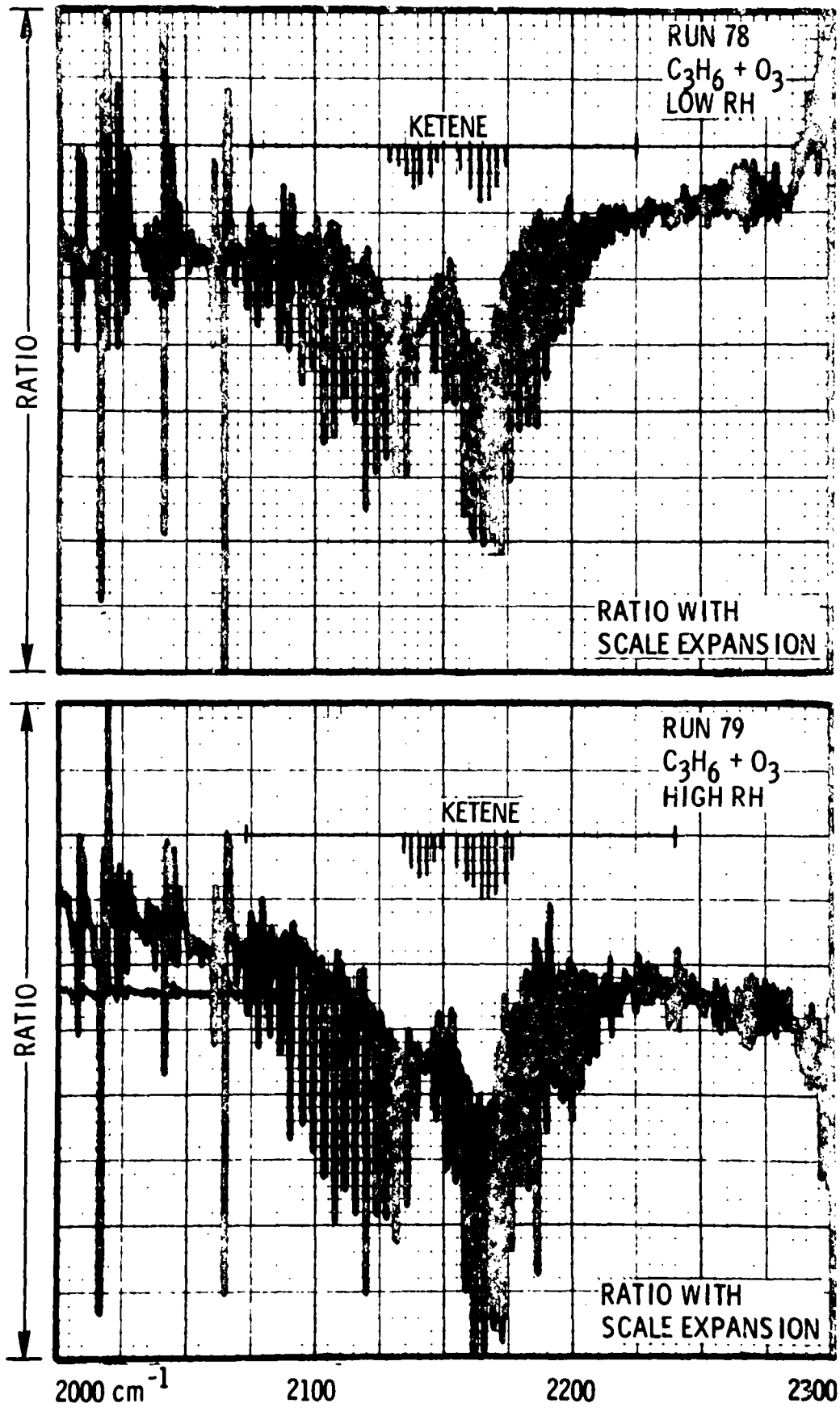

FIGURE 5-10. INFRARED SPECTRA IN REGION OF CARBON MONOXIDE ABSORPTION.

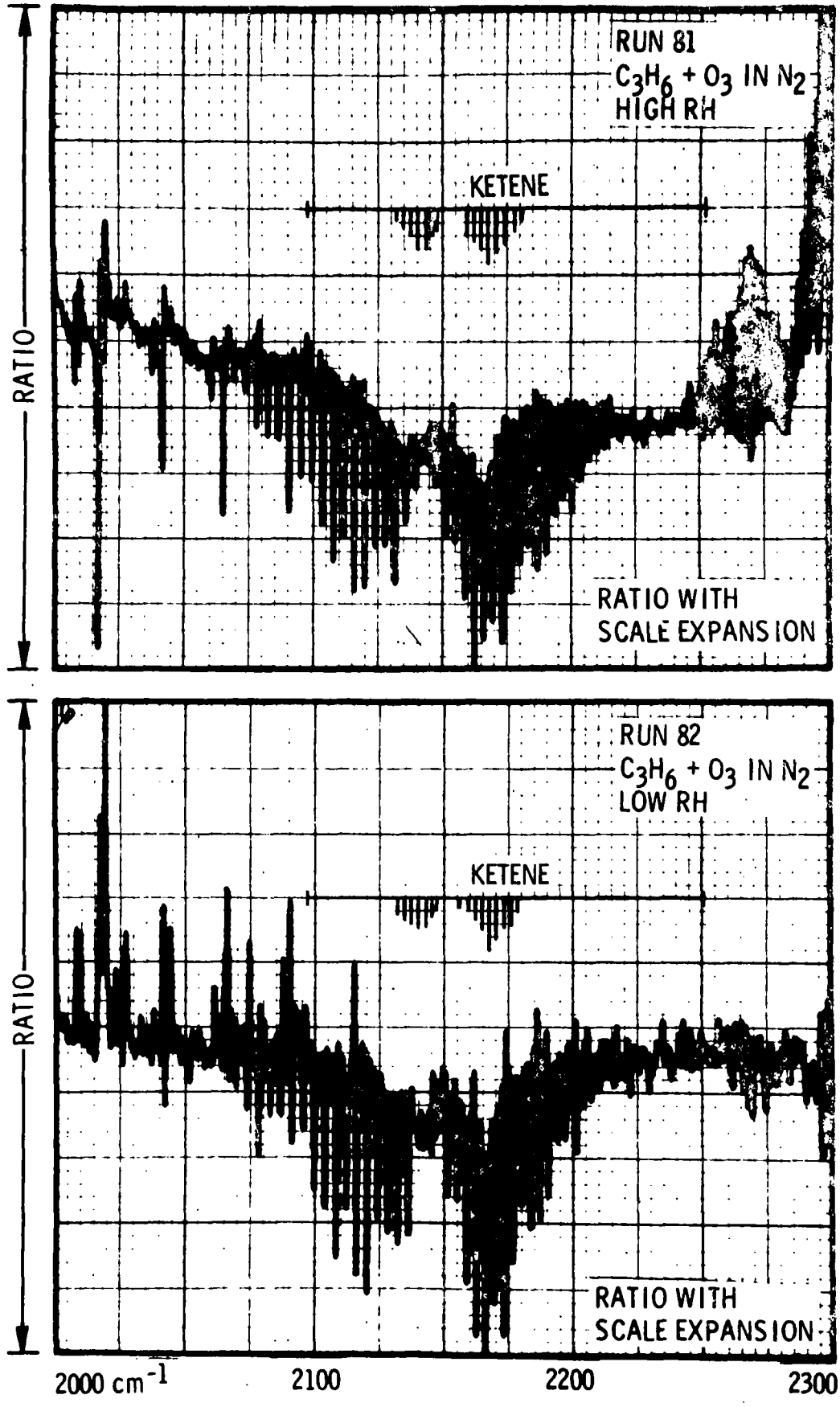

FIGURE 5-11. INFRARED SPECTRA IN REGION OF CARBON MONOXIDE ABSORPTION.

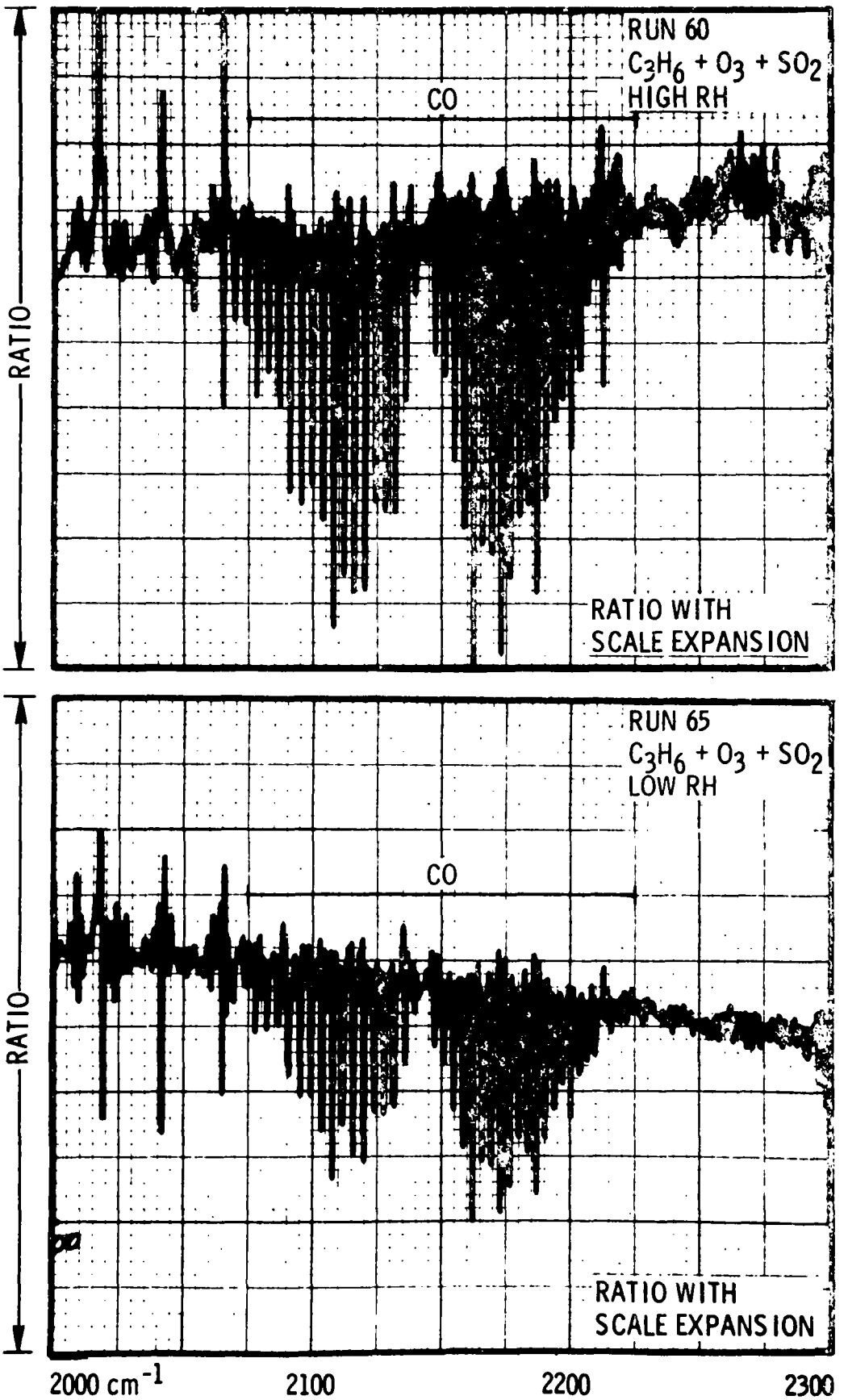

FIGURE 5-12. INFRARED SPECTRA IN REGION OF CARBON MONOXIDE ABSORPTION.

2000-2300 cm^{-1} and 2600-3000 cm^{-1} for two ethylene-ozone reactions are shown in Figure 5-13. Sulfur dioxide was included as a reactant in run 29 recorded in the lower spectrum. The products observed from these reactions are carbon monoxide, formyaldehyde, and in the case of Run 28 (without sulfur dioxide), a trace of formic acid. For Run 29, a quantifiable amount of formic acid was observed at approximately 1130 cm^{-1}.

The results of the product identification and measurement for all of the experiments analyzed by the Fourier transform spectroscopic method are listed in the Appendix. The concentration values tabulated are in parts per million (ppm) and were calculated by applying the Lambert-Beer equation to the absorption spectra as discussed in Chapter IV-B,6. A more detailed product evaluation is contained in Table 5-3 for eight of these runs. The run identification number, the relative humidity and the product concentration expressed as ppm product per ppm of ozone reacted are tabulated. The error term noted below each product species is based on the confidence with which the absorption coefficients used in the measurements are known and does not relate to the measurement itself. The absorption coefficient for ketene was not measured due to difficulties encountered in the quantitative isolation of pure ketene for calibration purposes. The value used for this species is, therefore, a best estimate (Gay, 1974) and the error term is believed to be realistic.

An evaluation of data in Table 5-3 shows that the production of carbon monoxide is unaffected by the addition of sulfur dioxide to the system. Analogous to the formation of ketene from the decomposition of the acetyl form of the intermediate species, carbon monoxide and water were speculated as forming from the decomposition of the formyl form of that species. For this analogy to hold, a higher concentration of carbon monoxide would be expected in the absence of sulfur dioxide. This

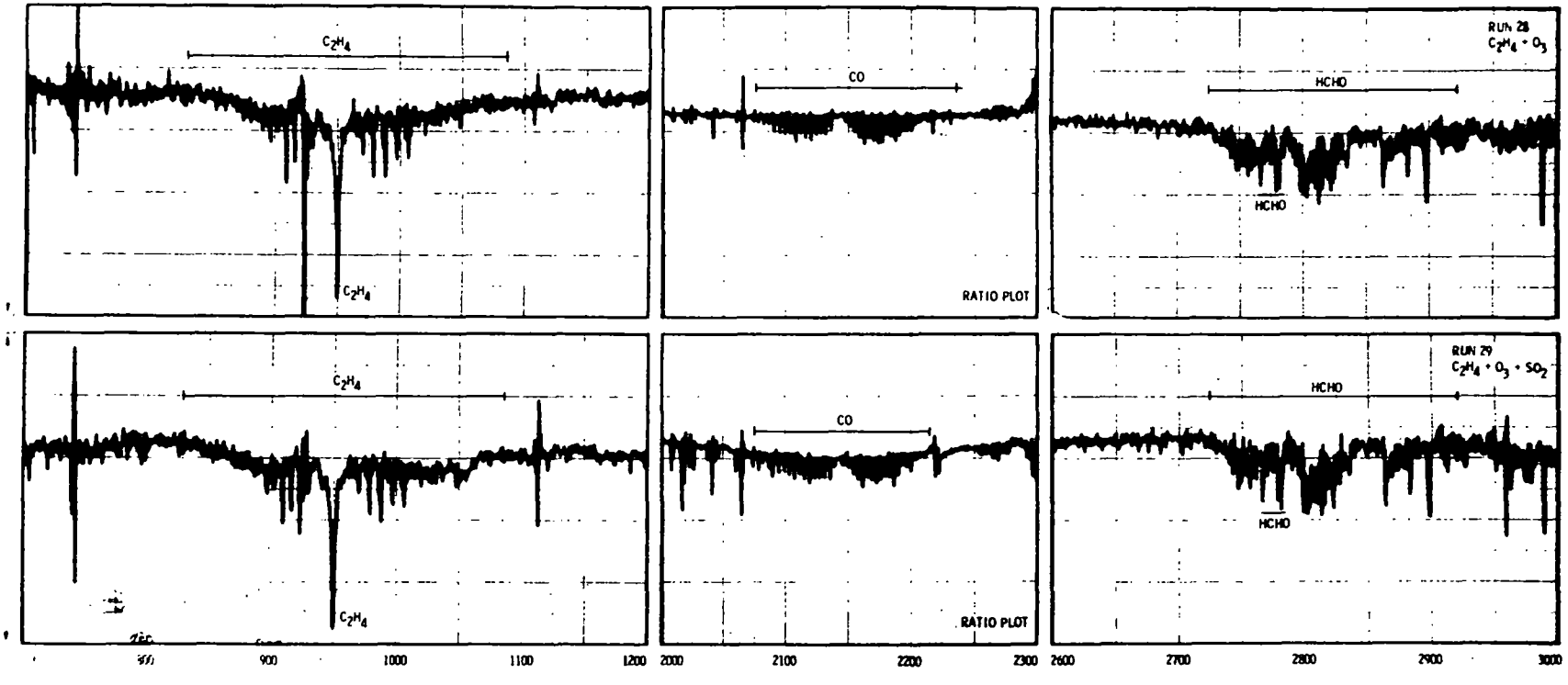

FIGURE 5-13. INFRARED ABSORPTION SPECTRA OF REACTOR CONTENTS.

Table 5-3

Product Analysis by Fourier Transform Infrared Spectroscopy

Propylene - Ozone Reaction

Run	RH %	CO* (± 0.02)	HCHO* (± 0.03)	CH_3CHO* (± 0.1)	CH_2CO* (± 0.03)	HCOOH* (± 0.07)
60 (with SO_2)	20	0.34	1.34	0.68	0	Trace
65 (with SO_2)	36	0.35	1.32	0.76	0	Trace
31 (with SO_2)	19	0.36	1.32	0.61	0	Trace
21 (without SO_2)	19	0.36	1.24	0.58	0.08	Trace
81 (without SO_2-in N_2)	36	0.18	0.56	0.32	0.08	0
82 (without SO_2-in N_2)	20	0.23	0.51	0.30	0.06	0

Ethylene - Ozone Reaction

29 (with SO_2)	20	0.38	1.42	0	0	0.07
28 (without SO_2)	22	0.28	1.38	0	0	Trace

*ppm/ppm ozone consumed

was not observed in these experiments as the production of carbon monoxide appeared constant relative to the rate of ozone consumption. Both forms of the intermediate species are operative in oxidizing the sulfur dioxide as evidenced by the formation of light scattering aerosols in both the ethylene and propylene systems (data follows in Section E). The formation of the carbon monoxide observed may still be via that decomposition reaction but direct evidence is lacking. Reaction 4, Chapter II-B indicates that carbon monoxide and methyl alcohol could be formed by another decomposition reaction. No methyl or other alcohol was observed in these analyses and, therefore, reaction 4 is apparently not operational or has a minor role in generating the carbon monoxide.

Formic acid was observed in each of the experiments conducted in the oxygen enriched system and is postulated to result from a recombination of the hydroxyl and the peroxyformyl radicals.

For the purpose of discussion, a mechanism is adopted which is similar to the three step mechanism proposed by Cox and Penkett (1972) in that the olefin-ozone reaction produces a reactive intermediate which subsequently can decompose, rearrange, or react with other than the two primary reactants and which is the oxidizing species for sulfur dioxide. The new mechanism does not, however, exclude additional reactions particularly those which involve a secondary attack on the principal reactants. Based on this mechanism, one should observe a higher production of formaldehyde in the ozone-ethylene reaction conducted in the presence of sulfur dioxide while in the absence of sulfur dioxide, production of formic acid and carbon monoxide should be higher. These features were not observed in the reactions with ethylene, and in fact the tendency, although slight, was in the opposite direction.

An increase in both formaldehyde and acetyaldehyde production was

also expected for reactions of propylene and ozone occurring in the presence of sulfur dioxide. The data listed in Table 5-3 demonstrates this feature in the case of formaldehyde but it is not well defined in the case of acetyaldehyde. A number of calculations were made to substantiate the increase in aldehyde yield consistent with the sulfur dioxide oxidative step in the mechanism producing the products sulfur trioxide and stable aldehyde. The nine propylene runs listed in the Appendix were used to determine the formation ratio of the two aldehyde species. The observed mean of the ratio of formaldehyde to acetyaldehyde with one standard deviation for the nine experiments was 1.85 ± 0.20. This finding tends to confirm the increase in the acetyaldehyde production concurrent with that of the formaldehyde. The ratio of the formaldehyde concentration to that of carbon monoxide was also calculated for the seven runs conducted in an oxygenated atmosphere. Four of the runs were conducted without any sulfur dioxide in the system and for these the mean ratio was calculated as 3.17 ± 0.26. In the other three experiments which included sulfur dioxide, the mean ratio was 3.80 ± 0.16. A t-test shows these mean ratios to be significantly different at the 95% level. As the carbon monoxide concentration apparently remains constant, the difference in the mean ratio values is due to a change in the formaldehyde concentration. This result supports the finding of increased formaldehyde, or more generally, aldehyde production in the propylene-ozone thermal reaction when conducted in the presence of sulfur dioxide.

The competition for the reactive intermediate was affirmed by noting that a gain in carbon for run 21 was 0.40 ppm accounted for in the species ketene while the corresponding loss relative to run 31 was 0.43 ppm carbon accounted for in the two aldehyde species. Although the initial reactant concentrations were not precisely the same, it is also interesting to note

that 0.20 ppm sulfur dioxide was consumed in run 31 while 0.17 ppm ketene was formed in run 21. To determine whether this indication establishes a real relationship between the two species would require further experimentation.

A product analysis of the two propylene-ozone experiments conducted in a reduced oxygen atmosphere and listed in the table in the Appendix indicates that no formic acid was formed. This finding refutes the mechanistic step shown as reaction 7 in Chapter II-B, in which the acid results from the decomposition of the formyl form of the intermediate species. An oxygen enriched atmosphere is required for the production of the formic acid as it is for the formation of the hydroxyl radical. The other species which was formed with the hydroxyl radical from one of the proposed interactions of the reactive intermediate with molecular oxygen is the peroxyformyl radical. It is speculated that a recombination of these two radical species could result in the formation of the formic acid according to

$$H\overset{O}{\overset{\|}{C}}OO\cdot + \cdot OH \rightarrow O_2 + HCOOH \qquad (28)$$

The species shown, however, is also known to be very unstable and rapidly decomposes as

$$H\overset{O}{\overset{\|}{C}}OO\cdot \rightarrow CO + \cdot HO_2 \qquad (22)$$

A decomposition reaction of this form can also account for the essentially constant production per ppm of ozone consumed of carbon monoxide in the oxygen enriched system. The occurrence of such a reaction in this system is reinforced by the observation that the carbon monoxide was lower in the oxygen deprived atmosphere.

One further observation noted from these two experiments which made use of nitrogen as the diluent gas is the marked reduction in the produc-

tion of both aldehyde species compared to the runs conducted in air. The production of formaldehyde for these two runs averaged about 0.54 ppm/ppm of ozone reacted and for the acetyaldehyde was 0.31 ppm/ppm of ozone consumed. This result can be accounted for by another reaction of the intermediate species with oxygen resulting in the formation of ozone and aldehyde, reaction 13, Chapter II-B, for example. It is also significant to note that this reaction would contribute a major fraction of the aldehyde formed.

Ammonia was not observed as a product or a contaminant in these experimental runs.

Scott et al. (1957) also observed formaldehyde, acetyaldehyde, carbon monoxide and ketene in the reaction of propylene with ozone. In addition, they reported values for carbon dioxide and water and an upper limit for acid production. The initial concentration for each of the two reactants used in their experiments was 32 ppm. The results described herein are in good qualitative agreement with their findings. Vrbaski and Cvetanović (1960) also conducted an extensive product analysis of the propylene-ozone reaction although at considerably higher reactant concentrations. Carbon monoxide and formaldehyde were not included in their analyses performed by gas-liquid chromatography. Products reported were acetyaldehyde, propionaldehyde, acetone, methyl alcohol, carbon dioxide and formic acid. The yield reported for formic acid (0.34 ppm/ppm of ozone consumed) was considerably higher than observed in this study or in the study of Scott et al. (1957). The values reported for propionaldehyde and acetone were very low being 0.003 and 0.008 ppm/ppm of ozone consumed respectively while that for the alcohol was 0.033 ppm/ppm ozone reacted.

Although there is some variation in product formation among the different investigations, there is general agreement relative to the

formation of aldehydes as a major product of the olefin-ozone reactions. These species result from the attack on and the rupture of the double bond by ozone and the addition of an oxygen atom onto one of the fragments. Through this mechanism and as observed in this study ethylene produces formaldehyde and the propylene yields acetyaldehyde and formaldehyde. There is also general agreement that carbon monoxide and carbon dioxide are among the major products although carbon dioxide was not measured in this study. Alterations in the product inventory and yield due to the presence of the sulfur dioxide are not reported elsewhere.

It was not possible during these experiments to identify quantitatively all of the minor products formed during the reactions. Some of the products were below the detection limits of the instrumentation while the characteristic absorption spectra of others appears in the region of major products and were completely masked. Carbon dioxide was not quantitated as there existed a short free air path in the experimental arrangement between the cell and the detector. Despite these limitations, it was still of interest to calculate a material balance on carbon, i.e., to calculate the ratio of the concentration of carbon atoms found in the identified products to the concentration of carbon atoms in the reacted olefin. This ratio was 62.5% for run 31 which included sulfur dioxide and 66.6% for run 21 which included only the propylene and ozone. The ethylene reactions yielded a carbon balance of 56.3% for run 29 with sulfur dioxide and 54.7% for run 28 which did not contain the sulfur species. Assurance that this difference was not due to equipment failure was obtained by comparing the results of the olefin and acetyaldehyde measurements made by the Fourier transform infrared spectrometer and the gas chromatograph. The four measurements of propylene and acetyaldehyde

agreed to approximately ten percent and the two measurements of ethylene agreed to within three percent.

C. Tentative Reaction Mechanism

To summarize the evidence presented in the previous sections, the following scheme provides the salient features of a mechanism for the propylene-ozone-sulfur dioxide system which is consistent with the data observed in these experiments. The initial steps of the tentative mechanism are those which directly influence the concentration of either the sulfur dioxide or the species responsible for its oxidative consumption. The final steps in the mechanism are presented to account for other products observed in the various experiments conducted.

One scheme which is generally accepted for the ozonalysis reaction is the Criegee mechanism in which the reactive intermediates are the zwitterions. The structure and reactivity of these species are considered in popular practice to be biradical in character (Calvert, 1973). It is proposed that these reactive intermediates are responsible for the oxidation of the sulfur dioxide in the system. The products of the initial reaction are stable aldehydes and the active biradical species according to the equations

$$O_3 + CH_3\text{-}CH{=}CH_2 \rightarrow HCHO + CH_3\dot{C}HOO\cdot \qquad (1)$$

$$\rightarrow CH_3CHO + H\dot{C}HOO\cdot \qquad (1a)$$

The intermediate can only interact with the olefin, molecular oxygen and the sulfur dioxide. The finding that the stoichiometry of the reaction is affected by the presence of oxygen indicates that the intermediates are not directly involved in a secondary attack on the olefin. Interactions of the intermediate with molecular oxygen occur as follows:

$$\dot{R}CHOO\cdot + O_2 \rightarrow \cdot OH + R\overset{O}{\overset{\|}{C}}OO\cdot \qquad (11)$$

$$\dot{R}CHOO\cdot + O_2 \rightarrow O_3 + RCHO \qquad (13)$$

A secondary attack on the olefin by species other than ozone generated in the system has been demonstrated and through the calculated addition of a prescribed amount of carbon monoxide, the agent responsible for the secondary attack was tentatively identified as the hydroxyl radical. A reduction in the aldehyde yield observed in experiments conducted in a reduced oxygen atmosphere indicates that reaction 13 is also active in the system. This ozone production is apparently offset by the increasing participation of ozone in reactions involving unidentified products of the primary reaction.

An apparent decomposition reaction of the acetyl form of the biradical intermediate was noted in the propylene-ozone interactions and resulted in the production of ketene according to the reaction

$$CH_3\dot{C}HOO\cdot \rightarrow CH_2{=}C{=}O + H_2O \ . \qquad (5)$$

The rate of this reaction must be slow since the ketene was not observed in systems which included sulfur dioxide as a reactant. This result along with a materials balance analysis enforced the identification of the intermediate as the species which oxidized the sulfur dioxide particularly as none of the other species under consideration form ketene.

The hydroxyl radical was involved in a secondary attack on the olefin species. The rate constant for these reactions is approximately one hundred times greater than is the rate constant for the hydroxyl radical-sulfur dioxide reaction thus eliminating that species from consideration as the oxidizing agent. The propylene-hydroxyl radical reaction is itself chain propagating:

$$\cdot OH + CH_3\text{-}CH{=}CH_2 \rightarrow CH_3\dot{C}H\text{-}CH_2OH \quad . \qquad (14)$$

The final step in the proposed mechanism is the oxidative consumption of the sulfur dioxide by the reactive biradical species:

$$R\dot{C}HOO\cdot + SO_2 \rightarrow SO_3 + RCHO \quad . \qquad (29)$$

Other potentially oxidizing species for the sulfur dioxide have been eliminated in the preceding sections.

The mechanistic steps which follow next are advanced to account for other products observed by the infrared spectroscopic analysis.

An oxygen effect was observed in the production of formic acid thereby eliminating the decomposition of the formyl form of the intermediate as being responsible for its formation. It is speculated, however, that a reaction between the hydroxyl and the peroxyformyl radicals will produce the acid observed:

$$\cdot OH + H\overset{O}{\overset{\|}{C}}OO\cdot \rightarrow O_2 + HCOOH \quad . \qquad (28)$$

The formation of carbon monoxide from another decomposition of the formyl form of the biradical species in analogy with the formation of ketene from the decomposition of the acetyl form was not observed. There was an oxygen effect noted in the formation of the carbon monoxide and in contrast to the ketene, the presence of sulfur dioxide did not affect the observed concentration. The peroxyformyl radical requires an enriched oxygen atmosphere for its formation in this mechanism (reaction 13), is known to be highly unstable and on decomposition can account for the carbon monoxide as follows:

$$H\overset{O}{\overset{\|}{C}}OO\cdot \rightarrow CO + \dot{H}O_2 \quad . \qquad (22)$$

The hydroxyl radical formed in the oxygen enriched system reacts with the aldehyde species with about the same rate constant as with the olefin. This reaction leads to the formation of formyl and acetyl radicals which in the presence of oxygen become an additional source of peroxyformyl and peroxyacetyl radicals:

$$\cdot OH + RCHO \rightarrow H_2O + R\overset{O}{\overset{\|}{C}}\cdot \qquad (16)$$

$$R\overset{O}{\overset{\|}{C}}\cdot + O_2 \rightarrow R\overset{O}{\overset{\|}{C}}OO\cdot \quad . \qquad (30)$$

The notable difference between the foregoing mechanism and the three-step mechanism employed by Cox and Penkett (1972) is the relatively large involvement of secondary reactions shown above. The deviation from 1:1 stoichiometry results from a secondary consumption of the olefin and secondary reactions between ozone and other products of the olefin-ozone-sulfur dioxide system. The observed oxygen effect in these studies which affected the stoichiometry and the yield of the various products indicates that in an oxygen deprived system, the consumption of ozone by product species becomes more significant relative to the olefin consumption. In an oxygen enriched system, however, additional ozone is regenerated as are the radical species.

D. Sulfate Analysis and Sulfur Mass Balance

Several samples, collected on Millipore Corporation Fluoropore filters, were studied in an attempt to perform a sulfur balance on the propylene-ozone-sulfur dioxide reaction and also to confirm the conversion of the sulfur dioxide to a sulfate aerosol. The filters were 37 mm in diameter and had a mean pore size of 0.2 μm. X-ray fluorescence spectroscopy, for a total sulfur measurement, and liquid chromatography, for measurement of water soluble sulfates, were used to estimate the sulfuric

acid mist loading on the filter. Both techniques were employed as they are still under development as methods for use on atmospheric samples of mixed components. Also, a test for consistency was desired particularly on this aerosol which is expected to contain only $SO_3(H_2O)_x$.

A summary of the analytical results from both methods is shown in Table 5-4. The total volume sampled, the calculated mass concentration of the sulfuric acid aerosol in $\mu g/m^3$, the equivalent concentration of sulfur dioxide in ppm and the measured amount of sulfur dioxide consumed are tabulated. Using the liquid chromatographic results as a basis the sulfur balance for the five samples analyzed by that method indicate that recoveries of from 77 to 100 percent were achieved. The two samples for which the recovery was essentially 100% were collected near the end of the first hour of the experiments while the other three samples were collected approximately one half hour later into the run. The fraction of the sulfur unaccounted for by the filter analysis is believed to have been lost to the system by diffusion to and absorbance on the reactor walls. The extensive sampling requirements for runs 16, 24 and 32 coupled with the late period in the run for the filter sampling, i.e., after the ozone had been depleted by 90%, left the bag nearly empty and the surface to volume ratio increased accordingly thereby enhancing the potential for diffusive losses.

As no ammonia was observed in the samples analyzed by the Fourier transform infrared spectrometer it was assumed that the total sulfate aerosol loading on the filters was due to sulfuric acid. It also follows from the high sulfur recoveries observed from the X-ray fluoresence spectroscopic and liquid chromatographic analyses that the dominant if not the only conversion for the sulfur dioxide is via an oxidative process resulting in the formation of the acid aerosol.

Table 5-4

Summary of Sulfuric Acid Analysis by X-ray Fluoresence Spectroscopy and Liquid Chromatography

X-ray Analysis

Sample	ng(s)/cm^2	μg(S)	H_2SO_4 (μg/m^3)	SO_2 (ppm)	Measured ΔSO_2 (ppm)
16	1348	10.84	1147	.187	.202
24	596	4.79	853	.139	.124
32	1071	8.61	1237	.202	.187
60	4149	33.37	1289	.210	.205
65	3417	27.48	1061	.173	.158

Liquid Chromatography

Sample	μg(S)/ml	μg($SO_4^=$)	H_2SO_4 (μg/m^3)	SO_2 (ppm)	% Recovery
16		29.3	1033	.168	83
24	1.97	9.85	585	.095	77
32	3.85	19.3	922	.150	80
60	3.32	99.6	1282	.209	100
65	2.50	75.0	966	.57	99

The results of the liquid chromatographic analysis were used as a basis as the system was calibrated with sulfuric acid during the same time period in which the samples were analyzed. Calibration samples were prepared by adding .1 N sulfuric acid aqueous stock solution to isopropyl alchohol in the prescribed volumetric ratio and taking aliquots to yield standards in the range of 0.5-5 μg ($SO_4^=$)/ml (a span that encompassed the samples collected). The plot of peak height for these standards vs concentration was non-linear in these low concentrations as was expected from solubilities and kinetics considerations (Tejada, 1974).

Analysis of samples by X-ray fluorescence spectroscopy for elements lighter than potassium (A=39) is hindered by the self-absorption (of the low energy characteristic X-rays) within the filter matrix or by the aerosol loading (Dzubay & Stevens, 1974). The correction for self-absorption for particles $\lesssim$ 2 μm, however, is small and the data to follow demonstrates that aerosol generated in the gas phase reaction of propylene-ozone sulfur dioxide consisted largely of sub-microscopic droplets. A ratio plot of the results of the total mass of sulfuric acid collected on the filter as estimated by the X-ray fluorescence and the liquid chromatographic technique is shown as Figure 5-14. The unit ratio is based on the acceptance of the results of the wet chemical analysis as a reference. Also, shown on this figure is the mass of the acid measured by the two methods.

Although the data are limited an initial evaluation of these results led to a postulate explaining the high results obtained by the X-ray fluorescence technique for low total mass loadings. X-ray fluorescence spectroscopic analysis under ideal conditions examines an area about 25 mm in diameter on the filter. The ratio of the examined to the total filter area of the 37 mm diameter filters used was about 0.45, and the sample

$\mu g\ H_2SO_4$

SAMPLE	X-RAY FLUORESCENCE	LIQUID CHROMATOGRAPHY	RATIO
24	14.68	10.06	1.46
32	26.37	19,65	1.34
60	102.18	101.68	1.00
65	84.16	76.56	1.10

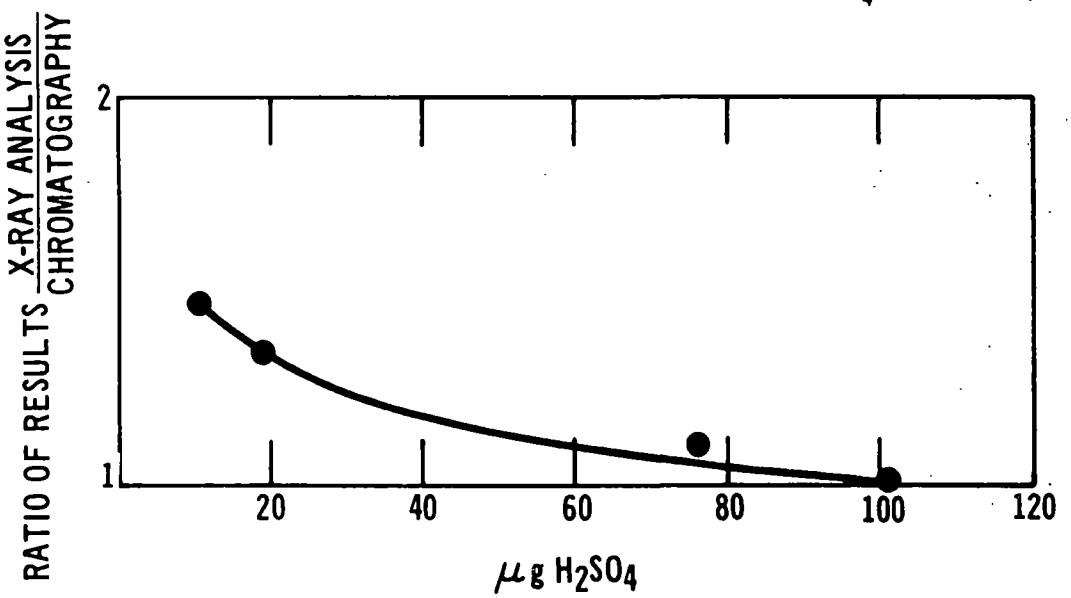

FIGURE 5-14. COMPARISON OF RESULTS FOR SULFURIC ACID ANALYSIS.

was assumed to be uniformly deposited over the total surface. Precautions were taken to facilitate the collection of a uniformly distributed sample on the filter by adding an extra spacer ring to the in-line filter holder to allow the captive aerosol more time to disperse laterally prior to entrapment. The data suggest, however, that the aerosol was preferentially loaded on the central portion of the filter first. For heavier loadings, the deposition became more uniformly distributed as the increasing pressure drop at the center made collection on the outer portion more favorable. The data further suggest that for a total mass loading of $\geq$100 μg of sulfuric acid and with the sampling arrangement and flow rate employed the results were comparable. This postulate was later substantiated by separately analyzing the central 1.98 cm^2 and the balance of filter sample number 16 by the liquid chromatographic technique. The mass loading per unit area was found to be 1.7 times higher over the central portion of the filter than over the outer ring.

E. Light Scattering Measurements.

An integrating nephelometer was used to measure the light scattering coefficient of the aerosol formed in the gas to particle conversion. Scatter from particulate material over an angle from about 8.5 to 168.8° was measured by this device.

According to this instrument, no light scattering aerosol was formed in reactions which did not include sulfur dioxide. In addition, no light scattering aerosol was observed over the lifetime of the experiment, in the reaction of ozone with sulfur dioxide.

The meteorological range or local visual distance was estimated from the measurement of the scattering coefficient according to equation IV-4 adjusted for the wavelength used by the eye in sunlight. These data are

reported for two representative experiments in Figures 5-15 and 5-16. Included in these figures is a plot of sulfur dioxide consumption with time and a plot of the variation in the total surface area with time as measured with the Electrical Aerosol Size Analyzer. The final stage of the latter curve is affected by the rapid growth of the acid aerosol out of the measurement range of this instrument. The important feature for the discussion and comparison to follow is related, however, to the initial rate of growth to the achievement of some apparent stable total surface area.

Figure 5-15 contains plots of these data for a propylene-ozone-sulfur dioxide reaction. The initial rate of sulfur dioxide consumption is the highest for the run and is responsible for the rapid establishment of a large total surface area due almost exclusively to a nucleation process. Although the total surface area is large, the newly formed embryos are too small at early times to scatter light efficiently. As the experiment progressed, however, the aerosol particles grew by nucleation, condensation and coagulation becoming increasingly more efficient in scattering light. The mean surface area diameter for this run was estimated at 15, 30 and 60 minutes as 0.22, 0.26 and 0.30 μm respectively. These mean surface area diameter estimates are affected by the growth of the aerosol out of the range of the analyzer and are, as a result, slightly smaller than would be expected. Concurrent with the increase in the scattering coefficient is a decrease in the visual distance which, at eight minutes into the run, was almost 16 kilometers (km) and which diminished to about 2 km within forty-five minutes.

Figure 5-16 contains plots for the ethylene-ozone-sulfur dioxide system which are similar to those shown in Figure 5-15. The ethylene-ozone reaction has been shown previously to be slower than the propylene-

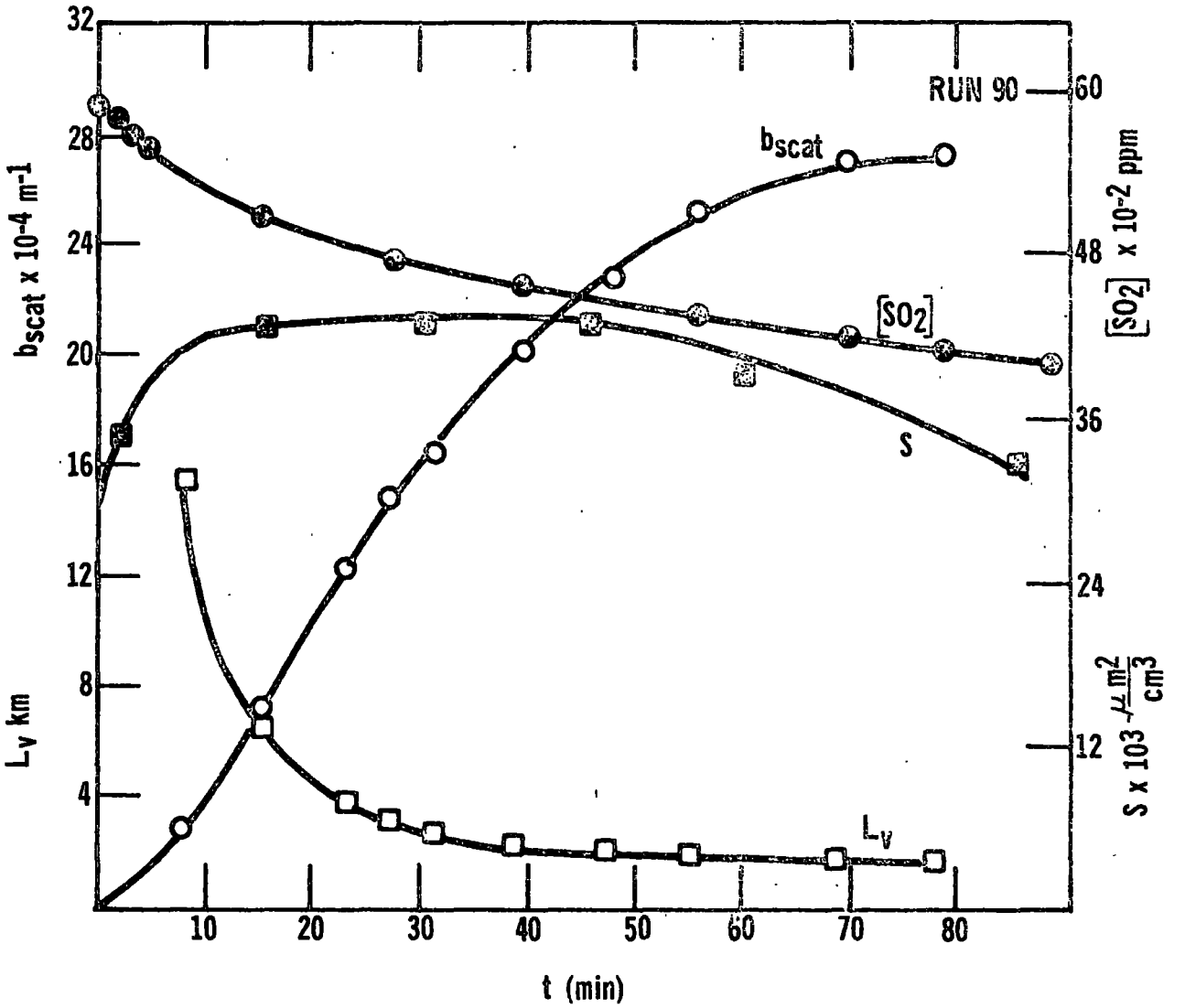

FIGURE 5-15. VARIATION OF THE SCATTERING COEFFICIENT, VISUAL RANGE, SURFACE AREA CONCENTRATION AND SULFUR DIOXIDE CONCENTRATION WITH TIME FOR A PROPYLENE-OZONE-SULFUR DIOXIDE EXPERIMENT.

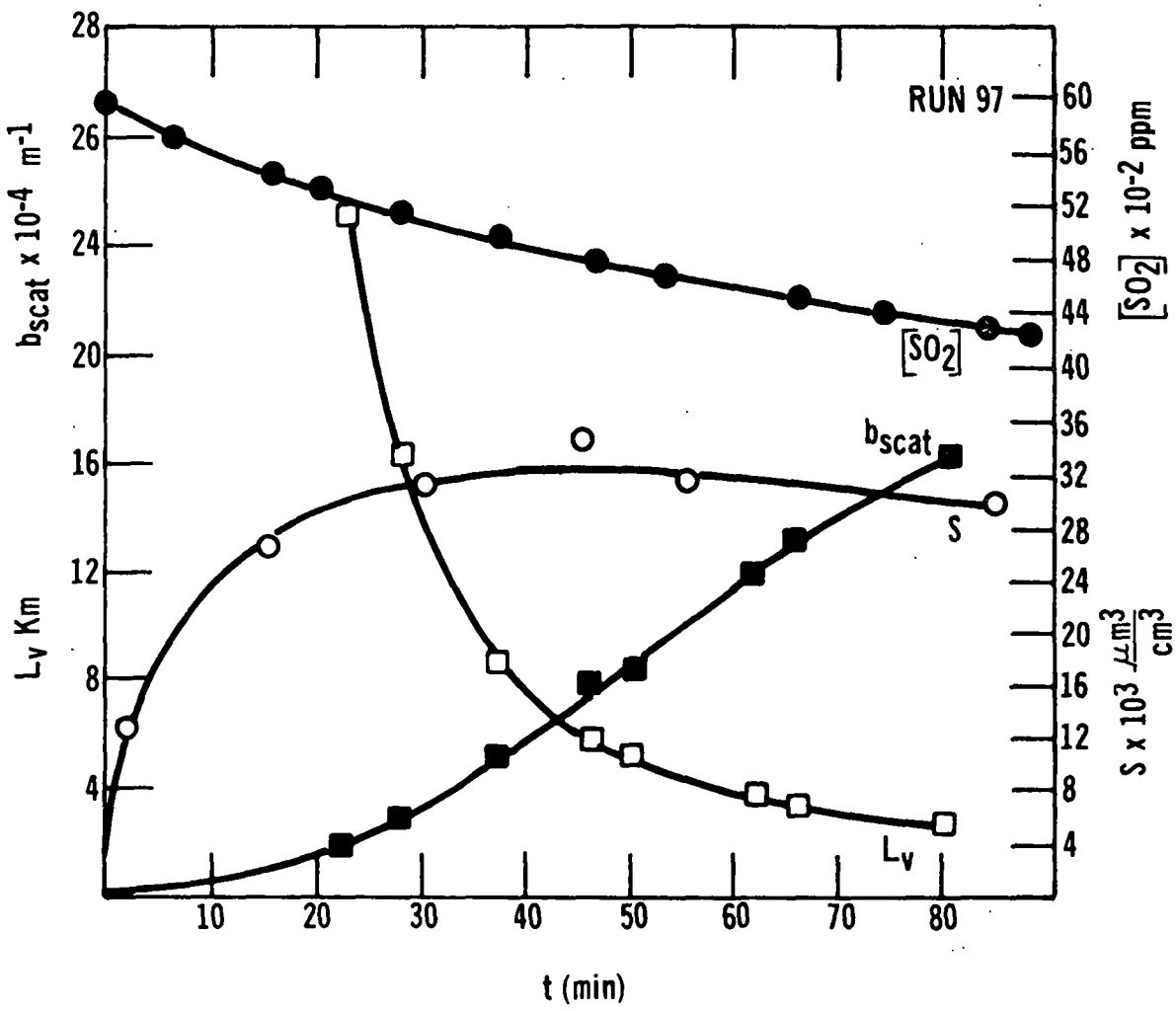

FIGURE 5-16. VARIATION OF THE SCATTERING COEFFICIENT, VISUAL RANGE, SURFACE AREA CONCENTRATION AND SULFUR DIOXIDE CONCENTRATION WITH TIME FOR AN ETHYLENE-OZONE-SULFUR DIOXIDE EXPERIMENT.

ozone reaction and the sulfur dioxide consumption is likewise slower. The rate of establishment of surface area is reduced compared to the propylene system and the stable total surface area level is also lower. The scattering coefficient measurement shows that the rise of this function is appreciably slower than in the propylene system although the mean surface diameter of the particles is essentially identical for the two systems at the times measured. The estimated diameter at 15, 30, and 60 minutes was 0.22, 0.25 and 0.31 μm respectively. This result indicates that although the nucleation process is more limited, the growth of the acid aerosol in the two systems follows the same pattern. The degradation of the visual distance with time likewise displays the relative slowness of the ethylene system. Visibility, which was reduced to about 16 km at eight minutes in the propylene system was essentially unlimited and at the end of forty-five minutes was greater than 6 km compared to 2 km in the propylene system.

F. Aerosol Development

The propylene-ozone reaction was monitored to determine if a nucleation process was active in this system and to follow the growth of any aerosol formed. A condensation nuclei counter was used to measure the total number concentration as a function of time while the electrical mobility analyzer was used to obtain an estimate of the total surface area and volume concentrations. These data, for a typical olefin-ozone reaction, are shown in Figure 5-17. An induction period lasting almost five minutes occurred prior to the initiation of the nucleation process. Once started, however, the nucleation proceeded rapidly reaching a peak concentration of approximately 95,000/cm^3 at fifteen minutes into the run. Although the nucleation process continued, the peak and subsequent decay

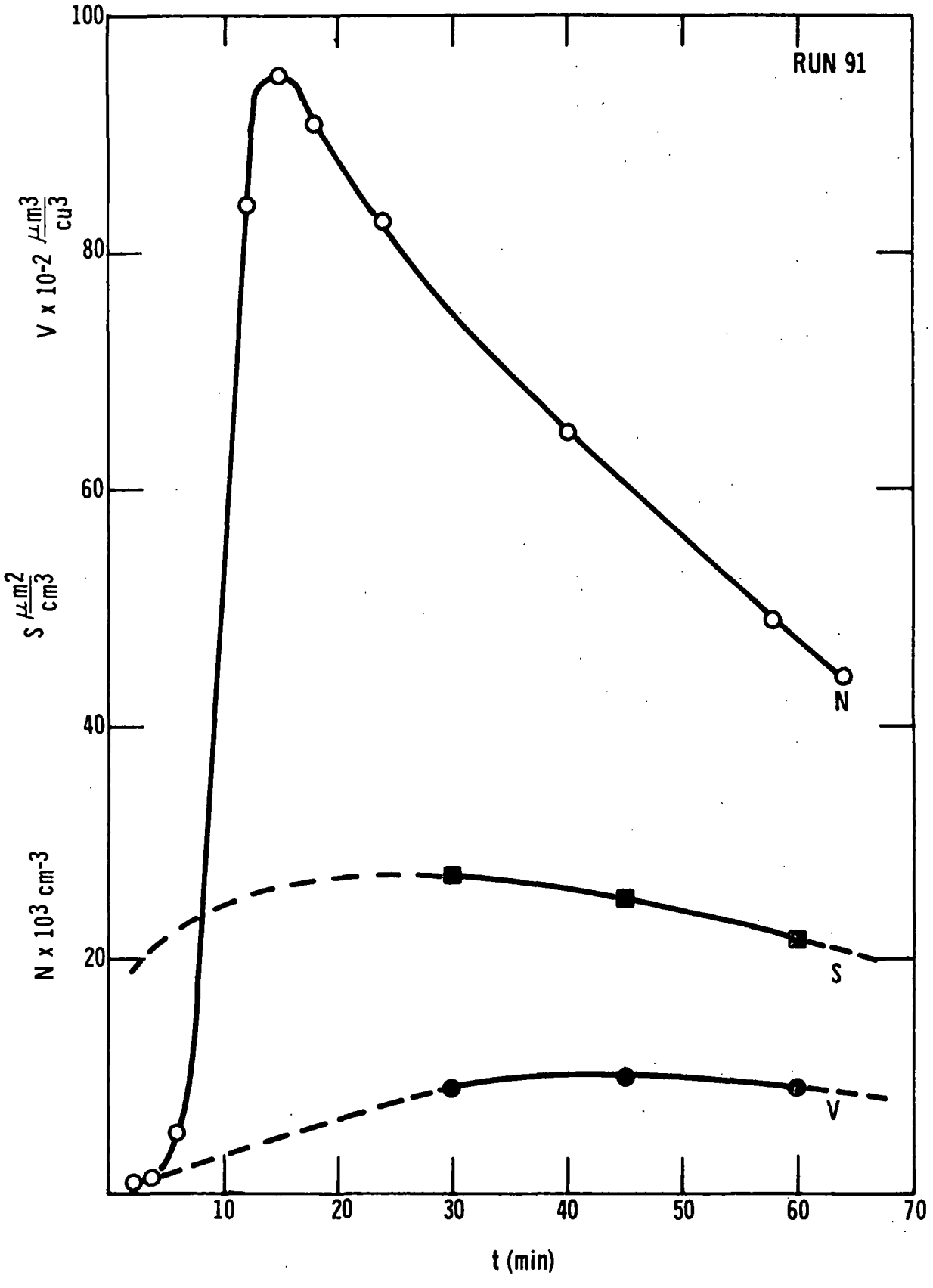

FIGURE 5-17. AEROSOL PARTICLE NUMBER, SURFACE AREA AND VOLUME DEVELOPMENT FOR A PROPYLENE-OZONE EXPERIMENT.

of the number concentration indicated that a transient equilibrium was attained between the two processes and which was followed by a period of increasing domination by the coagulation process. The curves drawn through these concentration data and those to follow were fitted by eye.

The total volume concentration was observed to increase linearly for almost thirty minutes and then remain essentially constant for the duration of the experiment. The conservation of the total volume is consistent with a system under the control of pure Brownian coagulation with no new material being added to the aerosol volume.

The total surface area concentration initially increased rapidly due to the large surface to volume ratio of the newly formed embryos. Condensable material was limited in this system and at an early stage of the aerosol's development, the coagulation process dominated causing the total surface area concentration to diminish.

There was no significant aerosol growth observed in the propylene-ozone system and the count mean diameter of the aerosol at sixty minutes was estimated by the electrical mobility analyzer as 0.018 μm. There were no particles $\geq$ 0.042 μm observed nor was any light scattering aerosol registered on the integrating nephelometer.

Figures 5-18 through 5-23 show the total volume, surface area and number concentrations for a series of six aerosol experiments which included sulfur dioxide as a reactant. The growth of the aerosol formed in these reactions was limited by design to remain essentially within the range of the electrical mobility analyzer. Wall losses evident at higher reactant concentrations were eliminated as were inaccuracies associated with coupling of size distribution data from different measurement devices. The initial reactant concentrations were also varied for these experiments to obtain a range of sulfur dioxide consumption values. One other variable

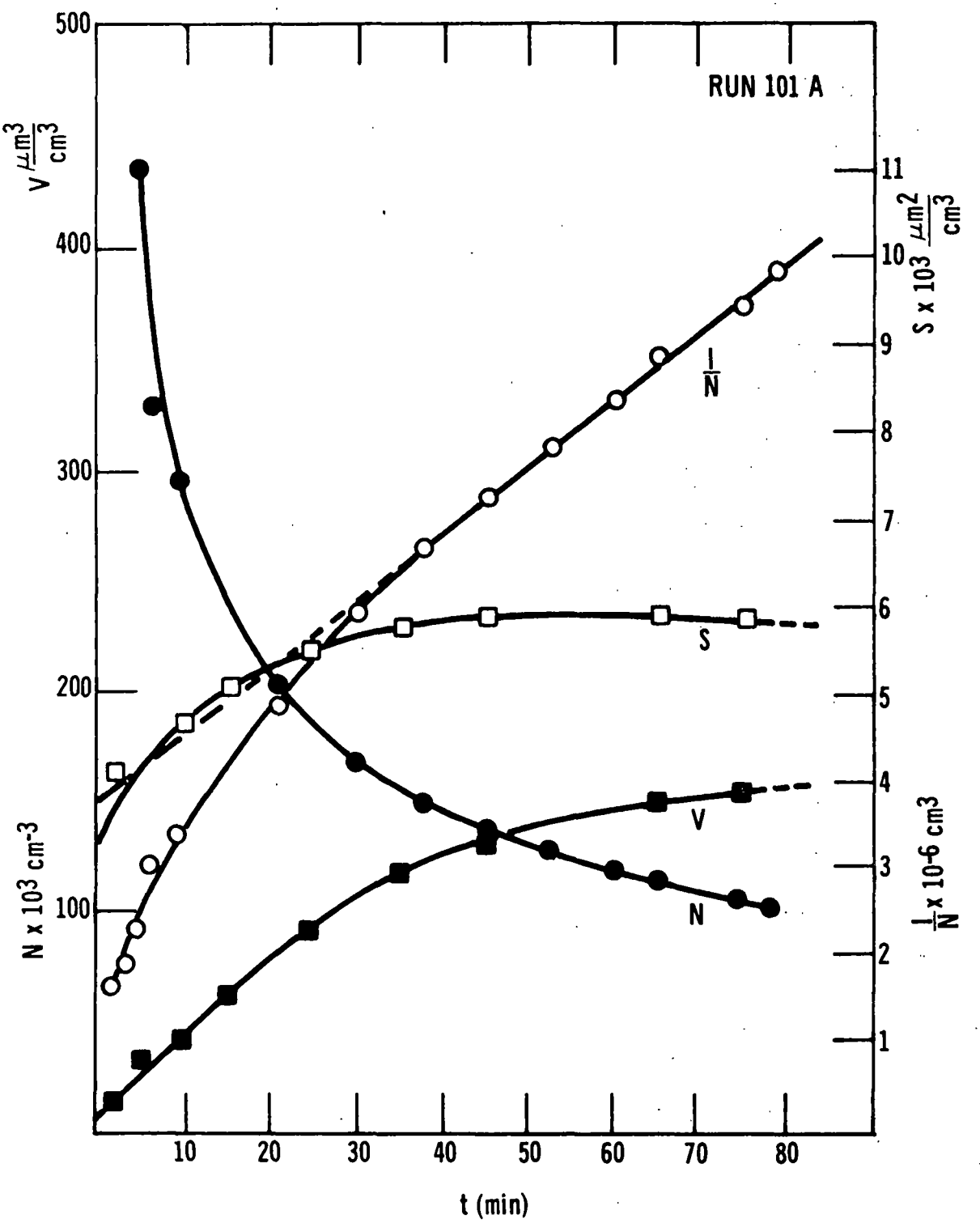

FIGURE 5-18. TOTAL VOLUME, NUMBER, RECIPROCAL OF NUMBER AND SURFACE AREA CONCENTRATION VERSUS TIME FOR THE DEVELOPING SULFURIC ACID AEROSOL.

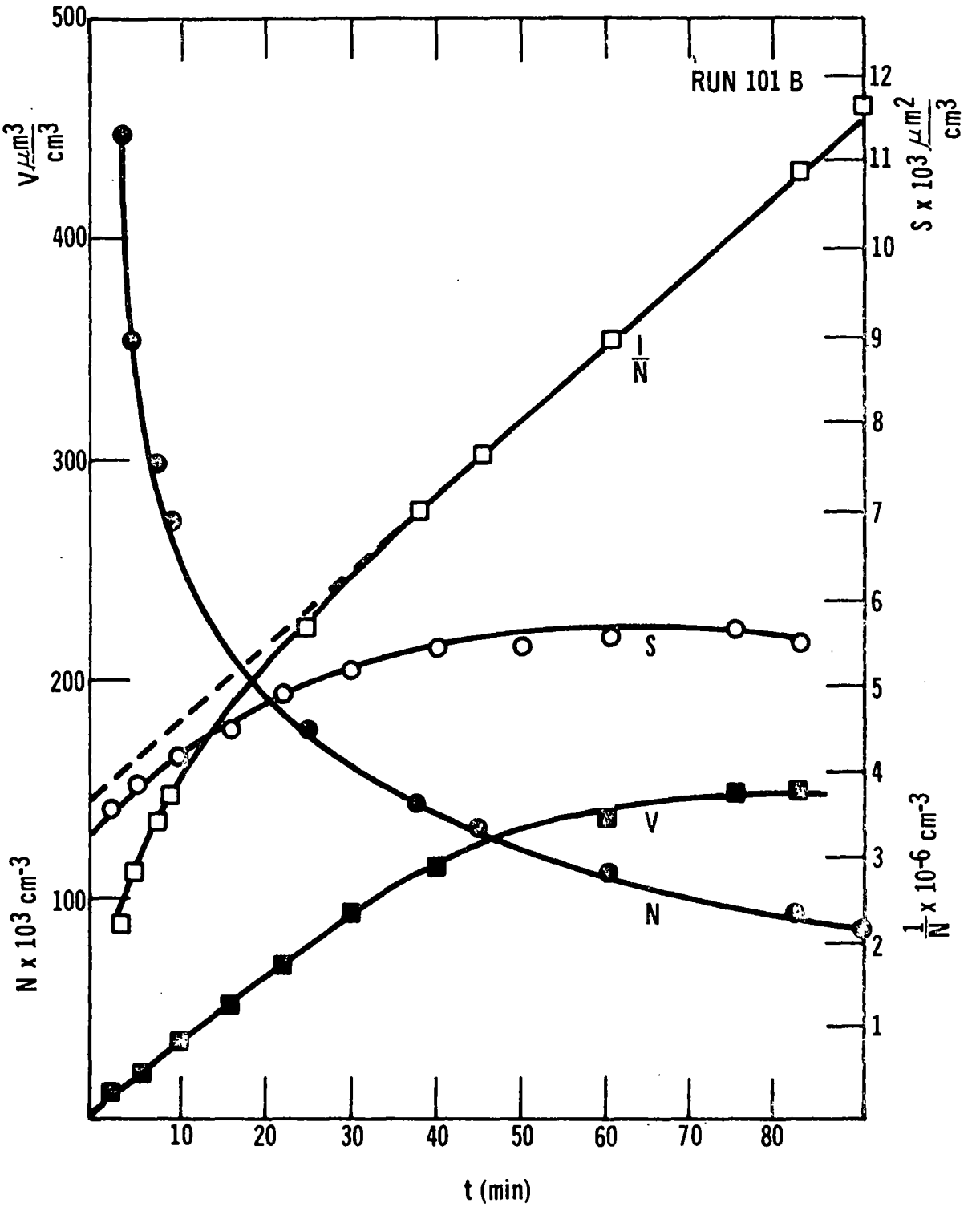

FIGURE 5-19. TOTAL VOLUME, NUMBER, RECIPROCAL OF NUMBER AND SURFACE AREA CONCENTRATION VERSUS TIME FOR THE DEVELOPING SULFURIC ACID AEROSOL.

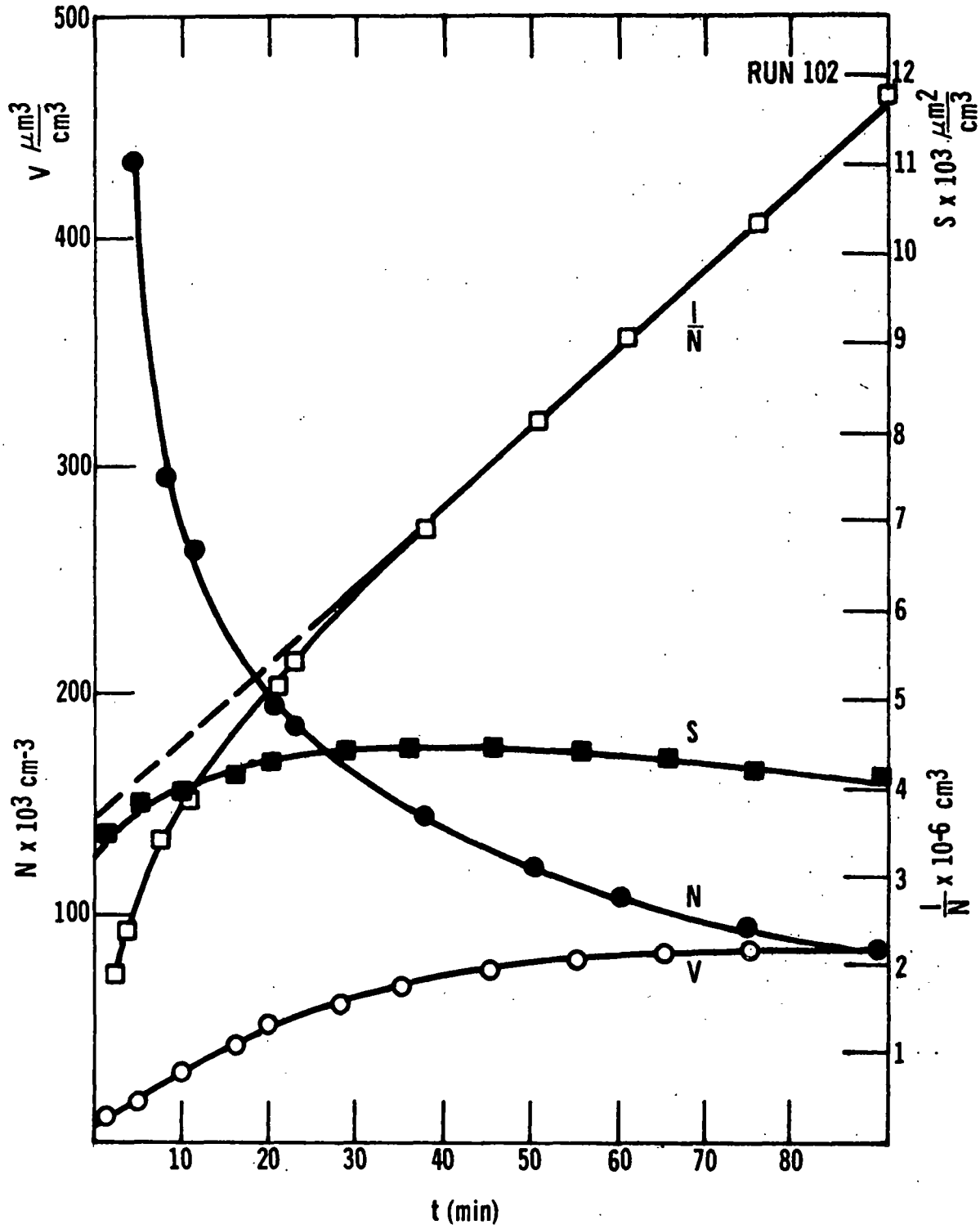

FIGURE 5-20. TOTAL VOLUME, NUMBER, RECIPROCAL OF NUMBER AND SURFACE AREA CONCENTRATION VERSUS TIME FOR THE DEVELOPING SULFURIC ACID AEROSOL.

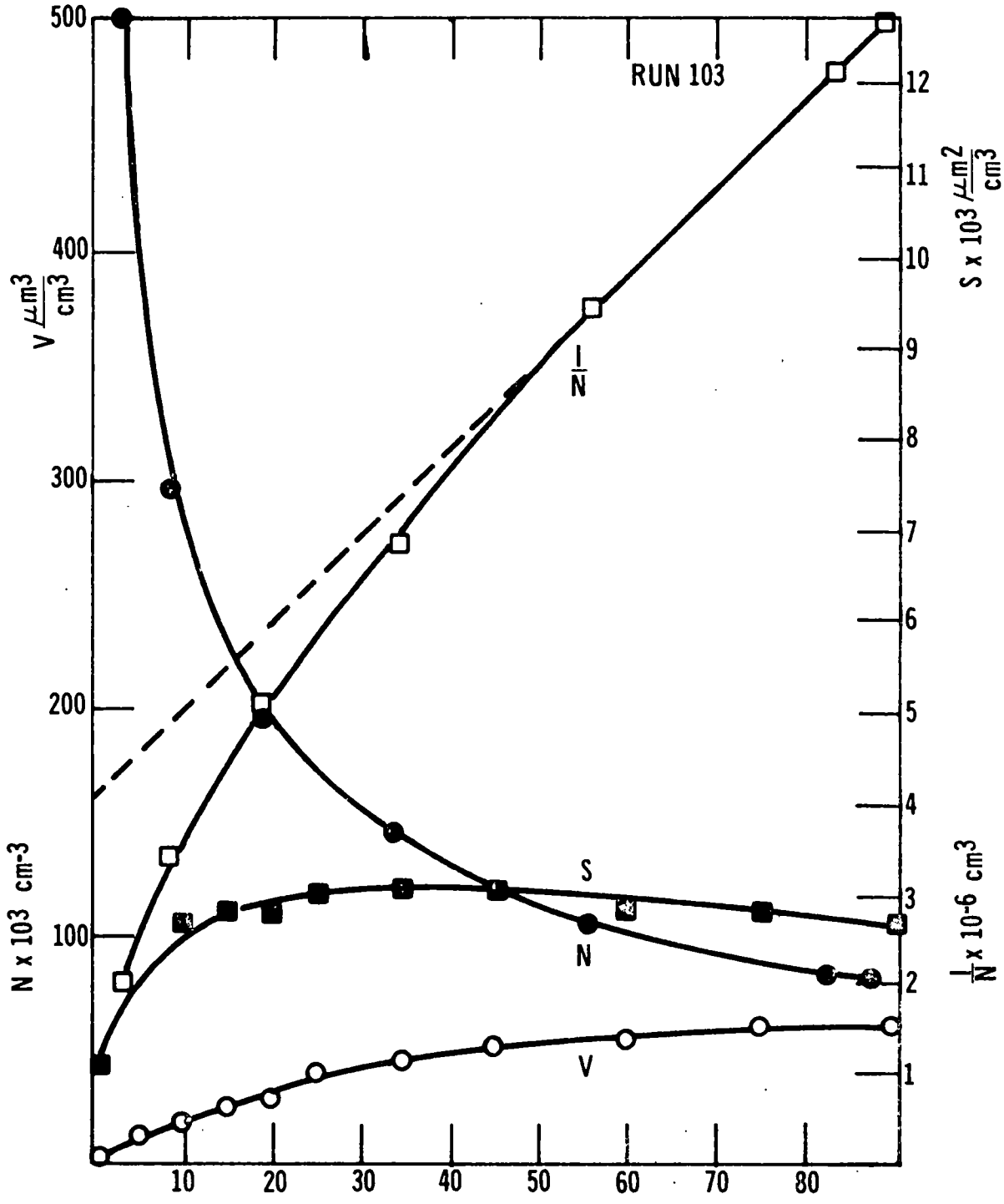

FIGURE 5-21. TOTAL VOLUME, NUMBER, RECIPROCAL OF NUMBER AND SURFACE AREA CONCENTRATION VERSUS TIME FOR THE DEVELOPING SULFURIC ACID AEROSOL.

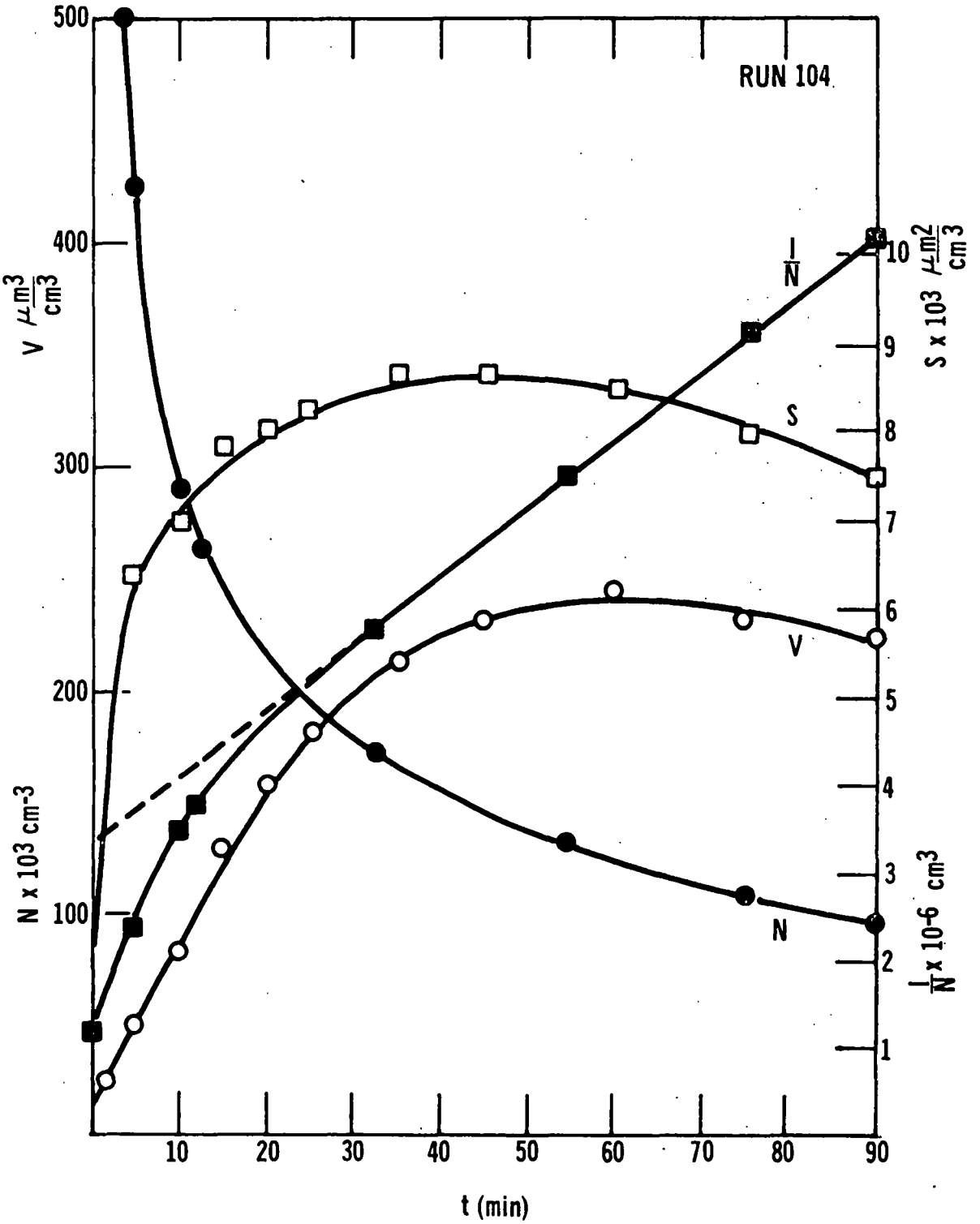

FIGURE 5-22. TOTAL VOLUME, NUMBER, RECIPROCAL OF NUMBER AND SURFACE AREA CONCENTRATION VERSUS TIME FOR THE DEVELOPING SULFURIC ACID AEROSOL.

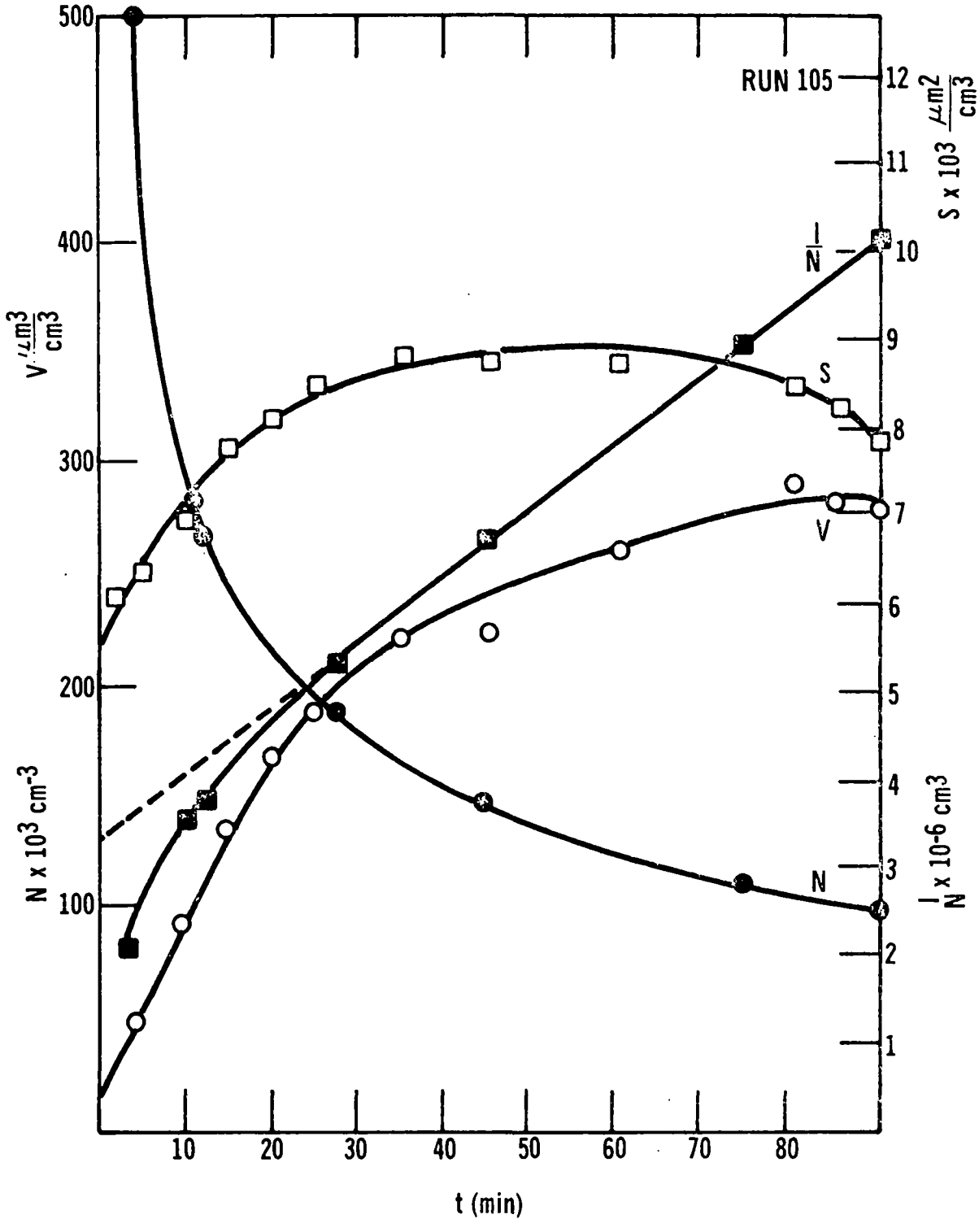

FIGURE 5-23. TOTAL VOLUME, NUMBER, RECIPROCAL OF NUMBER AND SURFACE AREA CONCENTRATION VERSUS TIME FOR THE DEVELOPING SULFURIC ACID AEROSOL.

is displayed on these plots, that being the reciprocal of the number concentration which is related to the coagulation constant by equation III-14. The general patterns in the formation and growth of the aerosol observed in this series of runs appeared similar for each run over the range of experimental conditions employed.

The process by which the acid aerosol was formed and developed in this system is postulated to include the three mechanisms of nucleation, condensation and coagulation. Initially, for a brief instant, the vapor phase mixture was free of all nuclei. Homogeneous nucleation then occurred spontaneously due to the diffusional or effusional aggregation of molecules in the supersaturated system. Supersaturation in this system is postulated to have been primarily achieved as a result of the gas phase reaction leading to the production of species of sufficiently low volatility which allowed the critical saturation to be exceeded. The surface free energy was critical to the stability of these newly formed embryos because of their small size.

The solution droplets formed persisted and grew by condensation because the supersaturation exceeded that required by equation III-8. The size of the nuclei apparently exceeded the critical diameter required by the Kelvin equation (III-4) and the supersaturation was maintained resulting in the continued growth of the droplets with a decrease in the free energy. Eventually the supersaturation diminished due to a depletion of the reactants in the gas phase and the subsequent reduction in the production of acid vapor. The vapor was extracted faster than it was being produced and a practical limit was reached.

The coagulation process in this system immediately followed the commencement of the nucleation phase because of the rapid buildup in the number concentration and the Brownian collisions which followed. The

rate of coagulation eventually became equal to the nucleation rate and the maximum number of nuclei was observed. The nucleation rate was finally surpassed and eventually the decay typical to a pure coagulation process was noted.

The number concentration was observed to be decaying at the start of the experiments indicating that the build up of the aerosol by nucleation was very rapid and was near completion at the recorded zero time or was at least dominated completely by the coagulation process. Ozone was added to the reactor late in the charging period of five minutes and was not added in the final thirty seconds for any of these aerosol runs. In an attempt to monitor the nucleation process, the condensation nuclei count was recorded through the reactor charging period for runs 104 and 105. In these two cases the ozone was added to the reactor, already partially charged with sulfur dioxide, propylene and air, for thirty seconds commencing at 3.75 minutes into the filling period. Prior to the addition of the ozone, the observed nuclei count was approximately $400/cm^3$. The initiation of the homogeneous nucleation process was essentially instantaneous with the maximum concentration of $940,000/cm^3$ attained approximately thirty seconds before the recorded zero time. Here also, the maximum concentration of nuclei corresponded to a transient equilibrium condition during which the rate of addition of particles to the system by nucleation was equal to the loss by coagulation.

The relationship between the number concentration data and the coagulation constant predicts that the reciprocal of the number concentration should increase linearly with time for a system in which coagulation is the only removal process. The slope of the line formed as a result of this relationship is numerically equal to the average coagulation constant of the polydisperse aerosol system. The plots of the reciprocal number

concentration in Figures 5-18 through 5-23 show that after some initial period, a linear relationship was established. Wall or sedimentation losses would have been demonstrated by an increasing slope of this curve commencing at the time of occurrence. It was expected that should this phenomena occur, as it did in some of the higher concentration experiments, it would happen late in the run when the surface to volume ratio of the reactor has increased significantly.

The higher value of the coagulation constant noted for the first several minutes of the runs can be accounted for by the relatively large difference between the diameter of the newly formed embryos and the mean diameter of the growing aerosol. According to the theory of coagulation, for particles of unequal sizes, the coagulation constant increases rapidly with an increasing diameter ratio (Table III-1 and equation III-13).

The total surface area concentration for the six runs was observed to rise rapidly commencing prior to the recorded zero time. The large number of nuclei formed as a result of the gas to particle conversion coupled with the large surface to volume ratio for the small particles was responsible for this initial increase in surface area. As the aerosol growth continued, condensation tended to increase while coagulation reduced the total surface area observed until an apparent equilibrium condition between these processes was established. The surface area function remained essentially constant until the condensable material in the system diminished and the growth process was dominated by coagulation.

The increase in the total volume concentration proceeded at an appreciably slower rate than did the surface area concentration, again because of the small volume and relatively large surface area of the nuclei. The initial rise in the total volume was due to nucleation and at some later time, when sufficient surface area had been established, to

condensation. When the condensation process ceased due to the depletion of the vapor phase the total volume concentration was conserved as there were no system losses such as to the reactor walls. The slight decline noted in the total volume concentration curve for run 104 was due to the growth of the aerosol, or more specifically to some of the aerosol particles exceeding the range of the electrical mobility analyzer. Losses to the walls were contraindicated as the reciprocal number concentration curve was linear through this period consistent with a pure coagulation process.

At any time in the developmental history of the aerosol produced in the thermal reaction of propylene, ozone and sulfur dioxide, the relative contribution of each of the three processes varys. The expression for the rate of generation of particles in a particular class of the size distribution per unit volume for the simultaneous occurrence of nucleation, condensation and coagulation takes the form (according to Hidy and Brock, 1970 and Brock 1974):

$$\frac{\partial n(v,t)}{\partial t} = \underbrace{\tfrac{1}{2}\int_0^v b(v_c,v')\, n(v_c)n(v')\, dv' - n(v,t)\int_0^\infty bn(v')dv'}_{\text{coagulation}}$$

$$\underbrace{\frac{\partial}{\partial v}\left[\Psi(v)n(v,t)\right]}_{\text{condensation}} + \underbrace{\dot{\gamma}_N}_{\text{nucleation}} . \qquad \text{V-4}$$

where n = concentration of species in number per unit volume

b = collision parameter for Brownian motion in the free molecule regime

v = volume of particular class of molecular aggregate

Ψ = rate of condensation

$\dot{\gamma}_N$ = rate of generation of particles in the class by nucleation.

The rate of change in the mass concentration of the sulfuric acid (S), which is coupled to the equation for the rate of generation, takes the

functional form

$$\frac{\partial[H_2SO_4]}{\partial t} = k_{30}[I][SO_2] - \int_0^\infty \Psi(v,s)n(v,t)dv - \int_0^\infty v\dot{\gamma}_N(v,s)dv \qquad \text{V-5}$$

assuming that k_{30} $[I][SO_2]$ equals the rate of formation of the acid species due to the thermal reaction. And, if a pseudo-steady state is proposed for the acid concentration then

$$k_{30}\ [I][SO_2] = \int_0^\infty \Psi n dv + \int_0^\infty v\dot{\gamma}_N dv \qquad \text{V-6}$$

Owing to the form of the nucleation term, nucleation will take place only at high acid concentrations but condensation, once an aerosol phase has been established, will occur at a much lower supersaturation.

Once an aerosol has been formed it is difficult to distinguish between continued nucleation and condensation relative to their respective contribution to the aerosol mass. Small nuclei attach to the established aerosol surface in much the same manner and according to laws of the same form as do the condensing molecules. For example, one variable measured during this study was the change in the mean volume diameter with time. The governing rate equation based on condensation is $\frac{d\ \bar{D}pv}{dt} = \alpha' S_{molecules}$ while for the attachment of nuclei the expression is $\frac{d\ \bar{D}pv}{dt} = \alpha'' S_{nuclei}$. The equations are of the same form differing in the constants α' or α''. For a constant mass of acid in molecular form and a constant acid mass as nuclei, $\frac{d\ \bar{D}pv}{dt}$ would also be constant as was observed in the initial period of growth in these experiments. This could occur when the rate of production of the acid is constant which, according to the initial linearity of the volumetric conversion rate, was the case for this series of experiments.

An empirical result of computer simulation studies performed by

Brock (1974) indicates that for a system involving only the nucleation and coagulation processes, the reciprocal number concentration curve is markedly curved during the early stages of aerosol development in agreement with observations made during the studies reported herein. In contrast, the results of a simulation involving only the condensation and coagulation processes indicate that the reciprocal number concentration increases linearly with time. These empirically determined results can be used for the six aerosol experiments to distinguish between the nucleation and condensation processes from the reciprocal number concentration curves. The nucleation process appears to persist for a longer period in systems with a lower sulfur dioxide consumption and a lower total surface area (run 103 for example) while for runs in which the loss of sulfur dioxide is greater, the surface and volume increase more rapidly at the expense of the supersaturation level. As the acid vapor drops below the critical saturation in these high sulfur dioxide consumption runs (runs 104 and 105 for example) condensation commences earlier and at a lower supersaturation state than required by nucleation.

The volumetric conversion rate, total volume at 80 minutes, volume mean diameter growth rate, coagulation constant and the sulfur dioxide consumption through the first 80 minutes, all calculated from the data shown in Figures 5-18 through 5-23, are listed in Table 5-5.

The relative humidity was approximately the same during each of these aerosol experiments. The volumetric conversion rate was calculated for the period during which this function was constant, i.e., for at least the first twenty minutes of the run. The values listed for the volume and the sulfur dioxide consumption reflect measurements made when the experiments were eighty minutes old and when the volume accumulation was becoming stabilized. The coagulation constant was calculated from the

Table 5-5.

Volumetric Conversion Rate, Total Volume at 80 minutes, Mean Volume Diameter Growth Rate, Coagulation Constant and Sulfur Dioxide Consumption at 80 minutes for Aerosol Experiments

Run	RH (%)	$\frac{dv}{dt}$ $(\frac{\mu m^3}{cm^3 hr})$	$V(\frac{\mu m^3}{cm^3})$	$\frac{d\bar{D}_{pv}}{dt}$ $(\frac{\mu m}{hr})$	$Kx10^{-9}(cm^3 sec^{-1})$	ΔSO_2 (ppb)
101A	19	217	158	.391	1.26	11
101B	19	182	150	.340	1.44	10
102	18	139	86	.295	1.49	8
103	20	89	61	.258	1.61	4.5
104	20	437	235	.655	1.27	17.5
105	18	483	290	.671	1.28	21.5

linear portion of the curve of the reciprocal of the number concentration versus time. The rate of change in the mean volume diameter related to the initial period of each run for which this function was apparently constant.

The mean coagulation constant with one standard deviation calculated from the reciprocal number concentration curves for these runs was 1.39 ± 0.14 (x 10^{-9} cm^3/sec). The mean, count mean diameter calculated from the data for the six runs which appears in the Appendix with one standard deviation was 0.064 ± 0.014 μm. According to Fuchs (1964), the coagulation constant for equal sized particles having diameters between 0.04 and 0.1 μm would be in the range of 0.72 x 10^{-9} to 1.10 x 10^{-9} cm^3/sec (Table III-1). The agreement between the theoretically predicted and the measured values is very high particularly when the polydispersity is considered.

The count mean diameters of the distributions indicate that the particles are larger than the molecules in the suspending gas. In this system in which the Knudsen number is greater than 13.2, i.e., the free molecule regime, the kinetic theory of gases may be applied to aerosol coagulation. This implies that the particles are behaving like giant molecules mixed in the gas in such a way that they merely constitute just another component of the multicomponent gas phase system.

For these low level runs, the total amount of sulfur dioxide reacted was small and the reaction rate was slow. The volumetric conversion rate was essentially constant during at least the first twenty minutes of these runs as evidenced by the total volume concentration curves on Figures 5-18 through 5-23. Based on the initial, near linear consumption of the sulfur dioxide, an estimate of the consumption rate of that species during the initial period where the volumetric conversion rate was constant could be calculated. In the performance of this calculation it was assumed that

the sulfur dioxide consumption was directly proportional to the formation of the sulfur trioxide during this period, that the sulfuric acid to water ratio in the particles was constant and that equilibrium existed between the vapor and the condensed phase of the aqueous sulfuric acid. Bray (1970) generated tabulations of the relative humidity and the water vapor pressure over aqueous solutions of sulfuric acid as a function of the temperature and density at the equilibrium condition. The tabulation also included a correlation of the percent acid and the density of the aqueous sulfuric acid solution as reported in the Chemical Engineers Handbook (1963).

The following expression relates the oxidation rate of the sulfur dioxide with the volumetric conversion rate of the aqueous sulfuric acid solution through the percent acid and the solution density data:

$$\frac{d[SO_2]}{dt} = \frac{d[V_{SO_3(H_2O)_x}]}{dt} \; f\rho \; \frac{M_{SO_2}}{M_{H_2SO_4}} \qquad \text{V-7}$$

where f = the mole fraction of sulfuric acid in the aqueous solution at the temperature and relative humidity of the system

ρ = density of the solution and

M = molecular weight of the species.

Using the average temperature of 27°C, average relative humidity of 19 percent for the six aerosol runs and data from Bray's tabulation (density = 1.477 g/cm^3; percent acid = 58.43), the initial reaction rate of the sulfur dioxide was calculated. Dividing this result by the initial sulfur dioxide concentration yields the oxidation rate by the reactive species in this dark reaction. The results of these computations are listed in Table 5-6.

The mean oxidation rate with one standard deviation calculated from these data is 0.360 ± .096 percent/hour which is in good agreement with

Table 5-6. Initial Sulfur Dioxide Reaction Rate and Oxidative Rate.

Run	$\frac{d[SO_2]_o}{dt}$ ($ppm^{-1}min^{-1}$)	Oxidative Rate (%/hr)
101A	7.80×10^{-4}	0.414
101B	6.54	0.299
102	4.97	0.229
103	3.17	0.476
104	15.67	0.435
105	17.36	0.307

Table 5-7. Calculated Sulfur Dioxide Consumption based on the Observed Volume Concentration.

Run	ΔSO_2 Calculated (ppm)	$\frac{\Delta SO_2 \text{ Calculated}}{\Delta SO_2 \text{ Observed}}$
101A	0.022	2.0
101B	0.021	2.1
102	0.012	1.5
103	0.008	1.8
104	0.033	1.9
105	0.041	1.9

the observations of Cox and Penkett (1971) who reported an oxidation rate of 0.4 percent per hour for sulfur dioxide in their studies.

It was also of interest to determine whether the total volume concentration of aerosol measured at eight minutes into the run correlated with the sulfur dioxide consumption using the density, percent acid, and equilibrium conditions assumed in the previous calculations. The sulfur dioxide concentration was calculated, which according to the assumptions would be responsible for the volume observed. The calculated sulfur dioxide concentration was then compared to the amount reacted. The results of this analysis are reported in Table 5-7. The mean ratio of the calculated to the observed sulfur dioxide consumption based on these data is 1.9 ± 0.2 indicating that the volume concentration measured was somewhat greater than can be accounted for by this type of computation. There are a number of factors which could possibly account for this difference including an inaccuracy in the original assumptions of constant acid to water ratio in the volume and equilibrium between the vapor and the condensed phase of the aqueous sulfuric acid. It is believed, however, that this error more probably stems from the lack of an absolute calibration on the aerosol measuring instrument.

The observed volume and the sulfur dioxide consumption data, both at eighty minutes into the run, were plotted for the six aerosol experiments (Figure 5-24). The line was fit through the origin by a least squares regression analysis and a slope of approximately 13.5 was obtained. These data demonstrate the linearity of the relationship existing between these two parameters and as predicted by equation V-7.

The data displayed in Figures 5-18 through 5-23 show that the total surface area concentration grows quite rapidly to some apparent equilibrium level where it remains essentially constant for a significant period of

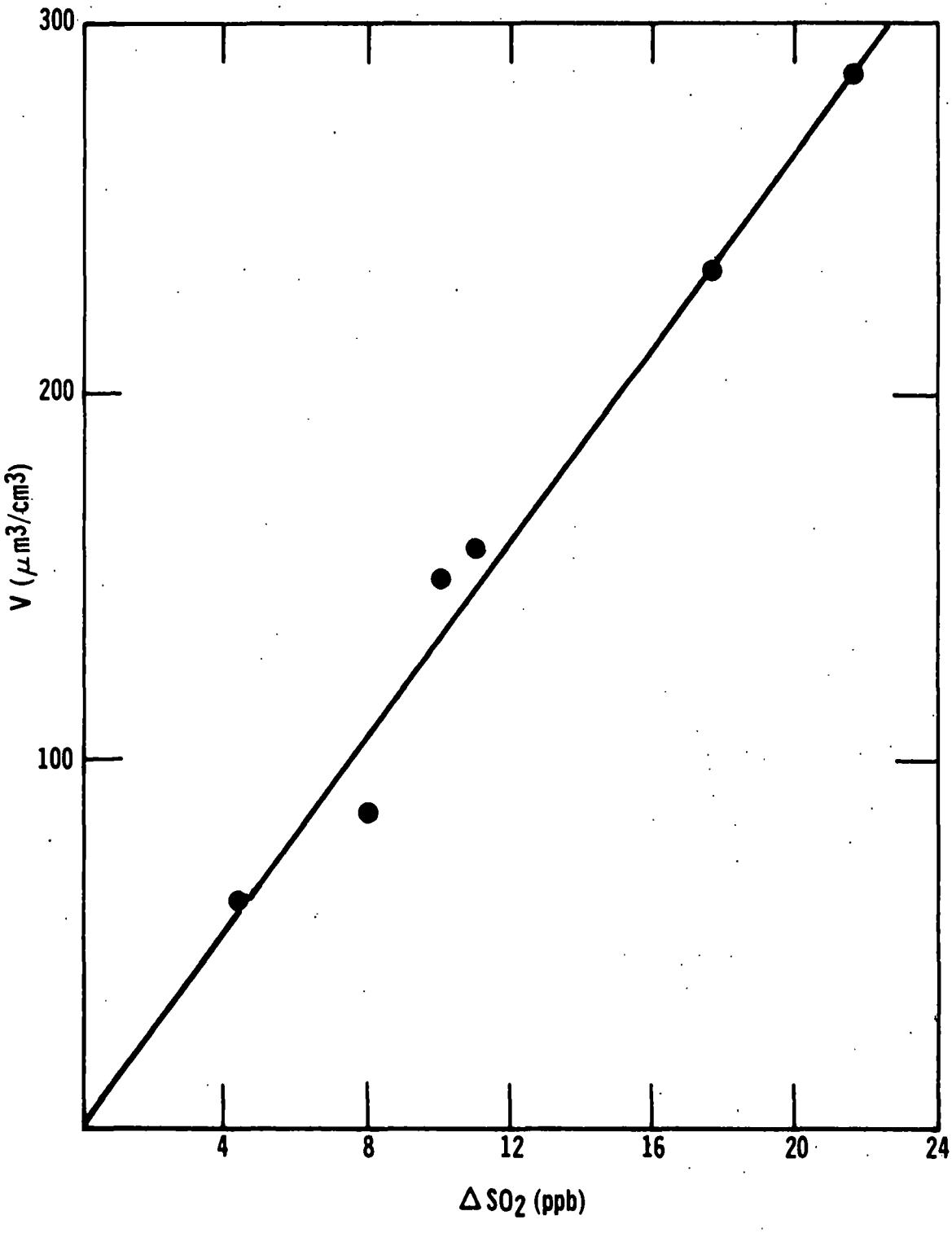

FIGURE 5-24. TOTAL VOLUME VERSUS SULFUR DIOXIDE CONSUMPTION AT T +80 MINUTES.

time. The total volume concentration of the aerosol can be seen to be increasing linearly to and in some cases beyond the time at which the equilibrium surface area is established. This indicates that the equilibrium condition is established as a result of the gain of surface area due to condensation and nucleation being offset by the loss due to coagulation. The equilibrium condition is destroyed when the reactants have largely been consumed, the degree of supersaturation diminished and new surface area is not being formed. The coagulation process continues and the total surface area is thereby reduced.

Clark (1972) noted, for his experiments dealing with the photooxidation of sulfur dioxide, a strong correlation between the equilibrium surface area and the volumetric conversion rate. A linear relationship was demonstrated in a log-log plot of the two parameters. This correlation was tested for the series of six aerosol experiments under discussion the results of which are shown in Figure 5-25. The line shown is fit to the six data points by the method of least squares regression analysis. The equation which best fits these data is given as

$$\log S_E = 0.583 \log \left(\frac{dv}{dt}\right) + 0.239 \qquad \text{(V-8)}$$

for which a correlation coefficient of 0.9933 was obtained.

Also plotted on this figure are the data from Clark's experiments as well as some data from sulfur dioxide photooxidation studies conducted by the University of Minnesota and by Calspan Corporation. Although it is generally considered a tenuous operation to extend a regression line beyond the limits of the data it was successfully done through more than two log decrements with these data. It is immediately apparent that all of the data plotted could be fit to a single regression line with a high correlation coefficient. Of note in this observation is the fact that

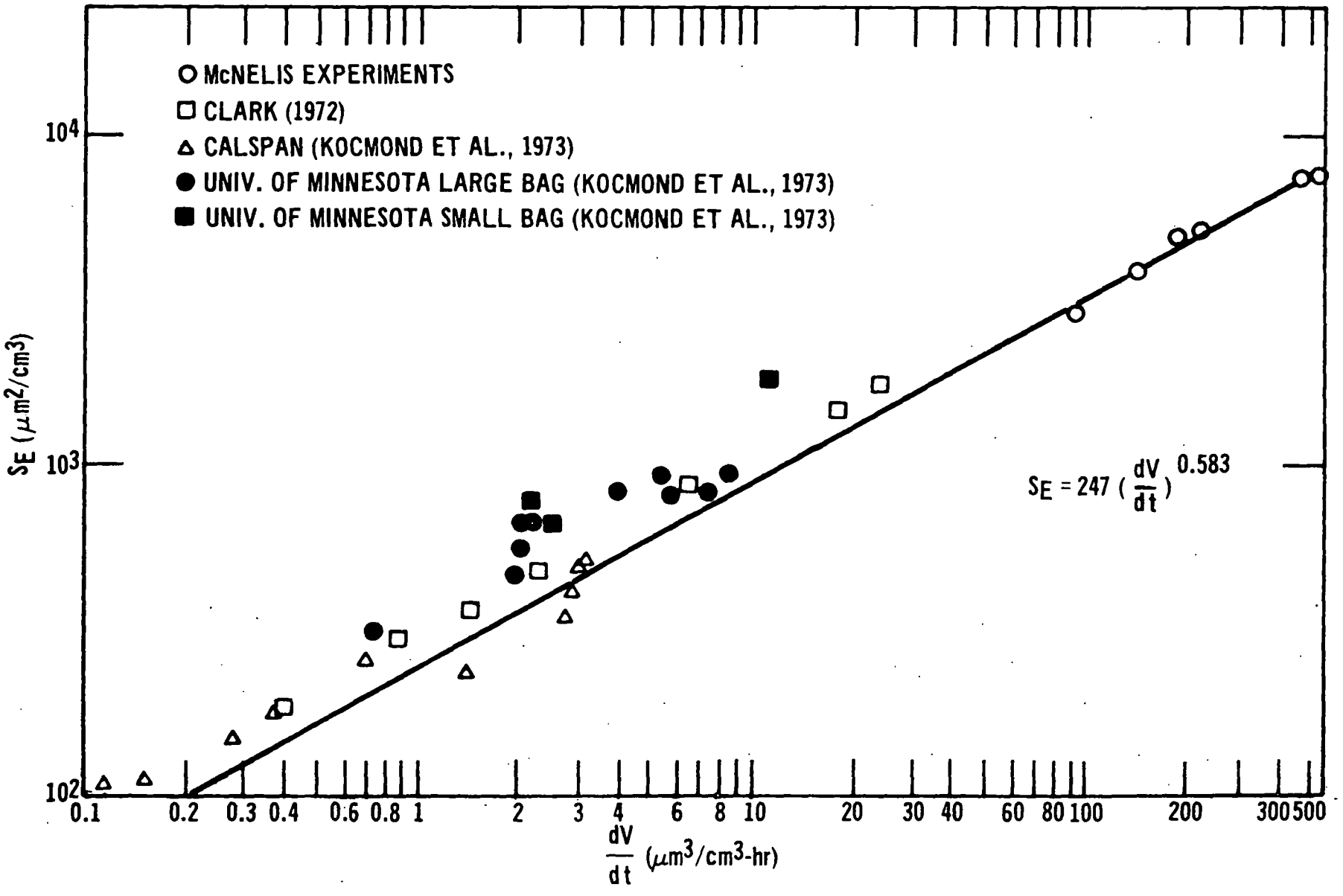

FIGURE 5-25. VARIATION OF THE EQUILIBRIUM SURFACE AREA WITH VOLUMETRIC CONVERSION RATE.

the data plotted for which the volumetric conversion rate $\leq$ 30 $\mu m^3/cm^3$-hr are from experiments involving the photooxidation of sulfur dioxide while those with the volumetric conversion rate > 80 $\mu m^3/cm^3$-hr are from a thermal reaction involving olefin-ozone-sulfur dioxide. The tendency toward the equilibrium surface area is controlled, therefore, by the physical processes of nucleation, condensation and coagulation rather than the particular chemical reaction leading to the gas to particle conversion.

The volumetric conversion rate measured for the initial period of the aerosol growth is plotted in Figure 5-26 against the product of the initial ozone and propylene concentrations for two different initial concentrations of sulfur dioxide. Included in this plot are eight of the experiments discussed earlier in this report for which both the reactant concentration data and the volumetric conversion rates were available and which involved higher reactant concentrations. The data point closest to the origin represents run 104 of the aerosol series. The curves shown are the least squares regression lines fit to the data and forced through the origin. The volumetric conversion rate for the higher concentration runs was estimated from $\frac{\Delta V}{\Delta t}$ over the first few minutes of the reactions only. These data indicate that for a given sulfur dioxide concentration, the aerosol formation follows second order kinetics with respect to the olefin and ozone concentrations. These data also indicate a predictive capability for the volumetric conversion rate which, for the low concentration runs, was observed to remain constant for a prolonged period.

The volume distribution of the aerosol was followed in time for the six runs. The distributions plotted at selected time intervals for these runs are shown in Figures 5-27 through 5-32. Depending on the time at which the distributions were measured they were influenced to a different degree by one or more of the three processes: nucleation, condensation

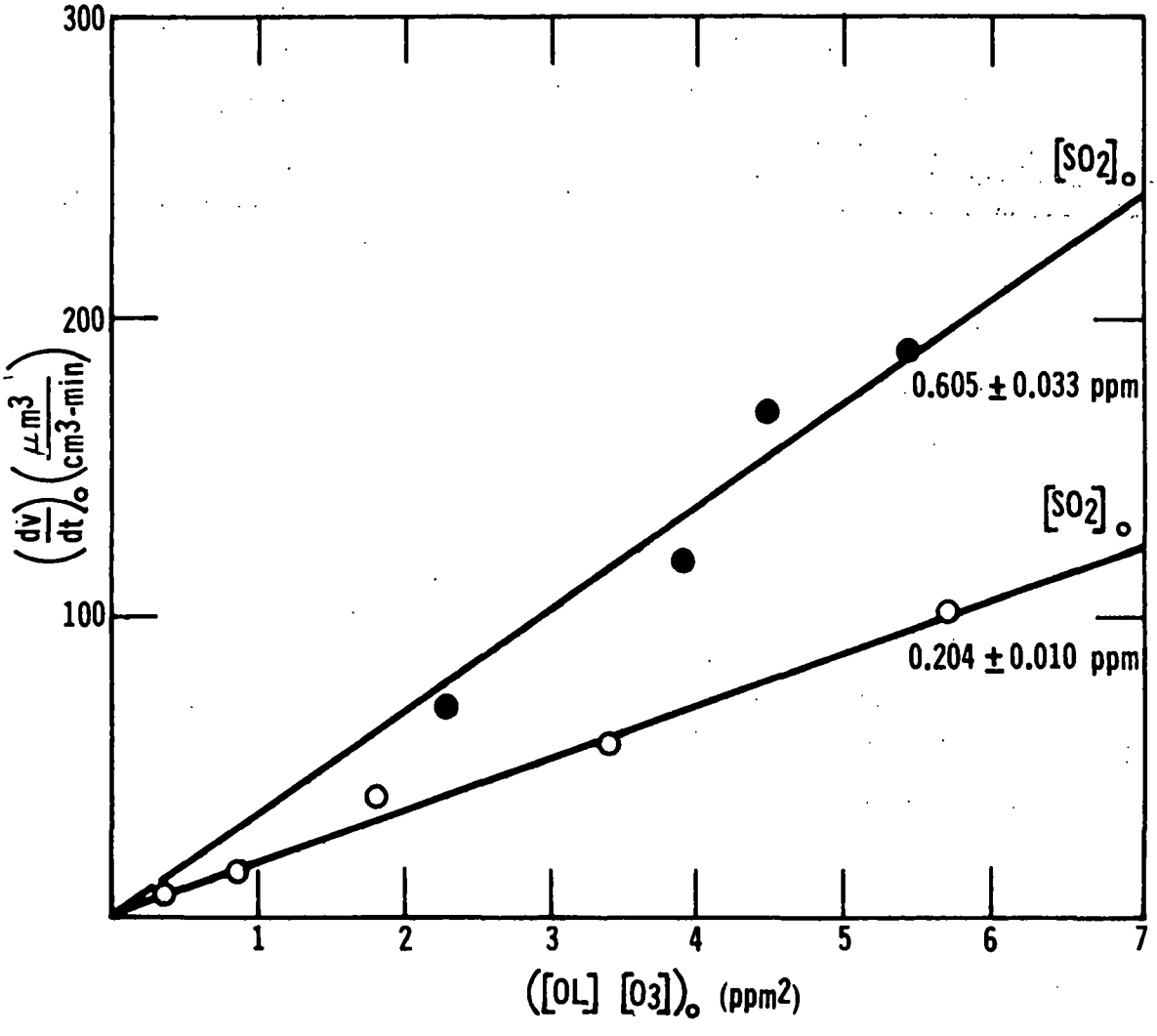

FIGURE 5-26. INITIAL VOLUMETRIC CONVERSION RATE VERSUS PRODUCT OF INITIAL PROPYLENE AND OZONE CONCENTRATIONS FOR DIFFERENT INITIAL SULFUR DIOXIDE CONCENTRATIONS.

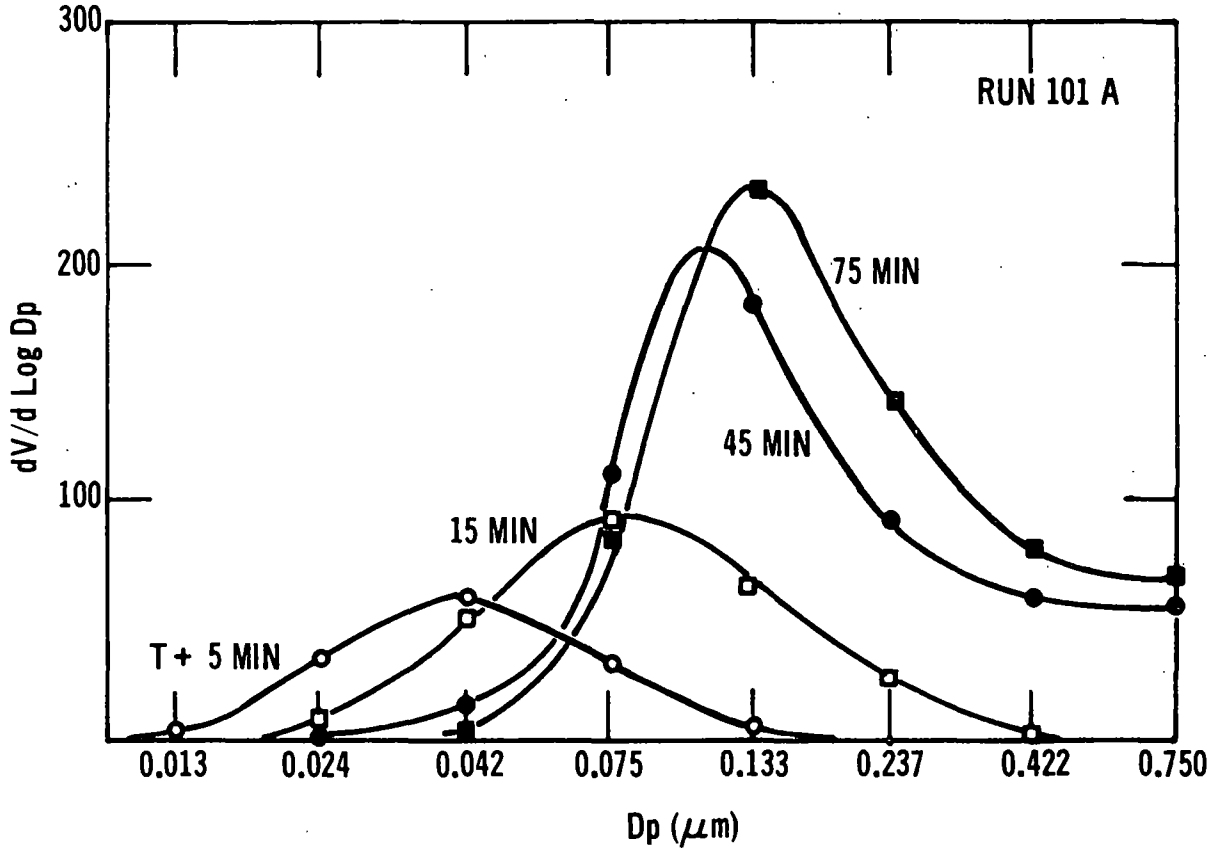

FIGURE 5-27. DEVELOPMENT OF THE VOLUME DISTRIBUTION WITH TIME.

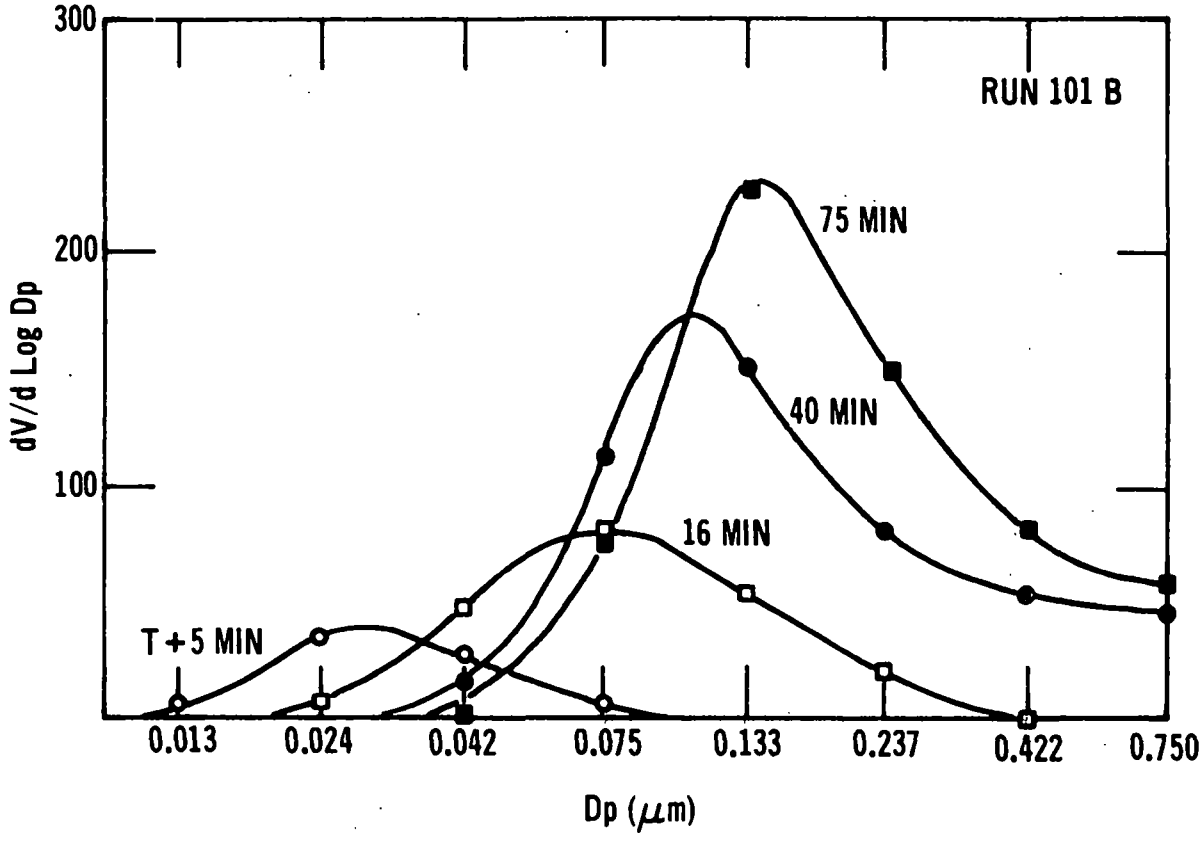

FIGURE 5-28. DEVELOPMENT OF THE VOLUME DISTRIBUTION WITH TIME.

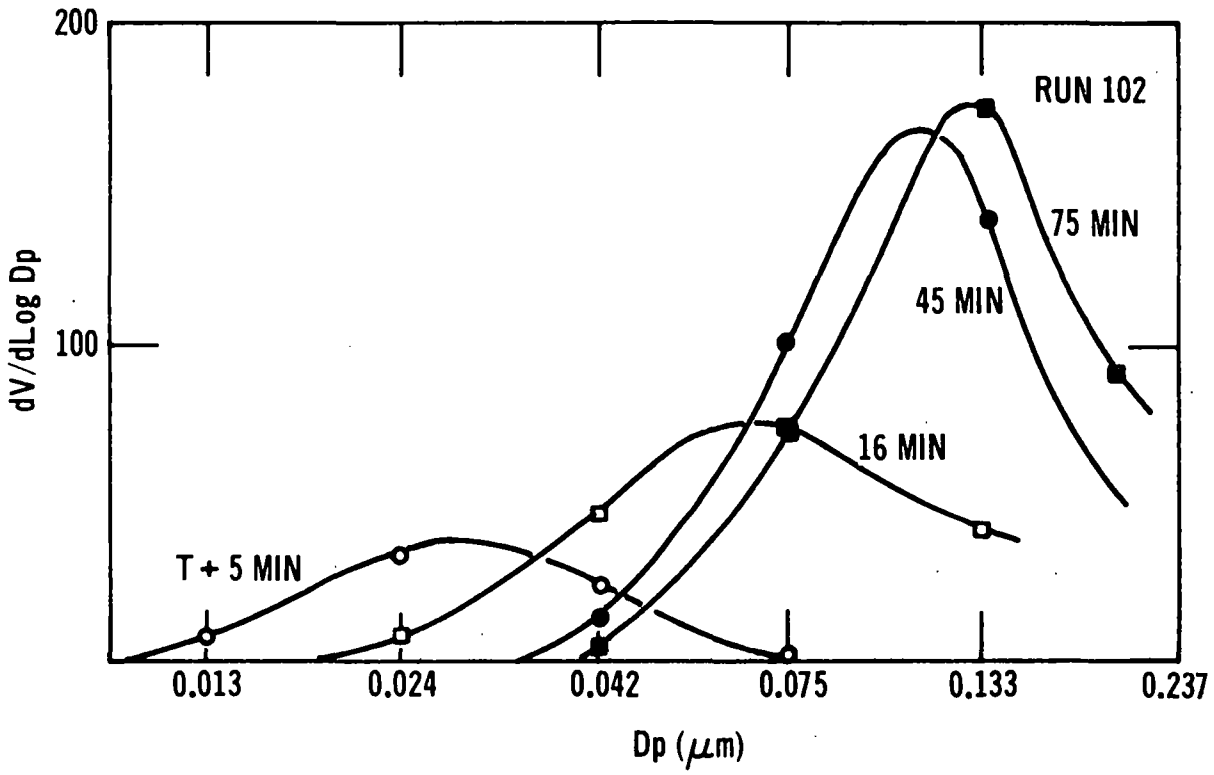

FIGURE 5-29. DEVELOPMENT OF THE VOLUME DISTRIBUTION WITH TIME.

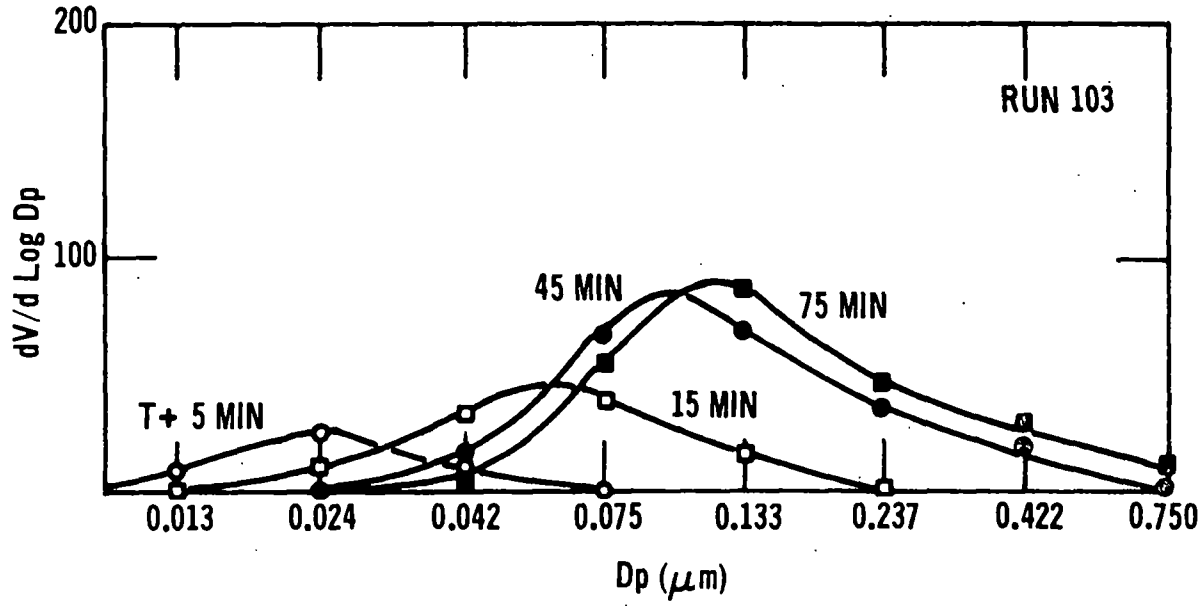

FIGURE 5-30. DEVELOPMENT OF THE VOLUME DISTRIBUTION WITH TIME

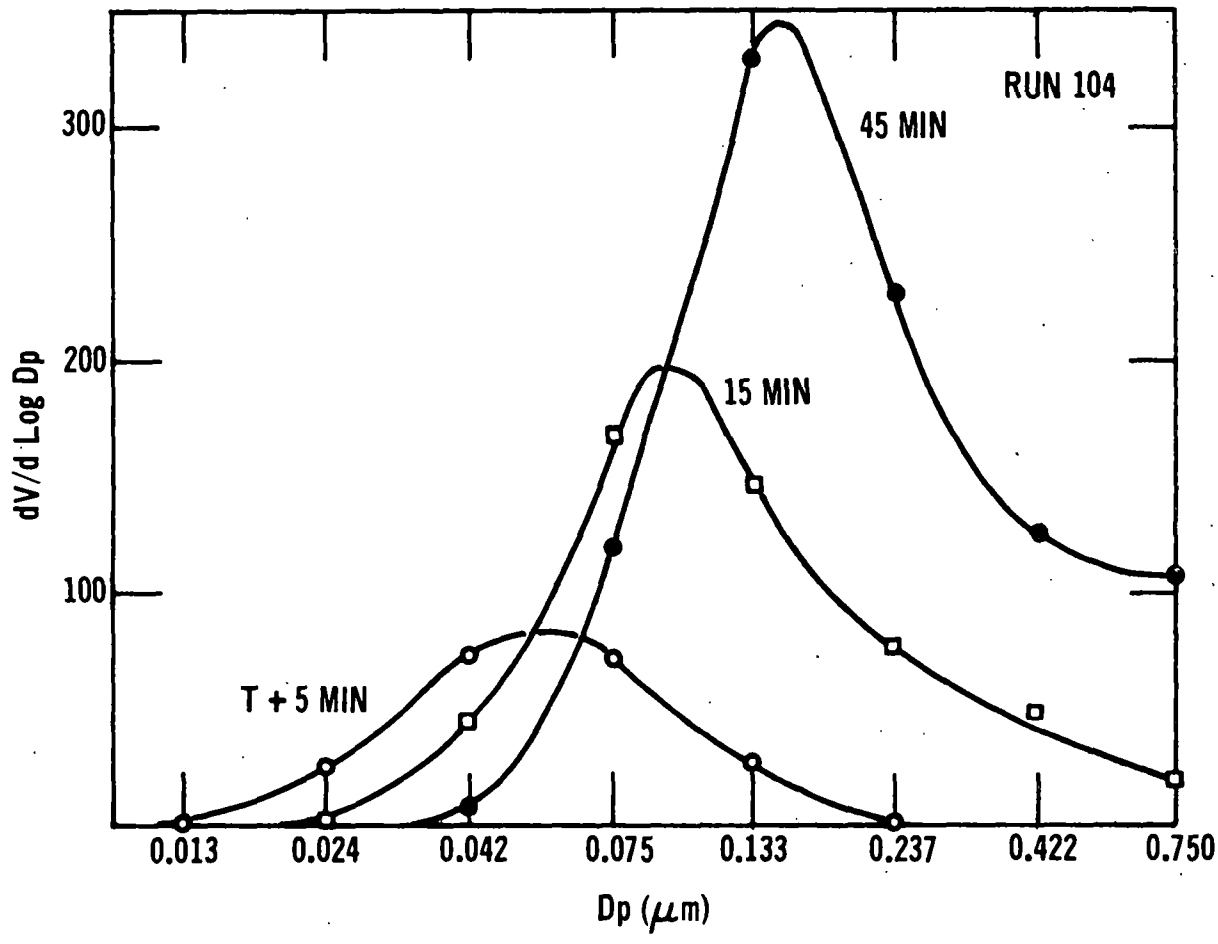

FIGURE 5-31. DEVELOPMENT OF THE VOLUME DISTRIBUTION WITH TIME.

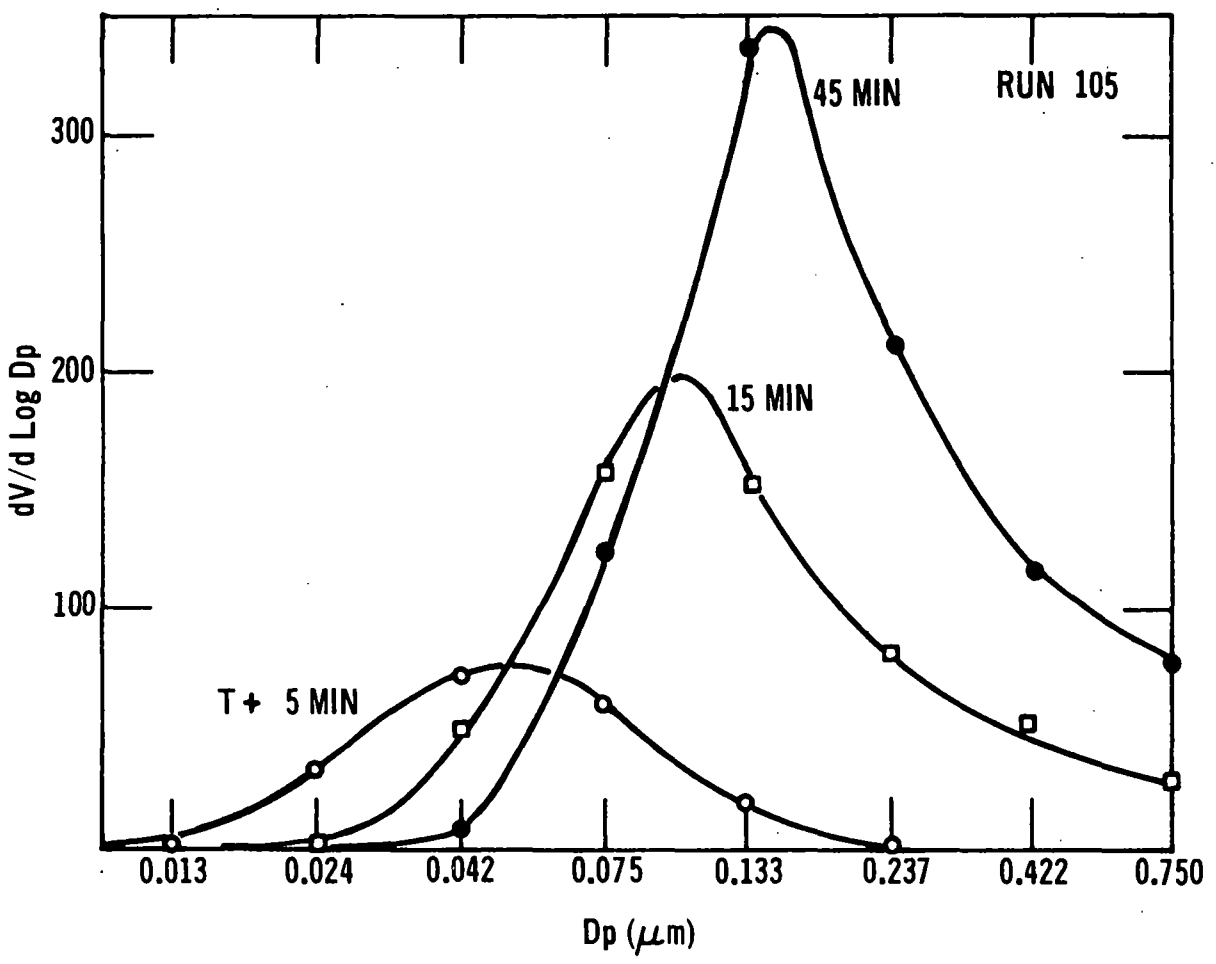

FIGURE 5-32. DEVELOPMENT OF THE VOLUME DISTRIBUTION WITH TIME.

and coagulation. The frequency parameter used in these plots, $\frac{dV}{d\log D_p}$, presents the distribution in such a manner that the area under the curve in a given size range is proportional to the volume in that range.

There are several notable features in these developmental volume distributions which were similar for each of the experiments. Most obvious is the shift in the distributions to larger mean diameters with time. The rate of change appears, however, to decrease at later times and the mean volume diameter appears to be approaching some limit. The increase in the total volume is also readily apparent, particularly in runs in which the sulfur dioxide consumption was highest.

Although in the logrithimic display of these data, it appeared that the distributions were becoming narrower, in fact the spread increased over a larger range of particle diameters. The count distribution data (included in the Appendix) also reflect the increasing polydispersity with time. From theoretical considerations, the tendency for the size distribution, due to droplet growth by diffusion of vapor, i.e., condensation, is to become narrower. The increasing polydispersity in this system, therefore, must have been due to the formation of larger particles by collisions and coalesence of smaller ones, also theoretically predicted. The tail of the distribution curves for measurements made late in the runs show that for the runs in which the amount of sulfur dioxide reacted was high, there was some few particles which outgrew the range of the electrical mobility analyzer.

The volume mean diameters of the growing aerosol were calculated for each of the runs at several different times out to beyond eighty minutes in most cases. These data are plotted in Figure 5-33 and show that the rate of change in the volume mean diameter is apparently constant for

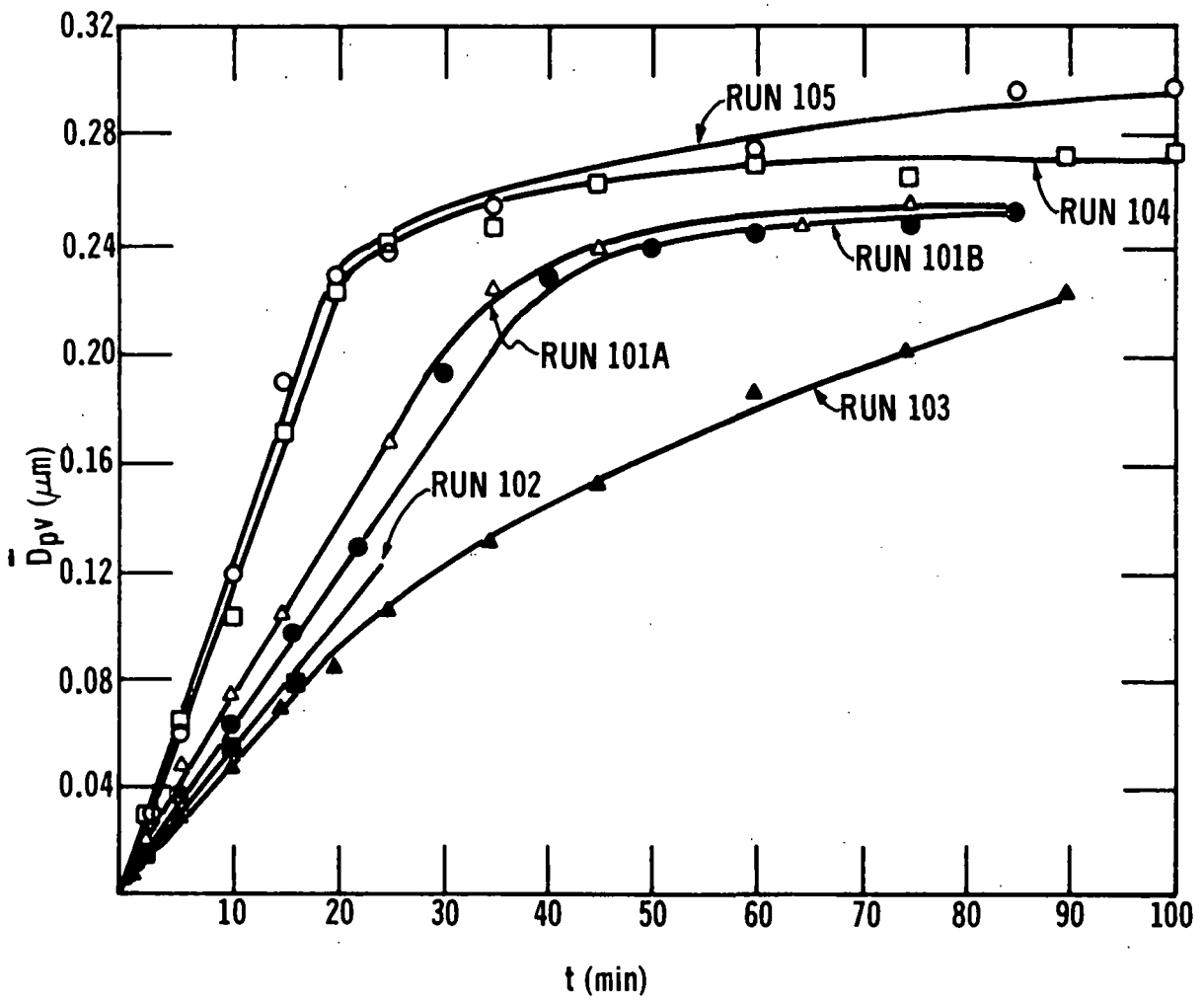

FIGURE 5-33. VARIATION OF VOLUME MEAN DIAMETER WITH TIME FOR SIX AEROSOL EXPERIMENTS.

the initial period of at least twenty minutes. The slopes of the linear portion of these curves are listed in Table 5-5 and range from 0.258 μm/hr for run 103 to 0.671 μm/hr for run 105. The higher rates correspond to the runs in which the largest amount of sulfur dioxide was reacted. The mean volume diameters for each of the runs tended to reach some upper limit of development which for the conditions of these experiments appeared to be about 0.25 to 0.30 μm.

The curves plotted in Figure 5-33 also indicate two distinct growth regimes which are more obvious on the curves having the higher initial rate of change in the mean volume diameter. The knee of these curves corresponds in time to the point at which the reciprocal number concentration curves became linear (Figures 5-18 through 5-23). The coagulation process essentially commences in these systems concurrently with the initiation of the gas phase reaction because of the very rapid increase in the number concentration of nucleated droplets and continues throughout the experimental period. The nucleation process, however, occurs initially when the supersaturation exceeds some critical value and recedes when either the supersaturation drops too low to support the process or when sufficient surface area is formed and the condensation process competes for the material in the vapor phase. It is suggested for these curves, that the initial linear increase in the volume mean diameter is due to a coupling of the nucleation and the coagulation processes while the later and slower increase is due to condensation and coagulation. The relative sharpness of the knee depends on the accumulative effect of the speed with which the critical surface area in the system develops and with which the acid in the vapor phase is depleted by condensation. The net result of this additive effect is a sharp decline in and termination of the homogeneous nucleation process.

The constant rate of change observed initially in the volume mean diameter was found to be linearly related to the volumetric conversion rate measured for each of the aerosol experiments through the logarithms of the two functions. These data are plotted in Figure 5-34 and the line shown is fit by the method of least squares regression analysis. The equation which best fits this data is given by

$$\log \left(\frac{d\bar{D}_{pv}}{dt}\right) = 0.6102 \log \left(\frac{dv}{dt}\right) - 1.8172$$

for which a correlation coefficient of 0.9880 was obtained.

The results of these aerosol characterization studies could have an immediate application in the generation of sulfuric acid mist of known physical properties for controlled laboratory animal exposures. The data displayed in Figure 5-26 indicate that the volumetric conversion rate of condensable material from the vapor to the aerosol phase is predictable from a knowledge of the initial reactant concentrations. And, for a given initial concentration of sulfur dioxide, the aerosol formation follows a second order rate law with respect to the two primary reactants, propylene and ozone. The curve drawn in Figure 5-34 shows that the rate of change in the mean volume diameter is also predictable based on the volumetric conversion rate. Finally, the curves previously discussed and displayed in Figure 5-33 show that some limit on the development of the mean volume diameter occurs in practical systems and is likewise predictable. For the conditions of these experiments a limit of 0.25 to 0.30 μm was imposed on the growth of the mean volume diameter.

Although it is believed that aerosols having other mean volume diameters could be generated through this mechanism, the mean volume diameter observed in these studies is of particular interest. Previous studies, summarized by Lewis et al. (1972), made use of aerosols of 0.8, 2.5 and

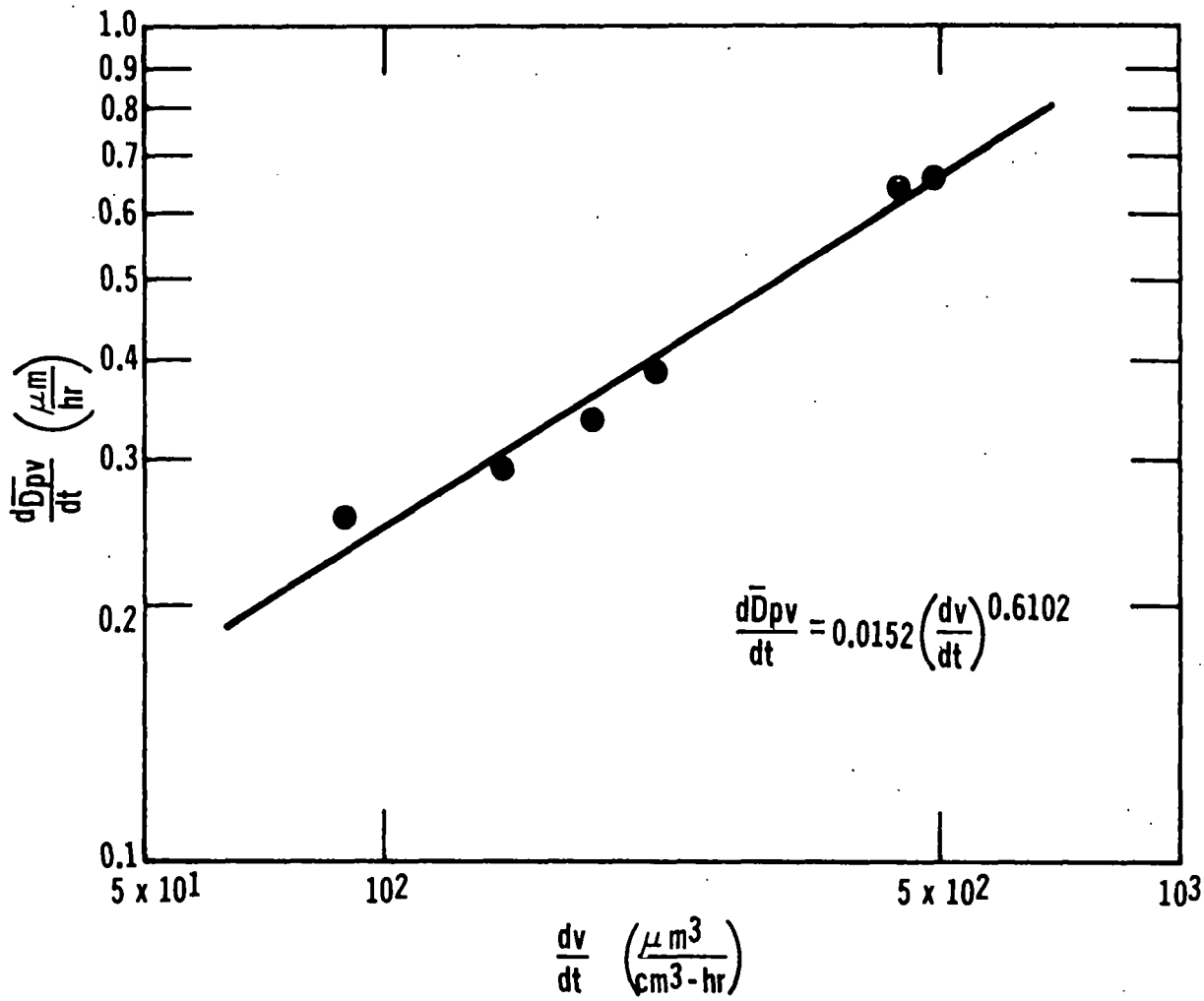

FIGURE 5-34. RATE OF CHANGE IN MEAN VOLUME DIAMETER VERSUS VOLUMETRIC CONVERSION RATE.

7.0 μm mass median diameters (mmd) to measure the effect of sulfuric acid mist on the pulmonary function of guinea pigs. Few particles of the largest size penetrate beyond the nasal-pharangeal region where they can cause an obstruction in the larger airways. The two smaller sizes can penetrate the lower regions of the respiratory system and interact with the smooth muscle lining around the terminal and other small bronchioles. It is this smooth muscle which contracts to produce in humans the symptoms of asthma, the physiological response most strongly associated with suspended particulate sulfate (Environmental Protection Agency, 1974). An acid aerosol with a mass mean diameter of the size generated during the aerosol studies discussed in this dissertation (approximately 0.3 μm) has not been used in exposure studies. It is suggested that these smaller particles would penetrate the alveoli, the division of the pulmonary region of the lung which has no smooth muscle and as a result, a different physiological or histopathological response may be observed.

G. Aerosol Measurements by Single Particle Light Scattering.

The aerosol generated in the series of the experiments just discussed was limited in growth by controlling the initial reactant concentrations. That series led to the development of an internally consistent mechanism to describe the relative contribution of the different processes leading to the production and growth of the acid aerosol. The aerosol produced in the higher reactant concentration experiments was also monitored with an optical aerosol analyzer. The results of these measurements for typical experimental runs are shown in Figures 5-35 and 5-36 for a propylene-ozone-sulfur dioxide system and for a ethylene-ozone-sulfur dioxide system respectively. The general trends displayed for the two different olefins are similar with the production of the light scattering aerosol occurring

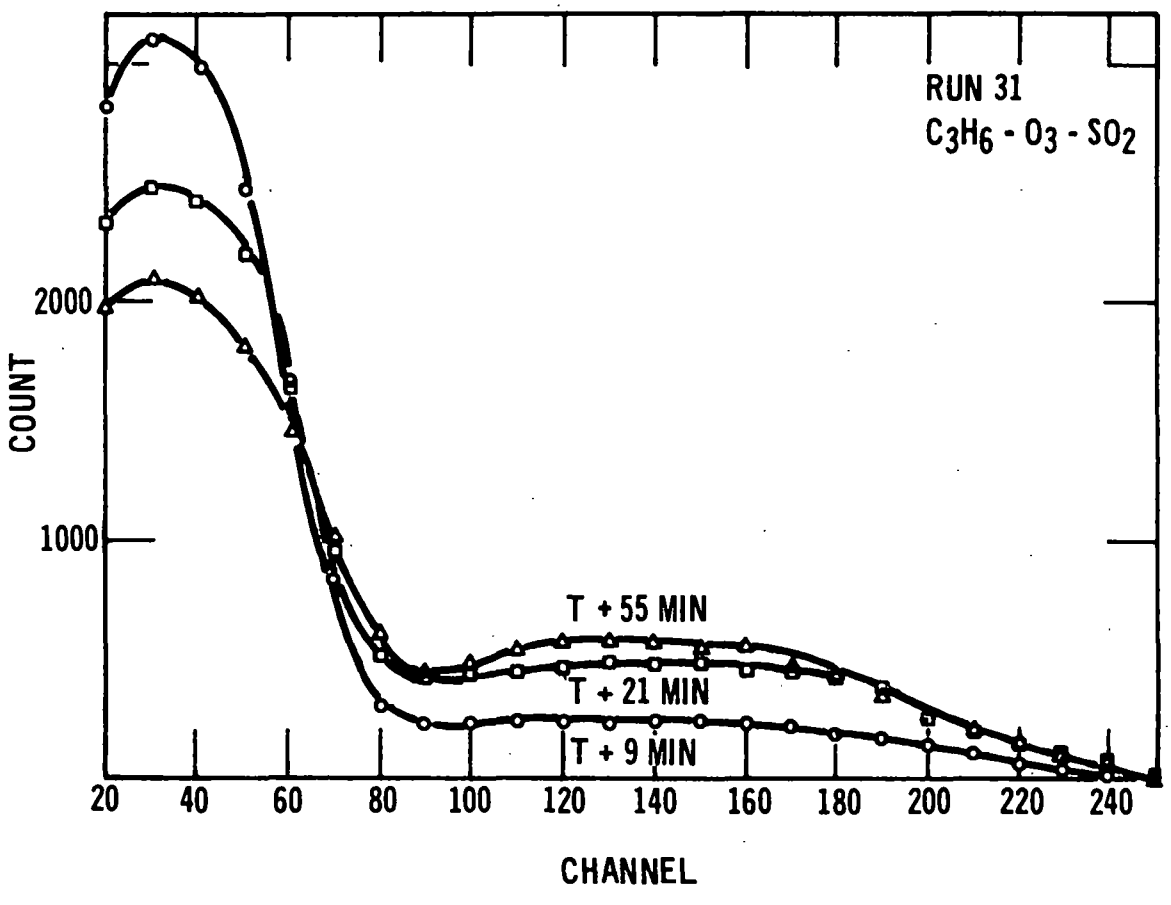

FIGURE 5-35. VARIATION OF AEROSOL SIZE DISTRIBUTION WITH TIME AS MEASURED WITH OPTICAL PARTICLE SIZE ANALYZER.

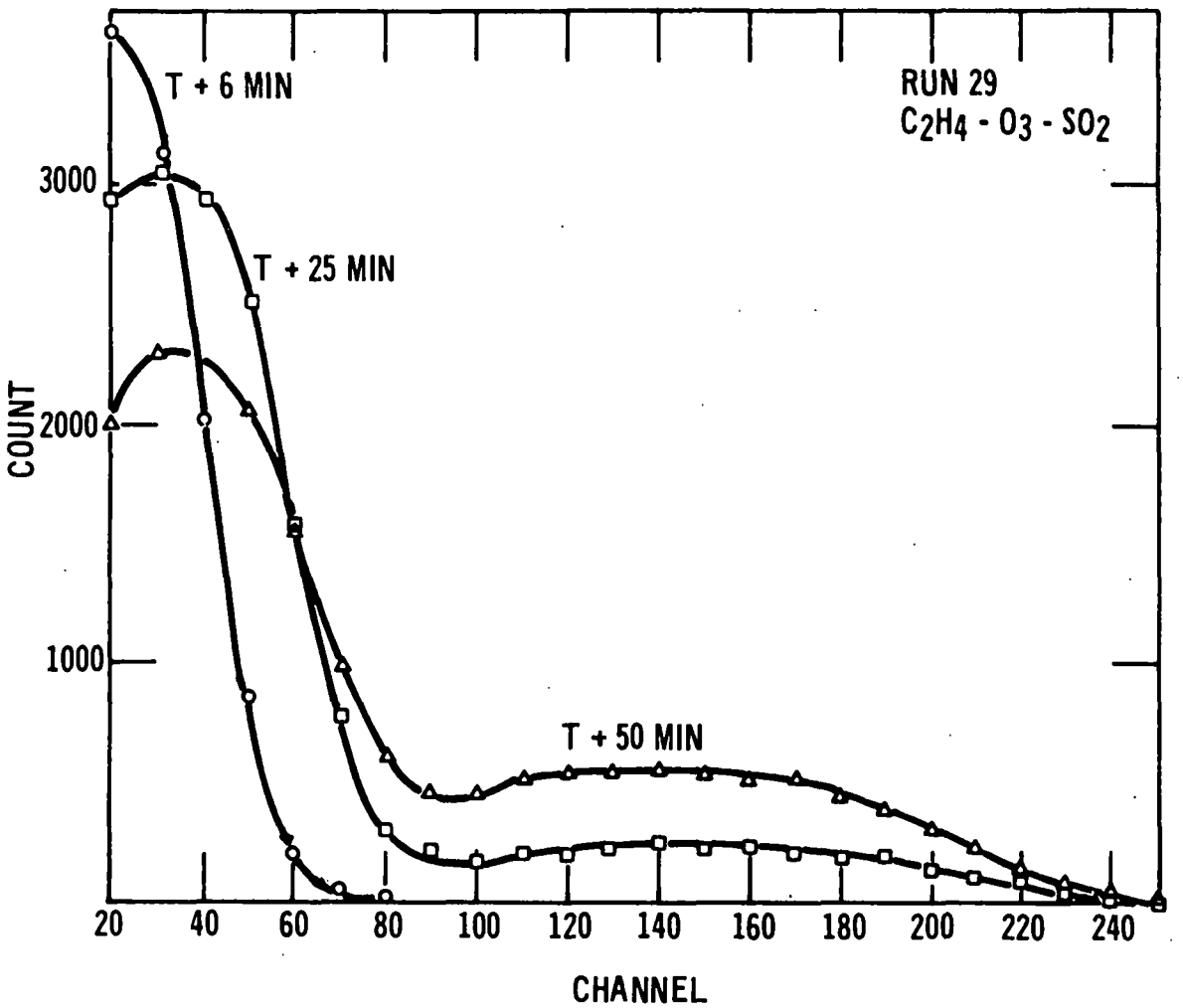

FIGURE 5-36. VARIATION OF AEROSOL SIZE DISTRIBUTION WITH TIME AS MEASURED WITH OPTICAL PARTICLE SIZE ANALYZER.

earlier and at a faster rate in the propylene system. The fact that ethylene produces a similar aerosol is itself of note supporting the basic features of the gas phase mechanism postulated earlier. Principal features of these aerosol size distributions are the first peak which occurs at about 0.38 μm, the saddle at approximately 0.76 μm and the second peak at channel 140 for which the diameter is 1.35 μm. Although the aerosol outgrew the range of the electrical mobility analyzer, the measurement by that instrument indicated a somewhat lower mean size for the first peak. More important, however, is the existence of the second peak which occurred in each of the higher concentration runs. It is speculated that this secondary peak and the saddle point occur as a result of the enhanced coagulation among particles of unequal sizes. This mechanism would account for the peak becoming more pronounced at the expense of the smaller particle sizes through the saddle point of the combined distribution for these systems of higher reactant consumption. More significant in the observation of the second peak is the fact that although only a relative few droplets grow to this larger size they can account for an appreciable fraction of the total aerosol mass.

CHAPTER VI

CONCLUSIONS AND RECOMMENDATIONS

As a result of the measurements made during these experiments and reported on in this dissertation, the mechanism leading to the oxidative consumption of sulfur dioxide is better understood. In addition, the mechanism leading to the production, growth and decay of a sulfuric acid aerosol from the thermal gas phase reaction has been explained in terms of the basic processes of nucleation, condensation and coagulation. Finally, the coupling of the gas phase and the aerosol information provides a unique set of data with which to evaluate atmospheric and photochemical smog chamber results. The principal conclusions reached as a result of these studies follow in a summarized format.

1. The reactor vessel and sampling system designed and assembled for these experiments were found to perform satisfactorily in the study of selected dark phase reactions and in the measurement of specific gas and condensed phase products. A reactor having a larger volume is suggested for use in any additional studies of the type conducted to allow for more nearly continuous sampling with all of the instrumentation.

2. Wall effects did not affect the results or the conclusions of this study significantly. The losses of the individual reactants were measured and found not to affect the stoichiometric results. The sulfur mass balance and the aerosol reciprocal number concentration measurements indicate that a measurable loss of sulfur to the walls occurred only at the terminus of the runs when the surface to volume ratio of the reactor became excessively large. The lower recovery of total carbon evaluated

near the end of the runs was believed due to the carbon content of unmeasured products.

3. The stoichiometry of the propylene-ozone reaction was found to be a smooth function of the initial concentration ratio of these species. The olefin/ozone consumption was > 1 for a system in which the olefin was initially in excess and < 1 for a system having an initial ozone excess. The consumption ratio was unaffected by the addition of sulfur dioxide to the reactor or by varying the relative humidity over the range of 20 to 38 percent.

4. Molecular oxygen had a significant effect on the reaction stoichiometry and product formation in the propylene-ozone thermal reaction. The propylene/ozone consumption ratio was lower in a system in which the molecular oxygen concentration was reduced. Oxygen also contributed to the regeneration of ozone and the production of the hydroxyl radical species, both of which interacted with the propylene and with products of the reaction. Although the formation of the hydroxyl radical had been postulated, these experiments provided the first direct evidence for its participation and its role.

5. Acetyaldehyde, formaldehyde, carbon monoxide, ketene and formic acid were observed products of the propylene-ozone reaction. The concentrations of acetyaldehyde, formaldehyde and carbon monoxide were affected by the molecular oxygen concentration. Ketene was apparently unaffected by the availability of oxygen while the production of formic acid depended on its presence. Ketene was not observed in any of the reactions involving sulfur dioxide as a reactant indicating that its rate of formation is significantly slower than the rate of the bimolecular reaction between sulfur dioxide and the intermediate species.

6. The mechanism which follows has been advanced in this dissertation

for the oxidative consumption of sulfur dioxide in the propylene-ozone-sulfur dioxide system and which is consistent both internally and with the data observed in this study. Secondary reactions are a distinctive feature of this model which incorporates relatively few reactions to explain the major characteristics of the system studied. The rate constant for the propylene ozonalysis step of the mechanism was estimated to be 1.40 ± 0.39 ($\times 10^{-2}$ ppm^{-1} min^{-1}). The steps of the proposed mechanism are as follows:

$$O_3 + CH_3\text{-}CH{=}CH_2 \rightarrow HCHO + CH_3\dot{C}HOO\cdot \qquad (1)$$

$$O_3 + CH_3\text{-}CH{=}CH_2 \rightarrow CH_3CHO + H\dot{C}HOO\cdot \qquad (1a)$$

$$R\dot{C}HOO\cdot + O_2 \rightarrow \cdot OH + R\overset{O}{C}OO\cdot \qquad (11)$$

$$R\dot{C}HOO\cdot + O_2 \rightarrow O_3 + RCHO \qquad (13)$$

$$CH_3\dot{C}HOO\cdot \rightarrow CH_2{=}C{=}O + H_2O \qquad (5)$$

$$\cdot OH + CH_3\text{-}CH{=}CH_2 \rightarrow CH_3\dot{C}H\text{-}CH_2OH \qquad (14)$$

$$R\dot{C}HOO\cdot + SO_2 \rightarrow SO_3 + RCHO \qquad (30)$$

7. Aerosol formation occurred in the dark reaction of propylene and ozone although the particulates formed did not grow to a size which efficiently scattered light. The addition of sulfur dioxide to the reactor markedly enhanced both the formation and subsequent growth of the aerosol. The rate of aerosol formation was also much faster in the system which included sulfur dioxide. For a given initial sulfur dioxide concentration the aerosol formation was found to follow second order kinetics with respect to the propylene and ozone concentrations.

8. The same general patterns of aerosol formation, growth and decay, were observed over an extensive range of volumetric conversion rates. These

patterns are consistent with a model which includes homogeneous nucleation, condensation and coagulation. Nucleation commenced in the system which included sulfur dioxide almost immediately upon initiation of the gas phase reaction. Coagulation of the newly formed embryos and the growing droplets commenced within seconds and persisted throughout the experimental period. Condensation began with the establishment of a stable aerosol phase and soon replaced nucleation as the primary gas to particle conversion process.

9. An apparent equilibrium surface area was established for the aerosol when the addition to the total surface area by condensation was equal to the loss by coagulation. A strong correlation was found to exist between this equilibrium surface area and the volumetric conversion rate. It was also found that the correlation could be extended considerably in range to include data from experiments conducted elsewhere in which the aerosol was photochemically generated. The establishment of the equilibrium surface area is due, therefore, to the physical processes rather than the chemical mechanism leading to its formation.

10. The volume distributions were observed to shift to larger sized droplets with time. An upper limit for droplet growth was noted and was attributed to the depletion of the reactant concentrations, of the concentration of the sulfuric acid in the vapor phase and of the number concentration of the aerosol droplets. The initial rate of change in the mean volume diameter was found to be highly correlated with the volumetric conversion rate according to a power function relationship.

11. Finally, the apparent dependence of the volumetric conversion rate on the initial reactant concentrations and of the rate of change of the mean volume diameter on the volumetric conversion rate provide a predictive capability potentially useful in the generation of a sulfuric

acid aerosol of known physical properties for controlled laboratory animal experimentation.

It is recommended that additional research be conducted to measure or to obtain through appropriate mathematical models the sulfur dioxide oxidation rate. The reaction scheme advanced in this dissertation with its mechanism for ozone regeneration and hydroxyl radical production could be tested in existing kinetic models comparing the results with the concentration profiles observed in this study.

Experimentation along the lines conducted in this study should also be continued to include other olefinic compounds. The structure and reactivity of the intermediate species and the reaction products would vary depending on the unsaturated hydrocarbon investigated. Tetramethylethylene, for example, would yield acetone as an initial product in lieu of the aldehydes. The hydroxyl radical reaction with the acetone is expected to be significantly slower than its reaction with the aldehydes and the product inventory and primary reaction stoichiometry would be affected. The products of the secondary reaction between the olefin and the hydroxyl radical require identification as do the products of the decomposition reactions of the hydroxyl radical-olefin adducts. The products of these composite reactions could be followed in time with a system like the Fourier Transform Infrared Spectrometer and the concentration profiles evaluated to determine the relative potential of the various olefins in photochemical smog development.

The hydroxyl radical is, perhaps, the most important oxidizing species in photochemical smog particularly in the early stages before the ozone concentration develops. Although the initial reaction of the hydroxyl radical with saturated and unsaturated hydrocarbons is established, its mode of reaction with aromatics is speculative. Experimental evidence is

needed to fix the exact mechanism of that reaction. Specification of the oxidation mechanism for sulfur dioxide in reactions involving the hydroxyl radical with olefins, parraffins and aromatic hydrocarbons is also needed. These reactions potentially contribute to the development of secondary aerosols in the ambient atmosphere which are largely responsible for the aggravation of respiratory ailments and reduced visibility associated with photochemical smog.

REFERENCES

Ahlquist, N.C. and Charlson, R.J., "Measurement of the Wavelength Dependence of Atmospheric Extinction Due to Scatter," Atmospheric Environment, Vol. 3, p. 551 (1969).

Altshuller, A.P. and Bufalini, J.J., "Photochemical Aspects of Air Pollution: A Review," Environmental Science and Technology, Vol. 5, p. 39 (1971).

Amelin, A.G., Theory of Fog Condensation, S. Monson Wiener Bindery Ltd., Jerusalem, 1967, pp. 1-39.

Bademosi, F., "Diffusion Charging and Related Transfer Processes in Knudsen Aerosols," Ph.D. Thesis, University of Minnesota, Minneapolis, 1971.

Bailey, P.S., "The Reactions of Ozone with Organic Compounds," Chemical Reviews, Vol. 58, p. 925 (1958).

Baulch, D.L., Drysdale, D..D and Lloyd, A.C., "High Temperature Reaction Rate Data," Department of Physical Chemistry, The University, Leeds, England, 1968.

Becker, R. and Döring, W., "Kinetic Treatment of Embryo Formation in Supersaturated Vapours," Annalen der Physik, Vol. 24, p. 719 (1935).

Blacet, F.E., "Photochemistry in the Lower Atmosphere," Industrial and Engineering Chemistry, Vol. 44, p. 1339 (1952).

Bray, W.H., "Water Vapor Pressure Control with Aqueous Solutions of Sulfuric Acid," Journal of Materials, Vol. 5, p. 239 (1970).

Brock, J.R., Private Communication, University of Texas, Austin, 1974.

Bufalini, M., "Oxidation of Sulfur Dioxide in Polluted Atmospheres," Environmental Science and Technology, Vol. 5, p. 685 (1971).

Bufalini, J.J., Private Communication, Environmental Protection Agency, Research Triangle Park, North Carolina, 1974.

Bufalini, J.J. and Altshuller, A.P., "Kinetics of Vapor-Phase Hydrocarbon-Ozone Reactions," Canadian Journal of Chemistry, Vol. 43, p. 2243 (1965).

Cadle, R.D. and Schadt, C., "Kinetics of the Gas Phase Reaction of Olefins with Ozone," Journal of the American Chemical Society, Vol. 74, p. 6002 (1952).

Cadle, R.D. and Schadt, C., "Kinetics of the Gas Phase Reaction between Acetylene and Ozone," The Journal of Chemical Physics, Vol. 21, p. 163 (1953).

Calvert, J.G., "Interactions of Air Pollutants," Presented at the National Academy of Sciences, Conference on Health Effects of Air Pollutants, Washington, D.C. (1973).

Charlson, R.J., Ahlquist, N.C., Selvidge, H. and MacCready, P.B. Jr., "Monitoring of Atmospheric Aerosol Parameters with the Integrating Nephlometer," Journal of the Air Pollution Control Association, Vol. 19, p. 937 (1969).

Clark, W.E., "Measurements of Aerosols Produced by the Photochemical Oxidation of SO_2 in Air," Ph.D. Thesis, University of Minnesota, Minneapolis, 1972.

Clark, W.E. and Whitby, K.T., "Concentration and Size Distribution Measurements of Atmospheric Aerosols and a Test of the Theory of Self-Preserving Size Distributions," Journal of Atmospheric Sciences, Vol. 24, p. 677 (1967).

Chemical Engineers Handbook, 4th Edition, (J.H. Perry, ed.), McGraw-Hill, New York, 1963, p. 3-79.

Cox, R.A. and Penkett, S.A., "Photooxidation of Atmospheric SO_2," Nature, Vol. 229, p. 486 (1971).

Cox, R.A. and Penkett, S.A., "Aerosol Formation from Sulfur Dioxide in the Presence of Ozone and Olefinic Hydrocarbons," Journal of the Chemical Society, Faraday Transactions I, Part 9, Vol. 68, p. 1735 (1972).

Criegee, R., Blust, G. and Zinke, H., "Eine Neuartige Synthese von Ozoniden," Chemische Berichte, Vol. 87, p. 766 (1954).

Criegee, R., Kerchav, A. and Zinke, H., "Der Bildungsbereich Monomerer Ozonide," Chemische Berichte, Vol. 88, p. 1878 (1955).

Doyle, G.J., "Self Nucleation in the Sulfuric Acid-Water System," The Journal of Chemical Physics, Vol. 35, p. 795 (1961).

Dzubay, T.G. and Stevens, R.K., "Applications of X-Ray Fluorescence to Particulate Measurements," Second Joint Conference on Sensing of Environmental Pollutants, Instrument Society of America, Pittsburgh, Pennsylvania, 1973, pp. 211-218.

Dupont Company, "Tedlar" PVF Film, Bulletin TD-3, Wilmington, Delaware.

Environmental Protection Agency, National Primary and Secondary Ambient Air Quality Standards, Part 410, Chapter IV, Title 42, Code of Federal Regulations, Federal Register, Vol. 36, p. 8195, 1971.

Environmental Protection Agency, Health Consequences of Sulfur Oxides: A Review from CHESS, 1970-1971, Environmental Health Effects Research Series, EPA-650/1-74-004, Research Triangle Park, North Carolina, 1974.

Friedlander, S.K., "Similarity Considerations for the Particle-Size Spectrum of Stratospheric Aerosols," The Journal of Meteorology, Vol. 17, p. 479 (1960).

Fuchs, N.A., Droplet Evaporation and Growth in a Gaseous Medium, Pergamon Press, London, 1959.

Fuchs, N.A., The Mechanics of Aerosols, MacMillan Company, New York, 1964.

Garvin, D. and Hampson, R.F. (editors), Chemical Kinetics Data Survey VII. Tables of Rate and Photochemical Data for Modelling of the Stratosphere. National Bureau of Standards, NBSIR 74-430, Washington, D.C., 1974, pp. 10-56.

Gay, B.W. Jr., Private Communication, Environmental Protection Agency, Research Triangle Park, North Carolina, 1974.

Goodeve, C.F., Eastman, A.S. and Dooley, A., "The Reaction between Sulfur Trioxide and Water Vapours and a New Periodic Phenomenon," Faraday Society, London. Transactions, Vol. 30, p. 1127 (1934).

Goulding, F.S., Jaklevic, J.M., Jarrett, B.V. and Landis, D.A., Advances in X-Ray Analysis, Plenum Press, London, 1972, p. 470.

Groblicki, P.J. and Nebel, G.J., "The Photochemical Formation of Aerosols in Urban Atmospheres," Chemical Reactions in Urban Atmospheres, (C.S. Tuesday, ed.), American Elsevier, New York, 1971, pp. 241-267.

Hampson, R.D. (editor), Chemical Kinetics Data Survey VI. Photochemical and Rate Data for Twelve Gas Phase Reactions of Interest for Atmospheric Chemistry, National Bureau of Standards, NBSIR 73-207, Washington, D.C., 1973.

Hanst, P.L., Lefohn, A.S. and Gay, B.W. Jr., "Detection of Atmospheric Pollutants at Parts-Per-Billion Levels by Infrared Spectroscopy," Applied Spectroscopy, Vol. 27, p. 188 (1973).

Hanst, P.L., Stephens, E.R., Scott, E.R. and Doerr, R.C., "Atmospheric Ozone-Olefin Reactions," The Franklin Institute, Philadelphia, Pennsylvania (1958).

Heicklen, J., "Photochemistry of CH_3ONO, Reactions of CH_3O Radicals, Reactions of CH_3O_2 Radicals," Reviews, Pennsylvania State University, University Park (1973).

Hendry, D.G., Private Communication, Stanford Research Institute, Menlo Park, California, 1974.

Hidy, G.M. and Brock, J.R., The Dynamics of Aerocolloidal Systems, Vol. 1, Pergamon Press, New York, 1970, pp. 47-358.

Horvath, H. and Noll, K.E., "The Relationship Between Atmospheric Light Scattering Coefficient and Visibility," Atmospheric Environment, Vol. 3, p. 543 (1969).

Husar, R.B., "Coagulation of Knudsen Aerosols," Ph.D. Thesis, University of Minnesota, Minneapolis, 1971.

Intersociety Committee, Methods of Air Sampling and Analysis, American Public Health Association, Washington, D.C., 1972, p. 103.

Kelvin, Lord, "On the Equilibrium of Vapour at a Curved Surface of a Liquid," Proceedings of the Royal Society, Edinburgh, Vol. 7, p. 63 (1870).

Kiang, C.S., Stauffer, D., Mohnen, V.A., Bricard, J. and Vigla, D., "Heteromolecular Nucleation Theory Applied to Gas-To-Particle Conversion," Atmospheric Environment, Vol. 7, p. 1 (1973).

Kocmond, W.C., Kittelson, D.B., Yang, Y.H. and Demerjian, K.L., "Determination of the Formation Mechanisms and Composition of Photochemical Aerosol," NC5365-M-1, Calspan Corporation, Buffalo (1973).

Landis, D.A., Goulding, F.S. and Jaklevic, J.M., "Performance of a Pulsed-Light Feedback Preamplifier for Semiconductor Detector X-Ray Spectrometers," Nuclear Instruments and Methods, Vol. 87, p. 211 (1970).

Langstroth, C.O. and Gillespie, T., "Coagulation and Surface Losses in Disperse Systems in Still and Turbulent Air," Canadian Journal of Research, Vol. 25B, p. 455 (1947).

Leighton, P.A., Photochemistry of Air Pollution, Academic Press, New York, 1961, pp. 158-183.

Lewis, T.R., Amdur, M.O., Fritzhand, M.D. and Campbell, K.I., Toxicology of Atmospheric Sulfur Dioxide Decay Products, Environmental Protection Agency, Research Triangle Park, North Carolina, 1972, pp. 1-17.

List, R.J., Smithsonian Meteorological Tables, Smithsonian Institution Press, Publication Number 4014, Washington, D.C., 1949.

Liu, B.Y.H., Whitby, K.T. and Pui, D.Y.H., "A Portable Electrical Aerosol Analyzer for Size Distribution Measurement of Submicron Aerosols," Presented at the 66th Annual Meeting of the Air Pollution Control Association, Chicago (1973).

Mason, B.J., The Physics of Clouds, Clarendon Press, Oxford, 1971, pp. 1-30.

Maxwell, J.C., "Theory of the Wet-Bulb Thermometer," Collected Scientific Papers, Cambridge, Vol. 11, p. 625 (1890).

Meloy Laboratories Incorporated, "Operation, Maintenance and Parts Manual for Portable SO_2 Gas Calibrator, Model CS-10," Springfield, Virginia, 1972.

Mirabel, P. and Katz, J.L., "Binary Homogeneous Nucleation as a Mechanism for the Formation of Aerosols," The Journal of Chemical Physics, Vol. 60, p. 1138 (1974).

Niki, H., Private Communication, Ford Motor Company, 1974.

Niki, H., Daby, E.E. and Weinstock, B., "Mechanism of Smog Reactions," Photochemical Smog and Ozone Reactions, American Chemical Society, Washington, D.C., 1972, pp. 27-34.

Nolan, P.J., "The Photoelectric Nucleus Counter," Proceedings of the Royal Society, Dublin, Series A, Vol. 4, p. 161 (1972).

O'Keeffe, A.E. and Ortman, G.C., "Primary Standards for Trace Gas Analysis," Analytical Chemistry, Vol. 38, p. 760 (1966).

O'Neal, H.E. and Blumstein, C., "A New Mechanism for Gas Phase Ozone-Olefin Reactions," International Journal of Chemical Kinetics, Vol. V, p. 397 (1973).

Payne, W.A., Stief, L.J. and Davis, D.D., "A Kinetics Study of the Reaction of HO_2 with SO_2 and NO," Journal of the American Chemical Society, Vol. 95, p. 7614 (1973).

Prager, M.J., Stephens, E.R. and Scott, W.E., "Aerosol Formation from Gaseous Air Pollutants," Industrial and Engineering Chemistry, Vol. 52, p. 521 (1960).

Pressman, J., Arin, L.M. and Warneck, P., "Mechanisms for Removal of CO from the Atmosphere," GCA-TR-70-6-G, GCA Corporation, Bedford, Massachusetts (1970).

Rasmussen, R.A., "Terpenes: Their Analysis and Fate in the Atmosphere," Ph.D. Thesis, Washington University, Saint Louis, Missouri, 1964.

Reiss, H., "The Kinetics of Phase Transitions in Binary Systems," The Journal of Chemical Physics, Vol. 18, p. 840 (1950).

Ripperton, L.A., Jeffries, H.E. and White, O., "Formation of Aerosols by Reaction of Ozone with Selected Hydrocarbons," Photochemical Smog and Ozone Reactions, American Chemical Society, Washington, D.C., 1972, pp. 219-231.

Sahni, D.C., "The Effect of a Black Sphere on the Flux Distribution in an Infinite Moderator," Journal of Nuclear Engineering, Vol. 20, p. 915 (1966).

Scott, W.E., Stephens, E.R., Hanst, P.L. and Doerr, R.C., "Further Developments in the Chemistry of the Atmosphere," Proceedings of the American Petroleum Institute, Vol. 37, p. 171 (1957).

Service, J., "A Users Guide to the Statistical Analysis System," Student Supply Stores, North Carolina State University, Raleigh (1972).

Shirnov, V.I., The Rate of Aerosol Particle Growth by Coagulation and Condensation, Gidrometeorozdat, Moscow, 1969.

Smith, W.S. and Gruber, C.W., Atmospheric Emissions from Coal Combustion - An Inventory Guide, Publication Number 999-AP-24, U.S. Department of Health, Education and Welfare, Washington (1966).

Smoluchowski, M. von, "Versuch einer Mathematischen Theorie der Koagulationskinetik Kolloider Lösungen," Zeitschrift fuer Physikalische, Chemie, Vol. 92, p. 129 (1917).

Stedman, D.H., Morris, E.D. Jr., Daby, E.E., Niki, H. and Weinstock, B., "The Role of OH Radicals in Photochemical Smog," Presented at the 160th Annual American Chemical Society National Meeting, Chicago (1970).

Stedman, D.H., Wu, C.H. and Niki, H., "Kinetics of Gas-Phase Reactions of Ozone with Some Olefins," The Journal of Physical Chemistry, Vol. 77, p. 2511 (1973).

Stuhl, F., "Determination of Rate Constants for the Reactions of OH with Propylene and Ethylene by a Pulsed Photolysis - Resonance Fluoresence Method," Berichte der Bunsengesellschaft fuer Physikalische Chemie, Vol. 77, p. 674 (1973).

Tejada, S., "Determination of Soluble Sulfates from CVS Diluted Exhausts: An Automated Method," Environmental Protection Agency, Research Triangle Park, North Carolina, in preparation.

Thermo Systems Incorporated, "Operating and Service Manual - Model 3030 Electrical Aerosol Size Analyzer," Saint Paul, Minnesota, 1974.

Van DeVate, J.F., "The Thickness of the Stagnant Air Layer in Aerosol Containments and the Aerodynamic Diameter of Aggregates of Small Spheres," Journal of Colloid and Interface Science, Vol. 41, p. 194 (1972).

Vbraski, T. and Cvetanović, R.J., "Relative Rates of Reaction of Ozone with Olefins in the Vapor Phase," and "A Study of the Products of the Reactions of Ozone with Olefins in the Vapor Phase as Determined by Gas-Liquid Chromatography," Canadian Journal of Chemistry, Vol. 38, pp. 1053 and 1063 (1960).

Walter, H., "Coagulation and Size Distribution of Condensation Aerosols," Aerosol Science, Vol. 4, p. 1 (1973).

Washida, N., Martinez, R.I. and Bayes, K.D., "The Oxidation of Formyl Radicals," Reviews, University of California, Los Angeles (1973).

Wei, Y.K. and Cvetanović, R.J., "A Study of the Vapor Phase Reaction of Ozone with Olefins in the Presence and Absence of Molecular Oxygen," Canadian Journal of Chemistry, Vol. 41, p. 913 (1963).

Weinstock, B., Chemical Reactions in Urban Atmospheres, (C.S. Tuesday, ed.), American Elsevier, New York, 1971, p. 54.

Whitby, K.T. and Clark, W.E., "Electrical Aerosol Particle Counting and Size Distribution Measuring System for the 0.015 to 1 μ Size Range," Tellus, Vol. 18, p. 573 (1966).

Williamson, D.G., Private Communication, California Polytechnic State University, San Luis Obispo, California, 1974.

Wilson, W.E. Jr., Merryman, E.L., Levy, A. and Taliaferro, H.R., "Aerosol Formation in Photochemical Smog I. Effect of Stirring," Journal of the Air Pollution Control Association, Vol. 21, p. 128 (1971).

Wood, W.P., Castleman, A.W. Jr. and Tang, I.N., "Mechanisms of Aerosol Formation from Sulfur Dioxide," Presented at the 67th Annual Meeting of the Air Pollution Control Association, Denver (1974).

3M Company, "Scotchpak" Data Sheet, St. Paul, Minnesota.

Appendix 1: Product Analysis by Fourier Transform Infrared Spectroscopy

Run		RH (%)	CO (ppm)	HCHO (ppm)	CH_3CHO (ppm)	CH_2CO (ppm)	HCOOH (ppm)
28	$C_2H_4 + O_3$	22	.84	4.14	0	0	Trace
29	$C_2H_4 + O_3 + SO_2$	20	1.09	4.06	0	0	.19
30	$C_3H_6 + O_3$	19	175	2.12	1.25	.18	Trace
21	$C_3H_6 + O_3$	19	.93	3.21	1.49	.20	Trace
31	$C_3H_6 + O_3 + SO_2$	19	.94	3.44	1.59	0	Trace
78	$C_3H_6 + O_3$	19	.56	1.77	.99	.32	Trace
79	$C_3H_6 + O_3$	33	.70	2.27	1.36	.34	Trace
60	$C_3H_6 + O_3 + SO_2$	20	.71	2.82	1.43	0	Trace
65	$C_3H_6 + O_3 + SO_2$	36	.79	2.97	1.70	0	Trace
81	$C_3H_6 + O_3$ in N_2	36	.73	2.23	1.30	.32	0
82	$C_3H_6 + O_3$ in N_2	20	.87	1.94	1.12	.22	0

Appendix 2: Observed and Smoothed Reactant Concentrations for Gas Phase Experiments.

Smoothed data are listed through the first half of the 'OBS' sequence followed by the observed concentration values. The time derivatives of the concentration values are indicated by the 'DOT' notation.

RUN # 21.

OBS	TIME	HC	HCDOT	O3	O3DOT	SO2	SO2DOT	FLAG	OLXO3
1	0.0	8.12507	-.320182	2.88215	-.236510	0	0	1	23.4177
2	1.5	7.66205	-.297188	2.54341	-.215139	0	0	1	19.4878
3	3.0	7.23351	-.274194	2.23673	-.193769	0	0	1	16.1794
4	4.5	6.83947	-.251199	1.96211	-.172398	0	0	1	13.4198
5	6.0	6.47991	-.228205	1.72000	-.149031	0	0	1	11.1454
6	9.5	5.77509	-.174552	1.32155	-.105180	0	0	1	7.6320
7	14.5	5.16662	-.111191	0.95053	-.066193	0	0	1	4.9110
8	20.5	4.73827	-.067231	0.66120	-.043283	0	0	1	3.1329
9	26.5	4.46861	-.040845	0.45569	-.030780	0	0	1	2.0363
10	35.0	4.20761	-.024703	0.27253	-.018168	0	0	1	1.1467
11	43.5	4.06259	-.009421	0.15747	-.008905	0	0	1	0.6397
12	52.0	4.04746	.005861	0.12115	.000358	0	0	1	0.4903
13	0.0							0	
14	1.5	7.70000		2.55000				0	
15	3.0			2.21000				0	
16	4.5	6.77300		2.00000				0	
17	6.0			1.70000				0	
18	9.5	5.79800		1.28000				0	
19	14.5	5.10900		0.95500				0	
20	20.5	4.77300		0.66200				0	
21	26.5	4.45400		0.44700				0	
22	35.0	4.20200		0.27300				0	
23	43.5	4.09200		0.17200				0	
24	52.0	4.03400		0.11400				0	

RUN # 25.

OBS	TIME	HC	HCDOT	O3	O3DOT	SO2	SO2DOT	FLAG	OLXO3
1	0.0	1.87786	-.0632034	2.37699	-.0772514	.582743	-.00535633	1	4.46365
2	1.5	1.78501	-.0605892	2.26547	-.0714405	.574805	-.00522694	1	4.04389
3	3.0	1.69609	-.0579751	2.16267	-.0656295	.567062	-.00509755	1	3.66808
4	4.5	1.61109	-.0553610	2.06858	-.0598186	.559513	-.00496815	1	3.33267
5	6.0	1.53001	-.0527469	1.99261	-.0496536	.552157	-.00483876	1	3.04871
6	7.5	1.45285	-.0501327	1.92047	-.0465367	.544996	-.00470937	1	2.79015
7	13.0	1.20348	-.0405476	1.70577	-.0360289	.518966	-.00418712	1	2.05286
8	20.0	0.96989	-.0301656	1.50335	-.0272264	.494454	-.00306539	1	1.45809
9	28.0	0.79430	-.0203730	1.32309	-.0201304	.475969	-.00204479	1	1.05093
10	38.0	0.63495	-.0139678	1.15703	-.0139203	.463097	-.00124745	1	0.73466
11	47.0	0.53740	-.0100405	1.06069	-.0102874	.454454	-.00093915	1	0.57002
12	57.0	0.45650	-.0073793	0.98858	-.0077714	.446463	-.00080307	1	0.45129
13	66.0	0.40226	-.0054750	0.92370	-.0071519	.439819	-.00083868	1	0.37157
14	75.0	0.35848	-.0039788	0.85641	-.0067102	.432438	-.00088237	1	0.30700
15	83.0	0.33503	-.0034759	0.80746	-.0060014	.424536	-.00090368	1	0.27053
16	91.0	0.31216	-.0031598	0.76169	-.0054422	.417090	-.00090212	1	0.23777
17	100.0	0.28179	-.0035897	0.71554	-.0048130	.409335	-.00082131	1	0.20163
18	109.0	0.24754	-.0040197	0.67506	-.0041839	.402307	-.00074049	1	0.16711
19	0.0	1.87600						0	
20	1.5			2.27000				0	
21	3.0			2.15000		.566000		0	
22	4.5			2.08000		.561000		0	
23	6.0	1.53900		1.98000		.552000		0	
24	7.5							0	
25	13.0	1.18700		1.70000		.520000		0	
26	20.0	0.97500		1.50000		.493000		0	
27	28.0	0.78800		1.33000		.476000		0	
28	38.0	0.64000		1.15000		.463000		0	
29	47.0	0.53400		1.06000		.455000		0	
30	57.0	0.45900		0.99600		.446000		0	
31	66.0	0.40300		0.92000		.440000		0	
32	75.0	0.35700		0.85700		.433000		0	
33	83.0	0.33300		0.80700		.424000		0	
34	91.0	0.31800		0.76300		.417000		0	
35	100.0	0.27700		0.71500		.410000		0	
36	109.0	0.24900				.402000		0	

RUN # 26.

OBS	TIME	HC	HCDOT	O3	O3DOT	SO2	SO2DOT	FLAG	DLXO3
1	0.0	3.54659	-.0833005	1.07984	-.0651314	.620152	-.00690040	1	3.82976
2	1.5	3.42474	-.0791711	0.98602	-.0599585	.610093	-.00651270	1	3.37688
3	3.0	3.30908	-.0750416	0.89997	-.0547857	.600614	-.00612500	1	2.97806
4	4.5	3.19961	-.0709122	0.82167	-.0496128	.591718	-.00573731	1	2.62902
5	6.0	3.09634	-.0667827	0.75113	-.0444400	.583402	-.00534961	1	2.32575
6	10.0	2.85124	-.0557708	0.61791	-.0320097	.565275	-.00411949	1	1.76182
7	17.0	2.52829	-.0365000	0.47074	-.0185722	.539787	-.00315637	1	1.19018
8	24.0	2.39025	-.0191743	0.36625	-.0135722	.521412	-.00225174	1	0.87544
9	32.0	2.28256	-.0133804	0.28003	-.0099257	.508221	-.00153991	1	0.63919
10	39.0	2.20528	-.0104328	0.22113	-.0077414	.500380	-.00118088	1	0.48755
11	47.0	2.13821	-.0068144	0.16859	-.0057763	.491768	-.00093265	1	0.36047
12	55.0	2.08635	-.0064363	0.13032	-.0042370	.484739	-.00076722	1	0.27189
13	64.0	2.04829	-.0045340	0.10151	-.0030956	.479418	-.00060213	1	0.20792
14	71.0	2.01263	-.0033217	0.08298	-.0024547	.475815	-.00047723	1	0.16700
15	80.0	1.99044	-.0016095	0.06345	-.0018860	.471807	-.00041340	1	0.12528
16	91.0	1.98425	.0004831	0.04652	-.0011908	.467689	-.00033539	1	0.09231
17	0.0							0	
18	1.5	3.46000		0.98000				0	
19	3.0			0.91800		.602000		0	
20	4.5					.590000		0	
21	6.0			0.72900		.583000		0	
22	10.0	2.76800		0.61300		.565000		0	
23	17.0	2.54200		0.46900		.540000		0	
24	24.0	2.40900		0.36700		.521000		0	
25	32.0	2.25600		0.28000		.508000		0	
26	39.0	2.23200		0.22200		.501000		0	
27	47.0	2.12800		0.16800		.492000		0	
28	55.0	2.07900		0.13000		.484000		0	
29	64.0	2.06900		0.10200		.480000		0	
30	71.0	2.00000		0.08400		.476000		0	
31	80.0	1.98000		0.06200		.471000		0	
32	91.0	1.99000		0.04700		.468000		0	

RUN # 27.

OBS	TIME	HC	HCDOT	O3	O3DOT	SO2	SO2DOT	FLAG	DLXO3
1	0.0	3.46134	-.0772213	.982809	-.0382698	.193853	-.00251325	1	3.40183
2	1.5	3.34849	-.0732458	.926709	-.0365298	.190161	-.00240866	1	3.10307
3	3.0	3.24160	-.0692704	.873220	-.0347858	.186627	-.00230408	1	2.83063
4	4.5	3.14068	-.0652949	.822340	-.0330499	.183249	-.00219949	1	2.58270
5	6.0	3.04571	-.0613194	.774070	-.0313099	.180028	-.00209490	1	2.35760
6	7.5	2.95672	-.0573440	.728583	-.0293636	.176964	-.00199031	1	2.15421
7	13.0	2.68141	-.0427673	.585979	-.0235634	.166933	-.00171984	1	1.57125
8	19.0	2.47733	-.0305264	.463225	-.0183446	.158338	-.00129989	1	1.14756
9	25.0	2.34688	-.0204922	.370396	-.0139269	.152078	-.00091121	1	0.87045
10	31.0	2.25512	-.0154364	.300375	-.0105452	.147390	-.00070778	1	0.67738
11	39.0	2.14585	-.0114171	.234851	-.0074631	.143300	-.00044588	1	0.50396
12	44.0	2.09757	-.0086417	.203164	-.0064592	.141573	-.00037727	1	0.42615
13	49.0	2.05646	-.0071885	.172506	-.0056367	.139563	-.00034488	1	0.35475
14	58.0	2.03249	-.0036872	.128499	-.0043124	.137532	-.00022347	1	0.26117
15	68.0	1.99317	-.0033086	.093630	-.0030305	.135553	-.00021454	1	0.18662
16	76.0	1.96670	-.0028160	.074564	-.0023237	.134028	-.00018539	1	0.14664
17	84.0	1.93491	-.0016489	.058035	-.0018085	.132517	-.00019237	1	0.11229
18	93.0	1.93495	.0016578	.044366	-.0012290	.130750	-.00020022	1	0.08585
19	101.0	1.95597	.0045970	.036595	-.0007138	.129120	-.00020720	1	0.07173
20	0.0	3.45800						0	
21	1.5			.928000				0	
22	3.0			.872000				0	
23	4.5			.821000		.182000		0	
24	6.0	3.05400				.181000		0	
25	7.5			.730000		.178000		0	
26	13.0	2.67500		.583000		.166000		0	
27	19.0	2.47300		.465000		.159000		0	
28	25.0	2.36000		.370000		.152000		0	
29	31.0	2.24100		.300000		.147000		0	
30	39.0	2.16300		.236000		.144000		0	
31	44.0	2.08400		.204000		.141000		0	
32	49.0	2.05500		.173000		.140000		0	
33	58.0	2.02000		.127000		.137000		0	
34	68.0	2.01200		.095000		.136000		0	
35	76.0	1.94800		.074000		.134000		0	
36	84.0	1.94800		.059000		.132000		0	
37	93.0	1.92900		.044000		.131000		0	
38	101.0	1.96100						0	

RUN # 28.

OBS	TIME	HC	HCDOT	O3	O3DOT	SO2	SO2DOT	FLAG	OLXO3
1	0.0	11.8498	-.145570	3.80672	-.0877223	0	0	1	45.1090
2	1.5	11.6368	-.138494	3.67754	-.0845148	0	0	1	42.7947
3	3.0	11.4344	-.131418	3.55317	-.0813074	0	0	1	40.6282
4	6.0	11.0613	-.117266	3.31887	-.0748925	0	0	1	36.7111
5	11.5	10.5001	-.093963	2.93931	-.0631319	0	0	1	30.8629
6	17.0	10.0644	-.081193	2.63336	-.0511641	0	0	1	26.5032
7	22.5	9.6343	-.070649	2.37533	-.0435306	0	0	1	22.8845
8	27.5	9.2907	-.058653	2.18218	-.0389075	0	0	1	20.2740
9	32.5	9.0327	-.051840	1.99914	-.0350000	0	0	1	18.0577
10	37.5	8.8315	-.046160	1.82686	-.0328000	0	0	1	16.1340
11	42.5	8.5778	-.043700	1.66971	-.0282000	0	0	1	14.3225
12	47.5	8.3489	-.039880	1.54457	-.0252000	0	0	1	12.8955
13	52.5	8.1824	-.030425	1.42567	-.0232458	0	0	1	11.6654
14	57.5	8.0697	-.024483	1.31398	-.0204060	0	0	1	10.6035
15	65.0	7.8996	-.025875	1.16381	-.0164605	0	0	1	9.1937
16	70.0	7.7715	-.023407	1.09662	-.0147936	0	0	1	8.5224
17	75.0	7.6382	-.025500	1.03477	-.0138800	0	0	1	7.9038
18	80.0	7.5139	-.021179	0.95780	-.0139278	0	0	1	7.1968
19	85.0	7.4188	-.016873	0.89021	-.0131113	0	0	1	6.6042
20	95.0	7.2931	-.008261	0.76726	-.0114784	0	0	1	5.5957
21	0.0	11.8500						0	
22	1.5							0	
23	3.0	11.4500		3.57000				0	
24	6.0	11.0300		3.29000				0	
25	11.5	10.5100		2.95000				0	
26	17.0	10.0500		2.63000				0	
27	22.5	9.6710		2.37000				0	
28	27.5	9.2510		2.19000				0	
29	32.5	9.0340		2.00000				0	
30	37.5	8.8570		1.82000				0	
31	42.5	8.5720		1.68000				0	
32	47.5	8.3280		1.53000				0	
33	52.5	8.2060		1.44000				0	
34	57.5	8.0430		1.31000				0	
35	65.0	7.9210		1.16000				0	
36	70.0	7.7720		1.10000				0	
37	75.0	7.6090		1.04000				0	
38	80.0	7.5550		0.95600				0	
39	85.0	7.3920		0.88500				0	
40	95.0	7.2970		0.76900				0	

RUN # 29.

OBS	TIME	HC	HCDOT	O3	O3DOT	SO2	SO2DOT	FLAG	OLXO3
1	0.0	12.5020	-.306241	3.61723	-.0776162	.529393	-.0121465	1	45.2226
2	2.5	11.8036	-.252446	3.42806	-.0737240	.500223	-.0111896	1	40.4635
3	5.0	11.2398	-.198650	3.24861	-.0698319	.473445	-.0102328	1	36.5136
4	10.0	10.7103	-.099454	2.91891	-.0620476	.427065	-.0083190	1	31.2625
5	15.0	10.2401	-.082960	2.62600	-.0552000	.391029	-.0065800	1	26.8904
6	20.0	9.8461	-.067920	2.37486	-.0486000	.362486	-.0053200	1	23.3832
7	25.0	9.5693	-.055700	2.15000	-.0432000	.339829	-.0043000	1	20.5740
8	30.0	9.3521	-.052080	1.94086	-.0386000	.320343	-.0036800	1	18.1512
9	35.0	9.0576	-.045580	1.76000	-.0330000	.303571	-.0031400	1	15.9413
10	40.0	8.8549	-.045447	1.61748	-.0295763	.289401	-.0027146	1	14.3226
11	45.0	8.6362	-.038772	1.47818	-.0267066	.276559	-.0023525	1	12.7659
12	53.5	8.3576	-.033168	1.25973	-.0230118	.259623	-.0018238	1	10.5284
13	58.5	8.1707	-.032937	1.14786	-.0205612	.251110	-.0015378	1	9.3789
14	64.0	8.0400	-.023632	1.06217	-.0161656	.243495	-.0012313	1	8.5398
15	77.5	7.7354	-.021487	0.96160	-.0135495	.231950	-.0004791	1	6.6648
16	87.0	7.5384	-.019979	0.74162	-.0117086	.229914	.0000503	1	5.5907
17	0.0	12.6800						0	
18	2.5	11.5400		3.42000		.501000		0	
19	5.0	11.2000		3.26000		.472000		0	
20	10.0	10.7200		2.92000		.428000		0	
21	15.0	10.2500		2.62000		.390000		0	
22	20.0	9.8200		2.38000		.363000		0	
23	25.0	9.5760		2.15000		.340000		0	
24	30.0	9.3590		1.94000		.320000		0	
25	35.0	9.0880		1.76000		.304000		0	
26	40.0	8.7620		1.61000		.289000		0	
27	45.0	8.7350		1.49000		.277000		0	
28	53.5	8.2740		1.25000		.259000		0	
29	58.5	8.2200		1.15000		.252000		0	
30	64.0	8.0160		1.05000		.243000		0	
31	77.5	7.7310		0.87700		.232000		0	
32	87.0	7.5420		0.73500				0	

RUN # 31.

OBS	TIME	HC	HCDOT	O3	O3DOT	SO2	SO2DOT	FLAG	OLXO3
1	0.0	8.55502	-.347250	2.71353	-.235492	.524980	-.0325282	1	23.2143
2	1.5	8.05260	-.322649	2.37742	-.212649	.482373	-.0242809	1	19.1445
3	3.0	7.58708	-.298048	2.07558	-.189807	.452138	-.0160334	1	15.7476
4	4.5	7.15846	-.273448	1.80800	-.166964	.436607	-.0114937	1	12.9425
5	5.5	6.89321	-.257047	1.66658	-.143902	.429385	-.0080189	1	11.4881
6	10.5	5.81298	-.175045	1.11775	-.092676	.397888	-.0052269	1	6.4974
7	18.5	5.08467	-.078146	0.60891	-.051840	.368151	-.0028558	1	3.0961
8	24.0	4.83663	-.046306	0.41815	-.032987	.358121	-.0017553	1	2.0224
9	32.0	4.62060	-.022449	0.24538	-.018640	.351134	-.0009143	1	1.1338
10	37.5	4.52596	-.016054	0.17306	-.012724	.347638	-.0007423	1	0.7833
11	46.0	4.43847	-.004532	0.09287	-.006143	.341452	-.0007133	1	0.4122
12	55.0	4.45258	.007667	0.06894	.006825	.335170	-.0006826	1	0.3070
13	0.0	8.62200				.526000		0	
14	1.5			2.38000		.480000		0	
15	3.0			2.07000		.453000		0	
16	4.5			1.81000		.436000		0	
17	5.5	6.77000		1.65000		.428000		0	
18	10.5	5.81200		1.08000		.397000		0	
19	18.5	5.06200		0.61900		.368000		0	
20	24.0	4.87700		0.42000		.358000		0	
21	32.0	4.62300		0.24500		.352000		0	
22	37.5	4.50200		0.17300		.347000		0	
23	46.0	4.47800		0.10200		.342000		0	
24	55.0	4.43800		0.06500		.335000		0	

RUN # 86.

OBS	TIME	HC	HCDOT	O3	O3DOT	SO2	SO2DOT	FLAG	OLXO3
1	0.0	.921686	-.0201141	1.96941	-.0342548	.201297	-.00588206	1	1.81518
2	1.0	.901668	-.0199232	1.93586	-.0328374	.195676	-.00536059	1	1.74550
3	1.5	.891720	-.0198277	1.91962	-.0321288	.193061	-.00509985	1	1.71178
4	3.0	.862203	-.0195412	1.87302	-.0300027	.185998	-.00431765	1	1.61493
5	4.5	.833106	-.0192546	1.82961	-.0270767	.180108	-.00353544	1	1.52426
6	6.0	.804435	-.0189684	1.79044	-.0279751	.176984	-.00264273	1	1.44030
7	11.0	.711984	-.0180136	1.67750	-.0193290	.167973	-.00155905	1	1.19435
8	17.0	.610521	-.0157915	1.56715	-.0146590	.160115	-.00119015	1	0.96899
9	23.0	.505346	-.0147920	1.51164	-.0123740	.153768	-.00089828	1	0.76390
10	29.0	.443813	-.0105506	1.44619	-.0111506	.149727	-.00068451	1	0.64184
11	37.0	.368326	-.0088446	1.34914	-.0102244	.145312	-.00048450	1	0.49719
12	47.0	.301665	-.0063608	1.26215	-.0075000	.141803	-.00037972	1	0.38075
13	57.0	.245941	-.0051698	1.20246	-.0062137	.138094	-.00034845	1	0.29573
14	65.0	.207574	-.0036720	1.16582	-.0055401	.135548	-.00028071	1	0.24199
15	73.0	.160029	-.0024125	1.11343	-.0052500	.133086	-.00026250	1	0.20045
16	81.0	.174743	-.0019500	1.07257	-.0045000	.131571	-.00016250	1	0.18742
17	89.0	.159019	-.0016083	1.04966	-.0041268	.130885	-.00019151	1	0.16692
18	97.0	.144336	-.0020026	1.01391	-.0048110	.129055	-.00026608	1	0.14634
19	114.0	.164254	-.0027129	0.91976	-.0062649	.123184	-.00042457	1	0.09589
20	0.0					.202000		0	
21	1.0	.909000						0	
22	1.5			1.91000		.192000		0	
23	3.0			1.89000				0	
24	4.5			1.83000		.180000		0	
25	6.0	.778000		1.78000		.176000		0	
26	11.0	.730000		1.68000		.168000		0	
27	17.0	.585000		1.58000		.160000		0	
28	23.0	.515000		1.52000		.154000		0	
29	29.0	.435000		1.44000		.149000		0	
30	37.0	.371000		1.36000		.146000		0	
31	47.0	.298000		1.25000		.141000		0	
32	57.0	.251000		1.21000		.139000		0	
33	65.0	.206000		1.17000		.135000		0	
34	73.0	.176000		1.11000		.133000		0	
35	81.0	.175000		1.07000		.132000		0	
36	89.0	.170000		1.05000		.130000		0	
37	97.0	.131000		1.02000		.130000		0	
38	114.0	.107000		0.91800		.123000		0	

RUN # 87.

OBS	TIME	HC	HCDOT	O3	O3DOT	SO2	SO2DOT	FLAG	OLXO3
1	0.0	1.11160	-.0262750	2.05569	-.0491465	.650706	-.00410461	1	2.28510
2	1.5	1.07261	-.0257125	1.98461	-.0456182	.644627	-.00399995	1	2.12872
3	3.0	1.03446	-.0251500	1.91883	-.0420900	.638706	-.00389530	1	1.98496
4	4.5	0.99716	-.0245875	1.85834	-.0385618	.632941	-.00379064	1	1.85307
5	8.0	0.91340	-.0232750	1.75180	-.0282022	.620101	-.00354644	1	1.60010
6	16.0	0.73920	-.0202750	1.56696	-.0197562	.593566	-.00298760	1	1.15830
7	24.0	0.57677	-.0165553	1.44498	-.0140006	.573175	-.00231829	1	0.83342
8	32.0	0.47589	-.0121465	1.35889	-.0110185	.556781	-.00191739	1	0.64668
9	41.0	0.39184	-.0086349	1.27473	-.0090150	.542474	-.00145676	1	0.49950
10	50.0	0.32611	-.0066120	1.19481	-.0077733	.530812	-.00120446	1	0.38964
11	59.0	0.27222	-.0053507	1.13102	-.0068353	.521174	-.00097612	1	0.30788
12	67.0	0.23874	-.0039449	1.08507	-.0058803	.514488	-.00078915	1	0.25905
13	76.0	0.20769	-.0034257	1.03339	-.0054581	.507768	-.00063919	1	0.21462
14	85.0	0.17911	-.0029255	0.98602	-.0050675	.502908	-.00044070	1	0.17660
15	93.0	0.15748	-.0024809	0.94687	-.0047203	.500089	-.00026427	1	0.14911
16	0.0	1.10100						0	
17	1.5			1.99000				0	
18	3.0			1.91000		.638000		0	
19	4.5			1.86000		.635000		0	
20	8.0	0.93700		1.74000		.618000		0	
21	16.0	0.73200		1.57000		.595000		0	
22	24.0	0.57500		1.44000		.572000		0	
23	32.0	0.47100		1.36000		.557000		0	
24	41.0	0.40100		1.28000		.543000		0	
25	50.0	0.31900		1.19000		.530000		0	
26	59.0	0.27500		1.13000		.522000		0	
27	67.0	0.24000		1.09000		.514000		0	
28	76.0	0.20400		1.03000		.508000		0	
29	85.0	0.18500		0.98500		.503000		0	
30	93.0	0.15500		0.94800		.500000		0	

RUN # 88.

OBS	TIME	HC	HCDOT	O3	O3DOT	SO2	SO2DOT	FLAG	OLXO3
1	0.0	3.28134	-.0283691	.273524	-.0120562	.207480	-.000853374	1	.897525
2	1.5	3.23994	-.0268321	.256070	-.0112163	.206220	-.000826182	1	.829650
3	3.0	3.20084	-.0252952	.239875	-.0103764	.205001	-.000798991	1	.767803
4	4.5	3.16405	-.0237582	.224940	-.0095365	.203823	-.000771800	1	.711724
5	6.0	3.12957	-.0222213	.211383	-.0090037	.202686	-.000744609	1	.661539
6	7.0	3.10786	-.0211966	.202266	-.0087549	.201950	-.000726481	1	.628613
7	13.0	2.99912	-.0150488	.158285	-.0065635	.197918	-.000617717	1	.474718
8	22.0	2.93428	-.0075727	.111033	-.0045476	.193106	-.000432187	1	.325802
9	29.0	2.87909	-.0060033	.085744	-.0034246	.190705	-.000293443	1	.246864
10	36.0	2.84561	-.0049590	.065424	-.0026655	.188952	-.000245821	1	.186172
11	45.0	2.81450	-.0028560	.045584	-.0018921	.187600	-.000135639	1	.128295
12	53.0	2.79193	-.0018518	.033364	-.0013545	.186613	-.000146571	1	.093149
13	61.0	2.78071	-.0011875	.024829	-.0009750	.185400	-.000150000	1	.069041
14	69.0	2.78130	.0004272	.018804	-.0006769	.184395	-.000148579	1	.052300
15	77.0	2.78685	.0009615	.014230	-.0004666	.183066	-.000183674	1	.039657
16	83.0	2.79382	.0013623	.011904	-.0003088	.181885	-.000209996	1	.033258
17	0.0	3.30600						0	
18	1.5			.256000				0	
19	3.0			.240000				0	
20	4.5			.225000				0	
21	6.0			.211000		.203000		0	
22	7.0	3.05500		.203000		.202000		0	
23	13.0	3.01100		.156000		.197000		0	
24	22.0	2.94200		.112000		.194000		0	
25	29.0	2.86900		.086000		.190000		0	
26	36.0	2.84400		.065000		.189000		0	
27	45.0	2.82500		.046000		.188000		0	
28	53.0	2.78000		.033000		.186000		0	
29	61.0	2.78500		.025000		.186000		0	
30	69.0	2.78500		.019000		.184000		0	
31	77.0	2.77500		.014000		.183000		0	
32	83.0	2.80000		.012000		.182000		0	

RUN # 89.

OBS	TIME	HC	HCDOT	O3	O3DOT	SO2	SO2DOT	FLAG	OLXO3
1	0.0	3.31782	-.0396135	.294753	-.0133694	.637251	-.00173412	1	.977936
2	1.5	3.26072	-.0365132	.275311	-.0125524	.634696	-.00157233	1	.897714
3	3.0	3.20828	-.0334128	.257096	-.0117354	.632234	-.00161053	1	.824834
4	4.5	3.16049	-.0303124	.240105	-.0109183	.629864	-.00154874	1	.758849
5	7.0	3.09116	-.0251452	.215418	-.0093294	.626121	-.00144575	1	.665892
6	13.0	2.98867	-.0133228	.167647	-.0071878	.618188	-.00119857	1	.501041
7	19.0	2.94850	-.0087489	.131815	-.0054665	.611975	-.00099051	1	.388657
8	26.0	2.90455	-.0059588	.100686	-.0040996	.605966	-.00081444	1	.292448
9	34.0	2.85921	-.0051314	.073722	-.0030091	.600173	-.00070402	1	.210785
10	44.0	2.80017	-.0035170	.050283	-.0020703	.593636	-.00057796	1	.140800
11	52.0	2.79586	-.0018419	.036865	-.0015407	.589276	-.00046381	1	.103070
12	63.0	2.77920	-.0011860	.023264	-.0009323	.585133	-.00028957	1	.064655
13	74.0	2.76977	-.0005301	.016354	-.0003240	.582906	-.00011534	1	.045297
14	0.0	3.33000						0	
15	1.5			.276000				0	
16	3.0	3.19000		.255000				0	
17	4.5			.242000		.630000		0	
18	7.0	3.09000		.214000		.626000		0	
19	13.0	2.99000		.167000		.618000		0	
20	19.0	2.93300		.132000		.612000		0	
21	26.0	2.92800		.100000		.606000		0	
22	34.0	2.84300		.074000		.600000		0	
23	44.0	2.81000		.050000		.594000		0	
24	52.0	2.78100		.037000		.589000		0	
25	63.0	2.80000		.024000		.585000		0	
26	74.0	2.76200		.016000		.583000		0	

RUN # 90.

OBS	TIME	HC	HCDOT	O3	O3DOT	SO2	SO2DOT	FLAG	OLXO3
1	0.0	2.73851	-.0771067	1.97049	-.0672579	.580315	-.00669454	1	5.39619
2	1.5	2.62523	-.0739234	1.87248	-.0634219	.570500	-.00639150	1	4.91569
3	3.0	2.51674	-.0707401	1.78022	-.0595859	.561140	-.00608846	1	4.48035
4	4.5	2.41301	-.0675569	1.69372	-.0557499	.552235	-.00578542	1	4.08697
5	9.0	2.18956	-.0601292	1.52317	-.0464426	.533223	-.00507832	1	3.33507
6	15.0	1.82065	-.0452739	1.24789	-.0351251	.502065	-.00379175	1	2.27197
7	23.0	1.54386	-.0314440	1.01499	-.0273047	.479342	-.00234598	1	1.56700
8	27.0	1.42899	-.0259903	0.91248	-.0232000	.471886	-.00198750	1	1.30392
9	31.0	1.35060	-.0216875	0.82547	-.0204154	.465237	-.00163486	1	1.11488
10	39.0	1.21466	-.0160125	0.69851	-.0141097	.454214	-.00131166	1	0.84845
11	47.0	1.10789	-.0125021	0.61114	-.0108605	.444872	-.00117401	1	0.67708
12	55.0	1.02832	-.0093736	0.53590	-.0089872	.436136	-.00110370	1	0.55108
13	69.0	0.91759	-.0068246	0.42505	-.0070730	.420877	-.00109513	1	0.39002
14	78.0	0.86769	-.0057272	0.36562	-.0059651	.411129	-.00113158	1	0.31725
15	88.0	0.81524	-.0046008	0.31411	-.0052988	.399639	-.00115905	1	0.25607
16	95.0	0.78448	-.0038541	0.27848	-.0046182	.391147	-.00108024	1	0.21846
17	103.0	0.75779	-.0028179	0.24373	-.0040686	.382920	-.00097653	1	0.18470
18	111.0	0.73939	-.0017816	0.21338	-.0035191	.375522	-.00087282	1	0.15777
19	0.0	2.74300						0	
20	1.5			1.87000				0	
21	3.0			1.78000		.559000		0	
22	4.5			1.70000		.555000		0	
23	9.0	2.18200		1.51000		.533000		0	
24	15.0	1.81600		1.25000		.502000		0	
25	23.0	1.54000		1.02000		.480000		0	
26	27.0			0.91400		.472000		0	
27	31.0	1.36200		0.81700		.465000		0	
28	39.0	1.20300		0.69900		.454000		0	
29	47.0	1.11700		0.60900		.445000		0	
30	55.0	1.02200		0.53800		.436000		0	
31	69.0	0.92000		0.42400		.421000		0	
32	78.0	0.86800		0.36600		.411000		0	
33	88.0	0.81800		0.31300		.400000		0	
34	95.0	0.78000		0.28300		.391000		0	
35	103.0	0.76000		0.23700		.382000		0	
36	111.0	0.73900		0.21600		.376000		0	

RUN # 91.

OBS	TIME	HC	HCDDT	O3	O3DDT	SO2	SO2DDT	FLAG	OLXO3
1	0.00	2.58000	-.0668333	1.66000	-.0368418	0	0	1	4.28280
2	2.25	2.43455	-.0624583	1.57743	-.0365571	0	0	1	3.84032
3	3.75	2.34305	-.0595417	1.52273	-.0363674	0	0	1	3.56784
4	6.00	2.21400	-.0551667	1.44123	-.0360827	0	0	1	3.19088
5	12.00	1.91600	-.0425000	1.22259	-.0308963	0	0	1	2.34493
6	15.00	1.79625	-.0376667	1.13627	-.0290167	0	0	1	2.04102
7	18.00	1.70418	-.0329412	1.05742	-.0257224	0	0	1	1.80203
8	24.00	1.52741	-.0248962	0.91670	-.0210933	0	0	1	1.40018
9	29.00	1.42435	-.0188258	0.81460	-.0188696	0	0	1	1.16027
10	35.00	1.34161	-.0148123	0.71900	-.0150558	0	0	1	0.96462
11	40.00	1.27663	-.0124117	0.65082	-.0129362	0	0	1	0.83085
12	46.00	1.20455	-.0116137	0.58253	-.0111151	0	0	1	0.70169
13	58.00	1.07193	-.0092838	0.46749	-.0082165	0	0	1	0.50107
14	64.00	1.02869	-.0084155	0.42226	-.0071015	0	0	1	0.43437
15	76.00	0.93606	-.0066893	0.35293	-.0053554	0	0	1	0.33107
16	85.00	0.89970	-.0052693	0.31351	-.0043975	0	0	1	0.28207
17	98.00	0.85388	-.0043954	0.26009	-.0038985	0	0	1	0.21766
18	104.00	0.81172	-.0039920	0.23716	-.0036254	0	0	1	0.19251
19	110.00	0.78898	-.0035387	0.21621	-.0033586	0	0	1	0.17058
20	116.00	0.76800	-.0031853	0.19686	-.0030919	0	0	1	0.15131
21	0.00	2.59000						0	
22	2.25			1.58000				0	
23	3.75			1.52000				0	
24	6.00	2.19000		1.44000				0	
25	12.00	1.93000		1.23000				0	
26	15.00			1.12000				0	
27	18.00	1.70000		1.07000				0	
28	24.00	1.53000		0.91300				0	
29	29.00	1.42000		0.81300				0	
30	35.00	1.34000		0.72300				0	
31	40.00	1.28000		0.64800				0	
32	46.00			0.58000				0	
33	58.00	1.07000		0.47400				0	
34	64.00	1.02000		0.41500				0	
35	76.00			0.35400				0	
36	85.00	0.90200		0.31400				0	
37	98.00			0.26000				0	
38	104.00			0.23700				0	
39	110.00	0.78800		0.21600				0	
40	116.00	0.76400		0.19700				0	

RUN # 92.

OBS	TIME	HC	HCDOT	O3	O3DOT	SO2	SO2DOT	FLAG	OLXO3
1	0.0	3.01199	-.101708	1.65081	-.0612303	0	0	1	4.97223
2	1.5	2.86400	-.095610	1.56165	-.0576526	0	0	1	4.47257
3	3.0	2.72516	-.089513	1.47785	-.0540748	0	0	1	4.02739
4	6.0	2.47491	-.077319	1.32636	-.0469193	0	0	1	3.28263
5	11.0	2.13912	-.056995	1.13297	-.0356942	0	0	1	2.42356
6	17.0	1.89550	-.036042	0.94988	-.0275990	0	0	1	1.90051
7	19.9	1.80167	-.028670	0.87432	-.0245152	0	0	1	1.57523
8	24.0	1.73424	-.024069	0.78773	-.0213022	0	0	1	1.36610
9	30.0	1.61616	-.018853	0.68063	-.0173978	0	0	1	1.10000
10	39.0	1.46108	-.015402	0.55023	-.0129848	0	0	1	0.80394
11	53.0	1.28124	-.008759	0.40312	-.0087985	0	0	1	0.51650
12	60.0	1.23847	-.007472	0.35038	-.0074636	0	0	1	0.43394
13	68.0	1.19214	-.005500	0.29882	-.0059137	0	0	1	0.35623
14	77.0	1.14684	-.004565	0.25136	-.0047541	0	0	1	0.28828
15	86.0	1.10996	-.003631	0.21558	-.0038290	0	0	1	0.23906
16	94.0	1.08424	-.002799	0.18747	-.0031475	0	0	1	0.20327
17	108.0	1.05523	-.001345	0.15176	-.0019551	0	0	1	0.16014
18	0.0	3.02000						0	
19	1.5			1.57000				0	
20	3.0			1.47000				0	
21	6.0	2.46200		1.32000				0	
22	11.0	2.13000		1.13000				0	
23	17.0	1.89300		0.95200				0	
24	19.9							0	
25	24.0	1.73300		0.76400				0	
26	30.0	1.62800		0.68000				0	
27	39.0	1.45300		0.55000				0	
28	53.0	1.28800		0.40300				0	
29	60.0	1.22800		0.35200				0	
30	68.0	1.21200		0.30000				0	
31	77.0	1.13600		0.24900				0	
32	86.0			0.21700				0	
33	94.0			0.18900				0	
34	108.0	1.05600		0.15100				0	

RUN # 93.

OBS	TIME	HC	HCDOT	O3	O3DOT	SO2	SO2DOT	FLAG	CLXC3
1	0.0	2.75300	-.0600925	2.57259	-.0993578	0	0	1	7.08235
2	1.5	2.66305	-.0590031	2.42836	-.0929463	0	0	1	6.46686
3	3.0	2.57599	-.0570813	2.29375	-.0865347	0	0	1	5.90869
4	6.0	2.41051	-.0532375	2.05338	-.0737115	0	0	1	4.94971
5	8.0	2.30660	-.0506750	1.93120	-.0642510	0	0	1	4.45451
6	14.2	2.01704	-.0427313	1.58751	-.0466190	0	0	1	3.20206
7	16.0	1.94220	-.0404250	1.54181	-.0424233	0	0	1	2.99451
8	24.0	1.65715	-.0311619	1.25198	-.0328215	0	0	1	2.07471
9	32.0	1.46415	-.0219356	1.03362	-.0250017	0	0	1	1.51338
10	41.0	1.31642	-.0154697	0.84093	-.0187910	0	0	1	1.10702
11	49.0	1.20939	-.0112881	0.72247	-.0148150	0	0	1	0.87374
12	58.0	1.14773	-.0091785	0.61362	-.0114303	0	0	1	0.70427
13	67.0	1.07674	-.0070786	0.51900	-.0095944	0	0	1	0.55883
14	76.0	1.01874	-.0058107	0.44773	-.0079481	0	0	1	0.45612
15	86.0	0.96768	-.0044020	0.37565	-.0064676	0	0	1	0.36351
16	94.0	0.93597	-.0032751	0.32865	-.0052832	0	0	1	0.30794
17	112.0	0.90084	-.0007394	0.25754	-.0026183	0	0	1	0.23200
18	0.0	2.74600						0	
19	1.5			2.42000				0	
20	3.0			2.31000				0	
21	6.0			2.04000				0	
22	8.0	2.32900		1.92000				0	
23	14.2							0	
24	16.0	1.91700		1.53000				0	
25	24.0	1.67100		1.26000				0	
26	32.0	1.45800		1.03000				0	
27	41.0	1.30200		0.84200				0	
28	49.0			0.71700				0	
29	58.0	1.16700		0.61500				0	
30	67.0	1.07000						0	
31	76.0	1.00500		0.44400				0	
32	86.0							0	
33	94.0	0.94200		0.33300				0	
34	112.0			0.25600				0	

FUN # 94.

OBS	TIME	HC	HCDOT	O3	O3DOT	SO2	SO2DOT	FLAG	OLXO3
1	0.0	2.92957	-.0813174	2.68281	-.107388	0	0	1	7.85949
2	1.5	2.81015	-.0779099	2.52669	-.100780	0	0	1	7.10037
3	3.0	2.69584	-.0743025	2.38047	-.094171	0	0	1	6.41738
4	5.0	2.55138	-.0699592	2.20094	-.085360	0	0	1	5.61544
5	11.0	2.17252	-.0563294	1.79184	-.060696	0	0	1	3.89280
6	12.0	2.11732	-.0540578	1.73241	-.058176	0	0	1	3.66806
7	17.0	1.87543	-.0425997	1.48265	-.046590	0	0	1	2.78060
8	24.0	1.66159	-.0288234	1.21952	-.034292	0	0	1	2.02534
9	32.0	1.46779	-.0210206	0.99821	-.025269	0	0	1	1.46516
10	41.0	1.33700	-.0143670	0.82002	-.018362	0	0	1	1.09636
11	49.0	1.23603	-.0119761	0.69432	-.014826	0	0	1	0.85820
12	57.0	1.15716	-.0090542	0.59111	-.012051	0	0	1	0.68401
13	71.0	1.05028	-.0062152	0.45375	-.008590	0	0	1	0.47657
14	79.0	1.00705	-.0045929	0.39237	-.007217	0	0	1	0.39513
15	87.0	0.97679	-.0029708	0.34025	-.005950	0	0	1	0.33235
16	94.0	0.96097	-.0015511	0.30230	-.004893	0	0	1	0.29050
17	102.0	0.95505	.0000713	0.26799	-.003684	0	0	1	0.25594
18	0.0							0	
19	1.5			2.54000				0	
20	3.0			2.37000				0	
21	5.0	2.57000		2.19000				0	
22	11.0	2.12500		1.78000				0	
23	12.0							0	
24	17.0	1.90800		1.49000				0	
25	24.0	1.63300		1.21000				0	
26	32.0	1.40600		1.00000				0	
27	41.0	1.32500		0.82300				0	
28	49.0	1.24500		0.69200				0	
29	57.0	1.15000		0.59100				0	
30	71.0			0.45500				0	
31	79.0			0.39200				0	
32	87.0	0.98000		0.34100				0	
33	94.0	0.95500		0.30200				0	
34	102.0			0.26800				0	

RUN # 95.

OBS	TIME	HC	HCDOT	O3	O3DOT	SO2	SO2DOT	FLAG	DLXO3
1	0.0	3.02490	-.0635928	1.81263	-.0699221	.558233	-.00546656	1	5.48302
2	1.5	2.93108	-.0615022	1.71052	-.0662244	.550147	-.00531432	1	5.01367
3	3.0	2.84039	-.0594115	1.61396	-.0625267	.542290	-.00516208	1	4.58427
4	4.5	2.75284	-.0573209	1.52294	-.0588291	.534661	-.00500984	1	4.19241
5	6.8	2.62459	-.0541152	1.39415	-.0531593	.523406	-.00477640	1	3.65922
6	9.0	2.50901	-.0510489	1.28979	-.0477266	.512349	-.00457407	1	3.23609
7	16.0	2.18582	-.0412925	1.01682	-.0357746	.485605	-.00364176	1	2.22696
8	24.0	1.92678	-.0304795	0.79480	-.0252097	.460639	-.00271643	1	1.53140
9	40.0	1.59480	-.0159087	0.51492	-.0140306	.429429	-.00140179	1	0.82120
10	48.0	1.46680	-.0110915	0.42488	-.0109594	.420580	-.00099844	1	0.63171
11	56.0	1.41877	-.0081819	0.35126	-.0085375	.416343	-.00073750	1	0.49835
12	64.0	1.37562	-.0060137	0.29291	-.0068375	.410486	-.00075000	1	0.40294
13	72.0	1.33550	-.0040172	0.24526	-.0055361	.404343	-.00078571	1	0.32754
14	80.0	1.31134	-.0020207	0.20522	-.0044754	.397914	-.00082143	1	0.26911
15	86.2	1.30361	-.0004734	0.18002	-.0036550	.392736	-.00084911	1	0.23467
16	0.0	3.02400						0	
17	1.5			1.71000		.549000		0	
18	3.0			1.61000		.543000		0	
19	4.5			1.53000		.536000		0	
20	6.8							0	
21	9.0	2.52400		1.28000		.512000		0	
22	16.0	2.15400		1.01000		.484000		0	
23	24.0	1.92100		0.79000		.462000		0	
24	40.0	1.59300		0.52100		.428000		0	
25	48.0			0.42600		.422000		0	
26	56.0	1.42600		0.35100		.416000		0	
27	64.0	1.38100		0.29300		.411000		0	
28	72.0	1.33600		0.24600		.404000		0	
29	80.0	1.31000		0.20500		.398000		0	
30	86.2			0.18000				0	

RUN # 97.

OBS	TIME	HC	HCDOT	O3	O3DOT	SO2	SO2DOT	FLAG	OLXO3
1	0.0	3.11228	-.0750811	2.10226	-.0236689	.588442	-.00495812	1	6.54282
2	1.5	3.00898	-.0626476	2.06753	-.0226331	.581254	-.00462497	1	6.22117
3	3.0	2.92433	-.0502141	2.03436	-.0215973	.574557	-.00429182	1	5.94915
4	4.5	2.85834	-.0377806	2.00274	-.0205615	.568379	-.00395867	1	5.72451
5	6.0	2.81099	-.0253471	1.97268	-.0195257	.562691	-.00362552	1	5.54518
6	8.5	2.80030	-.0142708	1.92602	-.0177994	.554321	-.00307027	1	5.39344
7	11.0	2.76659	-.0136027	1.88368	-.0160731	.548496	-.00235090	1	5.21136
8	15.5	2.69818	-.0143035	1.82963	-.0128995	.537719	-.00236143	1	4.93666
9	18.0	2.66274	-.0145299	1.79353	-.0119756	.531948	-.00226723	1	4.78903
10	20.5	2.62667	-.0137691	1.76975	-.0110515	.526491	-.00224554	1	4.64855
11	22.5	2.59942	-.0134352	1.74839	-.0103123	.521997	-.00224862	1	4.54478
12	28.0	2.52573	-.0128737	1.70574	-.0091372	.508731	-.00219786	1	4.30824
13	37.5	2.41229	-.0108049	1.63103	-.0084096	.489047	-.00183737	1	3.93452
14	46.5	2.32294	-.0103725	1.55542	-.0077507	.473652	-.00140323	1	3.61315
15	50.0	2.28800	-.0097140	1.52875	-.0074919	.469393	-.00138295	1	3.49777
16	53.0	2.25709	-.0099002	1.50660	-.0074949	.465277	-.00132240	1	3.40054
17	62.0	2.17262	-.0074083	1.44159	-.0069521	.453992	-.00114125	1	3.13232
18	66.0	2.14814	-.0069879	1.41457	-.0068182	.449754	-.00104998	1	3.03869
19	69.5	2.12556	-.0068059	1.39098	-.0066568	.446410	-.00104764	1	2.95663
20	74.0	2.09722	-.0068223	1.36327	-.0074580	.441629	-.00109156	1	2.85907
21	80.5	2.04629	-.0063659	1.31336	-.0080991	.434289	-.00118283	1	2.68751
22	84.0	2.02563	-.0073328	1.28498	-.0077298	.429909	-.00125961	1	2.60290
23	88.0	1.99613	-.0059027	1.24979	-.0075222	.424899	-.00128811	1	2.49474
24	91.5	1.97849	-.0084550	1.22762	-.0062198	.420206	-.00128005	1	2.42883
25	94.0	1.95074	-.0045518	1.21368	-.0072200	.417036	-.00125544	1	2.36757
26	96.5	1.94786	-.0042000	1.19486	-.0080000	.413929	-.00123084	1	2.32741
27	99.0	1.94000	-.0110000	1.17343	-.0091429	.410882	-.00120623	1	2.27645
28	101.5	1.90300	-.0185000	1.14914	-.0102857	.407897	-.00118162	1	2.18682
29	104.0	1.84700	-.0262000	1.12200	-.0114286	.404974	-.00115702	1	2.07233
30	0.0	3.13100						0	
31	1.5							0	
32	3.0	2.88000						0	
33	4.5			2.00000		.570000		0	
34	6.0	2.82700		1.98000		.560000		0	
35	8.5	2.80100		1.92000		.555000		0	
36	11.0	2.77000				.548000		0	
37	15.5	2.69400		1.82000		.538000		0	
38	18.0	2.66400				.532000		0	
39	20.5	2.63000				.526000		0	
40	22.5							0	
41	28.0	2.52400		1.71000		.510000		0	
42	37.5	2.41400		1.63000		.488000		0	
43	45.5	2.32300		1.58000		.474000		0	
44	50.0	2.29600				.470000		0	
45	53.0	2.25000		1.50000		.465000		0	
46	62.0	2.17800				.454000		0	
47	66.0	2.14400		1.42000		.450000		0	
						.446000		0	

RUN # 98.

OBS	TIME	HC	HCDOT	O3	O3DOT	SO2	SO2DOT	FLAG	CLXO3
1	0.0	2.82533	-.0796213	2.02467	-.0838182	.203914	-.0110857	1	5.72036
2	1.5	2.70833	-.0763853	1.90354	-.0776841	.189143	-.0086095	1	5.15541
3	3.0	2.59616	-.0731492	1.79161	-.0715499	.178086	-.0061333	1	4.65135
4	4.5	2.48888	-.0699131	1.68889	-.0654158	.172255	-.0043293	1	4.20344
5	6.0	2.38644	-.0666770	1.60364	-.0548492	.166552	-.0036240	1	3.82698
6	13.0	1.97255	-.0515753	1.29694	-.0368479	.147335	-.0023482	1	2.55828
7	21.0	1.63366	-.0371674	1.04250	-.0280129	.133743	-.0014557	1	1.70374
8	31.0	1.38291	-.0228488	0.83259	-.0191889	.124624	-.0008282	1	1.15140
9	38.0	1.24805	-.0172771	0.71737	-.0154101	.120291	-.0006346	1	0.89531
10	47.0	1.12531	-.0121975	0.60280	-.0117439	.115458	-.0004421	1	0.67833
11	55.0	1.05299	-.0094254	0.52008	-.0095344	.112575	-.0002977	1	0.54764
12	63.0	0.98511	-.0076500	0.45446	-.0078625	.110914	-.0002500	1	0.44769
13	71.0	0.92590	-.0062509	0.39732	-.0066090	.109571	-.0002300	1	0.36788
14	79.0	0.88776	-.0051001	0.34911	-.0056029	.107126	-.0002577	1	0.30993
15	89.0	0.84709	-.0044239	0.29870	-.0045344	.104190	-.0002207	1	0.25302
16	97.0	0.80926	-.0042482	0.26650	-.0036245	.102786	-.0001304	1	0.21507
17	106.0	0.77218	-.0039980	0.23800	-.0027106	.102070	-.0000288	1	0.18377
18	114.0	0.74111	-.0037718	0.21956	-.0018983	.102200	.0000615	1	0.16272
19	0.0	2.81200				.205000		0	
20	1.5			1.91000		.187000		0	
21	3.0			1.78000		.178000		0	
22	4.5			1.69000		.173000		0	
23	6.0	2.42400		1.60000		.166000		0	
24	13.0	1.93500		1.28000		.146000		0	
25	21.0	1.64400		1.05000		.134000		0	
26	31.0	1.39200		0.83100		.125000		0	
27	38.0	1.24100		0.72000		.120000		0	
28	47.0	1.12500		0.60100		.116000		0	
29	55.0	1.05700		0.52200		.112000		0	
30	63.0	0.98700		0.45300		.111000		0	
31	71.0	0.92100		0.39900		.110000		0	
32	79.0	0.88700		0.34800		.107000		0	
33	89.0	0.85300		0.29900		.104000		0	
34	97.0	0.80500		0.26700		.103000		0	
35	106.0	0.76800		0.23700		.102000		0	
36	114.0	0.74400		0.22000				0	

Appendix 3: Aerosol Droplet Number, Surface Area, and Volume Concentrations Distributions for Aerosol Experiments.

DP	Geometric Mean Diameter
AMP	Electrometer Current Sensed
DIFFERENCE	Current Difference
DX	$\frac{dx}{d \log D_p}$
$\frac{DX}{X}$	$\frac{dx}{x \, d \log D_p}$

101A 5

DP	AMP	DIFFERENCE	DN	DS	DV	DN/N	DS/S	DV/V
.0042	0.0	0.0	0.	0.0	0.0	0.0	0.0	0.0
.0075	9.2800	0.396E 06	1582248.	280.06	0.350	0.6516	0.0523	0.0105
.0133	9.1700	0.620E 06	2480079.	1378.92	3.050	0.9429	0.2573	0.0912
.0237	8.5900	0.119E 07	4776716.	8407.02	33.294	1.8161	1.5688	0.9952
.0422	4.6900	0.382E 06	1529624.	8550.60	60.114	0.5816	1.5956	1.7969
.0750	0.8140	0.371E 05	148598.	2630.18	32.840	0.0565	0.4908	0.9816
.1330	0.0360	0.848E 03	3393.	188.63	4.173	0.0013	0.0352	0.1247
.2370	0.0	0.0	0.	0.0	0.0	0.0	0.0	0.0
.4220	0.0	0.0	0.	0.0	0.0	0.0	0.0	0.0
.7500	0.0	0.0	0.	0.0	0.0	0.0	0.0	0.0
	0.0							

N	S	V
2630164.00	5358.85	33.46

101A 15

DP	AMP	DIFFERENCE	DN	DS	DV	DN/N	DS/S	DV/V
.0042	0.0	0.0	0.	0.0	0.0	0.0	0.0	0.0
.0075	0.0	0.0	0.	0.0	0.0	0.0	0.0	0.0
.0133	6.9500	0.107E 06	427602.	237.75	0.526	0.5644	0.0471	0.0085
.0237	6.8500	0.202E 06	808368.	1422.73	5.634	1.0670	0.2817	0.0914
.0422	6.1900	0.329E 06	1314151.	7346.10	51.646	1.7345	1.4545	0.8379
.0750	2.8600	0.105E 06	421919.	7467.96	93.244	0.5569	1.4786	1.5128
.1330	0.6510	0.137E 05	54753.	3044.29	67.347	0.0723	0.6027	1.0926
.2370	0.0700	0.922E 03	3688.	649.14	25.708	0.0049	0.1285	0.4171
.4220	0.0020	0.156E 02	62.	34.80	2.446	0.0001	0.0069	0.0397
.7500	0.0	0.0	0.	0.0	0.0	0.0	0.0	0.0
	0.0							

N	S	V
757635.25	5050.69	61.64

101A 45

DP	AMP	DIFFERENCE	DN	DS	DV	DN/N	DS/S	DV/V
.0042	0.0	0.0	0.	0.0	0.0	0.0	0.0	0.0
.0075	0.0	0.0	0.	0.0	0.0	0.0	0.0	0.0
.0133	5.5800	0.641E 05	256562.	142.65	0.316	0.7722	0.0243	0.0024
.0237	5.5200	0.153E 05	61240.	107.78	0.427	0.1843	0.0184	0.0032
.0422	5.4700	0.819E 05	327551.	1831.01	12.873	0.9859	0.3124	0.0969
.0750	4.6400	0.129E 06	515891.	9131.27	114.012	1.5528	1.5581	0.8583
.1330	1.9390	0.380E 05	152197.	8462.18	187.203	0.4581	1.4440	1.4092
.2370	0.3240	0.342E 04	13668.	2405.65	95.269	0.0411	0.4105	0.7172
.4220	0.0720	0.397E 03	1587.	887.31	62.382	0.0048	0.1514	0.4696
.7500	0.0210	0.669E 02	268.	473.76	58.885	0.0008	0.0808	0.4433
	0.0060							

N	S	V
332240.50	5860.40	132.84

101A 75

DP	AMP	DIFFERENCE	DN	DS	DV	DN/N	DS/S	DV/V
.0042	0.0	0.0	0.	0.0	0.0	0.0	0.0	0.0
.0075	4.7500	0.180E 06	719203.	127.30	0.159	1.9947	0.0218	0.0010
.0133	4.7000	0.107E 05	42761.	23.78	0.053	0.1186	0.0041	0.0003
.0237	4.6900	0.612E 04	24497.	43.11	0.171	0.0679	0.0074	0.0011
.0422	4.6700	0.138E 05	55249.	308.84	2.171	0.1532	0.0528	0.0140
.0750	4.5300	0.965E 05	385820.	6829.01	85.266	1.0701	1.1675	0.5483
.1330	2.5100	0.478E 05	191307.	10636.67	235.308	0.5306	1.8184	1.5131
.2370	0.4800	0.525E 04	20991.	3694.39	146.306	0.0582	0.6316	0.9408
.4220	0.0930	0.521E 03	2085.	1165.69	81.953	0.0058	0.1993	0.5270
.7500	0.0260	0.803E 02	321.	568.51	70.662	0.0009	0.0972	0.4544
	0.0080							

N	S	V
360558.00	5849.32	155.51

1018 5

DP	AMP	DIFFERENCE	DN	DS	DV	DN/N	DS/S	DV/V
.0042	0.0	0.0	0.	0.0	0.0	0.0	0.0	0.0
.0075	7.0300	0.432E 06	1726078.	305.52	0.381	0.5908	0.0778	0.0208
.0133	6.9100	0.108E 07	4318760.	2401.23	5.312	1.4781	0.6117	0.2901
.0237	5.9000	0.123E 07	4935940.	8687.25	34.403	1.6894	2.2131	1.8790
.0422	1.8700	0.169E 06	676807.	3783.35	26.599	0.2316	0.9638	1.4527
.0750	0.1550	0.740E 04	29605.	524.01	6.543	0.0101	0.1335	0.3573
.1330	0.0	0.0	0.	0.0	0.0	0.0	0.0	0.0
.2370	0.0	0.0	0.	0.0	0.0	0.0	0.0	0.0
.4220	0.0	0.0	0.	0.0	0.0	0.0	0.0	0.0
.7500	0.0	0.0	0.	0.0	0.0	0.0	0.0	0.0
	0.0							

N	S	V
2921797.00	3925.34	18.31

101B 16

DP	AHP	DIFFERENCE	DN	DS	DV	DN/N	DS/S	DV/V
.0042	0.0	0.0	0.	0.0	0.0	0.0	0.0	0.0
.0075	6.3100	0.719E 05	287673.	50.92	0.064	0.3864	0.0113	0.0012
.0133	6.2900	0.428E 05	171040.	95.10	0.210	0.2298	0.0212	0.0040
.0237	6.2500	0.224E 06	894105.	1573.62	6.232	1.2011	0.3501	0.1188
.0422	5.5200	0.302E 06	1207598.	6750.47	47.459	1.6222	1.5017	0.9044
.0750	2.4600	0.925E 05	370158.	6551.79	81.805	0.4972	1.4575	1.5589
.1330	0.5220	0.111E 05	44293.	2462.68	54.480	0.0595	0.5478	1.0382
.2370	0.0520	0.705E 03	2820.	496.40	19.659	0.0038	0.1104	0.3746
.4220	0.0	0.0	0.	0.0	0.0	0.0	0.0	0.0
.7500	0.0	0.0	0.	0.0	0.0	0.0	0.0	0.0
	0.0							

N	S	V
744421.00	4495.24	52.48

1018 40

DP	AMP	DIFFERENCE	DN	DS	DV	DN/N	DS/S	DV/V
.0042	0.0	0.0	0.	0.0	0.0	0.0	0.0	0.0
.0075	5.3900	0.719E 05	287673.	50.92	0.064	0.7678	0.0094	0.0005
.0133	5.3700	0.321E 05	128283.	71.33	0.158	0.3424	0.0132	0.0014
.0237	5.3400	0.612E 04	24495.	43.11	0.171	0.0654	0.0080	0.0015
.0422	5.3200	0.101E 06	402533.	2250.16	15.820	1.0744	0.4159	0.1364
.0750	4.3000	0.130E 06	518756.	9181.97	114.645	1.3846	1.6971	0.9886
.1330	1.5840	0.310E 05	123831.	6885.02	152.312	0.3305	1.2726	1.3134
.2370	0.2700	0.286E 04	11445.	2014.26	79.769	0.0305	0.3723	0.6879
.4220	0.0590	0.342E 03	1369.	765.53	53.820	0.0037	0.1415	0.4641
.7500	0.0150	0.535E 02	214.	379.01	47.108	0.0006	0.0701	0.4062
	0.0030							

N	S	V
374649.25	5410.32	115.97

1018 75

DP	AMP	DIFFERENCE	DN	DS	DV	DN/N	DS/S	DV/V
.0042	0.0	0.0	0.	0.0	0.0	0.0	0.0	0.0
.0075	4.5600	0.719E 05	287673.	50.92	0.064	1.0761	0.0090	0.0004
.0133	4.5400	0.321E 05	128283.	71.33	0.158	0.4798	0.0126	0.0010
.0237	4.5100	0.612E 04	24495.	43.11	0.171	0.0916	0.0076	0.0011
.0422	4.4900	0.158E 05	63142.	352.97	2.481	0.2362	0.0624	0.0165
.0750	4.3300	0.888E 05	355260.	6288.10	78.512	1.3289	1.1111	0.5207
.1330	2.4700	0.466E 05	186407.	10364.20	229.280	0.6973	1.8313	1.5207
.2370	0.4920	0.544E 04	21750.	3828.04	151.599	0.0814	0.6764	1.0055
.4220	0.0910	0.521E 03	2085.	1165.68	81.952	0.0078	0.2060	0.5435
.7500	0.0240	0.669E 02	268.	473.76	58.885	0.0010	0.0837	0.3905
	0.0090							

N	S	V
267340.50	5659.52	150.78

102 5

DP	AMP	DIFFERENCE	DN	DS	DV	DN/N	DS/S	DV/V
.0042	0.0	0.0	0.	0.0	0.0	0.0	0.0	0.0
.0075	6.9900	0.539E 06	2157608.	381.90	0.477	0.6189	0.0982	0.0294
.0133	6.8400	0.165E 07	6585036.	3661.28	8.100	1.8888	0.9413	0.4992
.0237	5.3000	0.115E 07	4593000.	8083.68	32.013	1.3174	2.0783	1.9732
.0422	1.5500	0.152E 06	607745.	3397.29	23.884	0.1743	0.8735	1.4722
.0750	0.0100	0.477E 03	1910.	33.81	0.422	0.0005	0.0087	0.0260
.1330	0.0	0.0	0.	0.0	0.0	0.0	0.0	0.0
.2370	0.0	0.0	0.	0.0	0.0	0.0	0.0	0.0
.4220	0.0	0.0	0.	0.0	0.0	0.0	0.0	0.0
.7500	0.0	0.0	0.	0.0	0.0	0.0	0.0	0.0
	0.0							

N	S	V
3486324.00	3889.49	16.22

102 16

DP	AMP	DIFFERENCE	DN	DS	DV	DN/N	DS/S	DV/V
.0042	0.0	0.0	0.	0.0	0.0	0.0	0.0	0.0
.0075	5.9700	0.108E 06	431516.	76.38	0.095	0.5700	0.0188	0.0023
.0133	5.9400	0.214E 05	85522.	47.55	0.105	0.1130	0.0117	0.0025
.0237	5.9200	0.236E 06	943095.	1659.85	6.573	1.2458	0.4075	0.1551
.0422	5.1500	0.300E 06	1199705.	6706.35	47.148	1.5848	1.6465	1.1125
.0750	2.1100	0.836E 05	334250.	5916.22	73.869	0.4415	1.4525	1.7430
.1330	0.3600	0.848E 04	33926.	1886.31	41.729	0.0448	0.4631	0.9846
.2370	0.0	0.0	0.	0.0	0.0	0.0	0.0	0.0
.4220	0.0	0.0	0.	0.0	0.0	0.0	0.0	0.0
.7500	0.0	0.0	0.	0.0	0.0	0.0	0.0	0.0
	0.0							

N	S	V
757003.25	4073.16	42.38

102 45

DP	AMP	DIFFERENCE	DN	DS	DV	DN/N	DS/S	DV/V
.0042	0.0	0.0	0.	0.0	0.0	0.0	0.0	0.0
.0075	4.6800	0.108E 06	431516.	76.38	0.095	1.1626	0.0172	0.0012
.0133	4.6500	0.214E 05	85522.	47.55	0.105	0.2304	0.0107	0.0014
.0237	4.6300	0.122E 05	48992.	86.23	0.341	0.1320	0.0194	0.0045
.0422	4.5900	0.858E 05	343337.	1919.25	13.493	0.9250	0.4313	0.1761
.0750	3.7200	0.114E 06	454580.	8046.06	100.462	1.2248	1.8081	1.3110
.1330	1.3400	0.283E 05	113088.	6287.68	139.098	0.3047	1.4130	1.8152
.2370	0.1400	0.190E 04	7594.	1336.47	52.927	0.0205	0.3003	0.6907
.4220	0.0	0.0	0.	0.0	0.0	0.0	0.0	0.0
.7500	0.0	0.0	0.	0.0	0.0	0.0	0.0	0.0
	0.0							

N	S	V
371156.50	4449.91	76.63

102 75

DP	AMP	DIFFERENCE	DN	DS	DV	DN/N	DS/S	DV/V
.0042	0.0	0.0	0.	0.0	0.0	0.0	0.0	0.0
.0075	3.9000	0.324E 06	1294562.	229.14	0.286	2.6466	0.0539	0.0033
.0133	3.8100	0.107E 05	42761.	23.78	0.053	0.0874	0.0056	0.0006
.0237	3.8000	0.306E 04	12247.	21.55	0.085	0.0250	0.0051	0.0010
.0422	3.7900	0.296E 05	118392.	661.81	4.653	0.2420	0.1557	0.0542
.0750	3.4900	0.836E 05	334250.	5916.22	73.869	0.6833	1.3918	0.8601
.1330	1.7400	0.353E 05	141360.	7859.61	173.873	0.2890	1.8490	2.0244
.2370	0.2400	0.325E 04	13018.	2291.10	90.733	0.0266	0.5390	1.0564
.4220	0.0	0.0	0.	0.0	0.0	0.0	0.0	0.0
.7500	0.0	0.0	0.	0.0	0.0	0.0	0.0	0.0
	0.0							

N	S	V
489146.75	4250.80	85.89

103 5

DP	AMP	DIFFERENCE	DN	DS	DV	DN/N	DS/S	DV/V
.0042	0.0	0.0	0.	0.0	0.0	0.0	0.0	0.0
.0075	5.4500	0.216E 06	863046.	152.76	0.191	0.2757	0.0500	0.0168
.0133	5.3900	0.198E 07	7910596.	4398.29	9.730	2.5272	1.4389	0.8595
.0237	3.5400	0.867E 06	3469857.	6106.95	24.185	1.1085	1.9978	2.1353
.0422	0.7070	0.690E 05	275853.	1542.02	10.841	0.0881	0.5045	0.9576
.0750	0.0080	0.382E 03	1528.	27.05	0.338	0.0005	0.0088	0.0298
.1330	0.0	0.0	0.	0.0	0.0	0.0	0.0	0.0
.2370	0.0	0.0	0.	0.0	0.0	0.0	0.0	0.0
.4220	0.0	0.0	0.	0.0	0.0	0.0	0.0	0.0
.7500	0.0	0.0	0.	0.0	0.0	0.0	0.0	0.0
	0.0							

N	S	V
3130219.00	3056.76	11.32

103 15

DP	AMP	DIFFERENCE	DN	DS	DV	DN/N	DS/S	DV/V
.0042	0.0	0.0	0.	0.0	0.0	0.0	0.0	0.0
.0075	0.0	0.0	0.	0.0	0.0	0.0	0.0	0.0
.0133	4.4100	0.428E 05	171040.	95.10	0.210	0.2598	0.0339	0.0085
.0237	4.3700	0.358E 06	1433016.	2522.11	9.988	2.1764	0.8997	0.4021
.0422	3.2000	0.210E 06	838610.	4687.83	32.957	1.2736	1.6723	1.3267
.0750	1.0750	0.443E 05	177248.	3137.29	39.172	0.2692	1.1192	1.5769
.1330	0.1470	0.346E 04	13853.	770.24	17.040	0.0210	0.2748	0.6859
.2370	0.0	0.0	0.	0.0	0.0	0.0	0.0	0.0
.4220	0.0	0.0	0.	0.0	0.0	0.0	0.0	0.0
.7500	0.0	0.0	0.	0.0	0.0	0.0	0.0	0.0
	0.0							

N	S	V
658441.25	2803.14	24.84

103 45

DP	AMP	DIFFERENCE	DN	DS	DV	DN/N	DS/S	DV/V
.0042	0.0	0.0	0.	0.0	0.0	0.0	0.0	0.0
.0075	3.5000	0.216E 06	863046.	152.76	0.191	1.8550	0.0496	0.0037
.0133	3.4400	0.214E 05	85522.	47.55	0.105	0.1838	0.0154	0.0020
.0237	3.4200	0.367E 05	146976.	258.68	1.024	0.3159	0.0839	0.0197
.0422	3.3000	0.101E 06	402533.	2250.16	15.820	0.8652	0.7302	0.3040
.0750	2.2800	0.754E 05	301780.	5341.50	66.693	0.6486	1.7335	1.2815
.1330	0.7000	0.139E 05	55602.	3091.45	68.390	0.1195	1.0033	1.3141
.2370	0.1100	0.126E 04	5044.	887.80	35.159	0.0108	0.2881	0.6756
.4220	0.0170	0.132E 03	529.	295.77	20.794	0.0011	0.0960	0.3995
.7500	0.0	0.0	0.	0.0	0.0	0.0	0.0	0.0
	0.0							

N	S	V
465257.00	3081.41	52.04

103 75

DP	AMP	DIFFERENCE	DN	DS	DV	DN/N	DS/S	DV/V
.0042	0.0	0.0	0.	0.0	0.0	0.0	0.0	0.0
.0075	0.0	0.0	0.	0.0	0.0	0.0	0.0	0.0
.0133	2.7000	0.107E 05	42761.	23.78	0.053	0.3038	0.0085	0.0009
.0237	2.6900	0.306E 04	12248.	21.56	0.085	0.0870	0.0077	0.0014
.0422	2.6800	0.434E 05	173641.	970.66	6.824	1.2336	0.3480	0.1148
.0750	2.2400	0.641E 05	256513.	4540.28	56.689	1.8224	1.6278	0.9533
.1330	0.8970	0.176E 05	70397.	3914.09	86.589	0.5001	1.4033	1.4560
.2370	0.1500	0.167E 04	6672.	1174.19	46.500	0.0474	0.4210	0.7819
.4220	0.0270	0.187E 03	747.	417.56	29.356	0.0053	0.1497	0.4936
.7500	0.0030	0.134E 02	54.	94.75	11.777	0.0004	0.0340	0.1980
	0.0							

N	S	V
140758.13	2789.21	59.47

104 5

DP	AMP	DIFFERENCE	DN	DS	DV	DN/N	DS/S	DV/V
.0042	0.0	0.0	0.	0.0	0.0	0.0	0.0	0.0
.0075	10.1700	0.252E 06	1006876.	178.22	0.223	0.5096	0.0284	0.0044
.0133	10.1000	0.192E 06	769681.	427.94	0.947	0.3896	0.0683	0.0186
.0237	9.9200	0.971E 06	3882614.	6833.40	27.062	1.9652	1.0900	0.5326
.0422	6.7500	0.474E 06	1894666.	10591.18	74.460	0.9590	1.6894	1.4654
.0750	1.9490	0.816E 05	326228.	5774.23	72.096	0.1651	0.9211	1.4189
.1330	0.2410	0.563E 04	22523.	1252.30	27.704	0.0114	0.1998	0.5452
.2370	0.0020	0.271E 02	108.	19.09	0.756	0.0001	0.0030	0.0149
.4220	0.0	0.0	0.	0.0	0.0	0.0	0.0	0.0
.7500	0.0	0.0	0.	0.0	0.0	0.0	0.0	0.0
	0.0							

N	S	V
1975673.00	6269.09	50.81

104 15

DP	AMP	DIFFERENCE	DN	DS	DV	DN/N	DS/S	DV/V
.0042	0.0	0.0	0.	0.0	0.0	0.0	0.0	0.0
.0075	0.0	0.0	0.	0.0	0.0	0.0	0.0	0.0
.0133	9.0800	0.203E 06	812442.	451.72	0.999	0.9992	0.0583	0.0077
.0237	8.8900	0.827E 05	330695.	582.02	2.305	0.4067	0.0751	0.0178
.0422	8.6200	0.302E 06	1207598.	6750.47	47.459	1.4852	0.8715	0.3660
.0750	5.5600	0.192E 06	767820.	13590.41	169.688	0.9443	1.7546	1.3085
.1330	1.5400	0.302E 05	120910.	6722.59	148.719	0.1487	0.8679	1.1468
.2370	0.2570	0.286E 04	11445.	2014.26	79.769	0.0141	0.2600	0.6151
.4220	0.0460	0.319E 03	1276.	713.33	50.150	0.0016	0.0921	0.3867
.7500	0.0050	0.223E 02	89.	157.92	19.628	0.0001	0.0204	0.1514
	0.0							

N	S	V
813068.00	7745.68	129.68

104 45

DP	AMP	DIFFERENCE	DN	DS	DV	DN/N	DS/S	DV/V
.0042	0.0	0.0	0.	0.0	0.0	0.0	0.0	0.0
.0075	0.0	0.0	0.	0.0	0.0	0.0	0.0	0.0
.0133	6.9200	0.107E 05	42757.	23.77	0.053	0.1620	0.0028	0.0002
.0237	6.9100	0.306E 04	12248.	21.56	0.085	0.0464	0.0025	0.0004
.0422	6.9000	0.355E 05	142070.	794.17	5.583	0.5381	0.0926	0.0240
.0750	6.5400	0.137E 06	548170.	9702.61	121.146	2.0764	1.1312	0.5197
.1330	3.6700	0.684E 05	273767.	15221.44	336.733	1.0370	1.7746	1.4445
.2370	0.7650	0.831E 04	33249.	5851.84	231.746	0.1259	0.6822	0.9941
.4220	0.1520	0.809E 03	3237.	1809.42	127.210	0.0123	0.2110	0.5457
.7500	0.0480	0.125E 03	500.	884.35	109.919	0.0019	0.1031	0.4715
	0.0200							

N	S	V
263999.00	8577.29	233.12

104 75

DP	AMP	DIFFERENCE	DN	DS	DV	DN/N	DS/S	DV/V
.0042	0.0	0.0	0.	0.0	0.0	0.0	0.0	0.0
.0075	5.8200	0.216E 06	863046.	152.76	0.191	2.1115	0.0193	0.0008
.0133	5.7600	0.107E 05	42757.	23.77	0.053	0.1046	0.0030	0.0002
.0237	5.7500	0.612E 04	24497.	43.11	0.171	0.0599	0.0054	0.0007
.0422	5.7300	0.109E 05	43410.	242.66	1.706	0.1062	0.0306	0.0073
.0750	5.6200	0.845E 05	338070.	5983.84	74.713	0.8271	0.7544	0.3198
.1330	3.8500	0.699E 05	279704.	15551.55	344.036	0.6843	1.9606	1.4726
.2370	0.8820	0.986E 04	39432.	6940.11	274.844	0.0965	0.8749	1.1764
.4220	0.1550	0.895E 03	3579.	2000.80	140.665	0.0088	0.2522	0.6021
.7500	0.0400	0.112E 03	446.	789.60	98.142	0.0011	0.0995	0.4201
	0.0150							

N	S	V
408735.00	7932.05	233.63

105 5

DP	AMP	DIFFERENCE	DN	DS	DV	DN/N	DS/S	DV/V
.0042	0.0	0.0	0.	0.0	0.0	0.0	0.0	0.0
.0075	10.4800	0.360E 05	143843.	25.46	0.032	0.0672	0.0040	0.0007
.0133	10.4700	0.428E 06	1710398.	950.98	2.104	0.7989	0.1510	0.0450
.0237	10.0700	0.114E 07	4544008.	7997.45	31.672	2.1224	1.2698	0.6770
.0422	6.3600	0.468E 06	1872566.	10467.64	73.592	0.8746	1.6620	1.5730
.0750	1.6150	0.696E 05	278478.	4929.05	61.544	0.1301	0.7826	1.3154
.1330	0.1570	0.370E 04	14796.	822.64	18.199	0.0069	0.1306	0.3890
.2370	0.0	0.0	0.	0.0	0.0	0.0	0.0	0.0
.4220	0.0	0.0	0.	0.0	0.0	0.0	0.0	0.0
.7500	0.0	0.0	0.	0.0	0.0	0.0	0.0	0.0
	0.0							

N	S	V
2141021.00	6298.30	46.79

105 15

DP	AMP	DIFFERENCE	DN	DS	DV	DN/N	DS/S	DV/V
.0042	0.0	0.0	0.	0.0	0.0	0.0	0.0	0.0
.0075	0.0	0.0	0.	0.0	0.0	0.0	0.0	0.0
.0133	8.7800	0.214E 06	855199.	475.49	1.052	1.1064	0.0622	0.0078
.0237	8.5800	0.490E 05	195969.	344.91	1.366	0.2535	0.0451	0.0151
.0422	8.4200	0.292E 06	1168134.	6529.87	45.908	1.5112	0.8542	0.3405
.0750	5.4600	0.183E 06	731530.	12948.07	161.668	0.9464	1.6938	1.1990
.1330	1.6300	0.318E 05	127318.	7078.89	156.601	0.1647	0.9260	1.1615
.2370	0.2790	0.305E 04	12204.	2147.90	85.062	0.0158	0.2810	0.6309
.4220	0.0540	0.358E 03	1432.	800.32	56.266	0.0019	0.1047	0.4173
.7500	0.0080	0.357E 02	143.	252.67	31.405	0.0002	0.0331	0.2329
	0.0							

N	S	V
772981.00	7644.53	134.83

105 45

DP	AMP	DIFFERENCE	DN	DS	DV	DN/N	DS/S	DV/V
.0042	0.0	0.0	0.	0.0	0.0	0.0	0.0	0.0
.0075	0.0	0.0	0.	0.0	0.0	0.0	0.0	0.0
.0133	7.2000	0.118E 06	470363.	261.52	0.579	1.2307	0.0301	0.0026
.0237	7.0900	0.612E 04	24495.	43.11	0.171	0.0641	0.0050	0.0008
.0422	7.0700	0.345E 05	138124.	772.11	5.428	0.3614	0.0887	0.0241
.0750	6.7200	0.146E 06	582550.	10311.13	128.744	1.5242	1.1852	0.5712
.1330	3.6700	0.696E 05	278479.	15483.43	342.529	0.7286	1.7797	1.5197
.2370	0.7150	0.782E 04	31296.	5508.18	218.136	0.0819	0.6331	0.9678
.4220	0.1380	0.786E 03	3144.	1757.23	123.540	0.0082	0.2020	0.5481
.7500	0.0370	0.937E 02	375.	663.26	82.439	0.0010	0.0762	0.3658
	0.0160							

N	S	V
382206.00	8699.99	225.39

105		75						
DP	AMP	DIFFERENCE	DN	DS	DV	DN/N	DS/S	DV/V
.0042	0.0	0.0	0.	0.0	0.0	0.0	0.0	0.0
.0075	5.6700	0.108E 06	431516.	76.38	0.095	1.4057	0.0088	0.0003
.0133	5.6400	0.428E 05	171040.	95.10	0.210	0.5572	0.0109	0.0007
.0237	5.6000	0.306E 04	12248.	21.56	0.085	0.0399	0.0025	0.0003
.0422	5.5900	0.118E 05	47357.	264.72	1.861	0.1543	0.0304	0.0062
.0750	5.4700	0.540E 05	215830.	3820.19	47.698	0.7031	0.4388	0.1589
.1330	4.3400	0.718E 05	287149.	15965.50	353.193	0.9354	1.8338	1.1765
.2370	1.2930	0.140E 05	55976.	9851.70	390.150	0.1823	1.1316	1.2996
.4220	0.2610	0.149E 04	5976.	3340.48	234.849	0.0195	0.3837	0.7823
.7500	0.0690	0.196E 03	785.	1389.69	172.730	0.0026	0.1596	0.5753
	0.0250							
			N	S	V			
			306968.75	8706.32	300.22			

INSTRUCTIONS

1. **REPORT NUMBER**
Insert the EPA report number as it appears on the cover of the publication.

2. **LEAVE BLANK**

3. **RECIPIENTS ACCESSION NUMBER**
Reserved for use by each report recipient.

4. **TITLE AND SUBTITLE**
Title should indicate clearly and briefly the subject coverage of the report, and be displayed prominently. Set subtitle, if used, in smaller type or otherwise subordinate it to main title. When a report is prepared in more than one volume, repeat the primary title, add volume number and include subtitle for the specific title.

5. **REPORT DATE**
Each report shall carry a date indicating at least month and year. Indicate the basis on which it was selected *(e.g., date of issue, date of approval, date of preparation, etc.)*.

6. **PERFORMING ORGANIZATION CODE**
Leave blank.

7. **AUTHOR(S)**
Give name(s) in conventional order *(John R. Doe, J. Robert Doe, etc.)*. List author's affiliation if it differs from the performing organization.

8. **PERFORMING ORGANIZATION REPORT NUMBER**
Insert if performing organization wishes to assign this number.

9. **PERFORMING ORGANIZATION NAME AND ADDRESS**
Give name, street, city, state, and ZIP code. List no more than two levels of an organizational hirearchy.

10. **PROGRAM ELEMENT NUMBER**
Use the program element number under which the report was prepared. Subordinate numbers may be included in parentheses.

11. **CONTRACT/GRANT NUMBER**
Insert contract or grant number under which report was prepared.

12. **SPONSORING AGENCY NAME AND ADDRESS**
Include ZIP code.

13. **TYPE OF REPORT AND PERIOD COVERED**
Indicate interim final, etc., and if applicable, dates covered.

14. **SPONSORING AGENCY CODE**
Leave blank.

15. **SUPPLEMENTARY NOTES**
Enter information not included elsewhere but useful, such as: Prepared in cooperation with, Translation of, Presented at conference of, To be published in, Supersedes, Supplements, etc.

16. **ABSTRACT**
Include a brief *(200 words or less)* factual summary of the most significant information contained in the report. If the report contains a significant bibliography or literature survey, mention it here.

17. **KEY WORDS AND DOCUMENT ANALYSIS**
(a) DESCRIPTORS - Select from the Thesaurus of Engineering and Scientific Terms the proper authorized terms that identify the major concept of the research and are sufficiently specific and precise to be used as index entries for cataloging.

(b) IDENTIFIERS AND OPEN-ENDED TERMS - Use identifiers for project names, code names, equipment designators, etc. Use open-ended terms written in descriptor form for those subjects for which no descriptor exists.

(c) COSATI FIELD GROUP - Field and group assignments are to be taken from the 1965 COSATI Subject Category List. Since the majority of documents are multidisciplinary in nature, the Primary Field/Group assignment(s) will be specific discipline, area of human endeavor, or type of physical object. The application(s) will be cross-referenced with secondary Field/Group assignments that will follow the primary posting(s).

18. **DISTRIBUTION STATEMENT**
Denote releasability to the public or limitation for reasons other than security for example "Release Unlimited." Cite any availability to the public, with address and price.

19. & 20. **SECURITY CLASSIFICATION**
DO NOT submit classified reports to the National Technical Information service.

21. **NUMBER OF PAGES**
Insert the total number of pages, including this one and unnumbered pages, but exclude distribution list, if any.

22. **PRICE**
Insert the price set by the National Technical Information Service or the Government Printing Office, if known.

INSTRUCTIONS

1. **REPORT NUMBER**
Insert the EPA report number as it appears on the cover of the publication.

2. **LEAVE BLANK**

3. **RECIPIENTS ACCESSION NUMBER**
Reserved for use by each report recipient.

4. **TITLE AND SUBTITLE**
Title should indicate clearly and briefly the subject coverage of the report, and be displayed prominently. Set subtitle, if used, in smaller type or otherwise subordinate it to main title. When a report is prepared in more than one volume, repeat the primary title, add volume number and include subtitle for the specific title.

5. **REPORT DATE**
Each report shall carry a date indicating at least month and year. Indicate the basis on which it was selected *(e.g., date of issue, date of approval, date of preparation, etc.)*.

6. **PERFORMING ORGANIZATION CODE**
Leave blank.

7. **AUTHOR(S)**
Give name(s) in conventional order *(John R. Doe, J. Robert Doe, etc.)*. List author's affiliation if it differs from the performing organization.

8. **PERFORMING ORGANIZATION REPORT NUMBER**
Insert if performing organization wishes to assign this number.

9. **PERFORMING ORGANIZATION NAME AND ADDRESS**
Give name, street, city, state, and ZIP code. List no more than two levels of an organizational hirearchy.

10. **PROGRAM ELEMENT NUMBER**
Use the program element number under which the report was prepared. Subordinate numbers may be included in parentheses.

11. **CONTRACT/GRANT NUMBER**
Insert contract or grant number under which report was prepared.

12. **SPONSORING AGENCY NAME AND ADDRESS**
Include ZIP code.

13. **TYPE OF REPORT AND PERIOD COVERED**
Indicate interim final, etc., and if applicable, dates covered.

14. **SPONSORING AGENCY CODE**
Leave blank.

15. **SUPPLEMENTARY NOTES**
Enter information not included elsewhere but useful, such as: Prepared in cooperation with, Translation of, Presented at conference of, To be published in, Supersedes, Supplements, etc.

16. **ABSTRACT**
Include a brief *(200 words or less)* factual summary of the most significant information contained in the report. If the report contains a significant bibliography or literature survey, mention it here.

17. **KEY WORDS AND DOCUMENT ANALYSIS**
(a) DESCRIPTORS - Select from the Thesaurus of Engineering and Scientific Terms the proper authorized terms that identify the major concept of the research and are sufficiently specific and precise to be used as index entries for cataloging.

(b) IDENTIFIERS AND OPEN-ENDED TERMS - Use identifiers for project names, code names, equipment designators, etc. Use open-ended terms written in descriptor form for those subjects for which no descriptor exists.

(c) COSATI FIELD GROUP - Field and group assignments are to be taken from the 1965 COSATI Subject Category List. Since the majority of documents are multidisciplinary in nature, the Primary Field/Group assignment(s) will be specific discipline, area of human endeavor, or type of physical object. The application(s) will be cross-referenced with secondary Field/Group assignments that will follow the primary posting(s).

18. **DISTRIBUTION STATEMENT**
Denote releasability to the public or limitation for reasons other than security for example "Release Unlimited." Cite any availability to the public, with address and price.

19. & 20. **SECURITY CLASSIFICATION**
DO NOT submit classified reports to the National Technical Information service.

21. **NUMBER OF PAGES**
Insert the total number of pages, including this one and unnumbered pages, but exclude distribution list, if any.

22. **PRICE**
Insert the price set by the National Technical Information Service or the Government Printing Office, if known.